TESIS DE LA UNIVERSIDAD DE ZARAGOZA

2023

190

Diego Pereira Leite

New methods for nanoparticles characterization by means of single particle Inductively coupled plasma mass spectrometry.

Director/es

Resano Ezcaray, Martín

Aramendia Marzo, María Teresa

ISSN 2254-7606

Prensas de la Universidad Universidad Zaragoza

ISSN 2254-7606

Universidad Zaragoza
1542

Tesis Doctoral

NEW METHODS FOR NANOPARTICLES CHARACTERIZATION BY MEANS OF SINGLE PARTICLE LNDUCTIVELY COUPLED PLASMA MASS SPECTROMETRY.

Autor

Diego Pereira Leite

Director/es

Resano Ezcaray, Martín
Aramendia Marzo, María Teresa

UNIVERSIDAD DE ZARAGOZA
Escuela de Doctorado

2021

Universidad Zaragoza
1542

Tesis Doctoral

NEW METHODS FOR NANOPARTICLES CHARACTERIZATION BY MEANS OF SINGLE PARTICLE INDUCTIVELY COUPLED PLASMA MASS SPECTROMETRY

Autor

Diego Pereira Leite

Director/es

Martín Resano Ezcaray

María Teresa Aramendía Marzo

Facultad de Ciencias/ Departamento de Química Analítica

2021

AGRADECIMIENTOS / ACKNOWLEDGEMENTS

Cinco años, cuatro meses y tres semanas después del día que dejé todo lo que conocía y había vivido para cruzar medio mundo con el objetivo de investigar y realizar un doctorado, finalmente, escribo estas palabras de agradecimientos, que son las últimas que escribo de mi tesis doctoral, aunque sean las primeras que se leen en esta memoria. Obviamente, no llegaría a escribirlas sin las numerosas ayudas que recibí a lo largo del camino.

En mi primer lugar y con mucho honor, agradezco a mis directores de tesis Martín Resano y Maite Aramendía. Muchas gracias, Martín, por toda la atención y paciencia recibida desde el primer momento, un año antes de venir a España, con todos los trámites para recibir la beca. Muchas gracias también por la asistencia al llegar en España, al empezar en el laboratorio y por la libertad de desarrollar la tesis doctoral. He podido comprobar por la calidad de los trabajos que este grupo genera por qué Martín Resano es un investigador tan respetado por los investigadores brasileños y, honestamente, no me imagino haciendo la tesis en otro sitio. Muchas gracias, Maite, por todos los conocimientos y experiencia transmitidos (¡no sólo en química analítica, en castellano también!), por todo el trabajo minucioso de codirección de tesis, por todo el apoyo desde Zaragoza cuando me encontraba lejos en mis estancias… y por todas las risas que echamos a lo largo de estos años!

Me gustaría decir muchas gracias *(e obrigado)* a mis compañeros del grupo M.A.R.T.E. A Esperanza García, por su amabilidad desde el primero momento que llegué al laboratorio. A Flavio Nakadi y Raúl Garde por compartir buenos momentos como compañeros de trabajo a lo largo de estos años. *Às minhas amigas brasileiras que vieram fazer doutorado sanduíche no laboratório Ananda Guarda, Raquel Machado e Priscila Vicentino, as quais tive o prazer de recepcioná-las em Zaragoza e realizar trabalhos em colaboração e à Prof. Dra. Convidada Márcia Veiga pelo companheirismo e inúmeras risadas.* A mis compañeras que también estuvieron de estancia en el laboratorio Águeda Cañabate y Mª Carmen García.

Me gustaría hacer una mención especial (in memoriam) a la Prof. Dra. Gemma Cepriá, que fue mi primer contacto de la Universidad y amablemente me envió la carta de aceptación y me recomendó a Martín para realizar la tesis doctoral.

Quero demonstrar a imensa gratidão que tenho ao Conselho Nacional de Desenvolvimento Científico e Tecnológico (CNPq) pela concessão da bolsa de Doutorado Pleno (processo n° 232487/2014-6).

Muchas gracias a la Fundación Ibercaja-CAI por la beca recibida a través del programa Ibercaja-CAI estancias de investigación sobre el tema: "Caracterización de nanopartículas Mediante Detección Individual de Partículas en Plasma de Acoplamiento Inductivo - Espectrometría de Masas con analizador de tiempo de vuelo (SP-ICP-TOF-MS)" en los laboratorios de LGC en Londres, Reino Unido.

A special thanks to the financial support provided by LGC through UK BEIS NMS Chemical and Biological Program to extend my secondment work in the UK.

A special thanks to the Prof. Dr. Frank Vanhaecke for the opportunity of working with his amazing research group and all the support during my stay in Ghent. Muchas Gracias a Eduardo Bolea-Fernández y Ana Rúa-Ibarz por el hospedaje en mis días en Gante y por el gran compromiso con el trabajo. No importaba si eran las diez de la noche o un fin de semana, siempre estaban motivados a ir a medir para mejorar todavía más el trabajo. Fue un gran privilegio estar este mes con vosotros.

A special thanks to the Glenn Woods from Agilent Technologies for the invitation to work with the new (at that time) ICP-MS/MS 8900 at the Agilent facilities in Cheadle, UK.

Muchas gracias al Prof. Dr. José Luís Todolí por recibirme en su grupo para la estancia de un mes en Alicante. Muchas gracias también a Raquel Sánchez y a Carlos Sánchez por toda la ayuda y compañerismo a lo largo de esta estancia.

Muchas gracias Al Prof. Dr. Javier Resano por el desarrollo de los scripts de tratamiento de datos con Octave.

Muchas gracias a Heidi Goenaga-Infante por recibirme en su grupo de investigación en LGC. Muchas gracias por la charla en congreso de CSI en Pisa y por aceptar que yo pudiera hacer una visita un año antes de, efectivamente, irme a Londres para la estancia. Vivir en Londres es algo que no imaginaba en mis mejores sueños y puedo decir que gracias al apoyo de mis directores y del suyo, he podido vivir experiencias académicas y personales inolvidables*. I would also like to give a special thanks to Dr. Dorota Bartczak and Alex Ramsay for all the support and understanding while I was doing my secondment in LGC. I would also give a special mention to Dr. Estela*

del Castillo for the help with the IDA work. Thanks to all the staff of the Inorganic Analysis team of LGC for having me those 6 months! I hope to visit you again in the future!

Finalmente, es la hora de los agradecimientos más personales (y emotivos).

Muito obrigado aos que ficaram no Brasil e entenderam que eu precisava sair de lá para viver essa experiencia. Muito obrigado à minha mãe Edileuza, ao meu pai de criação Toshio e à minha irmã Aline. À minha querida tia e segunda mãe Marcia Matos e às irmãs que a vida me deu, Jaqueline Matos e Télia Lima. A saudade não cabe no peito!

Muchas gracias a la nueva familia me acogió a lo largo de estos años.

A Abel. No encuentro palabras en castellano, en portugués, en inglés o en cualquier otro idioma que se hable en este inmenso mundo para expresar cuán importante eres para mí y lo inmensamente agradecido que estoy por todo.

A Daniel. Emigrar es difícil, pero tu amistad hizo todo muy fácil. Jamás imaginé que alguien me haría sentir como si fuera de Zaragoza de toda la vida. Eres el hermano que nunca tuve. Muchas gracias por tu amistad.

A Elisa. Gracias por el compañerismo, los momentos graciosos en el Local, en los viajes y los paseos por Zaragoza.

A Ricardo. De Londres a Madrid, pasando por Croacia. Eres un gran ejemplo e inspiración, como profesional y como persona. Ojalá se acaben pronto las restricciones y hagamos viaje que estamos hablando hace meses. ¡Gracias por la amistad!

Jordy, heel erg bedankt dat je een zeer goede vriend voor mij bent geweest tijdens deze pandemie en vanaf een grote afstand. Het was een zeer moeilijke periode en jij hebt mij er doorheen geholpen. Dag schat!

Na minha dissertação de mestrado, eu citei Fernando Pessoa com sua frase: "O homem é do tamanho dos seus sonhos". Se isso for verdade, hoje eu tenho o tamanho de toda a Espanha. Do fundo do meu coração, MUITO OBRIGADO!

"Creio no mundo como num malmequer,
Porque o vejo. Mas não penso nele
Porque pensar é não compreender ...

O Mundo não se fez para pensarmos nele
(Pensar é estar doente dos olhos)
Mas para olharmos para ele e estarmos de acordo...

Eu não tenho filosofia: tenho sentidos...
Se falo na Natureza não é porque saiba o que ela é,
Mas porque a amo, e amo-a por isso,
Porque quem ama nunca sabe o que ama
Nem sabe por que ama, nem o que é amar ...
Amar é a eterna inocência,
E a única inocência não pensar..."

Alberto Caeiro (heterônimo de Fernando Pessoa) – O guardador de rebanhos

"So I make a dress from my sorrows
And shoes from my sadness
And dance all the way into love
Trouble passes and beauty remains"

Paloma Faith / Bernard Joseph Butler / Fyfe Dangerfield Hutchins – Beauty Remains

PUBLICATIONS

During this PhD, the present author has participated in four articles. Two of them derive from the data presented in two chapters (Chapters 3 and 4) of the present thesis. Also, data from other two chapters (Chapters 5 and 6) have produced two draft articles that are being revised before submission.

Published articles presented in this thesis:

- **Characterization of SiO_2 nanoparticles by single particle-inductively coupled plasma-tandem mass spectrometry (SP-ICP-MS/MS)**
  Eduardo Bolea-Fernandez, Diego Leite, Ana Rua-Ibarz, Lieve Balcaen, Maite Aramendía, Martín Resano, Frank Vanhaecke
  Journal of Analytical Atomic Spectrometry, 2017, 32, 2140 - 2152

- **On the effect of using collision/reaction cell (CRC) technology in single-particle ICP-mass spectrometry (SP-ICP-MS)**
  Eduardo Bolea-Fernandez, Diego Leite, Ana Rua-Ibarz, Tong Liu, Glenn Woods, Maite Aramendía, Martín Resano, Frank Vanhaecke
  Analytica Chimica Acta, 2019, 24, 95 - 106

Another published articles throughout this PhD:

- **Direct mercury determination in blood and urine by means of high-resolution continuum source graphite furnace atomic absorption spectrometry using gold nanoparticles as a chemical modifier**
  Maite Aramendía, Ananda Guarda, Diego Leite, Martín Resano
  Journal of Analytical Atomic Spectrometry, 2017, 32, 2352-2359

- **Extraction induced by microemulsion breaking as a novel tool for the simultaneous determination of Cd, Mn, Pb and Sb in gasoline samples by ICP-MS and discrete sample introduction**

  Priscila O. Vicentino, Ricardo J. Cassella, Diego Leite, Martín Resano

  Talanta, 2020, 206

This work has been funded by:

- **Conselho Nacional de Desenvolvimento Científico e Tecnológico – Brasil (232487/2014-6).**
- **Ministerio de Economía y Competitividad (Proyecto CTQ2015-64684-P (MINECO/FEDER)) y Ministerio de Ciencia e Innovación (proyecto PGC2018-093753-B-I00 (MCIU/AEI//FEDER, UE)).**
- **Gobierno de Aragón a través de las convocatorias de Grupos de Investigación (Grupo M.A.R.T.E., E-41 (2015 y 2016), E43_17R (2017-19) y E43_20R (2020-2022), Fondo Europeo de Desarrollo Regional y FEDER Aragón 2014-2020)**
- **Proyectos OTRI 2016/1079 y 2015/0526**
- **LGC Limited (UK BEIS NMS Chemical and Biological Program)**

LIST OF ABREVIATIONS

A&MS - Atomic and Mass Spectrometry Research Group (University of Ghent)

AA - Axial Acceleration

AFM - Atomic Force Microscopy

AICIS- Australian Industrial Chemical Introduction Scheme

AMNM - Analytical Metrology for Nanomaterials

AN&N - Analytical Nanoscience and Nanotechnology

AS - Atomic Spectrometry

BEC - Background Equivalent Concentration

BG - Background

CCD - Charge-Coupled Device

CE - Capillary Electrophoresis

CRC- Collision/Reaction Cell

CRM - Certified Reference Material

DLS - Dynamic Light Scattering

DMF - Dynamic Mass Flow

DRC - Dynamic Reaction Cell

EC - European Commission

ECHA - European Chemicals Agency

EDS - Dispersive X-ray Spectroscopy

ENPs - Engineered Nanoparticles

EOF - Electroosmotic Flow

EU - European Union

EXAFS - X-ray Absorption Fine Structure

FDA - Foods and Drugs Administration

FFF - Field Flow Fractionation

GF AAS - Graphite Furnace Atomic Absorption Spectrometry

HDC - Hydrodynamic Chromatography

HR-SF - High Resolution Sector Field

ICP - Inductively Coupled Plasma

ICP OES - Inductively Coupled Plasma Optical Emission Spectrometry

ICP/MS-MS - ICP-tandem Mass Spectrometry

ICP-MS - Inductively Coupled Plasma Mass Spectrometry

IDA - Isotope Dilution Analysis

ISO - International Organization for Standardization

ISO/TC - International Organization for Standardization - Technical Committee

ISO/TR - International Organization for Standardization - Technical Recommendation

ISO/TS - International Organization for Standardization - Technical Specification

IUPAC - International Union of Pure and Applied Chemistry

KED - Kinetic Energy Discrimination

LA - Laser Ablation

LODs - Limits of Detection

LODsize - Size Limit of Detection

LOQ - Limit of Quantification

MALS - Multi Angle Light Scattering

MNM - Manufactured Nanomaterial

MNPs - Magnetic Nanoparticles

NIST - National Institute of Standards and Technology

NMs - Nanomaterials

NPs - Nanoparticles

NSTC - National Science and Technology Council

NTA - Nanoparticle Tracking Analysis

ORS - Octopole Reaction Cell

PEG - Polyethylene Glycol

PIS - Product Ion Scanning

Q - Quadrupole Mass Analyzer

Q1 - Quadrupole Mass Analyzer 1

Q2 - Quadrupole Mass Analyzer 2

REACH - Registration, Evaluation, Authorization and Restriction of Chemicals

RM - Reference Material

RSC - Royal Society of Chemistry

RSD - Relative Standard Deviation

SAXS - Small-Angle X-ray Scattering

SEC - Size-Exclusion Chromatography

SEM - Scanning Electron Microscopy

SP-ICP-MS - Single Particle Inductively Couple Plasma Mass Spectrometry

SPM - Scanning Probe Microscopy

SQ - Single Quad

SQ - Single Quadrupole

TE- Transport Efficiency

TEM - Transmission Electron Microscopy

TMAH - Tetramethylammonium hydroxide

TOF - Time Of Flight

TRA - Time Resolved Analysis

UK - United Kingdom

US Foresight Institute - United States Foresight Institute

USA - United States of America

USEPA - United States Environmental Protection Agency

UV-Vis - Ultraviolet-Visible Spectrometry

XANES - X-ray Absorption Near Edge Structure

XAS - X-ray absorption spectroscopy

XRD - X-ray Diffraction

XRF- X-Ray Fluorescence

CONTENTS

RESUMEN

El uso de las nanopartículas (NPs) ha incrementado de manera notable su importancia en el ámbito industrial, con el consecuente aumento de su consumo en la última década. Estos materiales poseen propiedades térmicas y ópticas diferentes del material macroscópico (sales o minerales) de misma composición, posibilitando su aplicación en diversas ramas industriales y de investigaciones innovadoras, tales como catálisis, paneles solares, baterías, dispositivos electrónicos, textiles, cosméticos, alimentación y productos farmacéuticos de diagnóstico y terapias antitumorales, moviendo un mercado evaluado en 20 mil millones de euros anuales. No obstante, el impacto generado por estos materiales en el medioambiente y en los seres vivos no se conoce completamente, y su intenso uso ha despertado la preocupación de diversos organismos internacionales en la última década, tales como la Comisión Europea, que han empezado por definir el término "nanomaterial" y sugerir técnicas que pueden ser usadas para su caracterización, complementando las legislaciones europeas de cosméticos y alimentos, en las cuales su control es obligatorio.

En este contexto, son necesarias nuevas metodologías analíticas capaces de caracterizar este tipo de materiales en los más diversos tipos de muestras, proporcionando información respecto a la nanopartícula (tales como la composición elemental, tamaño y sus concentraciones en masa y en número de partícula) de manera rápida y libre de interferencias. Actualmente existe una amplia gama de técnicas capaces de caracterizar nanomateriales, tales como las Microscopías Electrónicas de Transmisión (TEM) y de Barrido (SEM), Análisis de Rastreo de Partículas (PTA), Dispersión Dinámica de la Luz (DLS), Dispersión de Rayos-X a Bajo Ángulo (SAXS) o Espectrometría Ultravioleta-Visible (UV-Vis) , aunque todas ellas presentan diversas limitaciones, como elevados costes (tanto de análisis como de adquisición y mantenimiento de la instrumentación), incompatibilidad con algunos tipos de muestras y altos límites de detección (LOD), bien de tamaño y/o de concentración de nanopartículas.

La Detección Individual de Partículas mediante Plasma de Acoplamiento Inductivo con Detección por Espectrometría de Masas (SP-ICP-MS) es una técnica

emergente para análisis de NPs que supone una alternativa interesante y complementaria a las técnicas anteriores. En este modo de trabajo, una dispersión de nanopartículas altamente diluida se introduce en el ICP-MS y se obtiene una señal transitoria intensidad-tiempo con tiempos de adquisición relativamente cortos (10µs – 10ms), de modo que cada nanopartícula genera un pulso/conjunto de pulsos por encima de la señal de fondo. La intensidad de los pulsos está relacionada con la masa/tamaño de la nanopartícula, mientras que el número de pulsos por unidad de tiempo se relaciona con la concentración (número de nanopartículas por unidad de volumen) de la dispersión analizada. Inicialmente, en la técnica de SP-ICP-MS, se empleaban tiempos de adquisición de datos (td) en un rango de 3 a 10 ms. De esta manera y dado que la señal de una nanopartícula tiene una duración estimada de entre 400-500 µs, se asegura que cada nanopartícula genere un único pulso en el ICP-MS. Sin embargo, en los últimos años, se ha empezado a trabajar con td en la escala de los microsegundos, con posibilidad de llegar hasta 10 µs. De este modo, la señal de cada nanopartícula se obtiene como la integración de distintos pulsos consecutivos en el ICP-MS y se reduce la contribución del blanco a la señal de la misma. Por lo tanto, el uso de tiempos de adquisición en microsegundos mejora la separación entre las distribuciones de fondo y de NPs, posibilitando la caracterización de nanomateriales de menor tamaño.

Aunque la técnica de SP-ICP-MS presente algunas ventajas frente a las técnicas citadas anteriormente, todavía existe la necesidad de desarrollar métodos capaces de proporcionar resultados correctos y precisos cuando se analizan muestras complejas. Así, tal y como ocurre en cualquier otro método basado en el uso del ICP-MS, el desarrollo de métodos para nanopartículas compuestas de elementos afectados por interferencias espectrales con especies presentes en el plasma es uno de los principales desafíos para la técnica. Además, la detección y cuantificación de NPs en matrices complejas, tales como muestras medioambientales y biológicas se presenta como otro gran desafío para el desarrollo de métodos por SP-ICP-MS. Por esta razón, el objetivo de esta tesis doctoral es desarrollar métodos capaces de caracterizar NPs que presentan interferencias espectrales en el plasma, tales como Si y Fe, y explorar estrategias para la caracterización de NPs en matrices complejas.

En la primera parte de esta tesis doctoral (Capítulos 3 y 4), se usa la Celda de Colisión y Reacción (CRC) para la eliminación de interferentes espectrales presentes en el plasma.

En el capítulo 3, se desarrolla un método para la caracterización de SiO2NPs mediante Espectrometría de Masas con Plasma de Acoplamiento Inductivo en configuración Tándem (ICP-MS/MS). Primeramente, se optimizó el método para la determinación de Si libre de interferencias usando He como gas de colisión y H2, NH3, O2 y CH3F como gases de reacción. Los mejores resultados se obtuvieron con H2 (midiendo en la masa del analito – on mass) y CH3F (midiendo a la masa del aducto SiF+ m/z = 44– mass shift). Tras esta optimización, se procedió a la caracterización de SiO2NPs con los métodos desarrollados mediante SP-ICP-MS, utilizando un instrumento cuyo mínimo td era de 3 ms. De nuevo, los menores Limites de Detección de Tamaño (LODsize) se obtuvieron con H2 (on mass) y CH3F (mass shift) como gases de reacción, con valores de 75 y 85, respectivamente. Con estos métodos, pudieron caracterizarse correctamente SiO2NPs de 400, 300, 200 y 100 nm de diámetro nominal. Para la caracterización completa de una distribución de SiO2NPs de 80 nm, fue necesario utilizar una deconvolución de las señales del ruido de fondo y las NPs para una estimación correcta del de las concentraciones de masa y de numero de partícula. Seguidamente, el método desarrollado con H2 como gas de reacción se aplicó en otra instrumentación cuyo menor td era de 100 µs. Con este td se pudieron caracterizar las SiO2NPs de 80 nm directamente, sin la necesidad de usar el método de deconvoluciones desarrollado anteriormente.

Debido a la importancia del uso de la CRC en el desarrollo de métodos capaces de eliminar interferencias espectrales para determinados analitos, en el Capítulo 4 se evaluaron los efectos del uso de esta tecnología en la determinación de NPs mediante SP-ICP-MS. Se evaluó la influencia del tipo de gas utilizado en la CRC, así como el flujo de gas, tamaños y tipos de NPs analizadas. Primeramente, se inició el estudio con NPs de Ag, Au y Pt, utilizando un instrumento ICP-MS tradicional y un espectrómetro de masas ICP en tándem. Estas NPs no están afectadas por interferencias espectrales importantes, por lo que pueden medirse libres de interferencias con o sin CRC, lo que hace posible investigar los efectos del uso de gases de reacción/colisión sobre la señal obtenida. Se demostró que el uso de la tecnología CRC provoca un aumento significativo en el ancho de pico de la señal NP (de 0,5 a 3 ms). Este efecto es más prominente para un gas más pesado (NH3) que para uno más ligero (H2 o He). A un caudal de gas más alto y / o para tamaños de partícula mayores > 100 nm, la duración de la señal de las NP

se prolongó en mayor medida. A continuación, se estudiaron los efectos de la CRC en la determinación de Fe3O4NPs de 50 y 200 nm. Primeramente, se optimizó el método para la determinación de Fe en ICP-MS/MS libre de interferencias utilizando H2 y NH3 como gases de reacción y, seguidamente, se procedió con la caracterización de las Fe3O4NPs. En este caso, el uso de NH3 induce un ensanchamiento de pico muy significativo en comparación con el observado cuando se usa H2 (6.10 ± 1.60 frente a 0.94 ± 0.49 ms). Esta extensión del tiempo de detección de la partícula puede atribuirse a las colisiones / interacciones de la nube de iones con el gas de reacción. En general, el efecto de ensanchamiento de la duración de las señales de NPs es más pronunciado para partículas mayores. Para minimizar este efecto, se recomiendan gases ligeros y caudales de gas bajos.

En la segunda parte de esta tesis doctoral (Capítulos 5 y 6), se exploran estrategias para la determinación de AgNPs en matrices complejas, tal como la compatibilización de la matriz de la curva de calibración iónica (Capítulo 5) y Análisis por Dilución isotópica (Capitulo 6). En el Capítulo 5, se procedió con la caracterización de AgNPs extraídas de muestras de tejidos biológicos y sangre con una solución de Hidróxido de Tetrametilamonio (TMAH). En este estudio, se caracterizaron AgNPs de 40 y 75 nm y se midieron curvas de calibrado iónicas preparadas en 3 matrices distintas: 1% HNO3, 1 mM de citrato de sodio y 2.5% TMAH + 0.1% Triton X-100. Los resultados muestran que, con la compatibilización de la matriz de la calibración iónica, se obtienen tamaños de partícula más próximos a los valores de referencia determinados por TEM y proporcionados por el fabricante. Además, se aplicaron testes estadísticos para comprobar que los resultados de los diámetros obtenidos para cada curva de calibración eran diferentes entre ellos. De acuerdo con estos testes, los tamaños de NPs obtenidos (para ambas nanopartículas) en la matriz 2.5% TMAH + 0.1% Triton X-100 son estadísticamente distintos de los tamaños de NPs obtenidos con las otras dos curvas de calibración.

Otra estrategia comúnmente usada para determinación elemental en matrices complejas es la dilución isotópica (IDA), para lo que se requiere que puedan medirse al menos dos isótopos del analito de interés libres de interferencias. La aplicación de la IDA al análisis mediante SP-ICP-MS no es directa. En los ICP-MS equipados con un

cuadrupolo como separador de masas, las medidas de masas diferentes se hacen de manera secuencial y con tiempos de ciclo excesivamente largos como para medir las relaciones isotópicas de Ag para una sola NP. Sin embargo, los analizadores de masas de tiempo de vuelo (TOF), son capaces de registrar todo el espectro de masas (quasi) simultáneamente a una velocidad rápida (cada 30 μs para los instrumentos modernos). De esta manera, se pueden medir relaciones isotópicas de Ag para cada NP y, en consecuencia, se posibilita el uso de IDA. En el Capítulo 6, se desarrolla un método basado en IDA para la determinación del tamaño de partícula de muestras de AgNPs de 75 nm dispersas en 1 mM de citrato de sodio mediante el uso de un ICP-TOF-MS. Para el desarrollo de este método de análisis fue necesario realizar adaptaciones para aplicar la ecuación general IDA al análisis de SP. En este sentido se incluyó la eficiencia de transporte y del td en la ecuación. Además, se realizó un estudio sistemático sobre el efecto de diferentes parámetros en la precisión alcanzada para el análisis: parámetros instrumentales (modo de adquisición de datos y tiempo de integración), optimización de la concentración del patrón isotópico de dopaje y tratamiento de datos (corrección de eventos divididos y cálculo de la masa de la NP). Con el método optimizado se procedió a la caracterización de una muestra de AgNPs de 75 nm de diámetro nominal, obteniéndose valores satisfactorios de diámetro, concentración en número de partículas y concentración en masa. El método optimizado presentó resultados prometedores para la caracterización de AgNPs en matrices complejas por el método IDA.

CHAPTER 1

Introduction

1.1. Nanotechnology, nanomaterials and nanoparticles – definitions, uses and regulations

1.1.1. Nanotechnology: historic background and definition

Nanotechnology has become very important in the scientific community and industry over the past 20 years, being the vanguard technology for many discoveries in this century.[1] Nanotechnology had its initial step in 1959, with a lecture at the annual American Physical Society meeting at Caltech by the Physics Nobel Laureate Richard Feynman called "There's Plenty of Room at the Bottom", where he advocated for the manufacturing of really small things at an atom-by-atom scale. The term nanotechnology was first used in 1974 by Norio Taniguchi from the University of Tokyo, who spoke about improving the engineering precision of machines and finishing materials. In 1981, K. E. Drexler described a new approach called "bottom-up" (assembling objects from individual atoms), instead of using the approach "top-down" (manufacturing small objects from bulk materials), using the ideas previously described by Feynman and Taniguchi. In 1986, Drexler released the book "*Engines of Creation"* and the term nanotechnology was finally popularized.[2,3]

As with all the new emerging technologies, the definition of nanotechnology has been refined over the years as more scientific research groups started to dedicate their studies on the subject. Until 1999, the definition of nanotechnology encompassed terms such as size, ultra-precision engineering and ultra-dispersions. After consultation of experts from 20 different countries, the National Science and Technology Council (NSTC) adopted the new definition of nanotechnology from the National Science Foundation workshop.[4] Nowadays, the definitions by the International Organization for Standardization (ISO) and the United States Foresight Institute (US Foresight Institute) are widely used. [3,4] These definitions are gathered in Table 1.1.

Table 1.1. Nanotechnology definitions according to different international agencies / reports

Agency / Reports	Nanotechnology Definition
Nanotechnology Research Directions, 1999 (NSTC)	"Nanotechnology is the ability to control and restructure the matter at the atomic and molecular levels in the range of approximately 1–100 nm and exploiting the distinct properties and phenomena at that scale as compared to those associated with single atoms or molecules or bulk behavior. The aim is to create materials, devices, and systems with fundamentally new properties and functions by engineering their small structure."[4]
International Organization for Standardization - Technical Committee (ISO – TC)/229	"1. Understanding and control of matter and processes at the nanoscale, typically, but not exclusively, below 100 nanometers in one or more dimensions where the onset of size-dependent phenomena usually enables novel applications. 2. Utilizing the properties of nanoscale materials that differ from the properties of individual atoms, molecules, and bulk matter, to create improved materials, devices, and systems that exploit these new properties."[5]
US Foresight Institute	"Nanotechnology is a group of emerging technologies in which the structure of matter is controlled at the nanometer scale, the scale of small numbers of atoms, to produce novel materials and devices that have useful and unique properties." [6]

Other usual terms related to nanotechnology are:

- Nanobiotechnology: application of nanotechnology to biological sciences.
- Nanoscience: the science underlying nanotechnology.
- Nanoscale: scale that comprises the nanometer scale (10^{-9} m) – International Union of Pure and Applied Chemistry (IUPAC) definition.[7]
- Nanomaterials: the subject of study of nanotechnology.

In this thesis, characterization of nanomaterials and, in particular, of nanoparticles will be considered and hence, some further clarifications on this issue will be provided in the following sections.

1.1.2. Nanomaterials and nanoparticles: towards a technical definition

Nanomaterials (NMs) are the subject of study of nanotechnology. According to the International Organization for Standardization - Technical Recommendation (ISO/TR) 18401[8], a *nanomaterial* is defined as a "material with any external dimension in the nanoscale or having an internal structure or surface structure in the nanoscale". This normative also defines the term *manufactured nanomaterial* (MNM) as a "nanomaterial intentionally produced to have selected properties or composition". Regarding the term *nanoscale*, the same normative defines it as "length range approximately from 1 nm to 100 nm".

In another ISO document, the technical specification (TS) ISO/TS-80004-2,[9] NMs are divided into two main groups: nanoobjects and nanostructured materials (See Figure 1.1 for more details). Nano-objects are in turn divided into three categories that take into account the number of (outer) dimensions in the nanoscale range (size range from 1 to 100 nm):[10–12]

(i) nanoplates: 1 dimension in the nanoscale range with the other 2 dimensions significantly larger.

(ii) nanofibers: 2 dimensions in the nanoscale range with the other dimensions significantly larger.

(iii) nanoparticles: all the dimensions are in the nanoscale range.

Nanoparticles (NPs) are the subject of study of this thesis. The ISO definition presented is similar to the IUPAC definition, that states that a nanoparticle (NP) is a "particle of any shape with dimensions in the 1×10^{-9} and 1×10^{-7} m range", in other words, the dimensions of a NP are in the range between 1 and 100 nm.[13]

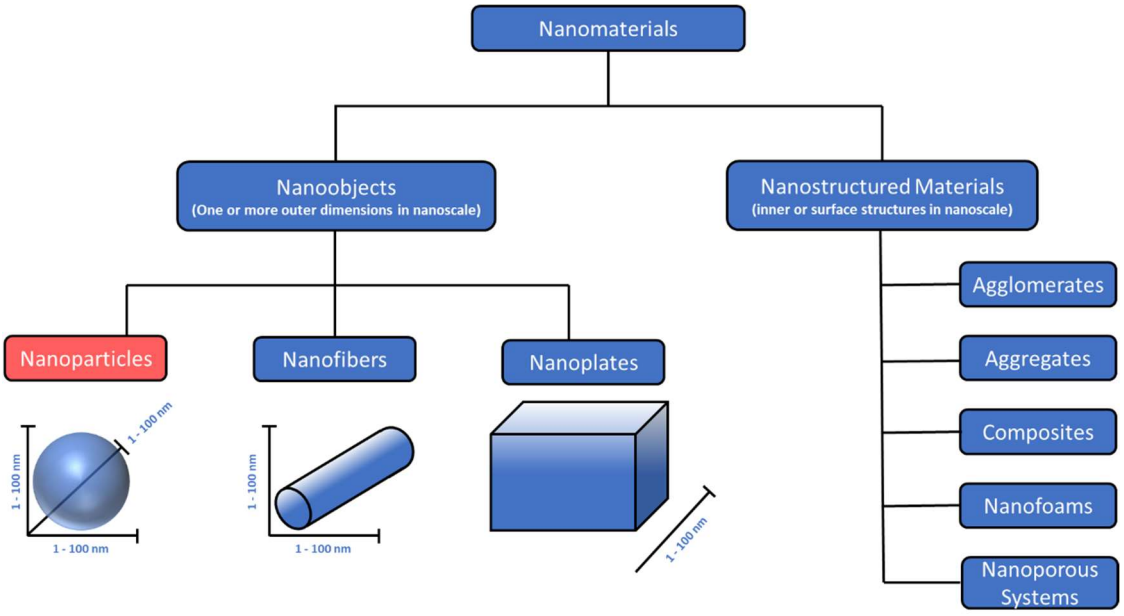

Figure 1.1. ISO classification of nanomaterials. Adapted with permission of John Wiley and Sons (License number: 4985260499083) from Krug & Wick.[12]

1.1.3. Nanoparticles: uses and impact

Although NMs have always been present in nature, as they are formed by natural processes in the environment and the biosphere,[14] the development of nanotechnology over the past 20 years and the increased importance of NMs in the industry, has generated a rise in consumption for this type of material. As an estimation, the use of NMs (NPs included) generated a world market that in 2013 was valued at US$ 22.9 billion and was expected to reach US$ 64.2 billion by 2019.[15] Among the different types of NMs, NPs play an important role in research and industry. Manufactured nanoparticles, also called engineered nanoparticles (ENPs), show physicochemical properties different from the bulk material of the same composition, such as unique thermic and optic properties or colloidal stability. These properties result from their high surface-to-volume ratio, which increases the reactivity at the molecular level. Furthermore, the NPs are largely used as catalysts and, due to their small size, they improve antibacterial properties of the bulk material.[16,17] These characteristics enable innovative industrial applications in different fields, such as electronics, textiles, cosmetics, food industry, pharmaceutical products, biomedicine, agriculture, cancer diagnosis, antitumoral therapies and many others.[10,14] In this context, the main types of NPs that are produced worldwide are:[14]

- Metallic: Ag, Au, Zn, Cu, Fe
- Metal oxides: TiO_2, Fe_2O_3, SiO_2, CeO_2, Al_2O_3, MnO_2
- Metal Sulfides: CuS, ZnS
- Nonmetallic: quantum dots (semiconductor nanocrystals that exhibit quantum mechanical properties),[18] graphene oxides
- Lipids: soybean, lecithin, stearic acid
- Polymers: alginate, chitosan, cellulose derivatives

The intense use of NPs and their subsequent disposal in the environment has increased exposure to this type of material. The concern about the effects on the environment and on human health is continuously rising, as NPs can cross biological barriers that other species cannot, thus introducing new types of hazards.[19,20] Exposure to NPs can occur by contact through direct ingestion of products containing ENPs or through the contaminated environment.[21] The most common emission routes to the environment are manufacturing processes, disposal (intentional or unintentional), sewage treatment, waste incineration, landfill and recycling processes.[22] As of present, the effects of NPs on the environment are not completely known and more information such as toxicity and environmental impact need further study. Thus, ENPs can be considered as emerging contaminants, in other words, pollutants that have only been investigated for the last 20 years due to the lack of availability of analytical methods that are able to detect their trace levels in environmental samples before.[23]

1.1.4. Nanomaterials: current regulations

In this scenario of a crescent NMs disposal, international governments, industries and standard agencies started to release instructive recommendations over the past decade in order to (i) define the term *nanomaterial* and (ii) guide the control and regulation concerning NMs.[24] Even though this work is focused on nanoparticle analysis, the term nanomaterial will be widely cited in this section as the international organizations do not refer specifically to NPs in their normative. However, as cited in

section 1.1.2., NPs are a specific type of NMs and, therefore, those recommendations are also applicable to nanoparticles.

Table 1.2. summarizes the definitions of the term nanomaterial for regulatory purposes by the main agencies around the world.[24,25] It is worth to point out that these definitions also take into account the ISO definitions for nanomaterials included in section 1.1.2.

Table 1.2. Definitions of nanomaterial for regulatory purposes by different agencies around the world.

Country/Region	Agency	Definition
European Union (EU)	European Commission (EC)	"Natural, incidental or manufactured material containing particles, in an unbound state or as an aggregate or as an agglomerate and where, for 50 % or more of the particles in the number size distribution, one or more external dimensions is in the size range 1 nm-100 nm. In specific cases and where warranted by concerns for the environment, health, safety or competitiveness the number size distribution threshold of 50 % may be replaced by a threshold between 1 and 50 %".[26]
Australia	Australian Industrial Chemical Introduction Scheme (AICIS)	"Nanoscale means the particle size range of 1 to 100nm. Your introduction is a 'specified class of introduction' if it is of a chemical that: • is introduced as a solid or is in a dispersion and • consists of particles in an unbound state or as an aggregate or agglomerate, at least 50% (by number size distribution) of which have at least one external dimension in the nanoscale."[27]

Canada	Health Canada	"a) It is at or within the nanoscale in at least one spatial dimension. b) It is smaller or larger than the nanoscale in all spatial dimensions and exhibits one or more nanoscale phenomena."[28]
United States of America (USA)	United States Environmental Protection Agency (USEPA)	No proper definition, but regulates the control of "solids at 25 °C and standard atmospheric pressure; that are manufactured or processed in a form where any particles, including aggregates and agglomerates, are in the size range of 1–100 nm in at least one dimension; and that are manufactured or processed to exhibit one or more unique and novel properties."[29]
	United States Food and Drug Administration (FDA)	FDA states that did not define nanomaterial, but considers nanomaterials as "materials that have at least one dimension in the size range of approximately 1 nm to 100 nm"[30]

As seen from table 1.2 and as reported in the study by Boverhof *et al.*,[24] which reviews 14 different recommendations, the particle size is the only common parameter in all recommendations, with the upper size limit varying according to the normative.[24] The concept of number size distribution is included in some of these definitions, pointing at the importance of measuring this parameter for control and regulatory purposes. However, many recommendations are not clear regarding to which parameters and methods of analysis should be used for NMs characterization. In the European context, the European Commission released in 2012 a report called *Requirements on Measurements for the Implementation of the European Commission Definition of the Term "Nanomaterial"*,[31] which describes several concepts on nanoscience that are presented in the cited European Recommendation. Furthermore, this report also details NMs sampling and sample preparation, requirements for measuring particle size and particle size distribution and analytical techniques that may be used for NMs characterization (the analytical techniques used for NMs and NPs characterization will be described in section 1.2.2.).

Besides these specific recommendations, several regulations exist in the EU that apply to NMs although not being specifically devoted to them. The Regulation EC No 1907/2006 concerning Registration, Evaluation, Authorization and Restriction of Chemicals (REACH), for example, does not mention NMs, but it is applied to chemical substances of any form and configuration. Thus, NMs are covered by the REACH regulation.[32,33] In order to fulfill the REACH requirements, the European Chemicals Agency (ECHA) has published a guidance document for information requirements and chemical safety assessment according to the REACH regulation.[34] This document comprises information such as physicochemical properties, toxicology characteristics and risk assessment, which lies on the European Recommendation for NMs.[32] Another specific regulations for NMs in cosmetics, agricultural, food and feed also exist in the UE.[32,33]

In conclusion, although great efforts are being made for understanding the physico-chemical properties of NMs, their behavior on the environment and their effects on human health, regulations regarding the control and disposal of these materials do not seem to be sufficiently clear in an international context. One of the reasons behind this circumstance might be the need for further improvements on analytical metrology and nanotoxicology that would enable new specific regulations on the subject to be proposed.[33]

1.2. Analytical Nanoscience and Nanotechnology and Analytical Metrology for Nanomaterials

1.2.1. Analytical Nanoscience and Nanotechnology - definition

As previously described, there is no doubt of the growing importance of nanotechnology on novel technological applications and in the quality of life of the general population with the use of nanomaterial-based products.[35] These impacts have also reached the Analytical Sciences (in which Analytical Chemistry plays a crucial role), creating a new field of study known as *Analytical Nanoscience and Nanotechnology* (AN&N).[36] In 2014, López-Lorente & Valcárcel[37] published a book chapter defining the two classical facets of AN&N and the "third way of AN&N", which idea was further

enforced by the same authors in a review article published in 2016.[35] Summarizing, the 3 approaches of the AN&N are (Figure 1.2.):[35,37]

1. **Nanomaterials as analytes in any type of samples**, such as cosmetics, environmental and clinical matrices. The number of AN&N studies dedicated to this approach ranges from 30 to 35%. Particularly, this thesis will explore this dimension of AN&N with the determination of different types of NPs in different sample matrices.
2. **Nanomaterials used as tools** in analytical processes (e.g., sensors, sorbents, electrical conductors, extractions, etc.) in order to improve an analytical method by exploiting the unique physicochemical properties of NMs. About 65 to 70% of the AN&N published works report the use of NMs as tools for analytical methods.
3. **Nanomaterials as analyte and tool in the same method** (third way of AN&N). The aim of this approach is to classify new current and future methods that might appear accompanying the development of nanotechnology. One example of the application of this approach lies in an analyte that at the same type improves the precision, sensitivity and selectivity of the method, in other words, this analyte is also a tool for improving the figures of merit of a certain method.

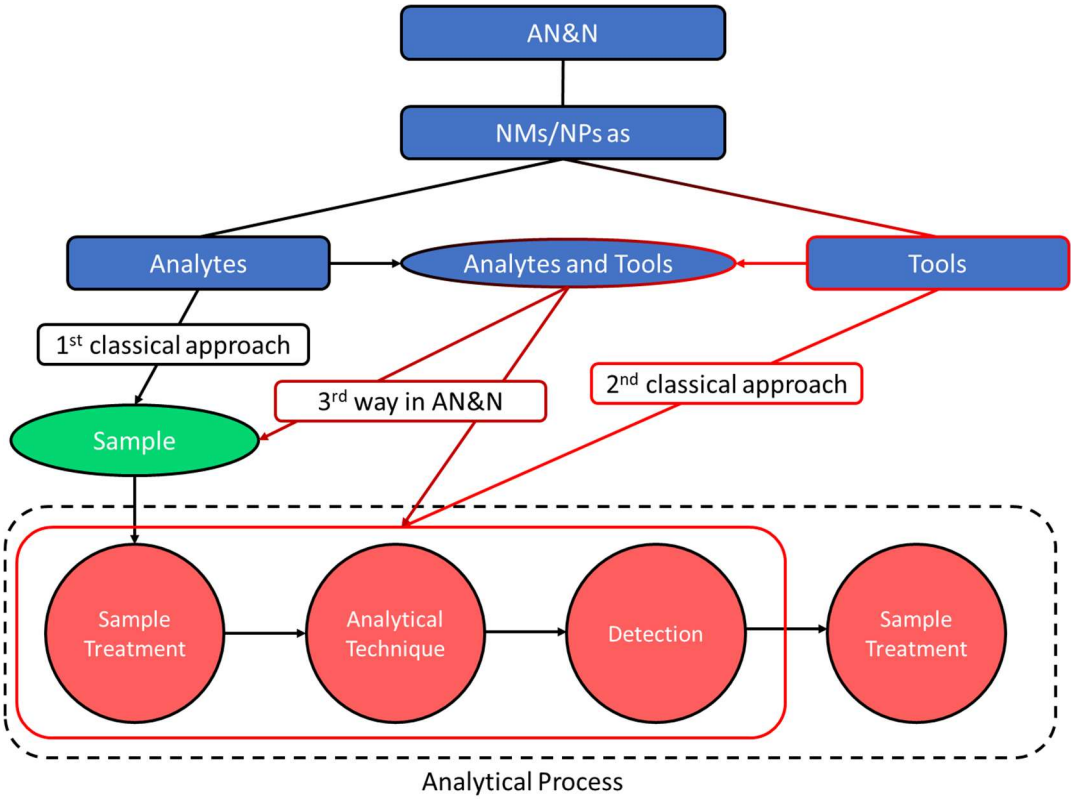

Figure 1.2. The 3 approaches of the AN&N according to the role played by NPs/NMs in the analytical process. Adapted with permission of Elsevier (License number: 4985260998655) from López-Lorente & Valcárcel.[35]

The use of NMs as tools, especially NPs, is the most developed field in AN&N, thanks to the new advances in nanotechnology and nanoscience. In fact, the current demand of NMs and NPs characterization is a direct consequence of the rising use of these materials. Besides this approach, and according to López-Lorente and Valcárcel, the main AN&N aspects that should be addressed in the near future are:[37]

1. Impact of NMs in the environment and human health.
2. Need for homogenous, pure and well-characterized NPs.
3. Development of different aspects of nanometrology.
4. Development of different aspects of nanomedicine, such as nanosystems (e.g. carbon nanotubes used as electrodes, or SiO_2NPs as replacements for conventional silica tips)[38] or nanostructured pharmaceuticals.

This thesis will try to create some knowledge regarding point 3: nanometrology.

1.2.2. Analytical Metrology for Nanomaterials - Nanometrology

As previously mentioned, nanometrology is one of the aspects of AN&N that needs further development from analytical chemists. Nanometrology is the discipline that standardizes physical measurements of materials at the nanometric scale,[20] in other words, is "the science of measurement at a nanoscale level".[37] Recently, the concept of Analytical Metrology for Nanomaterials (AMNM) was introduced in order to apply the principles of metrology science (as traceability and uncertainty) to the analysis of nanomaterials. In this regard, it is necessary to develop the key metrology parameters for reliable measurements in nanoanalysis, such as Certified Reference Materials (CRM), statistical calculations and standard methods.[33]

Both characterization and determination of NPs are subjects of study of AMNM. When speaking about NP characterization, NPs are the samples. Characterization is normally carried out for quality control purposes and/or use of the NP in a particular type of application just after their characterization. The complete characterization of NPs may be very time consuming and expensive, so the relevant information needed may vary according to the objective of the study. Nevertheless, there is a consensus in the scientific community that an accurate NMs characterization is a crucial step to assess their potential toxicological effects in environment and to the human health.[39]

On the other hand, determination refers to the application of an analytical method where the NPs are the analytes in a certain sample or matrix. Determination of NPs are frequently used as screening methods for obtaining rapid estimations in certain circumstances.[33]

There are eight main parameters usually measured by analytical techniques for NP characterization/determination: average size, size distribution, agglomeration, shape, structure, composition, surface and particle number concentration (Figure 1.3).[40]

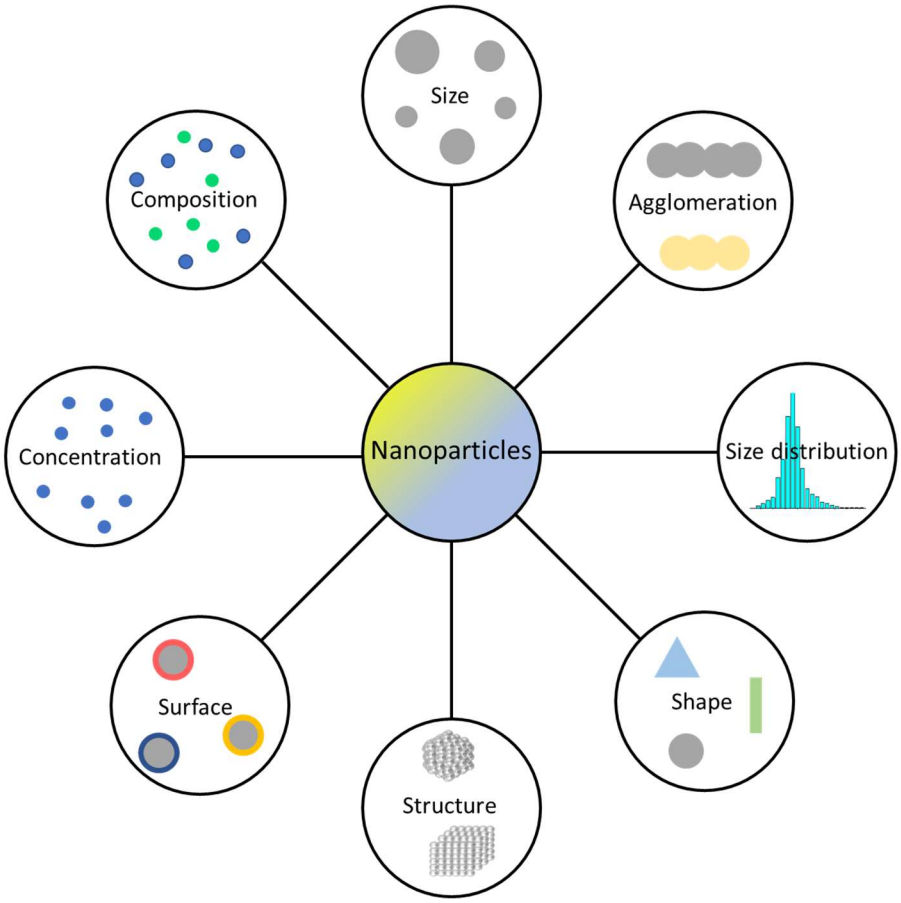

Figure 1.3. The 8 main physicochemical characteristics of NPs measured by analytical techniques. Adapted with permission of Elsevier (License number: 4985261257025) from Soriano *et al*.[40]

The analytical techniques deployed for gathering all this information can be grouped in 3 categories:[31,40,41]

1. **Counting methods:** methods that are used for counting and quantification purposes, providing the information particle by particle. In those methods, a large number of individual NPs has to be measured in order to guarantee a good representativity of the sample.
2. **Ensemble methods:** methods that are only capable of measuring a large number of particles at the same time (not individual NPs).
3. **Separation (fractionation) methods**: methods that separate the NPs present in a sample by one critical characteristic, such as size, surface or density. Coupling to other analytical technique providing a signal is necessary for analysis. Chromatographic techniques are mostly used for this purpose. Regarding these separation techniques, it is important to point out that they are usually coupled

to different detection techniques, such as Ultraviolet-Visible Spectrometry (UV-Vis), Multi Angle Light Scattering (MALS) and Atomic Spectrometry (AS) techniques. The AS techniques are not specific for nanoparticle characterization, but they offer advantages for NP characterization when coupled with a separation technique, such as low Limits of Detection (LODs) (μg L^{-1} to ng L^{-1}) and elemental specificity.[42] The main AS used for this purpose are:

- X-ray Absorption Spectroscopy (XAS): when X-rays are absorbed by atoms, the electron's binding energy is maximized generating a characteristic X-ray absorption spectrum. There are two types of XAS: X-ray Absorption Near Edge Structure (XANES), that provides information such as geometry and oxidation state, and extended X-ray Absorption Fine Structure (EXAFS), that provides the element coordination.[42,43]
- Graphite Furnace Atomic Absorption Spectrometry (GF AAS): in GF AAS, the atomization process occurs inside of a graphite furnace that can reach temperatures up to 2600°C, suitable for analysis of solids and few μL of liquid samples.[44] It has been demonstrated that ionic solutions have lower atomization delay than NPs at the same temperature, enabling the visualization of different species in the GF AAS. [45,46]
- Inductively Coupled Plasma (ICP) based techniques: Inductively Coupled Plasma Optical Emission Spectrometry (ICP OES) and Inductively Coupled Plasma Mass Spectrometry (ICP-MS) are normally coupled to separation techniques providing LODs at the μg L^{-1} and ng L^{-1} levels, respectively. Those techniques are used mainly to give the mass concentration information.[17,42]

Table 1.3. summarizes the most frequently used techniques for NP characterization/determination with their respective characteristics.

Table 1.3. Analytical techniques deployed for NP characterization/determination.

Technique	Fundamentals	Information provided	Benefits and Limitations
Counting Methods			
Transmission Electron Microscopy (TEM)[20,33,42,47,48]	• A beam of electrons is directed to the sample (under vacuum). After electron-sample interaction, transmitted electrons originate an image with sub-nanoscale resolution	• Size range: > 1 nm • Provides information on NP size, aggregation state and morphology.	✓ Can be coupled with X-ray techniques, such as Dispersive X-ray Spectroscopy (EDS), in order to obtain elemental information. ✓ Provides amplified images of the NMs structure × Sample preparation needed (deposition on sampling grids) × Time-consuming analysis × Measurement of, at least, a thousand of NPs to guarantee the representativity × Relatively small spatial resolution × The electron-beam can damage the NPs (depending on their nature)
Scanning Electron Microscopy (SEM)[20,33,47,48]	• A beam of electrons is directed to the sample (under vacuum). After electron-sample interaction, reflected electrons originate an image of the sample surface with sub-nanoscale resolution	• Size range: > 5 nm • Provides information on NP size and morphology	✓ Can be coupled with X-ray techniques, such as EDS, in order to obtain elemental information. ✓ Provides amplified images of the NMs structure × Sample preparation needed (deposition on sampling grids) × Destructive and time-consuming analysis × Measurement of, at least, a thousand NPs to guarantee the representativity × Relatively small spatial resolution × Unable to image non-conductive samples

Atomic Force Microscopy (AFM)[33,41,49–51]	• AFM is a type of Scanning Probe Microscopy (SPM), based on near-field interactions between a scanning tip and a sample, generating images • Analysis performed in ambient air and with liquid dispersions	• Provides size, morphology and surface texture and roughness information • Size range: 1 nm to 8 µm	✓ Capable of imaging almost all types of surfaces, including non-conductive samples ✓ Requires less laboratory space and is simpler to operate than TEM and SEM ✓ Requires less sample preparation than TEM and SEM × The geometry of the tip is very critical at the nanoscale and it must be very well characterized prior to NP analysis × Limited scan speed
Nanoparticle Tracking Analysis (NTA)[31,41,52]	• NTA combines a Charge-Coupled Device camera (CCD) with the laser light scattering microscopy, visualizing the individual nanoparticles, that moves under a Brownian motion • The movement and the NP size are related in the Stokes-Einstein Equation	• Standard method for particle number concentration, being capable of detecting NPs at concentrations up to 10^6 particles/mL • Size distributions range: 10 nm – 2 µm	✓ Possibility of measuring a large number of NPs ✓ Avoid NP changes during the analysis × Unable to analyze NPs in powder/solid form × The liquid used in the suspension needs to have known viscosity and be optically transparent and non-fluorescent at the wavelength of the equipment's laser source × Does not distinguish agglomerates and aggregates from NPs × The hydrodynamic diameter is calculated, which can differ from diameters determined by other techniques such as TEM and SEM

Single Particle Inductively Couple Plasma Mass Spectrometry (SP-ICP-MS)[40,42]	This methodology uses commercial ICP-MS in Time Resolved Analysis (TRA) mode at a very high data acquisition rates, in order to detect NPs as individual events over a continuous background baseline	• Elemental Composition • Provides Particle Number Concentration at very low limits (10^6 part L^{-1}) • Size limits of detection (LODsize) around 10 nm, depending on the NP • Provides the particle mass and elemental mass concentration (LOD ~ ng L^{-1})	✓ High mass sensitivity (ng L^{-1}) ✓ Very low particle number concentration limits (10^6 part L^{-1}) ✓ Fast analysis and suitable for screening purposes × Unable to determine the NP shape × Normally used only for liquid suspensions × Susceptible to sample matrix effects × Susceptible to ICP-MS spectral interferences × Requires NP CRMs for calibration
Ensemble Methods			
Dynamic Light Scattering (DLS)[31,41,53,54]	In this technique, the particles suspended in a liquid solvent undergo Brownian motion, scattering off the light from the particle suspension	• Provides information on size and size distribution • Size distributions range: 1 nm – 2 µm	✓ Good method for narrow size distributions ✓ Important for toxicological studies: analyzes the sample in the exposure media × Particle size is influenced by the presence of dust or agglomerates × Dispersion stability should be guaranteed × As NTA technique, hydrodynamic diameter is calculated and are greater than those provided by other techniques like TEM and SEM × Tendency of particles to aggregation during the measurements
X-ray Diffraction (XRD)[31,41]	Technique based on Bragg's law, which relates the lattice spacing with the angles when X-rays scatters from a crystalline material	• Size range: 1 – 100 nm • Determines the average size of a NP	✓ Non-destructive technique ✓ Used for crystalline structures ✓ Well-stablished technique × Only analyzes suspensions with a very high concentration of NPs × Not suitable for particle size distribution × Limited to crystalline particles

Small-Angle X-ray Scattering (SAXS)[31,41]	This technique is based on measuring at very low angles (0.05 - 5°) the X-rays scattered from a particle surface	• Provides particle size distributions and NP shape information • Size range: 1 – 100 nm	✓ Fast measurements × Unable to analyze NPs in powder/solid form × Not applicable to powders due to the particle-by-particle interaction × Size and size distributions are obtained only for relatively monodisperse NPs
X-Ray Fluorescence (XRF)[55–57]	High energy X-rays are used to excite the sample and generate X-ray fluorescence radiation. The radiation energies are specific for each element and the intensities are proportional to its concentration	• Provide images of the distribution of major, minor and trace elements • Provides mass concentration with LODs ~ µg L^{-1}	✓ Nondestructive analysis ✓ Multielemental technique ✓ Low sample preparation required × High LODs when compared with atomic spectroscopy detection techniques × Contamination in the sample surface may interfere with the results
Separation Methods			
Field Flow Fractionation (FFF):[31,33,40–42]	• FFF separates components of a sample by the action of an external field that is applied perpendicularly to a flow located inside of an empty, thin and long channel. • Separates particles in function of their hydrodynamic size	• Separates particles in the size range of separation: 2 nm – 100 µm • Offers the possibility of off-line collection for further analysis	✓ Well suited for polydisperse NP samples ✓ Minimum sample perturbation during the analysis ✓ The capability of coupling with different types of detectors makes FFF a very versatile technique × Reliable measurements only if the particles have the same behavior than the standards × Quantification depends on the detection method selected × Number of samples that can be analyzed by one run is limited by the buildup of the particles at the FFF channel × Careful sample preparation is needed in order to remove very large particles

Capillary Electrophoresis (CE)[41,42,58]	• CE separations are based on measuring the electrophoretic mobility of charged species (surface coating in the case of NPs) in an Electroosmotic Flow (EOF) inside of a thin capillary. • The EOF is generated by the application of a high voltage in the electrolyte located inside of the capillary. • Charged species migrate towards to the cathode and are separated on the base of their charge, shape and molecular weight	• Separates particles larger than 5 nm • Good characterization of surface functionalization and particle shape	✓ Minimum number of samples and chemicals are required ✓ Fast analysis with minimum generation of wastes ✓ Possibility of separation of NPs with similar surface-charge densities × Poor sensitivity when coupled with photometric detectors, one of the most used with CE × Requires high NP number concentration × NP surface may cause different surfactant-surface interaction and lead to different migration behaviors
Hydrodynamic Chromatography (HDC) and Size-Exclusion Chromatography (SEC)[18,31,41,42]	• Both are liquid chromatography techniques. Packed non-porous beads (HDC) or porous particles of different sizes ranging from 3 to 20 µm (SEC) are used for separation. • In both techniques larger species elute before smaller species	• Separation range sizes: HDC: 30 nm – 60 µm SEC: 1 nm - 2 µm	✓ Useful to separate NPs from other components (e.g. ionic analytic, other NPs types and molecules) present in the sample ✓ Rapid and easy handling method ✓ Can be used to obtain a fingerprint of the particle size distribution × NPs may adsorb in the column packing material, leading to a biased calibration and non-quantitative results × Requires well-characterized standards for calibration

As derived from information on Table 1.3, there is not a single analytical technique that can provide all the relevant information on NPs. All have their advantages and limitations and provide valuable information for different situations, although some are more popular than others. Out of these techniques, SP-ICP-MS is an emerging technique that has gained a lot of prominence over the past ten years in the analytical

community due to the advantages summarized on Table 1.3. Since its first introduction in 1993, there have been many improvements but there are still many aspects that need further attention so that the technique can be considered as well established for NP characterization/determination. In the following section, an overview of the technique history and evolution will be given, as well as the critical points of this technique that still need to be addressed by the analytical community.

1.3. Single Particle Inductively Coupled Plasma Mass Spectrometry (SP-ICP-MS)

1.3.1. Technique principles and historic development

In single particle mode, the ICP-MS is operated in time-resolved analysis (TRA) mode with very short integration (or dwell) times (in the range of a few milliseconds to a hundred microseconds), in which it is capable to perform particle-by-particle analysis. In this mode of operation, highly diluted NP dispersions are used so that NPs are individually introduced in the ICP-MS. Under these conditions, NP signals can be detected and counted as individual pulses (or an integration of a set of consecutive pulses) over a continuous background signal. Particle size and particle number density can be calculated based on the intensity of these pulses and their frequency, respectively, while both are used to provide mass concentration.[59–61]

Figure 1.4 shows the evolution of the number of articles published on SP-ICP-MS over the past decade. As seen from this figure, the interest of the analytical community in SP-ICP-MS has grown exponentially during this period, although measurement of single particles by atomic spectroscopy methods is not new. First publications on this subject date from 1968, where a flame spectrophotometer was used for studies on particle atomization processes on NaCl particles.[62–64] Single particle detection by plasma-based techniques was first developed in 1986 for the measurement of airborne particles by means of ICP OES.[65] In 1993 the use of mass spectrometry for the same purpose was reported for the first time.[66] In this study, Zn and Pb determination at femtogram levels was carried out in individual airborne particles with direct air introduction.

However, the first studies on SP-ICP-MS technique as it is currently known appeared in a series of papers published between 2003 and 2006 by Degueldre and collaborators, where they demonstrated the feasibility of the ICP-MS in single particle detection mode for analysis of colloids.[67–70] In these works, a single pulse above the instrumental background was related to a single colloidal particle, and hence the theoretical background for the technique was set.

Few years later, different research groups around the world started a series of fundamental studies that launched the interest on the SP-ICP-MS technique. In 2011, Laborda *et al.*[71] applied the single particle detection mode for the determination of silver nanoparticles (AgNPs) in a dispersion where also dissolved ionic silver was present. In this work, parameters such as the influence of dwell time and particle concentration on AgNPs detection, particle diameter and number concentration calculation were studied. The authors also characterized signal profiles for ionic silver and AgNPs in order to define a signal threshold for identification of NPs over the continuous background given by silver ions. Also in 2011, Pace *et al*.[59] published a work describing 3 different methods for determining the nebulization efficiency (later on referred as transport efficiency (TE) in the SP-ICP-MS literature) and presented a guide to count and measure particle diameters by means of SP-ICP-MS. In 2012, Olesik and Gray[62] studied some critical parameters for the characterization/determination of NPs by SP-ICP-MS, such as residence time of a NP in the plasma, adjustment of dilution for ensuring single particle conditions, the correct choice of dwell time for data acquisition and determination of particle number and analyte mass detection limits.

Thanks to the rising interest on NPs analysis by this new approach, the first review paper on SP-ICP-MS was published in 2014 by Laborda *et al*.[60] Also in 2014, Montaño *et al.*[61] developed a software for data collection that enabled the instrumental settling time elimination and data collection with dwell times at the microsecond range, changing the way that SP-ICP-MS used to be performed: from the detection of a single pulse to the detection and integration of a set of pulses above the instrumental background. This new approach improved the limits of detection achievable by this technique. Since this advantage was demonstrated, commercial ICP-MS instruments were improved accordingly so that the most recent works on SP-ICP-MS are performed with microsecond dwell times.

From this date on, many researchers focused their efforts on exploiting SP-ICP-MS as a routine technique for NP characterization/determination. In 2015, Peters *et al.*[72] developed an Excel based spreadsheet for straightforward NP characterization and determination. In 2016 Montaño *et al.*[73] published a tutorial review covering all the technique fundamentals (taking into account the recent advances in terms of microsecond detection) and discussing the remaining challenges for the SP-ICP-MS technique to become a routine analysis tool. Finally, Montoro Bustos *et al.*[74] carried out in 2018 a study for validation of NPs size and number concentration in routine analysis by SP-ICP-MS.

At the moment, many papers on applications of SP-ICP-MS for characterization/determination of NPs in different matrices are being published, while fundamental research addressing the remaining challenges for this technique and/or taking advantage of new instrumental developments is still carried out.[75–82]. The fundamentals, data processing main advantages and remaining challenges of this technique will be analyzed in more detail in the next section.

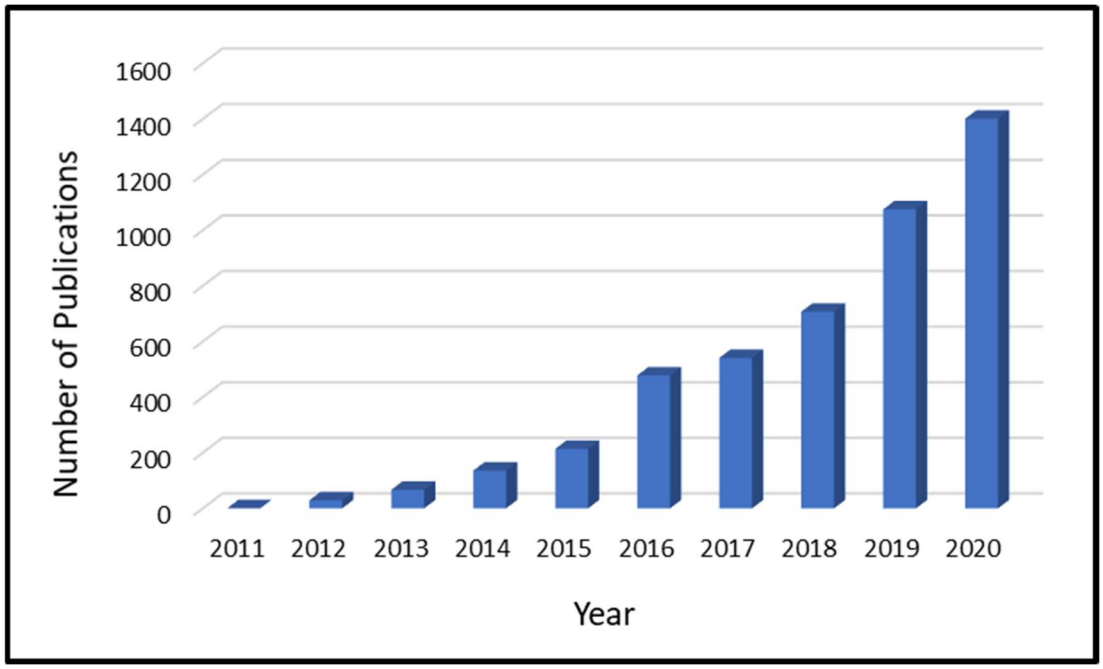

Figure 1.4. Evolution of number of articles published on SP-ICP-MS during the period 2011-2020. The two most common abbreviations for the technique found in the literature (SP-ICP-MS and spICP-MS) were used as searching routine in Web of Science. Since 2011, a total number of 4649 articles on SP-ICP-MS were found.
*The Web of Science data was updated on January 5th, 2021.

1.3.2. Fundamental principle of SP-ICP-MS and preliminary considerations

The fundamental principle of SP-ICP-MS is based on the possibility to detect each NP as an intense pulse of ions over a continuous background, which is given by instrumental noise plus the signal for any dissolved material present in the dispersion measured (Fig. 1.5). Under the single particle mode of operation, the intensity of the pulses can be related to the size of the NPs, while the frequency of the pulses detected over the background can be related to the particle number concentration in the dispersion measured.

As previously mentioned, in SP the ICP-MS is operated in TRA mode with very short dwell times (t_d). Additionally, for the most frequently used sequential ICP-MS instruments, detection is performed for only one element at a time, so that the settling time for the spectrometer can be eliminated. The purpose of all these measures is collecting as many points per time unit as possible to be able to characterize the transient signal given by a NP.

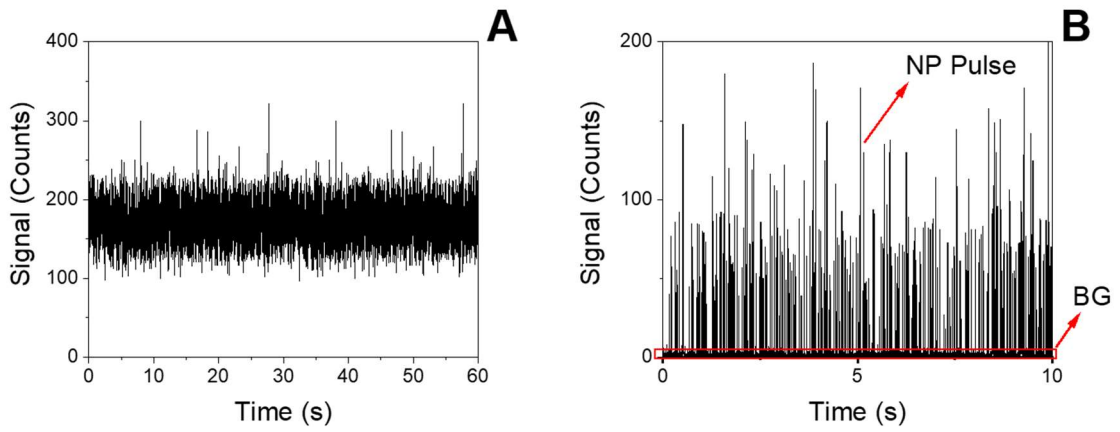

Figure 1.5. Generic example of (A) Ionic and (B) NP signals distribution over time of measurement (s) obtained by means ICP-MS in the TRA mode.

Working in the single particle mode of operation requires close control of the three following parameters, in order to obtain accurate results:[59]

(i) **Dwell time**: In 2012, Olesik & Gray[62] determined for the first time the signal duration of a 1 µm diameter SiO_2 particle, which was estimated to be

approximately 400 µs. Nowadays, it is accepted that the residence time of the ionic cloud generated by the atomization of the elements present in a single NP shows a duration ranging from 300 to 500 µs, depending on the NP.[73] In the beginnings of the SP-ICP-MS technique, the ICP-MS instrumentation available presented a fundamental limitation on the dwell times available for measurement, which could only start at 1 ms in best cases. These relatively long dwell times were not sufficient to fully characterize the transient signal generated by a NP, and dwell times had to be optimized to provide one signal pulse per NP. In this regard, the potential appearance for the following errors in the NP counting and diameter determination needed to be addressed (Figure 1.6)[73,83]:

- Appearance of double events for longer dwell times (generally above 5 ms): two or more NPs counted as a single NP. For a given dwell time, the probability for this error to happen can be minimized by reducing the NP dispersion number concentration[62] (see point iii below), although at the cost of longer analysis times.
- Split events for shorter dwell times (1 – 3 ms): the pulse of a single NP is split into two different events. The probability for this error to occur depends on the dwell time selected and increases with decreasing dwell times.

As a general rule, dwell times between 3-10 ms were used for NP determination with this type of instrumentation.

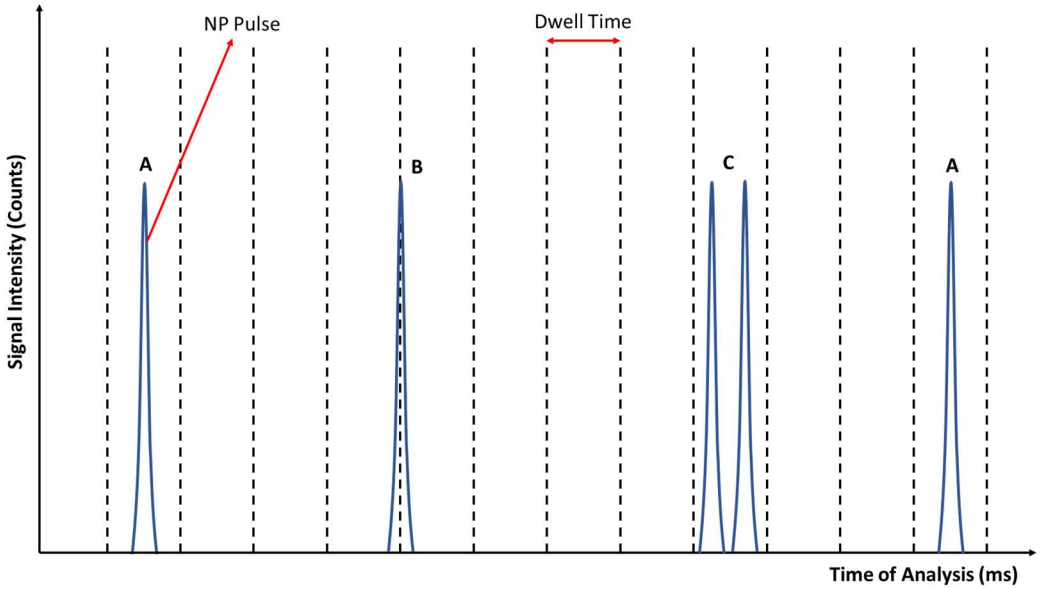

Figure 1.6. Generic example of NP signal detection with a dwell time in the millisecond range (1 – 20 ms). The following three possible situations are represented: (A) single pulse acquisition (B) Split event and (C) Counting of 2 NPs as one (double events).

From 2014, ICP-MS instruments with quadrupole analyzers were improved and dwell times in the microsecond range (10 – 500 µs) were made available. With the use of dwell times in the microsecond range, the NP signal is compounded by consecutive events above the background (Figure 1.7). These events have to be identified and integrated in order to obtain a single pulse intensity for a single NP.[73] With this strategy, there are no split events and the probability for detecting two or more NPs as a single NP is drastically reduced so that lower dilutions can be measured thus reducing the total analysis time. The use of ultrashort dwell times also decreases the background intensity measured together with the NP, improving the LODsize for NPs in the presence of dissolved ionic species in solution and/or polyatomic interferences generated in the plasma.[84] Currently, most SP-ICP-MS measurements are performed with dwell times in the range of 50-100 µs.[84,85]

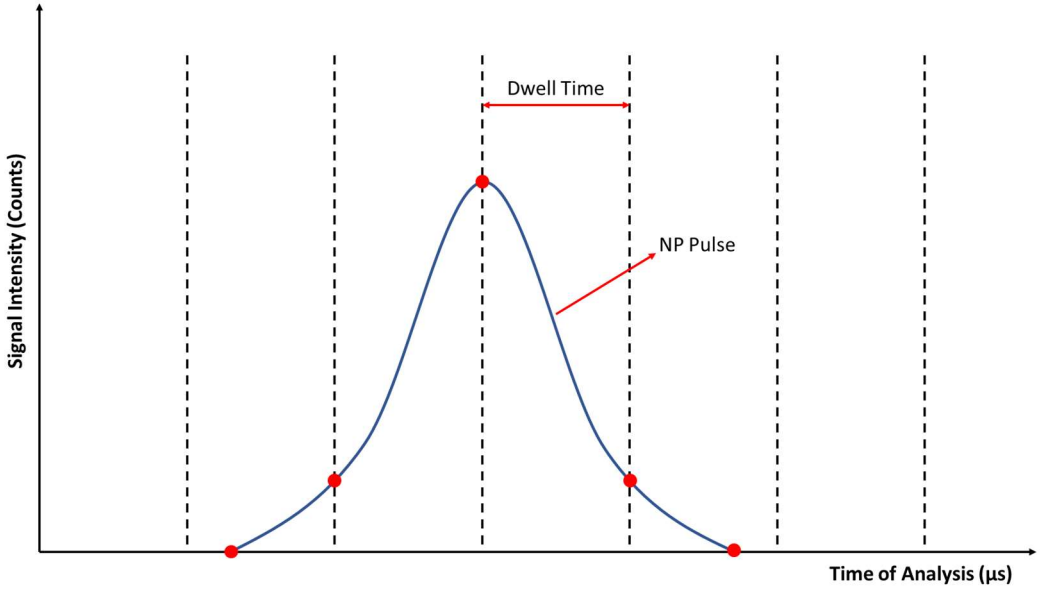

Figure 1.7. Generic example of NP signal detection with a dwell time in the microsecond range (50 – 500 µs). In order to obtain the full NP signal, the intensity represented by the red dotted points should be integrated and the result is the total signal pulse intensity.

(ii) **Sample flow rate to ICP-MS:** When a NP dispersion is measured in SP-ICP-MS, and once the pulse or set of pulses of NPs are collected, particle frequency is related to the dispersion particle number concentration, and pulse intensity is related to particle mass and size, provided that parameters such as density and shape are known/supposed for the NPs. Both parameters rely on maintenance of a constant flow rate of the dispersion to the ICP-MS instrument, that must be carefully measured on a daily basis for single particle analysis. The number concentration of NPs in solution can be calculated following Equation 1.1:[59]

$$N_p = \frac{f}{q\,\eta_n} \quad \textbf{(1.1)}$$

Where Np is the particle number concentration (part L^{-1}), f is the particle frequency (Hz), η_n is the TE and q is the sample flow rate to the ICP-MS ($L\ s^{-1}$). Calculation of the particle mass from the pulse intensity will be discussed in detail in section 1.3.3.2.

(iii) **Sample particle number concentration:** The particle number concentration of the measured sample plays a critical role on the quality of SP-ICP-MS measurements. As indicated in point (i) above, the frequency of the detected NPs (or the particle flux of NPs entering the plasma) should be limited in order to avoid the overlapping of NPs pulses (double events). As pointed out by Olesik & Grey,[62] Poisson statistics can be used to estimate the probability of more than one NP arriving simultaneously to the detector during one dwell time. The probability P_x of the signals from x nanoparticles to be detected simultaneously during the dwell time can be calculated according to equation 1.2:

$$P(x) = \frac{\lambda^x}{x!} e^{-\lambda} \quad \textbf{(1.2)}$$

Where x is the number of particles and λ is the nanoparticle detection frequency (NPs s^{-1}) multiplied by the dwell time (s). In the case of dwell times in the microsecond range, the time to be considered for the probability calculation is the residence time of a NP in the plasma (approximately 0.5 ms). Self-evidently, minimizing this probability is crucial for avoiding biases on the determination of NP number concentrations and hence, samples sufficiently diluted providing low detection frequencies (around 15 Hz for 3 ms) have to be measured. However, a sufficiently high number of NPs has to be measured to minimize the random error affecting counting events, which leads to the necessity of increasing the total analysis time for determining particle number concentrations with SP-ICP-MS or selecting compromise conditions for the measurements.

In this regard, Laborda *et al*.[86] presented 2 equations that govern the NP bias and the relative standard deviation when counting NPs with SP-ICP-MS as a function of the flux of NPs entering the plasma. If more than one NP are counted as one singe NP, this generates a negative bias on the number concentration. Assuming that only double events (2 NPs counted as one) are significant, the bias of the particle number ($bias_{NP}$) is given by equation 1.3.

$$bias_{NP} = \frac{t_d}{2} Q_{NP} \quad \textbf{(1.3)}$$

Where t_d is the dwell time (s) and Q_{NP} is the NP flux entering in the plasma (NPs s^{-1}). When working with dwell times in the microsecond range, the t_d is replaced by the width (w_{peak}) of the peak,[84] that, as previously cited, should be around 500 µs.

On the other hand, the random error when counting NPs is also governed by Poisson statistics and can be estimated from the total number of NPs counted. The relative standard deviation of the number of NPs (rsd_{NP}) is given by Equation 1.4:

$$rsd_{NP} = \frac{1}{\sqrt{t_i\, Q_{NP}}} \quad \textbf{(1.4)}$$

Where t_i is the total acquisition time (s) and Q_{NP} is the NP flux entering the plasma (NPs s^{-1}). Figure 1.8 presents the plots $bias_{NP}$ *vs* Q_{NP} and rsd_{NP} *vs* Q_{NP}: as seen from these plots, the relative bias increases linearly with Q_{NP}, whereas the rsd_{NP} decreases with the squared root of Q_{NP}. For a given dwell time (t_d) and total analysis time (t_i), the optimum Q_{NP} providing the lower $bias_{NP}$ and rsd_{NP} is obtained at the intersection of both curves.

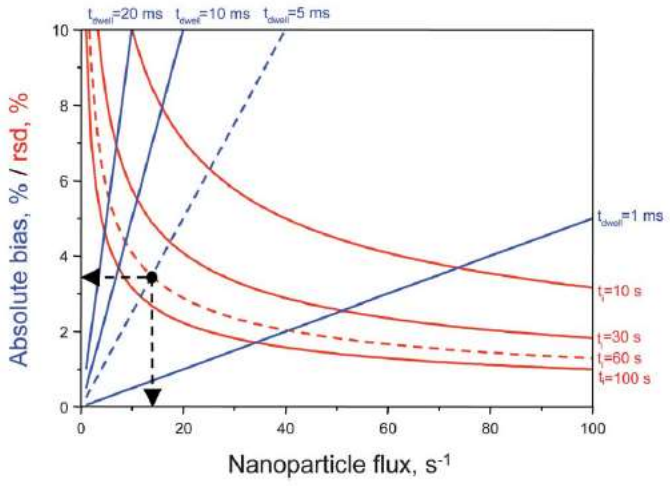

Figure 1.8. Plot of absolute bias/rsd versus Nanoparticle flux. The intersection point of both curves shows the optimum nanoparticle flux and the respective absolute bias. Reproduced with permission of Springer (License number: 4982450176798) from Abad *et al.*[84] (https://doi.org/10.1007/s00216-016-9515-y).

Laborda *et al*.[71] studied the effect of the coincidence of multiple NP pulses in the size distribution of a 113 nm AgNPs monodisperse suspension with dwell times in the millisecond range (Figure 1.9A) and Abad-Alvaro *et al*.[84] studied the detection of multiple NP pulses in the size distribution of a 60 nm AuNPs monodisperse suspension with dwell times in microsecond range (Figure 1.9B) (The conversion of pulse intensity to NP size will be discussed in more detail in section 1.3.3.2). Generally speaking, the presence of "multiple events" leads to additional peak distributions to the right of the main NP distribution. These additional peaks refer to the sum of two or three NP masses, that leads to a biased NP diameter of the overall NP size distribution if taken into account. Signal deconvolution might be used to eliminate this bias if detected after the measurements have been carried out.

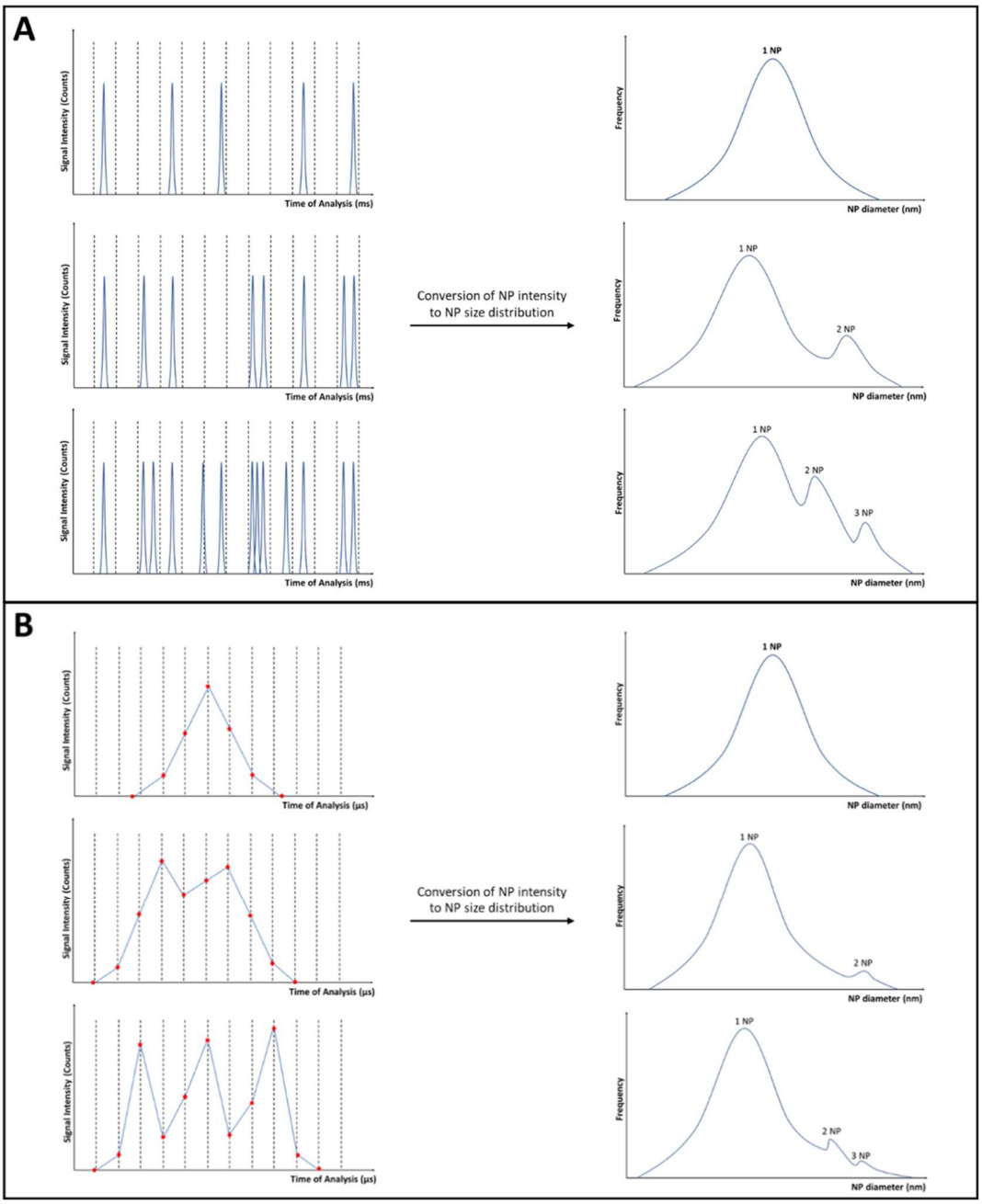

Figure 1.9. Effect of the detection of 1, 2 or 3 NPs as a single NP signal (A) with dwell times in the millisecond range and (B) with dwell times in the microsecond range. Adapted with permission of RSC (https://doi.org/10.1039/C0JA00098A) from Laborda *et al.*[71] and with permission of Springer (License number: 4982450176798) from Abad-Álvaro *et al.*[84] (https://doi.org/10.1007/s00216-016-9515-y).

1.3.3. Analysis protocol for SP-ICP-MS: Calibration

Analogously to all methods developed by means of ICP-MS, analysis by SP-ICP-MS also requires calibration against adequate standards to obtain quantitative results. Quantitative results that can be obtained with this technique are: the particle number concentration for a suspension, the size of individual nanoparticles (and hence the particle size distribution) and the total particle mass concentration as a combination of both the particle number concentration and the particle size distribution. Different approaches are used for calibration of each of these parameters.

For SP-ICP-MS, size calibration approaches must consider the transport of NPs into the plasma and equate correctly the intensity of each detected pulse with the analyte mass.[73] Currently, there are two main size calibration approaches for NP analysis by means SP-ICP-MS:

(i) Use of NP standards with known size: this calibration approach uses NP standard dispersions of the analyte of interest at different particle sizes to measure a calibration curve correlating the average signal intensity recorded vs. the average particle diameter for the dispersion. In this way, a direct relationship between diameter and instrumental response can be obtained. Even though this calibration approach is the most direct to determine the NP sizes of an unknown NP dispersion, the scarce availability of NP standard dispersions of different (monodisperse) sizes restricts the use of this calibration approach to a few elements, such as Au and Ag nanoparticles.[73]

(ii) Determination of Transport Efficiency (TE) and Ionic Calibration: this approach consists in carrying out an external mass-flux ionic calibration that takes into consideration the TE of the NP into the instrumentation. This is the method most commonly used in the SP-ICP-MS literature[60,73,87] and was chosen for all applications presented in this work. Details on this protocol are given in the following paragraphs.

1.3.3.1 Transport Efficiency (TE): definition and methods of determination

The Transport Efficiency (TE) is defined as the ratio between the number of particles (or analyte) detected and the number of particles (or analyte) aspirated. The TE affects the flux of NPs that reach the plasma (and hence the frequency at which NP are detected) but does not affect the pulse intensity recorded for each NP, that only depends on the NP size. *Pace et al*.[59] described 3 different methods to determine the TE and compared their performances:

Particle Frequency Method: this is the most frequently used method for determining the TE in SP-ICP-MS analysis. It consists in counting the NPs that arrive at the detector (frequency in pulses/s) and relate it to the total number of NPs that was introduced in the instrument via nebulization. The NP dispersion introduced into the nebulizer at a certain (known) constant sample flow rate must have a well-known number concentration. The rate of particles entering the plasma are detected by the instrumentation, whereas the number of aspirated particles depends on the suspension number concentration and the selected sample flow rate (the determination of the ideal particle number concentration of the NP dispersion to be introduced into the ICP-MS for avoiding biased results was described in section 1.3.2.). Finally, the TE is obtained using Equation 1.5:

$$\eta_n = \frac{f}{q\, N_p} \quad (1.5)$$

Where η_n is the TE (%), f is the frequency for the detected NPs (s^{-1} or Hz), q is the sample flow rate (mL min^{-1} or L s^{-1}) and N_p is the particle number concentration of the standard NP suspension (part L^{-1} or part L^{-1}). Usually, reference Au and Ag NPs from the National Institute of Standards and Technology (NIST) are used for this purpose due to its certified values and long-term stability.[88,89] Theoretically, this method can be used for any type

of NPs, even for those containing different analytes from the CRM used for TE calibration.

Particle Size Method: in this method, two calibration curves are created: (i) one using monodisperse NP suspensions of known size for the analyte of interest, for which the most frequent intensity is related to the most frequent (known) particle size and (ii) one using ionic solutions of the analyte of interest. Considering that TE should be the same for both the NP dispersions and the ionic solutions, and the fact that the intensity for each NP signal is not affected by the TE as it is the ionic solution, the ratio between the slope of the ionic calibration curve and the NPs calibration curve is equal to the TE (Equation 1.6).[59,73] The main limitation of this method is the scarce availability of monodisperse standard NP dispersions of different sizes for the same analyte.

$$\eta_n = \frac{Slope_{diss}}{Slope_{NP}} \textbf{ (1.6)}$$

Where η_n is the TE (%), $slope_{diss}$ is the slope of the ionic calibration curve and $slope_{NP}$ is the slope of the NP calibration curve.

Waste collection method: this method consists in weighting the volume of sample taken by the nebulizer and the volume of sample wasted at the exit of the spray chamber. The TE (η_n) is then indirectly determined by calculating the ratio between the difference of the total weight of the sample uptake and sample waste systems (including vials, tubing and solutions), Δtotal weight, before and after 60 s of analysis and the total aspirated sample volume (difference of the weight of the sample vial in the beginning and in the end of the 60 s analysis), Δsample weight (Equation 1.7).[59]

$$\eta_n = \frac{\Delta total\ weigh}{\Delta sample\ weight} \textbf{ (1.7)}$$

Even though this technique does not require the use of NP dispersions, the reported TE results are normally overestimated, which is attributed to the sensitivity of the indirect methods to small recovery losses. The waste method collection was revisited by *Cuello-Nuñez et.al*.[90] using what they called the Dynamic Mass Flow (DMF) approach. In this method, the mass flow of the sample reaching the plasma is measured using a vial where both sampling and waste tubings are located (Figure 1.10A). On the other hand, the mass flow of the sample uptake is measured using a vial containing the sample uptake tubing only (Figure 1.10B). Those vials are located on a balance that controls the weight while all the system works. A curve weight (g) vs. time (min) is obtained for both mass flows, and the TE (η) is calculated by dividing the slope of the flow of the sample reaching the plasma by the slope of the mass flow sample uptake. With this system, very good agreement between the TE determined by this method and the particle number concentration method results were compared with the particle frequency method by NTA analysis, with good agreement of the number concentration values.

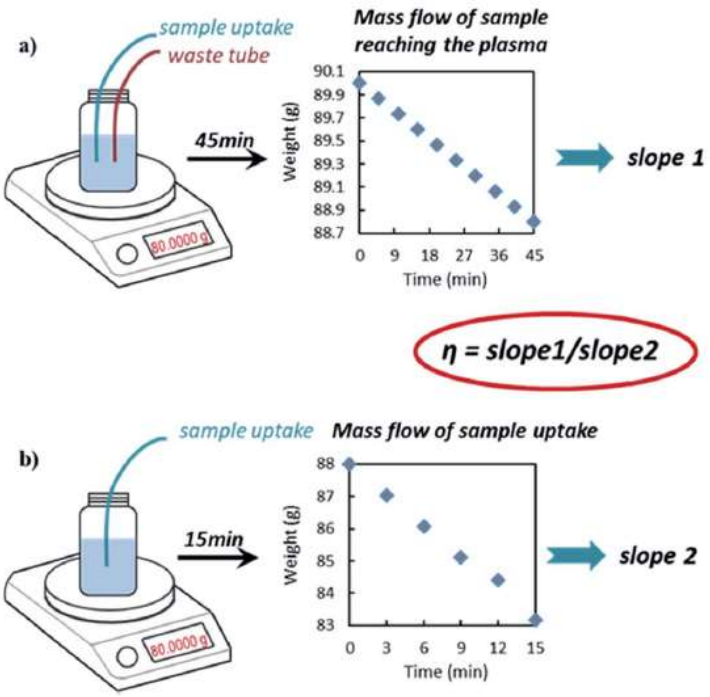

Figure 1.10. Schematic representation of the TE calculation by DMF approach. (A): determination of the mass flow of the sample reaching the plasma. (B) Determination of the mass flow of the sample uptake. This figure is reproduced with permission of Royal Society of Chemistry (RSC) from Cuello-Nuñez *et al*.[90] (https://doi.org/10.1039/C9JA00415G).

1.3.3.2. Determination of the mass-flux curve from dissolved ionic standards

After determining the TE, the next step is to measure the ionic calibration curve with the same analyte of the NPs of interest. The response curve for any ICP-MS measurement shows the instrumentation response (cps or counts) vs. concentration (or mass). The same type of curve is obtained for SP-ICP-MS. However, in this case, the NP mass is measured by event (per dwell time). Considering that the NPs in solution undergo complete ionization, it is reasonable to assume that, once in the plasma, the ions from an ionic solution will behave similarly from the ions of the NPs.[59] Therefore, the sensitivity obtained with the delivered mass from the ionic standard solution per event can be used to determine the mass of analyte generating the NP pulse. Equation 1.8 relates the ionic mass obtained per event with the concentration of the ionic standard:

$$W = \eta_n \, q \, t_d \, C \quad \textbf{(1.8)}$$

Where w is the mass per event, η_n is the TE (%), q is the sample flow (mL min^{-1} or L s^{-1}), t_d is the dwell time (ms or µs) and C the concentration of the ionic standard solution (µg L^{-1}). Applying this equation for all the ionic standards, a mass-flux is obtained for pulse intensity quantification (Figure 1.11). This calibration curve can be used to directly determine the mass of a NP generating a pulse of a given intensity. If density and shape for the NPs are known, the NP size can be subsequently derived.

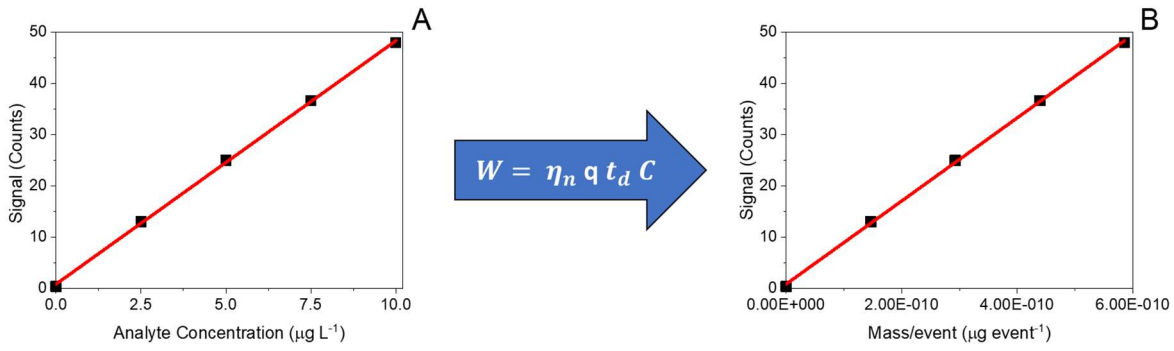

Figure 1.11: (A) Ionic Calibration Curve and (B) Mass-flux calibration curve after applying the Equation 3 to the calibration curve. Adapted with permission from Pace et al.[59] Copyright (2021) American Chemical Society.

1.3.4. Analysis protocol for SP-ICP-MS: Data acquisition, processing and treatment

As previously mentioned, NP signals are recorded as pulses: basically a set of intense signals above the background signal for the analyte of interest.[73] In contrast, if a ionic solution is analyzed in the TRA mode, a steady signal well above the background level will be observed. Prior to calculation of the particle mass for a given NP, it is necessary to differentiate the signal obtained from the NPs from the continuous background signal (caused by instrument noise and/or dissolved species).[73] Firstly, all the data acquired in the TRA mode (signal intensity versus time, Fig. 1.12A) is rearranged to obtain a graph signal frequency (commonly referred as just frequency) versus signal intensity (Fig. 1.12B). If there are NPs present in the analyzed sample, 2 different distributions will be found: the first one is the background signal distribution that follows a Poisson distribution,[71] whereas the second distribution is the NP distribution. As most detected events are coming from the Background (BG), normalization of the plot frequency vs. signal is normally carried out to observe both BG and NP distributions at the same time (Fig. 1.12C)

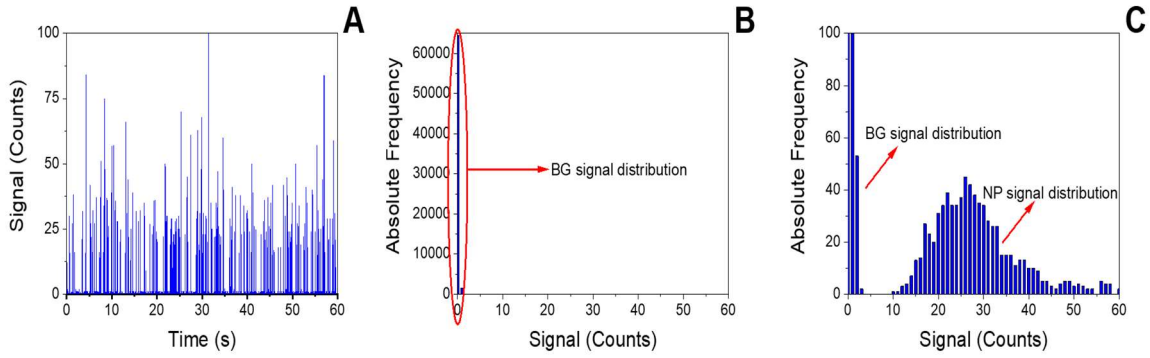

Figure 1.12: (A) Acquisition of NPs pulses by TRA mode (B) Plot of absolute frequency versus signal intensity with the data acquired on (A), where it is possible to observe the real dimension of the background distribution (C) Re-scaling from (B) graph by normalization, where it is possible to observe both BG and NP distribution

Once the plot presented in Fig. 1.12C is obtained, the most used strategy to differentiate the BG and NP distributions is an iterative approach in which a threshold value is determined and all the signals above this value are identified as NPs. In the first step of the iterative process, all data points (for both distributions) are averaged and all

data above a given threshold (usually three or five times the standard deviation, 3σ or 5σ) are excluded from the distribution. The remaining data are averaged again and, repeatedly, every data point above the 3σ/5σ threshold is excluded. This process ends when there is no data above the 3σ/5σ threshold left. Other threshold detection criteria, such as 7σ and 10σ have been also used in order to avoid the occurrence of false positives and improve the separation between the background and the NP distributions.[91] This method works properly for relatively large NPs, providing intensities well above the background level; for smaller NPs or suspensions with high dissolved content, however, it turns very difficult to differentiate both distributions. In such cases, deconvolution methods using a polygaussian probability function has been successfully applied.[92]

Different spreadsheets and guidelines to perform data treatment in SP-ICP-MS are available in the literature. In this thesis, a spreadsheet created by *Peters et al.*[72] was adapted for all parameters obtained by SP-ICP-MS calculations. This spreadsheet is composed of two interrelated worksheets. The first worksheet is used for calibration of the TE and, in the second worksheet, particle number concentration, mass concentration and particle size distribution are calculated for each sample by means of the response factor determined using a set of ionic standard solutions adapted to the type of NP analyzed. Taking into consideration that every single NP has 100% of ionization efficiency, the transformation of the peak intensity to NP mass is obtained following Equation 1.9:

$$M_P = \frac{I_{NP} - I_{BG}}{X_a\, m} \quad (1.9)$$

Where M_p is the particle mass (fg), I_{NP} is the intensity of the NP pulse (counts event^{-1}), I_{BG} is the average intensity of the background (counts event^{-1}), X_a is the mass fraction of the analyte in the NP distribution of the sample and m is the slope obtained in the mass-flux calibration curve (counts/µg event^{-1}).

To transform particle mass into size values (one of the most important parameters in NP characterization), knowledge on the particle geometry is needed. For

most frequently analyzed NPs, the assumption of spherical geometry for the NP is normally made and, hence, the diameter can be obtained by the using Equation (1.10):

$$D_{NP} = \sqrt[3]{\frac{6M_p}{\rho\,\pi}} \quad (1.10)$$

Where D_{NP} is the NP diameter (nm), M_p is the particle mass (fg) and ρ the particle density (g mL^{-1}) (normally the density of the bulk material is used although deviations from these values can be expected in some instances).[83] It is important to highlight that particles of any geometry can be analyzed by SP-ICP-MS. However, information on particle geometry is needed in order to apply Equation 1.10 (or any adaptation for other geometries).

As for particle number concentration, rearranging Equation 1.5, the number concentration of a NP dispersion can be obtained as indicated in Equation 1.1, presented in section 1.3.2.

All the NP analysis steps previously described are summarized in Figure 1.13.

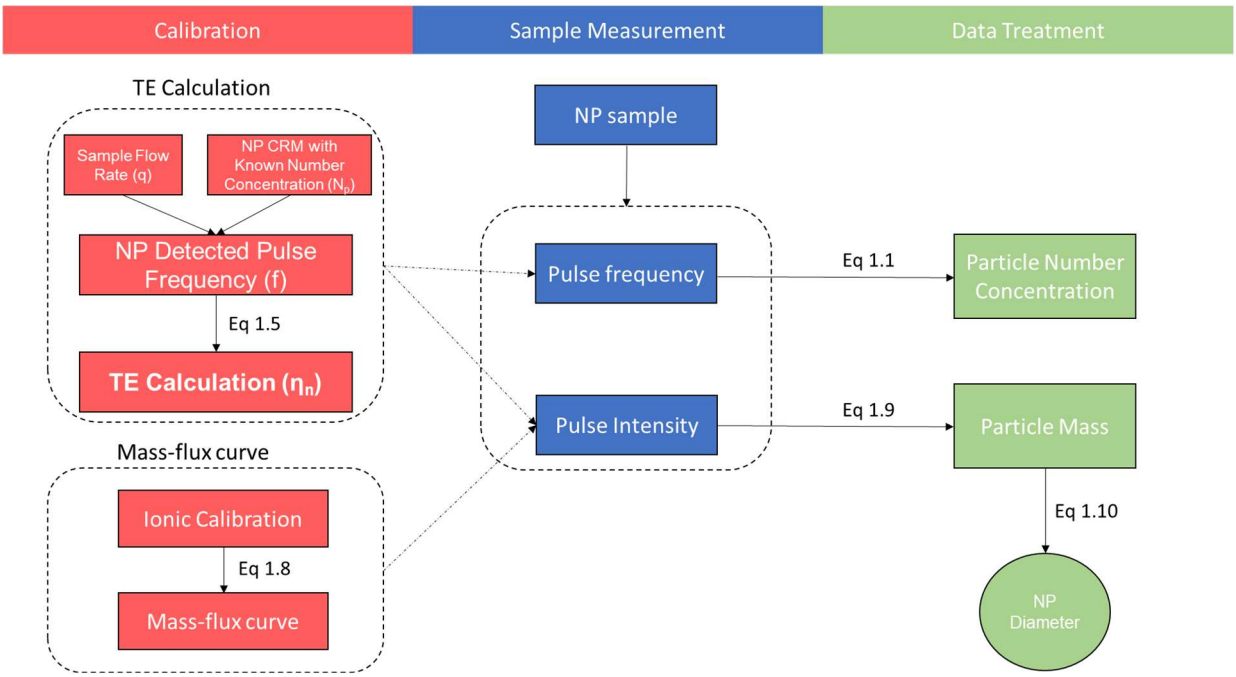

Figure 1.13: Main steps of NP characterization by SP-ICP-MS.

1.3.5. SP-ICP-MS: figures of merit, limitations and pending challenges

As previously discussed, SP-ICP-MS current applications mostly focused on various fields where NPs determination in different matrices is needed (e.g. ecotoxicology, etc.).[79] However, recent advances are also guiding the technique into the metrological area, mainly for the validation of the particle size and number concentrations, thus complementing electronic microscopy techniques.[74] In this regard, the technique capabilities are mostly instrumentally limited. Figures of merit for SP-ICP-MS are generally reported as particle number concentration and particle size limits of detection, which can be defined according to equations 1.11 and 1.12, respectively:[60]

$$LOD_{NP} = \frac{3}{\eta_n \, q \, t_i} \quad \textbf{(1.11)}$$

$$LOD_{size} = \left(\frac{18 s_B}{\pi \rho X_{NP} K_{ICPMS} K_M}\right)^{1/3} \quad \textbf{(1.12)}$$

Where η_n is the TE (%), q is the sample flow (mL min^{-1} or L s^{-1}), t_d is the dwell time (ms or µs), s_B is the standard deviation of the continuous background, ρ is the density of the NPs (g cm^{-3}), X_{NP} is the mass fraction of the element monitored in the NP, K_{ICPMS} is the detection efficiency (ratio of the number of ions detected *vs* the number of atoms introduced into the ICP) and K_M can be calculated as AN_{AV}/M_M where A is the atomic abundance of the isotope measured, N_{AV} the Avogadro number, and M_M the atomic mass of the analyte M. The product $K_{ICPMS}K_M$, on the other hand, can be calculated by Equation 1.13:[93]

$$K_{ICPMS} \, K_M = \frac{R}{\eta_n \, q \, C \, t_d} \quad \textbf{(1.13)}$$

Where R is the signal intensity (counts) of an ionic solution with mass concentration C (µg L^{-1}).

Equation 1.12 shows that LOD_{size} depends basically on the detection efficiency of the ICPMS (K_{ICPMS}), which mostly depends on the instrument. In fact, development of more efficient instrumental designs increasing transmission of ions to the detector would improve size detection limits achievable for SP-ICP-MS. With current instrumentation and for metallic NPs free from spectral interferences in the ICPMS, LODsize in the range of 10 nm can be achieved.[73,94] For elements showing spectral overlap with plasma polyatomic ions or from dissolved forms coming from the sample or as contamination (e.g. Si, Ti, Fe…), the magnitude of the continuous baseline worsens these size detection limits (through s_B). In such cases, the use of ultrashort dwell times has proven successful for lowering these limits,[61,84] while the use of collision and/or reaction cells for alleviating ICP-MS interferences has been frequently recommended for the same purpose. At the time this PhD thesis was initiated, however, no systematic studies on the effect of the use of such cell technologies for the determination of NPs by SP-ICP-MS had been published so far, so this was one of the goals selected for the present work.

As for the number concentration limit of detection (LOD_{NP}), and provided that only detectable NPs sizes above the LOD_{size} are considered, equation 1.11 shows that these limits do not depend on the NP composition, and can be improved by increasing the transport efficiency, increasing the sample flow rate and/or enlarging the total analysis time. With current instrumentation and maintaining the measuring time within reasonable limits, typical number concentration limits of detection around 10^6 part L^{-1} are reported. In fact, this is one of the main advantages of this technique, which allows to measure highly diluted suspensions at the concentration limits usually found in many real situations, such as environmental samples.[60]

This leads us again to the applied dimension of SP-ICP-MS where NPs have to be determined in a variety of matrices. At this point, it is important to stress that there are a series of limitations inherent to the technique that cannot be easily solved and define the kind of information that can be obtained with SP-ICP-MS. For instance, size information is typically given as NP diameter, for which it is assumed that the NPs have a spherical shape and that the NP density is equal to the bulk material density and independent from their size.[73] However, these assumptions may be inaccurate. First, the NP geometry has to be known in advance (e.g., by means of other techniques), as only

NP mass can be directly extracted from SP-ICP-MS measurements. TEM and SEM are the techniques most frequently used for this purpose. Regarding the NP density, on the other hand, a recent work from Tadjiki *et al*.[95] reported different density values for AgNPs in the range of 30 to 100 nm, being 18 to 24% lower than the density for the bulk material. The authors attribute this density difference on the NP porosity. Montaño *et al.* also reports different density values for SiO_2 NPs and colloidal suspensions from 100 and 1200 nm.[83] Density values for other NPs have not been reported so far, but it is fair to infer that errors in NPs sizing of are probably made when assuming the same density as for the bulk material.

The poor availability of well characterized NPs CRMs, on the other hand, may also show a serious impact on SP-ICP-MS method development, as in this technique CRMs are used for TE calculation. Currently, the CRMs most frequently used are provided by the NIST. In particular NIST Reference Material (RM) 8011, 8012, 8013 (AuNPs of 10, 30 and 60 nm nominal diameter, respectively) and NIST RM 8017 (AgNPs with 75 nm nominal diameter). However, until the last update from NIST on 18/08/2020, the NIST RM 8012 and 8013 were out of stock,[96,97] limiting even more the availability of CRMs for SP-ICP-MS analysis. LGC Limited also developed a CRM for gold nanoparticles with certified particle number concentration,[98] presenting an alternative CRM for the very demanded NIST AuNPs RM.

Besides these not easy to solve limitations, there are other challenges that, at least *a priori*, could be addressed with proper method development. Similarly to any ICP-MS application, SP-ICP-MS is also subjected to potential matrix effects and needs strategies to overcome them in order to reach accurate values for NP characterization,[75] especially when complex matrices and/or complex elements are under study. As previously mentioned, challenging elements subjected to severe spectral interferences in the ICP-MS might benefit from the use of collision/reaction cells, although this possibility was still to be fully tested at the onset of this PhD thesis. On the other hand, the determination of NPs on difficult matrices (such as environmental and biological samples) presenting high slurry contents, high concentration of organic matter and/or solvents or strongly acid and alkaline media,[73,88] is one of the main challenges for this technique and needs further investigation, mainly regarding to the accuracy of NP size

and mass concentration measurements. Strategies to overcome these potential matrix effects have also been seldom explored, so this was also selected as a goal for the PhD.

Finally, one of the main limitations of SP-ICP-MS is derived from the fact that most common ICP-MS used for measurements are sequential instruments (mostly quadrupoles). This limits the analysis to one isotope per run as the scanning frequencies of these mass analyzers are not sufficiently high for detecting the signal of different isotopes originating from a single NP event.[99] Detecting several isotopes simultaneously for SP-ICP-MS could find applications for analysis of NPs with more than one element in their composition, although more interestingly, they could help implementing strategies to cope with matrix effects such as internal standardization or Isotope Dilution Analysis (IDA). These possibilities could be realized by using Time-Of-Flight (TOF) mass analyzers, which are capable to register the whole mass spectrum simultaneously at a fast rate (every 30 µs for modern instruments). Recent instrumental advances have made available an ICP-TOF-MS instrument with is expected to feature an improved sensitivity when compared to older instruments,[76] which could be used for multielemental analysis of nanoparticles. Exploring the possibilities of this instrumentation for SP-ICP-MS, especially in the context of matrix effects overcoming, was also set as a goal for this work.

1.4. Objectives

Considering all of the above, the main goal for this thesis was set at the development of new methodological approaches for the accurate determination of NP sizes and particle number concentration in complex samples. In particular, solutions for overcoming spectral overlaps and/or mitigating matrix effects were aimed at. For achieving these goals, the following specific objectives were addressed:

- Exploring the possibilities of the use of ICP-tandem mass spectrometry (ICP-MS/MS) equipped with a collision/reaction cell (CRC) to determine NPs that are affected by severe spectral interferences on the ICP-MS. For this purpose, new methods for the determination of Si and Fe -containing NPs by SP-ICP-MS/MS were developed, in which the best suited CRC reaction/collision gases to be used were studied. Characterization of SiO_2 and Fe_3O_4 NPs was carried out.

- Systematic study of the effects of the use of CRC for determination of NPs by SP-ICP-MS, especially considering the duration of the NP signal events. Parameters such as type of gas, gas flow and type of NPs were considered for this purpose.
- Exploring the possibilities of matrix-matching for overcoming matrix effects on the determination of NPs in complex matrices. The determination of AgNPs in biological tissue digests was selected as a model for this study.
- Exploring the possibilities of ICP-TOF-MS for the determination of isotope ratios in individual NPs, thus enabling the application of isotope dilution analysis (IDA) for the determination of AgNPs.

CHAPTER 2

Experimental

2.1. Instrumentation

Measurements involving ICP-tandem mass Mass Spectrometry (ICP-MS/MS) were carried out with two different instruments. For the measurements with dwell times in the millisecond range used for the characterization of SiO_2NPs, an Agilent 8800 triple quadrupole ICP-MS/MS instrument (Agilent Technologies, Japan) located at the Atomic and Mass Spectrometry – 'A&MS' research group at Ghent University was deployed. In this case, the sample introduction system comprised a Micro mist nebulizer (400 µL min^{-1}) and a Peltier-cooled Scott-type spray chamber (2^oC). The instrument is equipped with two quadrupole mass analyzers (Q1 and Q2) and an octopole collision-reaction cell (ORS) mounted in-between the two quadrupole units (Q1-ORS-Q2). The tandem mass-spectrometry configuration enables this instrument to be operated in two different modes, single quadrupole (SQ) and MS/MS mode. In SQ mode, Q1 is fully open, while in MS/MS mode, both quadrupoles are used as mass filters with a single-mass bandpass window. Therefore, the MS/MS mode provides an improved control over the collisions/reactions occurring within the ORS. This setup also offers precursor and/or product ion scanning as powerful tools for method development, especially in the context of interference removal. In this work, the ORS was pressurized with various inert (He) and reactive gases (H_2, O_2, NH_3/He (10 % NH_3 in He) and CH_3F/He (10 % CH_3F in He)); also, no gas or "vented" mode was evaluated for illustrative purposes. The most relevant ICP-MS/MS instrument settings are listed in Table 2.1. All gases were introduced in the instrument *via* their corresponding inlets, except for the mixture of CH_3F/He that was introduced *via* the 4th line, which is originally intended for the use of O_2. Therefore, the CH_3F/He gas flow rates will be reported as their equivalent O_2 gas flow rates owing to the calibration of the gas flow controller for the latter. Although NH_3 and CH_3F were used as their corresponding mixtures with 90 % He, they will be further referred in this text to as NH_3 and/or CH_3F reaction gases.

Table 2.1. Instrument settings for the Agilent 8800 (ICP-MS/MS) instrument for SiO_2NPs characterization (dwell times in the millisecond range were used in this case).

Parameter	No gas "Vented" mode	He	H_2 On mass	H_2 Mass-shift	O_2	NH_3	CH_3F
Scan type	SQ MS/MS	MS/MS	SQ MS/MS	MS/MS	MS/MS	MS/MS	MS/MS
Plasma mode	Low matrix	Low matrix	Low matrix	Low matrix	Low matrix	Low matrix	Low matrix
RF power (W)	1550	1550	1550	1550	1550	1550	1550
Carrier gas flow rate (L min^{-1})	1.11	1.11	1.11	1.11	1.11	1.12	1.11
Extract 1 (V)	0.0	0.0	0.0	0.0	0.0	-3.0	-3.0
Q1 bias(V)	-3.0 0.0	0.0	-2.0 0.0	0.0	0.0	-1.0	-1.0
Octopole bias (V)	-8.0	-18.0	-18.0	-21.0	-5.0	-5.0	-5.0
Energy discrimination (V)	5.0	5.0	0.0	-5.0	-8.0	-8.4	-10.0
He flow (mL min^{-1})	---	1.5	---	---	---	1.0	---
H_2 flow (mL min^{-1})	---	---	1.5	4.5	---	---	---
3^{rd} gas flow (mL min^{-1})	---	---	---	---	---	1.0	---
4^{th} gas flow (mL min^{-1})	---	---	---	---	0.25	---	0.5
Q1 → Q2 masses	28 → 28	28 → 28	28 → 28	28 → 29	28 → 44	28 → 44	28 → 47
Extract 2 (V)	-180.0	-180.0	-170.0	-130.0	-145.0	-190.0	-190.0
Q2 bias (V)	-3.0	-13.0	-18.0	-26.0	-13.0	-13.4	-15.0
Settling Time (ms)	0	0	0	0	0	0	0
Dwell Time (TRA) (ms)	3	3	3	3	3	3	3
Total analysis time/sample (s)	60	60	60	60	60	60	60

For measurements with dwell times in the microsecond range, on the other hand, which were used for the characterization of SiO_2NPs, Fe_2O_3NPs and AgNPs and for the study on the effects of the CRC cell on the signal duration for AuNPs, an Agilent 8900 triple quadrupole ICP-MS/MS instrument (Agilent Technologies, Japan) from the Agilent Technologies R&D laboratory (Cheadle, United Kingdom) was deployed. The sample introduction system, the Q1-ORS-Q2 configuration and the SQ and MS/MS approach of analysis works in the same way as explained for the Agilent 8800 triple quadrupole ICP-MS/MS instrument. This setup also offers precursor and/or product ion scanning as powerful tools for method development, especially in the context of interference removal. The main difference between these models is the minimum achievable dwell time: in the 8800 model, the minimum t_d is 3 ms, whereas the 8900 model can lower dwell time values down to 100 µs. Furthermore, the 8900 model is equipped with the Single Particle Application Module of the MassHunter software for NPs data acquisition

and treatment, enabling analysis in single particle mode without the need for external applications. Different reaction/collision gases and different operating conditions were used in the different experiments performed in this work, as detailed next.

For the characterization of SiO_2NPs, in the first place, the ORS was pressurized with H_2 and all the analyses were carried out on the MS/MS on-mass mode. The operating conditions used in this case are shown in Table 2.2.

Table 2.2. Instrument settings for the Agilent 8900 (ICP-MS/MS) instrument for SiO_2NPs characterization with dwell times in the microsecond range.

Parameter	Condition
Scan type	MS/MS
Plasma mode	Low Matrix
RF power (W)	1600
Nebulizer gas flow rate (L min^{-1})	0.86
Auxiliary gas flow rate (L min^{-1})	0.90
Extract 1 (V)	0.00
Q1 bias(V)	-19.0
Octopole bias (V)	-12.0
Extract 2 (V)	-210.0
Energy discrimination (V)	0.0
Q1 → Q2 masses	28 → 28
Dwell Time	100 µs; 500 µs; 1 ms; 3 ms
Settling Time (µs)	0
Total Analysis Time/Sample (s)	60

For Fe_2O_3NPs characterization, the ORS was pressurized with H_2 and NH_3/He (10% NH_3 in He). The operating conditions used for SP-ICP-MS/MS analyses are shown in Table 2.3.

Table 2.3. Instrument settings for the Agilent 8900 (ICP-MS/MS) instrument for Fe_3O_4NPs characterization.

Parameter	H_2	NH_3
Scan type	MS/MS	MS/MS
Plasma mode	Low matrix	Low matrix
RF power (W)	1550	1600
Carrier gas flow rate (L min^{-1})	1.11	1.55
Extract 1 (V)	0.0	-29.0
Q1 bias(V)	0.0	-1.0
Extract 2 (V)	-245.0	-190.0
Octopole bias (V)	-5.0	-5.0
Energy discrimination (V)	-8.0	-7.0
CRC Gas flow (mL min^{-1})	1.5	1.5
Q1 → Q2 masses	56 → 56	56 → 90
Axial Acceleration (V)	2.0	0.2
Settling Time (ms)	0	0
Dwell Time (TRA) (µs)	100	100
Total analysis time/sample (s)	60	60

For the study on the effects of the CRC gases on the AuNPs signal duration, the ORS was pressurized with He, H_2 and NH_3/He (10% NH_3 in He). Also, no gas or "vented" mode was evaluated for comparative purposes. The operating conditions used for SP-ICP-MS/MS analyses are shown in Table 2.4.

Table 2.4. Instrument settings for the Agilent 8900 (ICP-MS/MS) instrument for the study on the effects of CRC gases on the signal duration for AuNPs.

Parameter	No gas	He	H_2	NH_3 On-mass	NH_3 Mass-Shift
Scan type	SQ	MS/MS	MS/MS	MS/MS	MS/MS
Plasma mode	Low matrix	Low matrix	Low matrix	Low matrix	Low matrix
RF power (W)	1600	1600	1600	1600	1600
Carrier gas flow rate (L min^{-1})	0.73	0.73	0.73	0.73	0.73
Extract 1 (V)	-8.1	-8.1	-8.1	-8.1	-8.1
Q1 bias(V)	-8.0	-3.0	0.0	-1.0	-1.0
Extract 2 (V)	-190.0	-190.0	-190.0	-190.0	-190.0
Octopole bias (V)	-9.0	-23.0	-20.0	-5.0	-5.0
Energy discrimination (V)	5.0	5.0	1.0	-7.0	-7.0
CRC Gas flow (mL min^{-1})	-	5.0	7.0	1.0	1.0
Q1 → Q2 masses	197	197 → 197	197 → 197	197 → 197	197 → 214
Axial Acceleration (V)	0.0	0.0	0.0	2.0	2.0
Settling Time (ms)	0	0	0	0	0
Dwell Time (TRA) (µs)	100	100	100	100	100
Total analysis time/sample (s)	60	60	60	60	60

The study on matrix matching possibilities for characterization of AgNPs in complex matrices was also carried out with an Agilent 8900 ICP-MS/MS instrument located at the Inorganic Analysis Research Group in LGC (London, United Kingdom). However, in this case the equipment was used in the single quad mode with no gas being pressured on the CRC, as Ag should not suffer from spectral interferences. The operating conditions used for SP-ICP-MS/MS analyses are shown in Table 2.5.

Table 2.5. Instrument settings for the Agilent 8900 (ICP-MS/MS) instrument for AgNPs characterization in different complex matrices.

Parameter	Condition
Scan type	SQ
Plasma mode	Low Matrix
RF power (W)	1550
Nebulizer gas flow rate (L min^{-1})	1.09
Auxiliary gas flow rate (L min^{-1})	0.90
Extract 1 (V)	-10.2
Q1 bias(V)	-7.0
Octopole bias (V)	-8.0
Extract 2 (V)	-235.0
Energy discrimination (V)	5.0
Q1 mass	107
Dwell Time (µs)	100
Settling Time (µs)	0
Total Analysis Time/Sample (s)	60

For comparison purposes, the effects of the use of CRC technology on NP signals was also carried out with a single quadrupole-ICP-MS instrument for the determination of different NPs (namely Au, Ag and PtNPs) with different sizes. In this case, a NexION 300X (Perkin Elmer, Waltham, USA) ICP-QMS instrument was used. The ICP-MS system was composed of a triple cone interface with a hyper skimmer cone used as an additional cone, which provided a gradual pressure reduction within the interface, mitigating the dispersion of the ion-beam. This instrument is also equipped with a quadrupole CRC (dynamic reaction cell – DRC) and with a quadrupole ion deflector to bend the ion beam over a 90 degrees angle before its introduction into the CRC. The sample introduction system comprised a 0.5 mL min^{-1} concentric quartz nebulizer and a quartz cyclonic spray chamber. Analysis of NPs was performed with the Syngistix Nano Application Software Module for Single Particle ICP-MS, which allows the ionic calibration, TE calculation and NP size determination without the need for external

software. The operating conditions of the NexION 300X are gathered in the Table 2.6, while the gas flow inside the DRC was changed along the experiment by means of the Syngistix software.

Table 2.6. Instrument settings for the Perkin Elmer NexION 300X instrument for the study on the effects of the CRC on the characterization of Ag, Au and Pt NPs.

Parameter	Condition
RF power (W)	1600
Nebulizer Gas Flow (L min^{-1})	0.96
ICP-MS Mode	Kinetic Energy Discrimination (KED)
Plasma Gas Flow (L min^{-1})	15.0
Discriminator Threshold (V)	12.0
Deflector Voltage (V)	-5.75
Quadrupole Rod Offset (V)	-12.0
Cell Entrace Voltage (V)	-8.0
Cell Exit Voltage (V)	-23.0
Cell Rod Offset (V)	-13.5
Axial Field Voltage (V)	475.0
RPq	0.5
Analyzed Isotopes	^{197}Au, ^{107}Ag, ^{195}Pt
Settling Time (ms)	0
Dwell Time (TRA) (µs)	100
Total analysis time/sample (s)	60

Finally, determination of AgNPs using the isotope dilution analysis (IDA) protocol was carried out with a Tofwerk icpTOF 2R instrument (Tofwerk, Thun, Switzerland). This instrument is a combination of the ion/optics, collision/reaction cell, gas and vacuum systems of an iCAP Qc from Thermo Fisher Scientific (Thermo Fisher Scientific, Waltham, USA) and the notch filter and TOF mass analyser from Tofwerk.[76] With this instrument, the mass range spectra from $^{7}Li^{+}$ to $^{254}UO^{+}$ can be obtained simultaneously. This equipment allows for two acquisition data modes: continuous and triggering mode. In continuous acquisition mode, the fastest rate of detection is 1000 Hz (33 TOF extractions per mass spectrum). Thus, the minimum integration time for the icpTOF 2R is 2.7 ms. In this mode all the spectra range can be recorded, but it is also possible to select certain m/z in the method parameters in the TofDaq software. In this mode large data files are

generated, as the data also include the background noise intensity. On the other hand, in Trigger-mode acquisition the data is recorded for a specific m/z above some threshold defined by the user. In this mode, only the particle above the background is recorded. As the background noise is not recorded, the file size of the sample is significantly reduced. For this reason, this mode is used when the particle composition is known or predefined.[100]

The sample introduction system comprises a Micromist nebulizer (400 µL min^{-1}) and a Peltier-cooled Scott-type spray chamber. The instrument is equipped with 3 software packages: Qtegra (version 2.7.2426.165) for sample introduction and ion optics control parameters, ToF Pilot (version 2.5.4.0.54) for the set up and configuration of the TOF system and Tofware (version 3.0.2) for data processing.

For AgNPs characterization, the collision/reaction cell was not used as the spectral interferences for $^{107}Ag^+$ and $^{109}Ag^+$ are expected to be negligible. The sensitivity and the mass calibration were adjusted daily in order to achieve the optimal operating conditions of the equipment. The working conditions finally selected are summarised in Table 2.7

Table 2.7. Instrument settings for the Tofwerk ICP-TOF-MS instrument for the isotope dilutions for AgNP determination.

Parameter	Condition
RF power (W)	1550W
Nebulizer Gas Flow (L min^{-1})	1.05 L/min
Plasma Gas Flow (L min^{-1}	14.0 L/min
Auxiliary Gas Flow (L min^{-1})	0.80 L/min
Monitored Isotopes	^{107}Ag, ^{109}Ag
Settling Time (ms)	0
Integration time (TRA) (ms)	3 ms
Total analysis time/sample (s)	60

For validation purposes most NP samples were also analyzed by Transmission Electronic Microscopy (TEM). A Tecnai T20 TEM instrument (Thermo Fisher Scientific, Waltham, USA) from “Laboratorio de Microscopias Avanzadas" at "Instituto de Nanociencia de Aragón” - Universidad de Zaragoza was used for this goal. This

equipment has 0.25 nm resolution and a working voltage range between 80 and 200 kV. In this work, a working voltage of 200kV was used.

2.2. Standards and Reagents

For SiO_2NPs and Fe_3O_2NPs particle number concentration and size determination, ultra-pure water (resistivity > 18.2 MΩ cm) was obtained from a Milli-Q Element water purification system (Millipore, France). Appropriate dilutions from 1 g L^{-1} single-elemental standard solution of Si and Fe (Instrument Solutions, The Netherlands) were prepared freshly on a daily basis under the form of the dissolved analyte and were used for method development and calibration purposes (concentrations ranging between 0 and 5 µg L^{-1}).

For the study on the effects of the CRC on Ag, Au and PtNPs carried out with the NexION 300X, ultrapure water obtained from an ultra-purification Milli-Q system (Millipore, Bilerica, USA) was employed for all the NPs dilutions.

For the study on matrix-matching for AgNPs determination and AgNPs determination by isotope dilution, ultrapure water (18.2 MΩ, 25 °C) was obtained from an Elga water purification unit (Elga, Marlow, Buckinghamshire, United Kingdom (UK)). For the matrix-match ionic calibration studies, appropriate dilutions were freshly and daily prepared from an Ag stock solution (Romil, Cambridge, UK) of 984.54 mg L^{-1}. All the Ag ionic solutions were prepared in 3 different media: 1 mM trisodium citrate, 1% v v^{-1} HNO_3 and 2.5% w w^{-1} TMAH with 0.1% w w^{-1} Triton X-100. Nitric acid (suprapure) was purchased from Romil (Cambridge, UK), Tetramethylammonium Hydroxide (TMAH) from Alfa Aesar (lot: S02C014) (Lancashire, UK) and Trisodium citrate tribasic dihydrate with purity higher than 99.5% w w^{-1} and Triton® X-100 from Sigma Aldrich (Gillingham, UK). For AgNPs determination by isotope dilution, a ^{109}Ag-enriched standard solution with a certified Ag ionic concentration of 9.97 µg g^{-1} in 2% (v v^{-1}) HNO_3 media and an isotopic abundance of 99.8% for ^{109}Ag and 0.2% for ^{107}Ag was purchased from ISC Science (Oviedo, Spain). All the Ag ionic solutions and isotopically enriched spikes intermediary solutions were prepared in 1 mM trisodium citrate media.

2.3. NPs samples and sample preparation

For the determination of SiO_2NPs with the Agilent 8800 (dwell times in the millisecond range), SiO_2NPs suspended in water were obtained from nanoComposix (non-functionalized NanoXact^{TM} Silica, Czech Republic). Particle size distributions and mass concentrations for these suspensions, determined by TEM and gravimetric analysis, respectively, are provided by the manufacturer. All the information on these NPs is gathered in Table 2.8. For TE calculation in this part of the work, a reference material NIST SRM 8013 – Gold Nanoparticles (AuNPs), of 60 nm nominal diameter (certified diameter: 56.0 ± 0.5 nm) was purchased from the National Institute of Standards Technology (NIST) (Gaithersburg, USA). All NP suspensions were shaken vigorously and sonicated during 10 minutes before their use to avoid particle agglomeration.

Table 2.8. Information on particle size (TEM) and particle concentration (gravimetric analysis) provided by nanoComposix for the SiO_2 NP suspensions for NPs characterization with the Agilent 8800 (dwell times in the millisecond range).

Nominal NP size (nm)	NP real size (mean) (nm)	Particle concentration (particles mL^{-1})	Mass concentration SiO_2 ($g\ L^{-1}$)
80	82.6 ± 4.7	1.5×10^{13}	10.0
100	99.2 ± 5.8	9.5×10^{12}	10.7
200	197 ± 14	1.1×10^{12}	10.1
300	297 ± 12	3.4×10^{11}	10.4
400	401 ± 26	1.4×10^{11}	10.3

In order to minimize the occurrence of double events in SP-ICP-MS mode with dwell times in the millisecond range, appropriate dilutions of the original NP suspensions were prepared. To calculate the dilution factor needed for each of the NP suspensions analyzed, probability calculations based on Poisson statistics were carried out taking into account the exact experimental parameters finally selected for the measurements (*i.e.* dwell time, transport efficiency and sample uptake rate) as to ensure a probability of double events to occur below 5%.[62] For the suspensions of NPs with a diameter below 100 nm, for which the particle distribution signal partially overlapped with that of the

background, lower dilution factors leading to increased probabilities of double events were used, as will be discussed in section 3.2.2.2.

For the determination of SiO_2NPs with the Agilent 8900 (dwell times in the microsecond range), suspended SiO_2NPs in water, with nominal size of 50 and 80 nm, were also obtained from nanoComposix. Particle size distributions and mass concentrations for these suspensions were also are provided by the manufacturer and are gathered in Table 2.9. For TE calculation in this part of the work, a reference material NIST SRM 8012 – Gold Nanoparticles (AuNPs), of 30 nm nominal diameter (certified diameter: 27.6 ± 2.1 nm) was used. All NP suspensions were shaken vigorously and sonicated during 10 minutes before their use to avoid particle agglomeration.

Table 2.9. Information on particle size (TEM) and particle concentration (gravimetric analysis) provided by nanoComposix for the SiO_2 NP suspensions for NPs characterization with the Agilent 8900 (dwell times in the microsecond range).

Nominal NP size (nm)	NP real size (mean) (nm)	Particle concentration (particles mL^{-1})	Mass concentration SiO_2 ($g\ L^{-1}$)
50	47 ± 3	9.1×10^{13}	10.6
80	81 ± 6	1.7×10^{13}	10.5

For the determination of Fe_3O_4NPs, custom-made Fe_3O_4NPs suspended in water were obtained from nanoComposix. Particle size distributions and mass concentrations for these suspensions, determined by TEM and gravimetric analysis, respectively, are provided by the manufacturer. All the information related to these NPs is gathered in Table 2.10. It needs to be noted that manufacturing monodisperse 200 nm Fe_3O_4 NPs proved difficult, resulting in a wider bimodal size distribution (see section 4.2.2.). For TE calculation in this part of the work, the reference material NIST SRM 8012 – Gold Nanoparticles (AuNPs), of 30 nm nominal diameter (certified diameter: 27.2 ± 2.1 nm) was used. All NP suspensions were shaken vigorously prior to their use to avoid particle agglomeration.

Table 2.10. Information on particle size (TEM) and particle concentration (gravimetric analysis) provided by nanoComposix for the Fe_3O_4NPs suspensions.

Nominal NP size (nm)	NP real size (mean) (nm)	Particle concentration (particles mL^{-1})	Mass concentration Fe_3O_4 (g L^{-1})
50	54 ± 5	9.1×10^{13}	10.6
200	196 ± 64	2.0×10^{10}	10.5

For the determination of the size distribution of Fe_3O_4NPs, dilution factors leading to less than 1000 NPs per minute were used in all cases. It needs to be noted that all measurements were carried out at ultra-fast data acquisition speed (dwell time of 100 μs). The dilution factors were calculated based on Poisson statistics to minimize the occurrence of double events during SP-ICP-MS/MS measurement.

For the study of the effects of the CRC on the signal duration, various suspensions of spherical (nano)particles from nanoComposix with different sizes and chemical compositions were used. Size distributions, particle number densities and mass concentrations for these (nano)particle suspensions were provided by the manufacturer (determined by TEM and gravimetric analysis). All the information is gathered in Table 2.11.

Table 2.11. Information on particle size (TEM) and particle concentration (gravimetric analysis) provided by nanoComposix for the study on the effects of CRC on the signal duration of Ag, Au and PtNPs.

Analyte	Nominal NP size (nm)	NP real size (mean) (nm)	Particle concentration (particles mL^{-1})	Elemental mass concentration (g L^{-1})
Ag	50	51 ± 6	3.0×10^{10}	0.021
	80	79 ± 7	7.6×10^{9}	0.021
	100	98 ± 13	4.1×10^{9}	0.021
	200	202 ± 29.7	4.8×10^{8}	0.022
Au	50	49.9 ± 2.2	4.2×10^{10}	0.053
	70	71 ± 9	1.4×10^{10}	0.052
	100	97 ± 10	5.7×10^{9}	0.053
Pt	50	46.2 ± 5.1	4.1×10^{10}	0.052
	70	72.2 ± 4.2	1.2×10^{10}	0.050

Also, 75 nm AgNPs (74.6 ± 3.8, NIST SRM 8017) and 30 nm AuNPs (27.6 ± 2.3, NIST SRM 8012) from NIST were used as NP reference materials for TE determination. The NIST SRM 8017 was reconstituted with 2 mL of ultrapure water, resulting in a mass

concentration of 1072 mg mL^{-1}. Additionally, and for comparison purposes, the NPs on Table 2.11 were evaluated by TEM. Some of the results obtained will be provided in section 5.2.2.2. The NP suspensions were gently stirred and sonicated before dilution. For all the experiments intended to measure the average signal duration of individual NP events, no more than 3000 NP events per minute were detected (in most cases, this value was lower than 1000 NP events per minute).

For the studies on matrix matching for AgNPs determination, AgNPs suspended in water with nominal size of 40 nm were acquired from nanoComposix. The certificate of analysis provided by the manufacturer reports a mean size for the particles of 41 ± 4 nm measured by TEM, mass concentration of Ag of 0.021 mg mL^{-1} measured by ICP-MS and a particle number concentration of $5.6x10^{10}$ particles mL^{-1}. For TE calculation and NP characterization, NIST SRM 8017 (74.6 ± 3.8 nm) was used. All the NPs samples were prepared in 2.5% w w^{-1} TMAH and 0.1% w w^{-1} Triton X-100 media. A revisited waste collection method[90] was carried out by LGC personnel to determine in house the particle number concentration of both AgNPs used in this part of the work, resulting in a number concentration of $5.6x10^{13}$ part L^{-1} for 40 nm AgNPs and 4.69×10^{14} part L^{-1} for 75 nm AgNPs.

For AgNPs determination by IDA, NIST SRM 8017 (74.6 ± 3.8 nm) was also used for TE determination and NP characterization. Again, a revisited waste collection method was carried out by LGC personnel to determine the particle number concentration of AgNPs dispersions in this part of the work,[90] resulting in a particle number concentration of 4.66×10^{14} part L^{-1}. To calculate the dilution factor needed for the NP suspensions analyzed, probability calculations based on Poisson statistics were carried out taking into account the exact experimental parameters finally selected for the measurement (integration time, transport efficiency and sample uptake rate) as to ensure a probability of double events to occur below 5%.[62] According to these calculations, the ideal particle number concentration of AgNPs diluted dispersion used for IDA analysis was, approximately, 4.50×10^7 particles L^{-1}. The AgNPs stock dispersion was vigorously shaken prior to preparation of all the NP dilutions. Each diluted AgNPs dispersion was spiked with a proper dilution of the ^{109}Ag isotopically enriched solution for reaching a final Ag ionic concentration of 1.5 µg g^{-1}. All the AgNPs dispersions (with

or without ^{109}Ag spike) were prepared in 1 mM trisodium citrate media. Dispersions were vigorously shaken prior to analysis.

2.4. General SP-ICP-MS data treatment for studies performed with quadrupole instruments

For experiments conducted with the Agilent 8800 triple quadrupole ICP-MS/MS instrument, the raw data obtained using the Agilent ICP-MS MassHunter Software operated in Time Resolved Analysis (TRA) mode were treated and evaluated externally using a modified spreadsheet previously published by Peters *et al.*[72] This spreadsheet is composed of two interrelated worksheets used for TE calculation and NPs characterization, respectively. The TE was calculated using the NIST SRM 8013 (AuNPs) and was determined according to the particle frequency method described by Pace *et al.*[59] In the second worksheet, sample mass and particle concentration and particle size distribution are calculated for each sample by means of the mass-flux curve determined using the ionic Si standard solutions and the TE. The NP pulses are differentiated from the background signal using the 3σ criterion, as previously described. For SiO_2NP distributions that are difficult to discern from the background, a deconvolution approach using OriginLab (OriginLab, Northampton, Massachusetts, USA) was used for modeling. This approach relies on approximating the raw distribution by a Gaussian model. The Equation thus obtained was used to calculate the particle diameter and particle and mass concentrations (see section 1.3.2.2).

For experiments conducted with the Agilent 8900 triple quadrupole ICP-MS/MS instrument, the raw data obtained using the Agilent ICP-MS MassHunter Software operated in Time Resolved Analysis (TRA) mode were also treated and evaluated externally. For NP integration, a script from Octave GNU (Free Software Foundation, Boston, USA) was developed for our group by Dr. Javier Resano (i3A, Universidad de Zaragoza). In this script, the threshold for integration was inserted prior to the NPs integration. This threshold was defined as the average plus 3 times the standard deviation of all the data. After performing the NP integration, the software generates a new spreadsheet with 3 data columns: time (ms), signal intensity and number of

integrated points per particle. In this spreadsheet, the nonintegrated values (background) remain as a single value (in counts) in the signal intensity column, the integrated signal for each NP is displayed in this signal intensity column next to the time of the first point of integration, whereas the other points of integration display no value. The integrated data are then inserted into the modified data treatment spreadsheet, based on that developed by *Peters et al*.[72] The most important modification regards the correction of the particle mass by the background contribution: the background intensity subtracted from the NP pulse intensity has to take into account the number of integrated events per particle (given in the third column in the Octave script) in order to obtain the corrected NP peak intensity and thus, the corrected particle mass (Equation 2.1):

$$M_P = \frac{I_{NP} - nI_{BG}}{X_a\, m} \quad (2.1)$$

Where M_p is the particle mass, I_{NP} is the intensity of the NP pulse, I_{BG} is the average intensity of the background, n is the number of integrated events per particle (obtained from the third column of the spreadsheet generated by the GNU Octave script), X_a is the mass fraction of the analyte in the NP and m is the slope obtained in the mass-flux calibration curve.

For the study on the effects of the CRC on the signal duration for Ag, Au and PtNPs and for the determination of Fe_3O_4NPs, an Hyper Dimensional Image Processing (HDIP) software developed at the Atomic and Mass Spectrometry – 'A&MS' research group at Ghent University was used to accurately calculate the NP signal duration in addition to the SP software packages available from the instruments deployed in these experiments: the MassHunter 4.4 Workstation for the Agilent 8900 ICP-MS/MS unit (Agilent Technologies, Inc. 2017) and Syngistix for ICP-MS Nano Aplication Software module, version 2.1. for the NexION 300 X (Perkin Elmer Inc., 2018). This HDIP software was developed for post-processing of spectral data and images in the context of laser ablation (LA) ICP-MS and is meanwhile commercially available from Teledyne Cetac Technologies for this purpose, but it was deployed to identify the individual NP events

appearing randomly during SP-ICP-MS measurements. By using the HDIP software, the average signal duration (at different %-ages of the peak height) and the average peak shape of NP events measured under different conditions could be calculated easily (Figure 2.1). Additionally, outliers resulting from instrument-derived signal spikes or other artifact resulting from the software data treatment were removed. For this purpose, any data point more than 1.5 interquartile ranges (IQRs) below the first quartile or above the third quartile was considered an outlier and was removed.

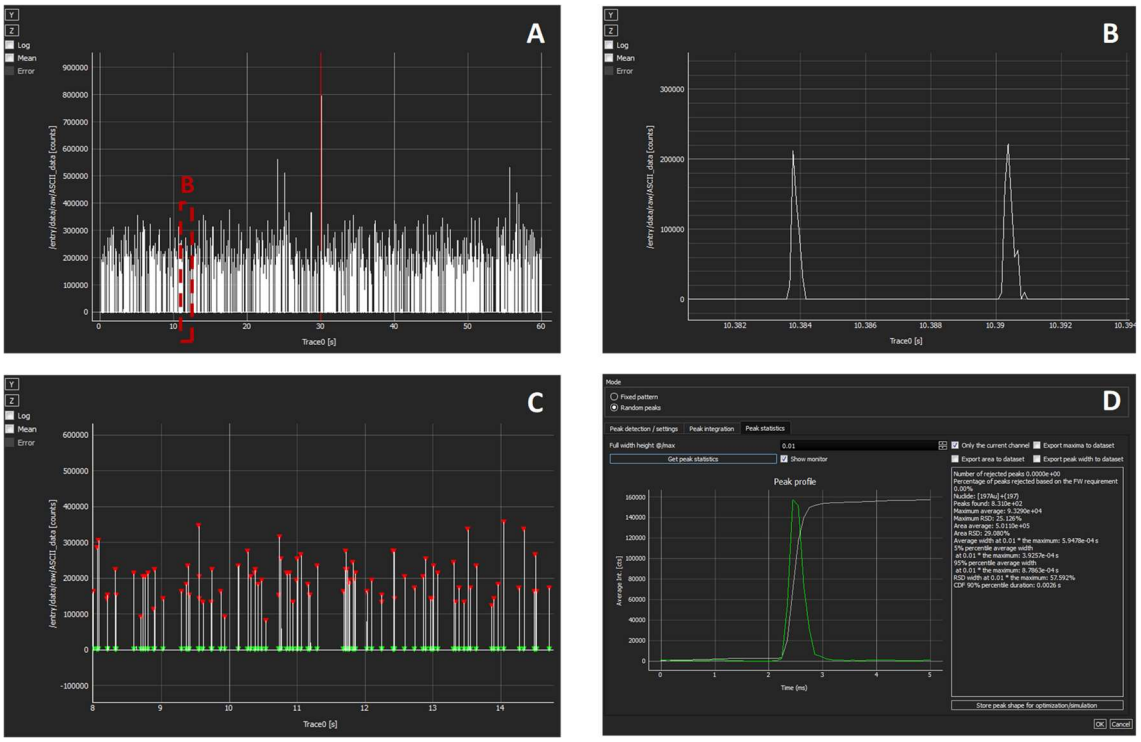

Figure 2.1. SP-ICP-MS data treatment using the A&MS (Ghent University) developed HDIP software. **Figures 2.1A** and 2.**1B** show the raw data (intensity *vs* time) from one measurement replicate of a AuNP standard. **Figure 2.1C** illustrates the identification of the signal spikes corresponding to single NP events; the selection criterion was based on different parameters, such as intensity, lower relative maximum threshold and higher relative minimum threshold. **Figure 2.1D** shows the average peak profile and the results obtained for the complete data set (peak profile, signal duration, number of peaks found, area average, *etc.*). This figure is reproduced with permission of with permission of Elsevier. (https://doi.org/10.1016/j.aca.2019.05.077)

All data treatment on the study of matrix matching for AgNP determination was carried out with the Single Particle Application Module of the ICP-MS MassHunter software (G5714A) from the Agilent 8900 ICP-MS/MS. Particle diameter and number

concentration were directly provided by the software according to the TE determination and the ionic calibration performed in the equipment.

2.5. SP-ICP-MS data treatment for experiments performed with ICP-TOF-MS instruments

2.5.1. AgNPs characterization by IDA approach

For the mass determination of a single AgNP detected by IDA approach, the following equation was used for this purpose (this equation will be explained with more details in the section 6.2.1.):

$$m_{NP} = \eta_n \cdot t_{int} \cdot c_{spike} \cdot d \cdot f \cdot \frac{M_s}{M_{sp}} \left(\frac{R_m A_{sp}^b - A_{sp}^a}{A_s^a - R_m A_s^b} \right) \textbf{(2.2)}$$

Where η_n is the TE, t_{int} is the integration time (s), c_{spike} is the spike mass concentration (ng L^{-1}), d is the density of the spike (ng L^{-1}), f is the sample flow (L s^{-1}), M_s and M_{sp} are the atomic weights of the element in the sample and the spike respectively, Rm is the isotope ratio a/b in the mixture, which varies with time as a result of the chromatographic separation and A_s^i and A_{sp}^i are the isotope abundances for the isotope i in the sample and the spike.

Before analysis, the sample flow f was measured in order to minimize the introduction of systematic errors in the TE calculation and in the AgNP characterization by IDA, as this parameter is critical for both calculations. For this purpose, a vial containing a 2.5 µg g^{-1} ionic Ag solution in citrate media was placed on an analytical balance placed next to the ICP-TOF-MS. After system stabilization, the weight of the vial was registered every 3 minutes for 15 minutes. Each registered weight was plotted against monitorization time, resulting in a linear sample uptake mass flow graph. The slope of the linear regression obtained is the sample flow (in g·min^{-1}). This procedure was repeated every day before analysis was carried out.

In addition to the general mass calibration performed daily at the beginning of the working session, re-calibration of the mass spectra was performed at the beginning and at the end of each analysis batch, using 2.5 ng mL^{-1} Ag ionic standards with natural isotope composition in 1 mM citrate matrix. This re-calibration was performed to correct for potential mass-calibration drifts for Ag isotopes.[100] On each batch the measurements of the TE, calibration standards for all operations described in this protocol and IDA samples were carried out. Re-calibration of mass spectra was carried out in data acquisition, with the Tofware data post processing software (a TOFWERK data analysis package running in the IgorPro environment).

In order to correct for mass-bias between the theoretical and the experimental isotope ratio, it is necessary to determine the mass discrimination factor (which we called K factor) prior to the IDA analysis. In this work, the K factor is defined as K = Rtrue/Rmeasured, where Rtrue = (107Ag/109Ag) natural = 1.075. A set of Ag ionic solutions of 2.5, 5.0, 7.5 and 10.0 µg L^{-1} with natural isotope composition was used for K factor calculation. These solutions were prepared and measured daily, and the K factor was obtained as the median of the values determined for each of the measured solutions. All the solutions utilized for this purpose were prepared in 1mM citrate media.

TE was determined following the particle frequency method,[59] using matrix-matching between the analyzed NP suspensions and the standard NP suspensions whenever required. The TE was determined daily prior to the IDA analysis of isotopically enriched AgNPs suspension. Five replicates were taken for the TE calculation and the median value was used for IDA calculations.

Continuous mode was selected for data acquisition (see section 6.2.2.1. for more details on this acquisition mode). For all data points on each TOF-MS time trace, complete mass spectra are recorded along with integrated data from each isotope. These data are stored in the instrument and can be treated after the acquisition has finished.

In this sense, different post-acquisition treatments were carried out using either the standard TOF-MS acquisition software or the Tofware. Re-calibration of mass spectra was performed using 2.5 ng mL^{-1} Ag ionic standards, as previously described. Moreover, baseline fitting and correction was also performed after data acquisition. The baseline in ICP-TOF-MS is a complex function of overlapping peak shapes and the

contribution of stray ions from the most abundant species in the plasma. As ions of all m/z are measured, by design, in each TOF extraction, intense peaks originated from the matrix can result in an elevation of the baseline by several orders of magnitude.[100] Under these circumstances, baseline fitting and subtraction seems imperative, especially if complex matrices are introduced in the ICP-TOF-MS instrument. For baseline fitting, a smoothing function that takes the rolling minimum of a defined number of TOF data points was selected.[100]

Following data acquisition in Tofware software, a file containing the time of analysis and only the traces for m/z 107 and 109 was obtained. Before applying the IDA equations into the isotope ratios of each sample, background correction was carried out for each sample. Considering that all NP dispersions are spiked with the enriched isotopic standard, a different blank solution was measured for this purpose. The average background for each Ag isotope determined from this solution was subtracted for each individual value per integration time in each NP sample.

The corrected mass-spectral signals were processed with an Excel spreadsheet developed in collaboration with the Inorganic Analysis Research Group in LGC (London, United Kingdom, using equations from section 6.2.1. Considering that the isotopically enriched spike is mostly ^{109}Ag, the trace at m/z 107 is used for identifying NP signals. For this purpose, a frequency-intensity histogram is built for the ^{107}Ag isotope and a threshold is applied for separating NPs signals from those of the background. The threshold follows the 5σ criteria, where σ is defined by the m/z=107 background standard deviation.[91] Next, $^{107}Ag/^{109}Ag$ isotope ratios are calculated for each event that matches the threshold condition. IDA equation described in section 6.2.1. (eq. 6.3) is then applied for each isotope ratio providing the particle mass for each detected event. As an additional measure, a script for correction of split events was written for our group by Dr. Javier Resano (i3A, Universidad de Zaragoza) in GNU Octave (Free Software Foundation, Boston, USA). With this script, NP signals that fall into two consecutive time events are integrated. The corrected particle mass is then reintroduced in the IDA spreadsheet to finally provide the NP diameter, assuming spherical form and density of bulk silver (10.49 g cm^{-3}).

2.5.2. AgNPs characterization by external calibration approach

For comparison purposes, characterization of the AgNPs used in this study was also carried out by the regular SP-ICP-MS method deploying external calibration with ionic standards. Data treatment was carried out following a similar protocol as that described in section 2.4 for quadrupole instruments. Determination of sample flow, recalibration of mass spectra and determination of transport efficiency needed for calculations were performed as described in section 2.5.1.

CHAPTER 3

Characterization of SiO_2 Nanoparticles by Single Particle – Inductively Coupled Plasma – Tandem Mass Spectroscopy (SP-ICP-MS/MS)

- The figures and the tables shown in this chapter are reproduced with permission of RSC. (https://doi.org/ 10.1039/c7ja00138j).
- The content of this chapter is adapted with permission of RSC (https://doi.org/ 10.1039/c7ja00138j).

3.1. Introduction

As non-metal oxides, silica nanoparticles (SiO_2NPs) are used in a large variety of applications, such as in food additives, drugs, coatings, sensors and cosmetics.[52,83,101] Furthermore, SiO_2 NPs are widely used for chemical mechanical planarization (CMP), in which their abrasive properties are relied on to polish materials in the semiconductor industry.[102]

The characterization of SiO_2NPs by means SP-ICP-MS is not straightforward, as all Si isotopes are subjected to spectral interferences coming from polyatomic ions formed in the plasma or Si ion background leaching from glass components in the instrumentation. The most abundant isotope at m/z = 28 (relative abundance: 92.22%) is mainly interfered by $^{14}N^{14}N^+$ and $^{12}C^{16}O^+$ species, while the other two Si isotopes at m/z= 29 and 30 (relative abundances: 4.69% and 3.09%, respectively) are interfered by $^{14}N^{15}N^+$, $^{14}N_2{}^1H^+$, $^{15}N_2{}^+$, $^{14}N^{15}N^1H^+$, $^{14}N^{16}O^+$ and $^{12}C^{18}O^+$.[103]

One of the most common strategies to overcome spectral interferences in ICP-MS operated with quadrupole mass analyzers is the use of Collision/Reaction Cells (CRC). A CRC is usually a second quadrupole or an octopole, which is placed before the mass analyzer and can be pressurized with a collision/reaction gas. The gas within the cell interacts with the analyte and (poly)atomic ions and helps mitigating the interferences mainly by two different mechanisms: (i) either by collision and kinetic energy discrimination: polyatomic ions have larger cross-sections than analyte ions of the same mass and collide with the CRC gas with higher frequency. As a result, their kinetic energy is decreased to a larger extent, which is used to eliminate the interference by setting a kinetic energy barrier that only the analyte ions can pass. (ii) or by chemical reactions: the CRC gas induces specific chemical reactions, mostly with the interferent species, which are thus detected at a different mass/charge ratio.[104]

Although the use of CRCs has proved successful for overcoming many usual polyatomic interferences in the ICP-MS, this strategy is not very efficient to solve the spectral interferences affecting some analytes, mainly those with m/z below 40 amu, that are mostly affected by interferences resulting from the recombination of light elements in the plasma (H, C, N and O). In face of this challenge, the relatively recent

(2012) introduction of ICP-tandem Mass Spectrometry (ICP-MS/MS) was a significant breakthrough and dramatically improved the capabilities of ICP-QMS for avoiding the problem of spectral interferences.[105,106]

ICP-MS/MS instruments are equipped with two quadrupole units (Q1 and Q2) located before (Q1) and after (Q2) a collision/reaction cell, thus enabling for a double mass selection if required. In the MS/MS mode, all ions with a mass-to-charge ratio different from that of the target nuclide are filtered out by Q1, thus enhancing the control over the collisions/reactions taking place in the CRC and permitting a much more efficient resolution of interferences (Figure 3.1).[107,108]

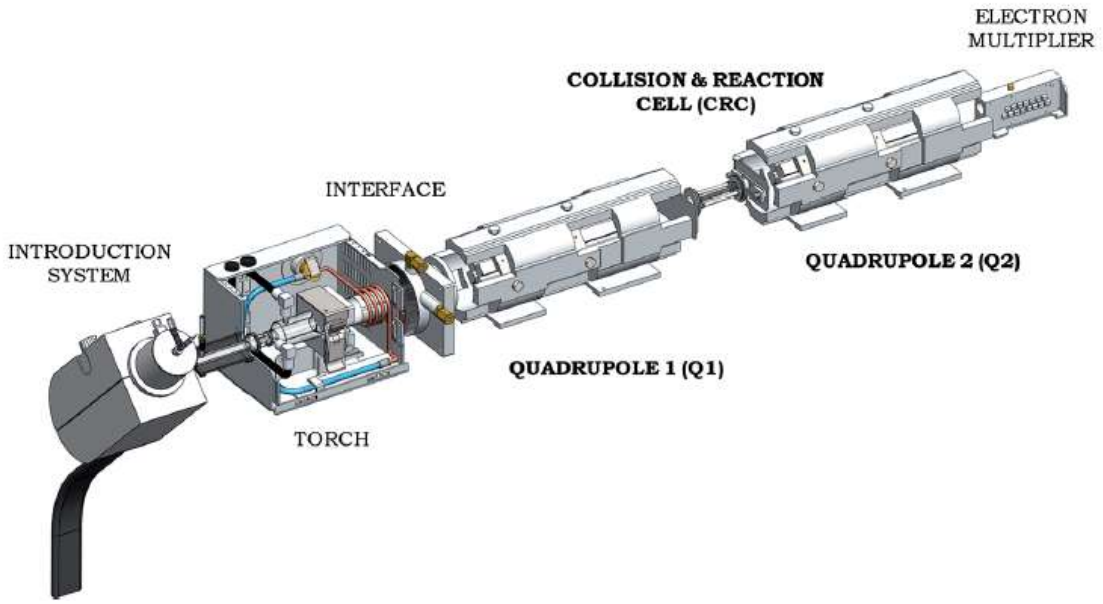

Figure 3.1: Graphical representation of ICP-MS/MS This figure is reproduced with permission of RSC from *Bolea-Fernandez et al.*[108] (https://doi.org/10.1039/C7JA00010C).

The ICP-MS/MS can be operated in two different configurations: *on-mass* and *mass-shift*. In the *on-mass* configuration, both quadrupoles have the same m/z ratio selected. The reaction of the gas and the interferent generates a product with a different m/z ratio, that is filtered out by Q2. As a result, the interference contribution to the analytical signal is eliminated. On the other hand, in the *mass-shift* approach, the selected mass on Q2 is different from the mass of the Q1. The Q1 is adjusted to let only the mass of the element of interest pass and, after reaction with the reaction gas within

the CRC, a product with a different is formed. Such m/z ratio is the only mass that the Q2 will let through and will, therefore, arrive to the detector. In this mode, the main interest is the reaction between the gas and the analyte. The parameters of the cell to induce the reaction have to be set to obtain the highest reaction yield and, consequently, achieve the best sensitivity for the analysis.[108]

Over the last years, selective ion-molecule chemistry in the CRC (usually referred to as chemical resolution) in ICP-MS/MS instrumentation has been relied on for the interference-free determination of ultra-trace concentrations of several analytes in the most diverse and complex sample matrices. In addition to the more common collision/reaction gases (e.g., He, H_2 and/or O_2), the potential of using highly reactive gases, such as NH_3 or CH_3F, has been demonstrated.[109,110] In the particular case of Si, O_2 and H_2 have been used as reaction gases for the determination of Si in different types of matrices such as HNO_3 1%, biodiesel, diesel, lubricating oils and nuclear waste glasses.[111–113] In the case of SiO_2NPs, characterization by ICP-MS/MS after separation by Field Flow Fractionation has been reported,[114] while characterization by SP-ICP-MS has only been reported by conventional quadrupole ICP-MS, using NH_3 and H_2 as reaction gases in the collision/reaction cell.[83]The objective of this chapter is to characterize SiO_2NPs by means SP-ICP-MS/MS, evaluating the effect of different collision/reaction gases in the data acquisition and NP characterization. The influence of the dwell time on the LODsize achievable for these NPs will be also studied.

3.2. Method development for interference-free determination of Si *via* ICP-MS/MS

Prior to the determination of the SiO_2NPs, method optimization for interference-free Si determination by ICP-MS/MS was carried out. In MS/MS mode, the CRC was operated under different conditions:

(i) **Vented mode.** The cell is not pressurized with any gas and both quadrupoles are set at the same m/z. This mode does not eliminate the spectral interferences and was used for comparison purposes.

(ii) **Kinetic energy discrimination (KED) mode:** The cell is pressurized with He as collision gas and both quadrupoles are set at the same m/z. Under these conditions the interfering polyatomic ions, with larger cross

sections, collide with higher frequency than the analyte ions, and thus their kinetic energy is reduced to a greater extent. The elimination of the interferences occurs by setting a kinetic energy discrimination barrier that only analyte ions should pass.

(iii) **Chemical resolution modes**: the cell is pressurized with H_2, O_2, NH_3 and/or CH_3F. The Q1 is always set at the m/z of the analyte while the Q2 might be set at the same m/z of the Q1 (*on-mass approach*) or at a different m/z (*mass-shift approach*). In the on-mass approach, the elimination of interferences occurs through chemical reactions with the interfering ions that are no longer detected at the m/z of the analyte, whereas in the mass-shift approach the chemical reaction occurs between the reaction gas and the analyte, which is then detected at a different m/z free of interferences.

In the chemical resolution mode with mass-shift detection, the mass at which the Q2 has to be set is determined *via* Product Ion Scanning (PIS). For performing a PIS, a standard solution of the analyte of interest is analyzed under the following conditions: the Q1 is fixed at the analyte m/z and the cell is pressurized with different reaction gases at different flow rates. The reactivity of the analyte towards these gases is then evaluated by performing a scan with Q2 over the entire mass spectrum (2 – 260 amu). In this particular case, this experiment was carried out with the most abundant isotope for Si at m/z = 28, and reactivity towards H_2, O_2, NH_3 and/or CH_3F was evaluated at different flow rates.

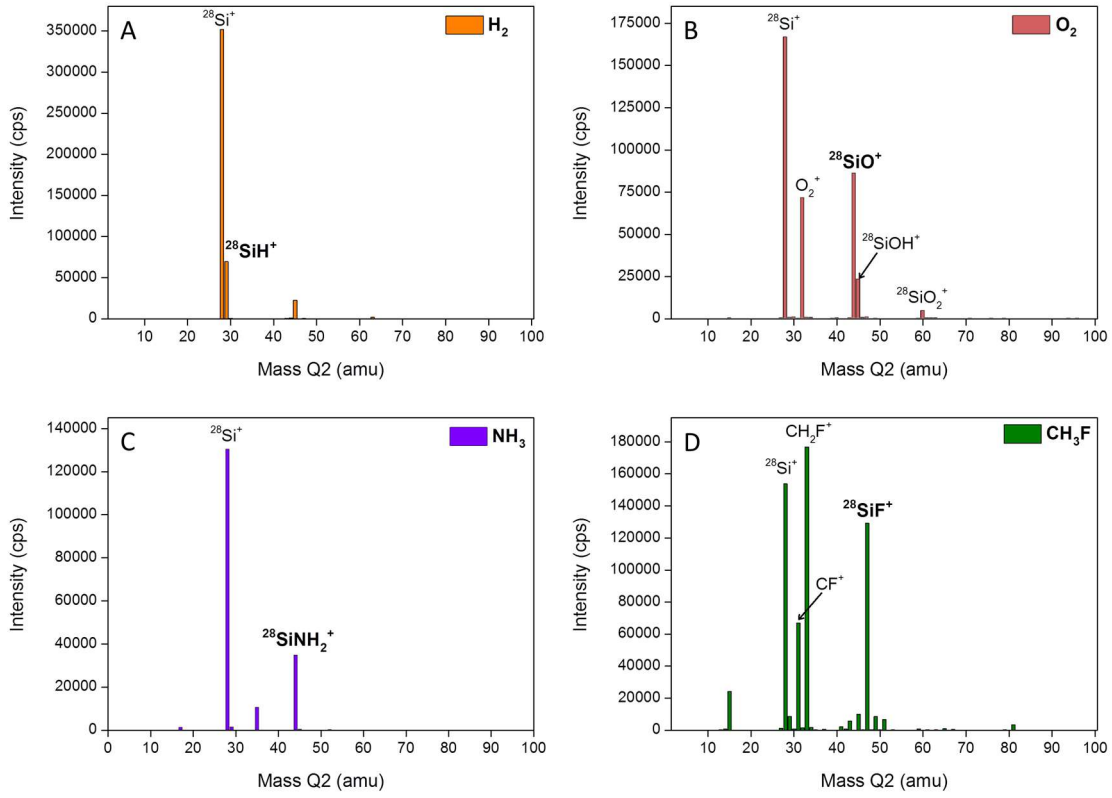

Figure 3.2: Full mass spectra in the range of interest (2 – 100 amu) obtained by product ion scanning for 10 µg L^{-1} Si standard solution with the addition of H_2 (5 mL min^{-1} - A), O_2 (0.2 mL min^{-1} - B), NH_3 (1 mL min^{-1} – C) or CH_3F (0.5 mL min^{-1} – D) reaction gases. The best suited reaction product ions finally selected are highlighted in bold.

Figure 3.2 shows an example of the mass spectra obtained in the region 2 – 100 amu (where most of the product ions appear) for the different gases used in the chemical resolution mode and using the optimum gas flow rates for maximizing the sensitivity for the reaction product ions that were finally selected (see below for details). Analysis of the full set of PIS spectra obtained at different gas flow rates allowed for the selection of the best suited reaction product ions. The reaction product ions selected for Si determination were SiH^+ (+1, m/z=29), SiO^+ (+16, m/z=44), $SiNH_2^+$ (+16, m/z=44) and SiF^+ (+19, m/z=47) with H_2, O_2, NH_3 and CH_3F, respectively. In addition to mass-shift approaches, the use of H_2 in an on-mass approach was evaluated for its capability to remove CO^+ and N_2^+ polyatomic interferences *via* reaction towards H_2. In this case, as previously cited, it is not necessary to perform the PIS analysis and the Q1 will be set at m/z = 28. For fine-tuning, the "ramp cell gas" option available in the instrument's

software was used to select the optimum gas flow rates for every method to maximize the signal-to-background ratio (intensity for 5 µg L^{-1} Si in MiliQ H_2O). Results for this optimization are shown in Figure 3.3.

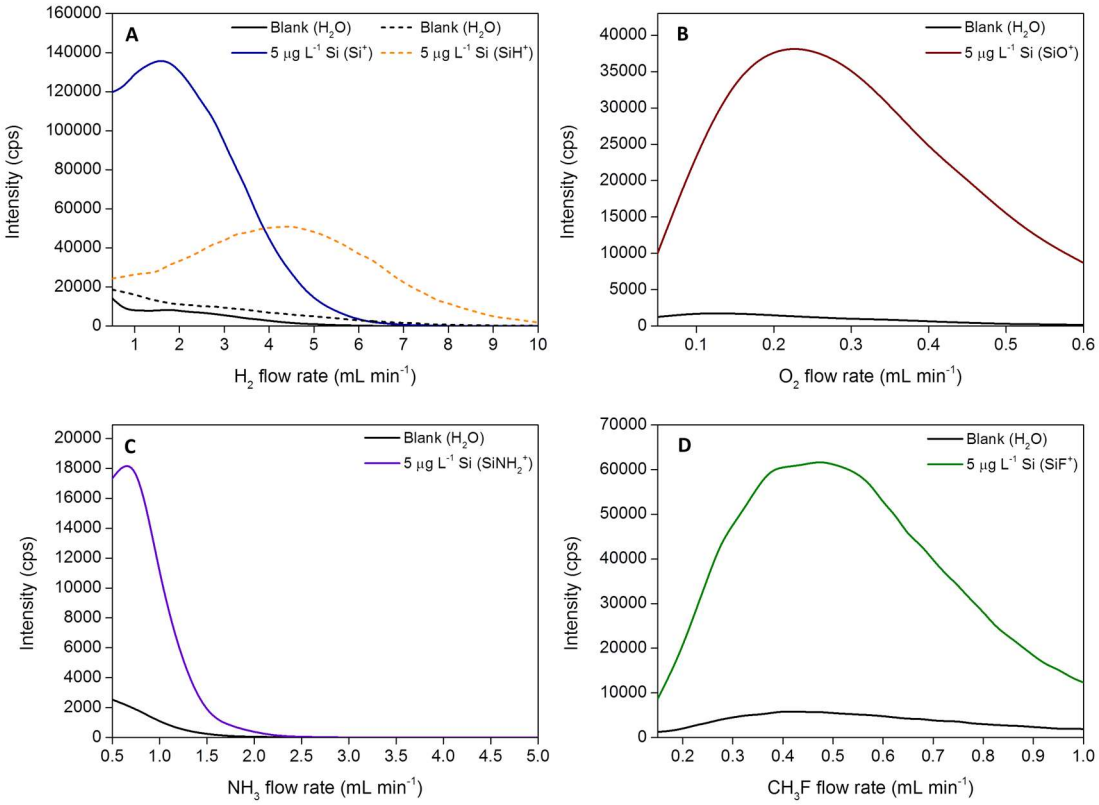

Figure 3.3: Selection of the optimum gas flow rate for the product ions selected in the case of (A) H_2 (Si^+ and SiH^+, 1.5 and 4.5 mL min^{-1}, respectively); (B) O_2 (SiO^+, 0.25 mL min^{-1}); (C) NH_3 ($SiNH_2^+$, 1.0 mL min^{-1}); and (D) CH_3F (SiF^+, 0.5 mL min^{-1}).

In this figure, the initial improvement in ion sensitivity observed at low flow rates for the H_2 can be attributed to a collisional focusing effect typical for instruments equipped with collision/reaction cells.[104,115] Despite the fact that interference-free conditions were achieved, there were still background signals above zero obtained for every m/z monitored and every reaction gas investigated. In all cases, this background signal corresponds to a Background Equivalent Concentration (BEC) of 0.29 ± 0.02 µgL^{-1} of Si, which indicates that there was a slight dissolved Si contamination in the MiliQ water used, even working in clean room conditions, an issue well documented for Si determination.[116,117] Table 3.1. summarizes the different reaction pathways of analyte and interfering ions for the different operation modes evaluated in this work.

Table 3.1. Summary of the reaction pathways of Si^+ and interfering ions for different operation modes

(1) No gas – Vented mode	**(2) Helium – He KED mode**
$^{28}Si^+ \rightarrow {}^{28}Si^+$ (on-mass)	$^{28}Si^+ + He \rightarrow {}^{28}Si^+$ (on-mass)
$^{28}CO^+ \rightarrow {}^{28}CO^+$	$^{28}CO^+ + He \rightarrow$ Removed by collisions + KED
$^{28}N_2^+ \rightarrow {}^{28}N_2^+$	$^{28}N_2^+ + He \rightarrow$ Removed by collisions + KED
(3) Hydrogen – H_2	**(4) Oxygen – O_2**
$^{28}Si^+ + H_2 \rightarrow {}^{28}Si^+$ (on-mass)	$^{28}Si^+ + O_2 \rightarrow {}^{44}SiO^+$ (mass-shift)
$^{28}Si^+ + H_2 \rightarrow {}^{29}SiH^+$ (mass-shift)	$^{28}Si^+ + O_2 \rightarrow {}^{60}SiO_2^+$ (mass-shift)
$^{28}CO^+ + H_2 \rightarrow {}^{29}COH^+ + H^+$	$^{28}CO^+ + O_2 \rightarrow {}^{44}CO_2^+$
$^{28}N_2^+ + H_2 \rightarrow {}^{29}N_2H^+ + H^+$	$^{28}N_2^+ + O_2 \rightarrow {}^{44}N_2O^+$
(5) Ammonia – NH_3	**(6) Methyl fluoride – CH_3F**
$^{28}Si^+ + NH_3 \rightarrow {}^{44}SiNH_2^+$ (mass-shift)	$^{28}Si^+ + CH_3F \rightarrow {}^{44}SiF^+ + CH_3$ (mass-shift)
$^{28}CO^+ + NH_3 \rightarrow$ No reaction	$^{28}CO^+ + CH_3F \rightarrow$ No reaction
$^{28}N_2^+ + NH_3 \rightarrow$ No reaction	$^{28}N_2^+ + CH_3F \rightarrow$ No reaction

In addition to the MS/MS mode, the different approaches developed were tested for their capabilities to avoid spectral overlap when the instrument was operated in single quadrupole (SQ) mode, in other words, with Q1 fully open. In this approach, the instrument is used as a regular ICP-MS compounded by a CRC and a quadrupole. SQ was evaluated as a possible approach in the case of the vented mode and of H_2 – on-mass only, as for O_2, NH_3 and CH_3F, the background signal was found to be very high due to the occurrence of spectral interferences at the m/z ratios of the reaction product ions selected. This may be related with the formation of unwanted product ions in the CRC, especially for highly reactive gases, such as NH_3 and CH_3F. For H_2, however, the signal of $^{28}SiH^+$ overlapped with that of other Si isotope (^{29}Si – 4.69 % abundance), thus only allowing to preserve the Si isotopic pattern by using the MS/MS mode. For 5 µg L^{-1} Si, the signal-to-background ratio for He-KED mode was found to be compromised by a strong reduction in sensitivity. This reduction was even more pronounced in SQ, and therefore, this approach was not further considered in the context of this work.

Once the different methods were optimized, calibration data and instrumental limits of detection (LODs) and of quantification (LOQs) were calculated by measuring 5

standard solutions (concentration ranging between 0 and 5 µg L^{-1} Si). The results obtained for the different operation modes are summarized in Table 3.2.

Table 3.2. Calibration data and instrumental limits of detection (LODs) and of quantification (LOQs) obtained for Si determination using ICP-MS/MS operated in different modes. LODs and LOQs were calculated as 3 and 10 times the standard deviation on 10 consecutive measurements of a blank solution (MQ H_20), divided by the slope of the calibration curve, respectively.

Gas	Mode	Approach	Q1 (amu)	Q2 (amu)	Sensitivity (L counts s^{-1} μg^{-1})	Intercept (counts s^{-1})	R^2	LoD (µg L^{-1})	LoQ (µg L^{-1})
No gas	SQ	On-mass	--	28	34800	830000	0.9996	0.90	3.00
	MS/MS	On-mass	28	28	21800	76100	0.9996	0.05	0.20
He	MS/MS	On-mass	28	28	287	471	0.9992	0.20	0.60
H_2	SQ	On-mass	--	28	43700	24300	0.9991	0.05	0.20
	MS/MS	On-mass	28	28	26900	7430	0.9999	0.02	0.05
	MS/MS	Mass-shift	28	29	4980	4240	0.9998	0.05	0.20
O_2	MS/MS	Mass-shift	28	44	8700	2470	0.9998	0.02	0.05
NH_3	MS/MS	Mass-shift	28	44	3160	948	0.9999	0.03	0.10
CH_3F	MS/MS	Mass-shift	28	47	13100	4070	0.9997	0.01	0.03

The instrumental LODs and LOQs were calculated as 3 and 10 times the standard deviation on 10 consecutive measurements of a blank solution (MQ H_20), divided by the slope of the calibration curve, respectively. For No gas and H_2, a reduction of the background signal and an improvement in the signal-to-background ratio was seen when switching from SQ to MS/MS mode, which can be attributed to a better transmission efficiency for atomic ions (Si^+) throughout the tandem mass spectrometer than for polyatomic ions (*e.g.*, CO^+ and N_2^+). Selection of the best approaches was based on the sensitivity of the corresponding method and on the ability to create interference-free conditions (best BEC approach[118]). Hence, the use of He (KED mode) and of O_2 (mass-shift – SiO^+) were considered less suitable owing to the poor sensitivity in the first case, and the possible occurrence of spectral interferences in the second (see Table 3.1.), which could become relevant in cases where the sample matrix contains higher concentrations of C and/or N, such as added nitric acid or organic solvents. In the case of O_2, it was also evaluated whether increasing the O_2 gas flow rate for monitoring SiO_2^+ as reaction product ion would result in a method suitable for Si determination. However,

although this approach was successfully applied by Gourgiotis *et al*.[113] in the context of isotopic analysis of Si for alteration studies of nuclear waste glasses, the method obtained was not sufficiently sensitive for ultra-trace Si determination.

The use of H_2 (on-mass and mass-shift) and of NH_3 and CH_3F (mass-shift) seem to be the methods of choice for the determination of Si at low concentration levels. As indicated in Table 3.2, instrumental LODs ranging between 0.01 and 0.05 µg L^{-1} were achieved using these approaches. With H_2 (on-mass), the highest sensitivity was obtained, but with CH_3F (mass-shift), the lowest LOD was provided. Thus, these two methods were selected for further SP-ICP-MS/MS method development, although results of other approaches will be provided for comparative purposes.

3.3. Analysis of SiO_2 NPs *via* SP-ICP-MS/MS with dwell times in the millisecond range

3.3.1. Detection of SiO_2NPs

Once the different approaches were optimized for interference-free determination of ultra-trace concentrations of Si, their suitability for characterizing SiO_2 NPs was evaluated. As described in the experimental chapter, NIST SRM 8013 (AuNPs) was used to determine the transport efficiency with the particle frequency method,[59] which is required in order to convert the particle detection rate obtained for SiO_2NPs into the particle number concentration. The transport efficiency was found to be 7.2 ± 0.4 %, (the standard deviation corresponds to 3 different replicates) without significant variations between experimental sessions.

For SP-ICP-MS/MS, the measurement of fast transient signals with a dwell time < 10 ms in TRA mode should enable the detection of every single NP. In this context, the dwell time is an important parameter that needs to be carefully selected considering the characteristics of the ICP-MS instrument used. In this regard, there tends to be an agreement in the SP-ICP-MS community to use dwell times of 3-5 ms as the most suitable for instruments allowing dwell times in the microsecond range.[60,72] In the particular case of SiO_2NPs, due to the occurrence of contamination issues affecting ultra-

trace Si determination, a dwell time of 3 ms was finally chosen, as this is the shortest time selectable for the Agilent 8800 ICP-MS/MS instrument. Once this selection was made, all NP suspensions to be measured with the optimized parameters were adequately diluted with MilliQ water to minimize the occurrence of double events.

The different methods developed in the previous section were tested for their capability to distinguish the number of ICP-MS intensity spikes from a given SiO_2NPs suspension from the background signal. First, the theoretical size limits of detection (LOD_{size}) for every approach were calculated as described by Laborda *et al.*,[60] according to the Equations 1.12 and 1.13 described in Chapter 1. For the standard deviation of the continuous background (S_B) calculation in each measurement mode, all of the SiO_2NPs suspensions and the water blank provided similar results, indicating that the potential effect of the introduction of larger NPs on the plasma conditions (e.g., plasma cooling)[62,73] was negligible for the range of NP sizes evaluated. Theoretical $LODs_{size}$ are summarized in Table 3.3.

However, different experimental $LODs_{size}$ may be found in the characterization of SiO_2NPs due to the dissolved Si^+ that comes from the Milli-Q water used in all the experiments, generating an experimental cut-off point between the background and the NPs distributions that is different from the value calculated by Equation 1.12. Taking this into consideration, Figure 3.4 shows the practical $LODs_{size}$ obtained from the frequency distributions for the dispersions of the smallest of the NPs tested that could be differentiated from the background. The practical $LODs_{size}$ seen from Figure 3.4 are also gathered in Table 3.3.

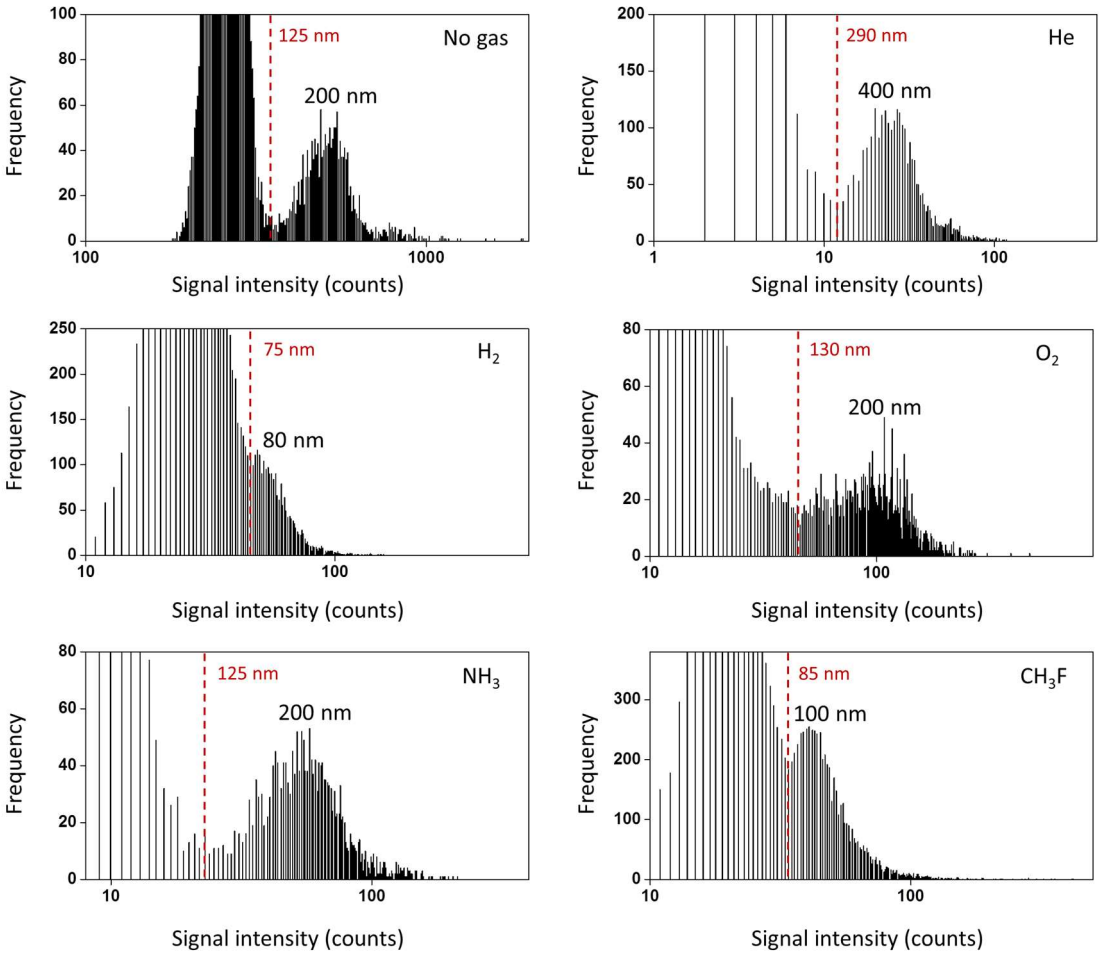

Figure 3.4. Frequency distribution for the lowest sizes detectable using the different approaches evaluated in this work. Practical $LODs_{size}$ are indicated in red in each figure. Frequency refers to the number of events of each type (background or NP) detected.

Table 3.3. Theoretical and experimental LOD_{sizes} for each reaction/collision gas

Gas	Theoretical LOD_{size} (nm)	Experimental LOD_{size} (nm)
No gas	90	125
He	160	290
H_2	50	75
O_2	80	130
NH_3	80	125
CH_3F	70	85

From these results, it is evident that practical $LODs_{size}$ are always higher than theoretical $LODs_{size}$, being especially noticeable for the He – on-mass mode. These differences are related with the relatively high intensity of the background observed in

all measurements due to slight dissolved Si contamination, as indicated before. Thus, the use of higher purity water and/or of controlled environments (such as clean room facilities) may enable smaller NPs to be detected using the same approaches. At this point, it is also interesting to point out that, in the case of no gas (vented mode), the LOD_{size} will increase with the addition of elements at the origin of polyatomic interferences (*i.e.,* N and/or C). In any case, it seems clear that the use of H_2 (Si^+, on-mass) and of CH_3F (SiF^+, mass-shift) appear to be the best approaches for SiO_2 NP characterization. Figure 3.5 shows the frequency distribution (*i.e.,* number of particles detected) of SiO_2 NPs with diameters ranging from 80 to 400 nm as a function of signal intensity (cps) when using H_2 – on-mass.

It can be seen that, while the signals for NPs with diameters of 80 and 100 nm are partially obscured by the background signal, the signals of NPs > 100 nm are found to be completely resolved by using this approach, thus enabling for the determination of their particle size, particle number concentration and mass concentration.

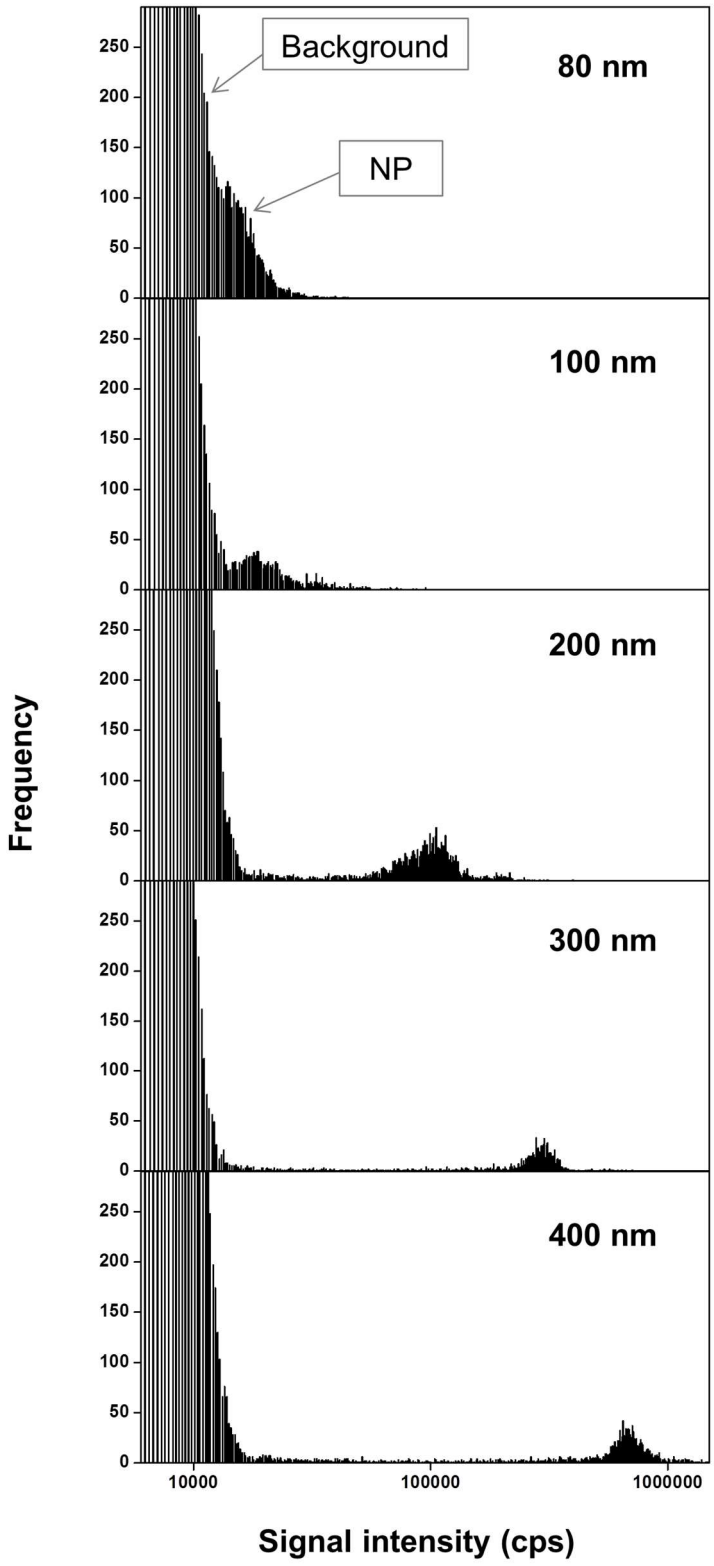

Figure 3.5. Frequency distributions of SiO_2NP suspensions (0.1 – 5 µg L^{-1}) with different NP diameters (ranging between 80 and 400 nm) when using H_2 in an on-mass approach. Frequency refers to the number of events of each type (background signal or NP) detected

3.3.2. Characterization of SiO_2NPs

As indicated before, H_2 – on-mass and CH_3F – mass-shift were the methods selected in this work for characterizing SiO_2NPs. Once detected, the ICP-MS intensity pulse generated by a single NP enables the NP mass determination and, consequently, the NP diameter, while the number of events recorded during the analysis time (frequency) allows the particle number concentration (number of particles per volume unit) determination. As previously indicated, all measurements were performed using a dwell time of 3 ms and total measuring time of 60 s. The dilution factor of each solution was calculated based on Poisson statistics[62,86] in order to minimize the occurrence of double events (2 or more NPs counted as a single event), as described in section 1.3.2.3. of Chapter 1. In this work, all the suspensions of SiO_2NPs were diluted from the original vessel within a range of 3.4×10^7 to 4.75×10^8 part L^{-1}. The dilution factors and the final particle and mass concentration used for each sample are summarized in Table 3.4.

Table 3.4. Dilution factor and final particle number and mass concentration of each SiO_2NPs dispersion measured using CH_3F (mass-shift) and H_2 (on-mass) as reaction gases in ICP-MS/MS

Methyl fluoride (CH_3F) – MS/MS – Mass-shift approach			
Particle diameter (TEM) (nm)[a]	**Dilution Factor**	**Final Particle Number Concentration (part L^{-1})**	**Final Mass Concentration (µg L^{-1})**
99.2 ± 5.8	2.00E+07	4.75E+08	0.54
197.1 ± 13.5	1.00E+07	1.10E+08	1.01
297.2 ± 11.5	4.00E+06	8.50E+07	2.60
401.0 ± 25.5	2.00E+06	7.00E+07	5.15
Hydrogen (H_2) – MS/MS – On-mass approach			
Particle diameter (TEM) (nm)[a]	**Dilution Factor**	**Final Particle Number Concentration (part L^{-1})**	**Final Mass Concentration (µg L^{-1})**
82.6 ± 4.7	1.00E+08	1.50E+08	0.10
99.2 ± 5.8	1.00E+08	9.50E+07	0.11
197.1 ± 13.5	1.00E+07	1.10E+08	1.01
297.2 ± 11.5	1.00E+07	3.40E+07	1.04
401.0 ± 25.5	2.00E+06	7.00E+07	5.15

The raw data were treated using a modified spreadsheet previously described by Peters *et al.,*[72] and described in section 2.4 of Chapter 2. The SiO_2 particle number concentration in each suspension (particles L^{-1}) was calculated considering the number of NP events detected, the transport efficiency (7.2 ± 0.4 %) and the sample flow rate (calculated prior to each sequence of analysis and corresponding to 0.34 mL min^{-1}). The NP mass was calculated following Equation 1.6 on Chapter 1, considering that the mass fraction of Si (X_a) in the NP (SiO_2/Si) is 2.14. Thereafter, the NP diameter was calculated as a function of the NP mass and its density (2.634 g cm^{-3}), assuming that SiO_2NPs has a spherical shape (Equation 1.10 on Chapter 1).

Finally, the particle size, particle number concentration and mass concentration of SiO_2NPs suspensions ranging from 80 to 400 nm were calculated for the two measurement modes tested, H_2 (on-mass) and CH_3F (mass-shift). The final size distributions for each sample and measurement mode are shown in Figure 3.6.

As already indicated in section 3.1.2.1 (Figures 3.4. and 3.5), the distributions for NPs with diameters higher than 100 nm were found to be completely resolved from that of the background signals, therefore allowing for a straightforward characterization of these SiO_2 NPs. However, for NPs of 100 nm (CH_3F – mass-shift approach) and of 80 and 100 nm (H_2 – on-mass approach), the NPs and the background distribution overlap and only a part of the NP distribution is visible in Figure 3.6. The results of particle diameter (nm), particle number concentration and mass concentration (recoveries, %) obtained with this approach are provided in Table 3.5 in the column *raw distribution*.

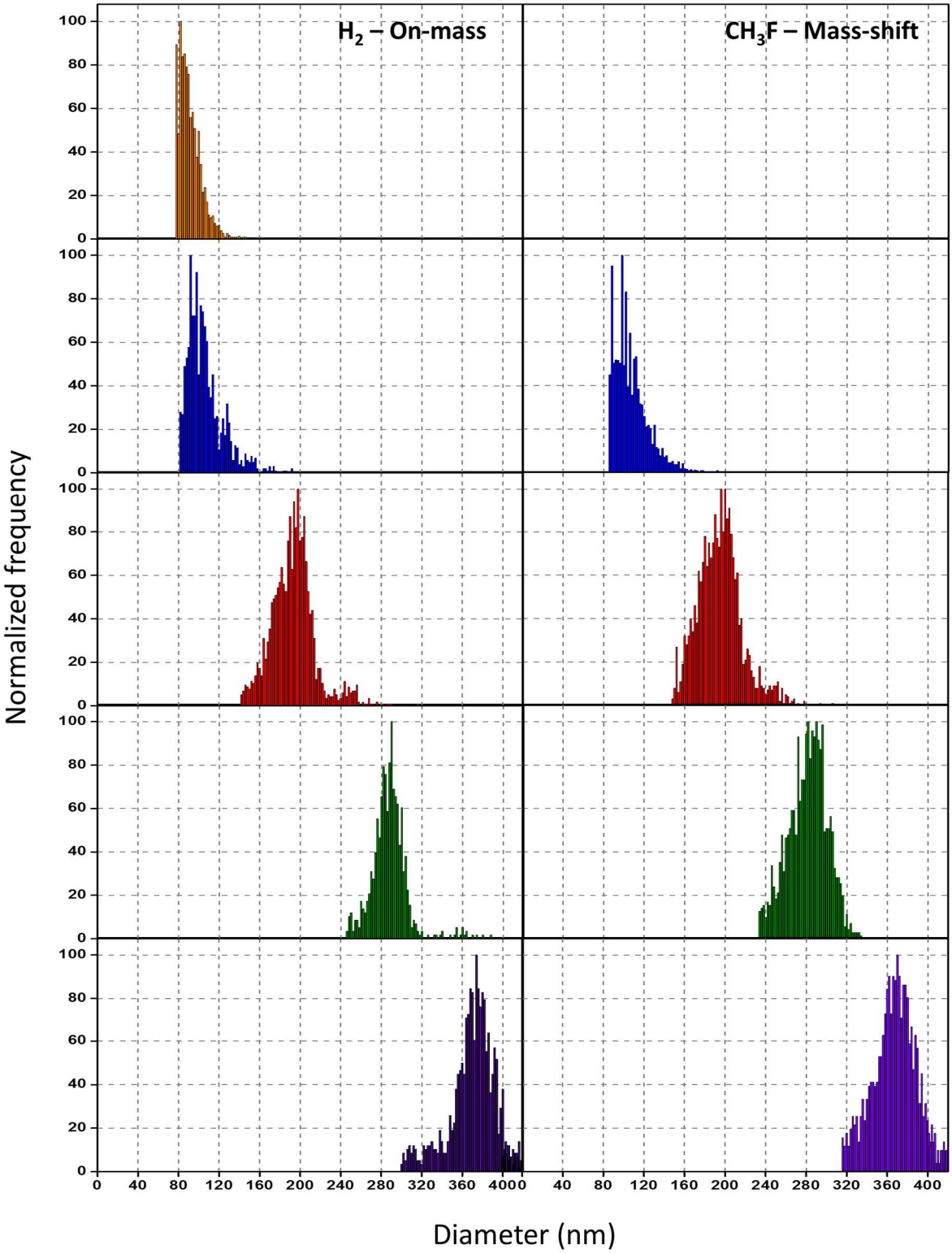

Figure 3.6. Particle size distributions calculated for SiO_2 NP suspensions of different sizes ranging from 80 to 400 nm using H_2 (on-mass) and CH_3F (mass-shift) approaches in ICP-MS/MS, with concentrations of the SiO_2 NP suspensions ranging between 0.1 – 5 and 0.5 – 5 µg L^{-1} for H_2 and CH_3F, respectively. Normalized frequency refers to the number of NPs detected of each size normalized to the number of NPs counted at the peak maximum.

Table 3.5. Characterization of SiO_2NPs using CH_3F (mass-shift) and H_2 (on-mass) as reaction gases in ICP-MS/MS

Methyl fluoride (CH_3F) – MS/MS – Mass-shift approach

Particle diameter (TEM) (nm)[a]	Particle diameter (nm)[b]		Particle number concentration Recovery (%)[c]		Mass concentration Recovery (%)[c]	
	Raw distribution	Deconvolution approach	Raw distribution	Deconvolution approach	Raw distribution	Deconvolution approach
99.2 ± 5.8	106 ± 20	94 ± 13	57 ± 2	82 ± 2	90 ± 3	94 ± 4
197.1 ± 13.5	191 ± 19	188 ± 16	94 ± 8	100 ± 8	100 ± 4	105 ± 3
297.2 ± 11.5	282 ± 24	283 ± 14	94 ± 1	100 ± 1	95 ± 1	101 ± 2
401.0 ± 25.5	378 ± 34	368 ± 12	92 ± 2	105 ± 2	95 ± 2	101 ± 2

Hydrogen (H_2) – MS/MS – On-mass approach

Particle diameter (TEM) (nm)[a]	Particle diameter (nm)[b]		Particle number concentration Recovery (%)[c]		Mass concentration Recovery (%)[c]	
	Raw distribution	Deconvolution approach	Raw distribution	Deconvolution approach	Raw distribution	Deconvolution approach
82.6 ± 4.7	90 ± 9	80 ± 10	64 ± 3	106 ± 4	100 ± 3	111 ± 2
99.2 ± 5.8	104 ± 15	93 ± 12	66 ± 2	84 ± 6	98 ± 2	94 ± 6
197.1 ± 13.5	191 ± 18	190 ± 14	87 ± 3	101 ± 2	92 ± 3	107 ± 2
297.2 ± 11.5	285 ± 15	286 ± 12	93 ± 2	97 ± 5	96 ± 2	102 ± 7
401.0 ± 25.5	381 ± 37	373 ± 16	90 ± 2	95 ± 4	96 ± 3	108 ± 8

[a] Uncertainty values for the particle diameter determined by TEM are those provided by the manufacturer and correspond to the standard deviation of the size distribution for the NPs.
[b] Uncertainty values for the particle diameter determined by SP-ICP-MS/MS correspond to the standard deviation of the size distribution for the NPs.
[c] Uncertainty values for the particle number concentration and mass concentration recoveries correspond to the standard deviation of three replicate measurements of 60 s each.

From these results, it can be concluded that this approach provides accurate NP sizing (errors below 5% for the NP diameter, corresponding to errors below 15% in the NP volume) for NPs with a nominal diameter above 100 nm, with particle number concentration and mass concentration recoveries ranging between 87.0 and 99.5%. For 80 and 100 nm, however, the results obtained with the raw distributions reflect the overlap with the background signal, resulting in lower recoveries for particle number concentrations (56.3 – 66.3 %), and the anomalous results for NP sizing. In fact, the NP diameter was shown to be significantly higher than the values obtained by TEM, which is certainly related to an incorrect average size calculation (biased high) due to the impossibility to discriminate the signals from the smaller NPs, also present in the NP

distribution, from the background. The mass concentration derived from the raw distributions was found to be less affected by this problem, which is attributed to a significant contribution of the background signal to the NP mass concentrations and to the fact that the detectable NPs are the larger/heavier ones, thus contributing to a higher extent to the final mass concentration.

In order to improve the characterization of SiO_2NPs in those cases in which the distribution partially overlaps with the background, a straightforward and user-friendly deconvolution approach using the software OriginLab was evaluated. This approach was based on a deconvolution of the overlapping distributions of both background and NP signals. The deconvolution was used to resolve or decompose the overlapping peaks into their separate components. Thus, by applying a simple deconvolution, a corrected distribution for the corresponding NPs was generated by approximating the "raw" distribution by a Gaussian function (see Equation 3.1).

$$y = y_0 + \frac{A}{w\sqrt{\pi/2}} * e^{-2\frac{(x-x_0)^2}{w^2}} \quad (3.1)$$

Where y_0 = offset, x_0 = center, w = width and A = area. The application of this deconvolution method becomes more successful as the intensity of the NP distribution peak (number of NPs detected) is maximized relative to the background distribution peak (number of events identified as background), as the software can identify and separate better both distributions. Due to the slight ionic analyte contamination and considering that this contamination is the same for all the NPs solutions (as the same Milli-Q water is used to prepare all the dilutions of this work), this could only be done by increasing the concentration of the NP suspension, in order to increase the NPs events frequency and, consequently, the peak of the NP distribution. In this case, just increasing the total measurement time would not work, as extending it would increase both peaks proportionally. However, increasing the NPs number concentration also increases the probability of occurrence of double events. Thus, as can be seen from Table 3.5, suspensions for the NPs of 80 nm using the H_2 – on-mass approach, and 100 nm for the CH_3F – mass-shift approach were more concentrated (in terms of particles L^-

[1]) for this reason. With the dilution factors used, an increased probability of double events up to 10% in the case of H_2 – on-mass, and 28% in the case of CH_3F – mass-shift was calculated; nevertheless, this option was preferred as it is the only way to obtain accurate results for the sizing of these NPs. An example of the use of this approach is presented in Figure 3.7, in which it can be seen that both background and NP distributions approximate their corresponding functions well. Therefore, the use of this approach should enable the characterization of SiO_2NPs that cannot be fully resolved from the background signal.

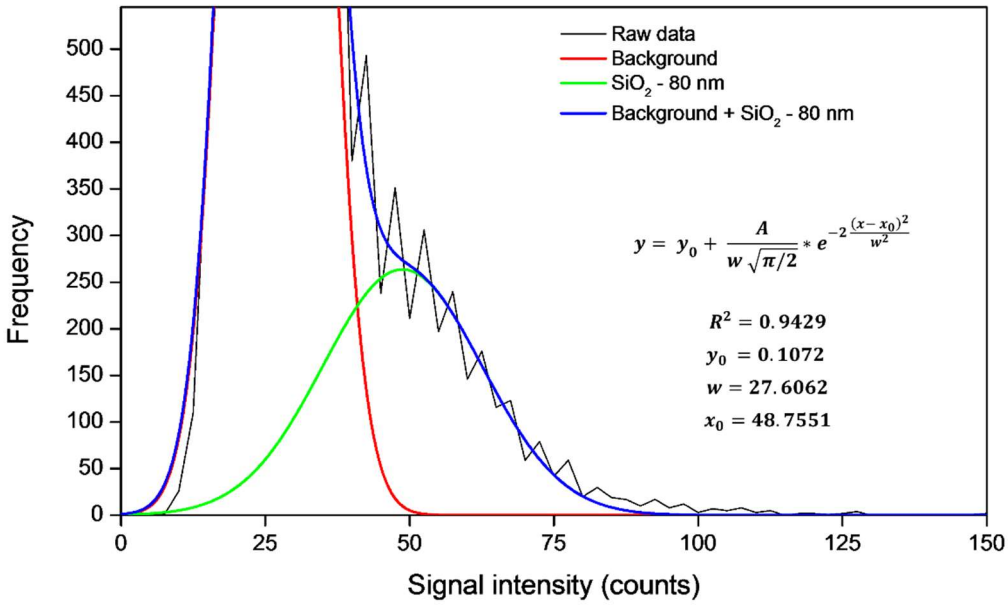

Figure 3.7. Deconvolution of the signal distribution of 80 nm SiO_2NPs, overlapping with the background signal distribution for SP-ICP-MS/MS using a H_2 – on-mass approach and following a Gaussian model.

In order to evaluate the suitability of the deconvolution approach for characterization of NP distributions, the method was also applied to SiO_2NPs with particle sizes higher than 100 nm that were fully resolved for comparison purposes, besides the SiO_2NPs distributions not fully resolved from the background, *i.e.,* 80 and 100 nm (H_2) and 100 nm (CH_3F). The results obtained are shown in Table 3.5, under the designation *deconvolution approach*. It can be seen that accurate results for particle diameter, particle number concentration and mass concentration for SiO_2NPs higher than 100 nm were achieved when applying the corresponding model to complete NP distributions, which validates the use of the Gaussian fitting for the NP distributions. For

the NP distributions partially overlapping with the background, accurate sizes were obtained in all cases, while particle number concentration deviated slightly from the expected values (82 – 106 % recoveries). This observation can be explained by the design of the experiment itself, that used an initial particle number concentration of the solutions with high probability of occurrence of double events. This fact can be seen on Figure 3.7 (80 nm SiO_2NPs with H_2 – on mass approach), where the right part of the NP distribution is not fully coincident with the model, which could indicate the existence of this second population of double events. This second distribution does not seem to significantly affect sizing of the primary distribution, and accurate results are obtained for this parameter upon application of the deconvolution model. However, the particle number concentration values cannot be 100% accurate if double events are occurring and a negative bias is expected, which occurs for 80 nm SiO_2NPs with CH_3F – Mass-shift approach and 100 nm SiO_2NPs with H_2 – on-mass approach. However, the particle number concentration recovery for 80 nm SiO_2NPs with H_2 – on-mass approach is 106%, which indicates a particle overcounting, probably due to the modelling of the functions of both distributions in the deconvolution process (only approximately 57% of the particles could be seen without the deconvolution approach, which indicated a less precise separation of the NPs and background distributions). Nevertheless, results for the particle number concentration recoveries with the deconvolution model are much closer to the expected values than with the raw distributions.

As a final test for method robustness, calibration curves (signal intensity vs. NP volume) for the different NPs measured were drawn and are shown in Figure 3.8.

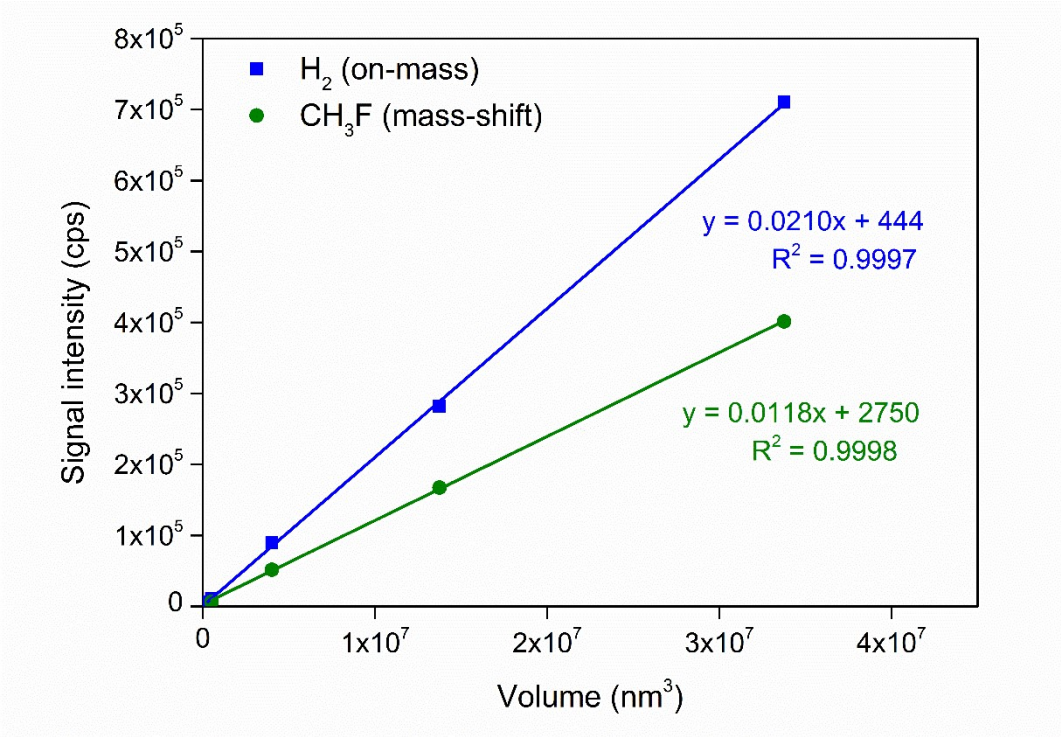

Figure 3.8. Calibration curves for the SiO_2NPs with diameters of 80 (only H_2 – on mass), 100, 200, 300 and 400 nm obtained with the H_2 – on mass and CH_3F – mass shift methods.

It has been shown that linearity for these calibration plots can be lost due to different factors, two of which have been identified as the most serious.[119] On the one hand, the linear dynamic range of electron multipliers operated in pulse counting mode is limited, although this problem can be easily solved working in dual detection mode (pulse counting and analog modes), provided adequate cross-calibration at the beginning of the measuring session.[62] A more serious problem can arise due to different degrees of vaporization/ionization for the smaller and the larger particles, which may require specific optimization of the measuring conditions for SP-ICP-MS, especially concerning forward ICP power and sample gas flow rate.[62,119] As seen from Figure 3.8, however, linear calibration curves (R^2 = 0.9997 and 0.9998 for H_2 – on mass and CH_3F – mass shift approaches, respectively) were obtained in this case covering the entire range of NP sizes studied (80 – 400 nm diameter), which is in good agreement with literature for SiO_2 NPs.[62,72,83,120] It is interesting to point out that data shown in the calibration plots were obtained on different days and that no specific optimization other than that reported in section 3.2.1 was performed for measurement of the NPs, which indicates

that the methods developed are robust for characterizing SiO_2NPs of different sizes in the range of 80 to 400 nm.

3.3.3. Effects of dwell time in the microsecond range on the LOD_{size} on the analysis of SiO_2 NPs *via* SP-ICP-MS/MS

As previously discussed, ICP-MS instrumentation has undergone several improvements over the past years, thus enabling more accurate NP characterization especially affecting limits of detection. In this part of the work, an Agilent 8900 ICP-MS/MS was used for characterization of smaller SiO_2NPs of 50 nm and 80 nm. This instrumentation presents three main advantages compared to the previous version (Agilent 8800 ICP-MS/MS) when it comes to NPs characterization:

- Possibility of working with ultrashort dwell times (minimum t_d = 100 µs);
- Elimination of the settling time in the TRA mode analysis;
- Improved sensitivity in comparison with the previous version, which helps to further improve the LOD_{size}.

Although both H_2 – on-mass and CH_3F – mass-shift methods developed in the previous section seem to perform fine for SiO_2NPs characterization, the instrument used in this part of work has no CH_3F gas line connected to the equipment, so further experiments were only carried out with H_2 as reaction gas (on-mass approach).

According to Abad-Álvaro *et al.*,[84] the LOD_{size} for the determination of NPs in presence of ions decreases with shorter t_d values. As ionic Si is expected to be found in the Milli-Q water, even when the work is carried out under clean environments, a comparison study with different dwell times (100 µs, 500 µs, 1 ms and 3 ms) was carried out in order to compare the LODsize achievable for SiO_2NPs characterization when ultrashort dwell times are used.

The NP characterization was carried using the same method described in section 3.2.2.1. First, the sample flow rate was calculated (0.34 mL min^{-1}) and the TE was determined with AuNPs 30 nm from NIST (NIST RM 8012). A TE value of 4.52 ± 0.15%, (the standard deviation corresponds to 3 different replicates) was found for this setup.

Then, the ionic calibration was performed, and the sensitivity value found was 53142 L counts s^{-1} μg^{-1}, twice the value obtained with the Agilent 8800 ICP/MS-MS (26900 L counts s^{-1} μg^{-1}). Theoretical $LODs_{size}$ determined according to Equations 1.2 and 1.3 were: 43 nm (100 µs), 54 nm (500 µs), 61 nm (1 ms) and 75 nm (3 ms). Again, practical limits of detection were calculated applying the 5σ threshold criteria measuring the SiO_2NPs dispersion of 50 nm nominal diameter (47 nm according to the certificate of analysis provided by nanoComposix). The signal intensity and particle size distributions obtained for this dispersion with the different dwell times are shown in Figure 3.9.

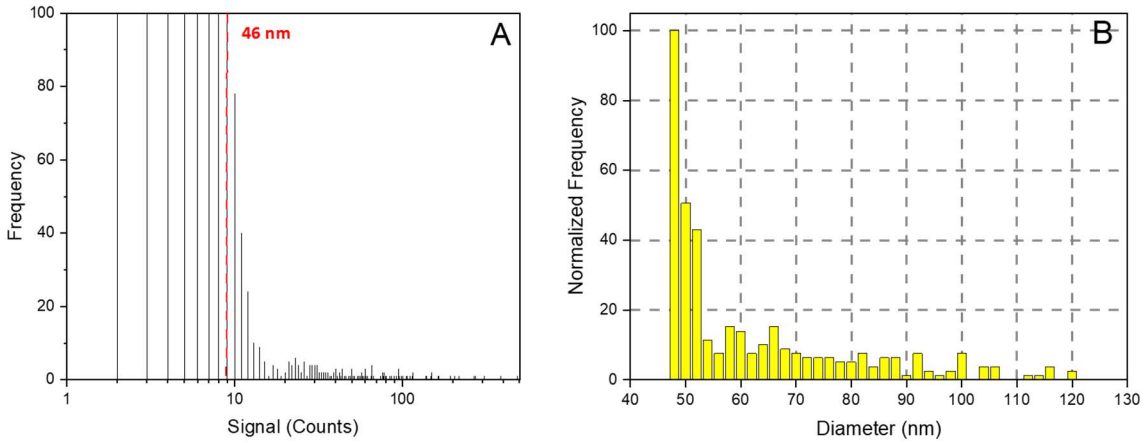

Figure 3.9. Frequency distribution with practical $LODs_{size}$ indicated in red (a) and particle size (b) distribution for the SiO_2 NPs 50 nm (H_2 – on mass) using the dwell time of 100 µs.

According to this picture, it is evident the overlapping between the background and the NPs distributions. As previously cited, the background peak intensity comes from the dissolved Si in the NPs solution, that in this case is equivalent to 0.33 ± 0.02 μgL^{-1} of Si. Furthermore, it can be observed that the experimental LOD_{size} (46 nm) is higher than the calculated LOD_{size} (43 nm). It is worth to remember that the cut-off point between NPs and background was determined by the 5σ criteria. In this case, if the 3σ criteria would have been applied, the cut-off point would be, approximately 5 counts, which is not suitable for this case, otherwise part of the background distribution would be counted as NPs. In the particle size distribution, it can be observed that the NP size ranges from 48 to 120 nm, and the most abundant size is 48 nm. This implies that less

than a half of distribution was obtained and, consequently, a full characterization of the 50 nm SiO_2NPs is not possible to be carried out with this current method.

The values of LOD_{size} also indicates the possibility of a full characterization of 80 nm SiO_2NPs with dwell times lower than 3 ms. The frequency distributions of both NPs and background can be seen in the Figure 3.10.

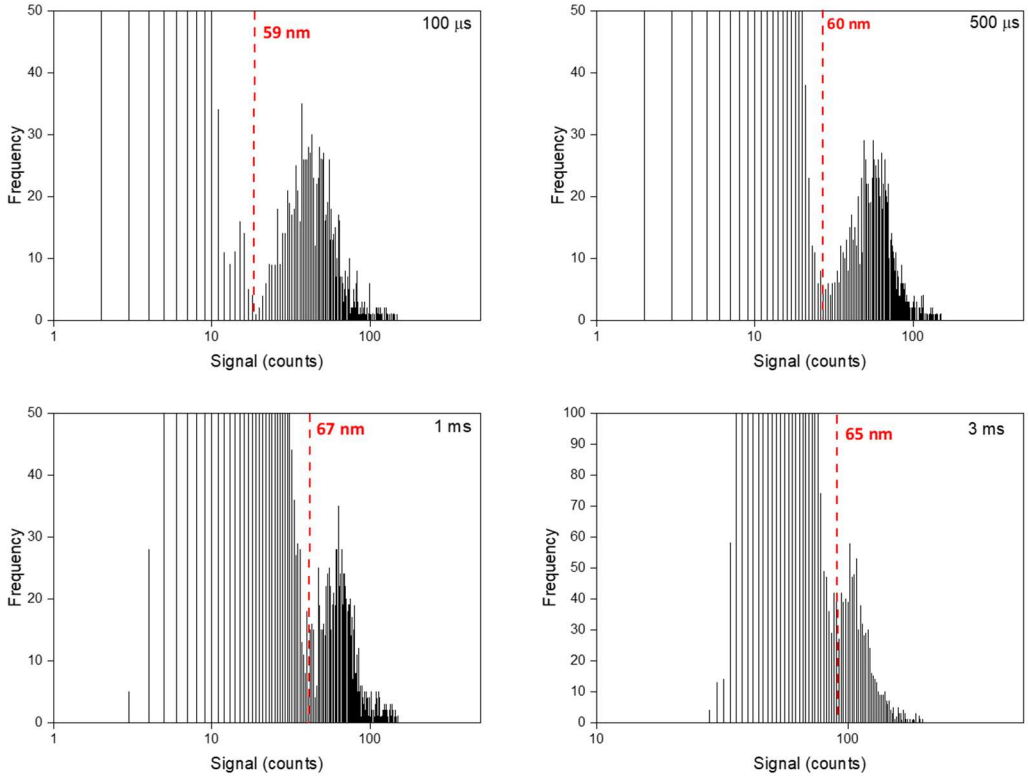

Figure 3.10. Frequency distribution with practical $LODs_{size}$ are indicated in red (for the SiO_2 NPs 850 nm (H_2 – on mass) using the dwell time of 100 µs.

It can be observed a total separation between the background and NPs distributions for dwell times in the microsecond range, whereas a slight overlap can be observed for 1 ms and a partial overlap for 3 ms. It confirms that as shorter is the dwell time, the better is the separations between the background and NPs distribution, thus better the NP characterization, as the intensity of the background is lower with shorter the dwell times while the NP intensity remains the same due to the data integration. It can be verified, therefore, the advantage of the use of dwell times in the microsecond

range to improve the characterization of 80 nm SiO_2NPs using H_2 as reaction gas with the on-mass approach by SP-ICP-MS/MS.

3.4. Conclusion

In this work, the capabilities of ICP-MS/MS using different collision/reactions gases (including He "KED" mode, and H_2, O_2, NH_3 and CH_3F "chemical resolution" modes) and no gas or "vented" mode, were evaluated for obtaining interference-free conditions for ultra-trace Si determination. After a comprehensive study, the H_2 – on-mass and of CH_3F – mass-shift modes were selected to avoid spectral overlap, providing an instrumental LODs < 15 ng L^{-1}. The methods developed were evaluated for characterizing SiO_2NPs (ranging between 80 and 400 nm) *via* SP-ICP-MS/MS with dwell times in the microsecond range. The use of a conventional approach was demonstrated to provide accurate particle size, particle number density and mass concentration for sizes > 100 nm, while for 80 and 100 nm, the distribution was found to be partially overlap with that of the background signals. Despite some dissolved Si contamination (BEC = 0.29 ± 0.02 µg L^{-1}), the use of a simple deconvolution approach following a Gaussian model enabled acceptable results to be obtained for NPs of 80 and 100 nm as well, which were at the time the lowest SiO_2NP sizes that have been detected so far *via* SP-ICP-MS/MS. Then, following the advances of the ICP-MS instrumentations that enabled working with dwell times in the microsecond range, the H_2 – on-mass was selected to characterize 50 and 80 nm SiO_2NPs. In this case, dissolved ionic Si contamination was also found (BEC = 0.33 ± 0.02 µg L^{-1}), but both background and NPs distributions were completely separated for 80 nm NPs, improving the results obtained with dwell times in the microsecond range. Even though this method improved the capabilities of characterization of 80 nm SiO_2NPs, it was not possible to fully characterizing 50 nm SiO_2NPs, mainly due to the instrumental LOD_{size} and the Si contamination, which makes the background distribution overlaps with NPs distribution.

CHAPTER 4

On the effect of using collision/reaction cell (CRC) technology in single-particle ICP-mass spectrometry (SP-ICP-MS)

- The figures and the tables shown in this chapter are reproduced with permission of Elsevier. (https://doi.org/10.1016/j.aca.2019.05.077)
- The content of this chapter is adapted with permission of RSC (https://doi.org/10.1016/j.aca.2019.05.077)

4.1. Introduction

As commented on in previous chapters and demonstrated for SiO_2NPs, SP-ICP-MS is not free from the influence of spectral interferences, which are inherent to the ICP-MS technique.[86,121,122] Although High Resolution-Sector Field (HR-SF) instrumentation is a classical alternative to overcome spectral interferences in ICP-MS,[123,124] this type of instrumentation is not routinely used for single-particle analysis.[125] In fact, most SP-ICP-MS works in the literature are developed with quadrupole instruments for which instrumental improvements and dedicated software have been developed in the past years. For these quadrupole instruments, the use of collision/reaction cell (CRC) technology is the approach of choice for addressing spectral interferences, which has become even more attractive with the introduction of tandem ICP-mass spectrometry (ICP-MS/MS) in 2012.[105,107,108,111,126–128] As previously explained in Chapter 3, ICP-MS/MS benefits from a better control over the ion-molecule processes occurring within the CRC, as a result of the double mass selection provided by the additional quadrupole located before the CRC.

However, the use of the CRC technology for overcoming spectral overlap also brings about specific challenges when aiming at operating quadrupole ICP-MS instruments in SP mode. Kálomista *et al.*[129] have recently demonstrated that pressurizing a CRC with an inert gas (for overcoming spectral overlap relying on kinetic energy discrimination – KED) influences the signal duration of a single NP event. However, no work to date has systematically studied the potential effect of introducing reaction gases to avoid spectral overlap *via* chemical resolution on NP signals, although this approach is widely used within the ICP-MS(/MS) community to achieve interference-free conditions for elemental analysis.

Peak broadening and peak shape have been extensively studied in the case of hyphenation of, *e.g.*, chromatographic techniques or Laser Ablation (LA) as a sample introduction system to ICP-MS. Detection capabilities can be strongly degraded when working with wide chromatographic peaks,[130] while in the context of LA-ICP-MS, recent efforts have been devoted to minimize aerosol dispersion aiming to achieve shorter washout times, thus providing a better imaging resolution.[131] However, peak shape and

duration was not systematically addressed in the case of SP-ICP-MS yet, most likely because the lowest dwell times attainable with previous-generation ICP-MS instrumentations did not allow well-defined peaks to be obtained, as these dwell times were usually longer than the duration of a single NP event. In other words, only recent ICP-MS instrumentation provides sufficient temporal resolution to accurately define the peak generated by a single NP event with multiple data points, instead of reporting a single data point per NP. Additionally, suitable software allowing one to accurately calculate the parameters defining a NP peak is mandatory to achieve such information. As a result, there is a common lack of information on the potential influence of introducing a CRC gas on SP-ICP-MS measurements.

In this chapter, the effects of pressurizing the CRC of two different ICP-QMS instruments (a single quadrupole and a tandem ICP-MS unit) are assessed. The instruments were operated in SP mode for the characterization of different NP types using different CRC gases: Au, Ag and PtNPs were used as model NPs while He, H_2 and NH_3 were tested as CRC gases. The conclusions from this model were further demonstrated by analyzing Fe_3O_4NPs, which strongly suffer from the occurrence of spectral interferences. From all results obtained, critical considerations on and practical recommendations for the use of CRC technology in ICP-MS operated in SP mode are provided.

4.2. Effect of the CRC conditions on the signal duration of single NP events

To assess the effect of the CRC mode on the signal duration of single NP events, different methods were developed by pressurizing the CRC system of an ICP-MS/MS (Agilent 8900 ICP-MS/MS) and of an ICP-QMS (NexION 300X) with different gases. On the ICP-MS/MS, the CRC was pressurized with He, H_2 or NH_3, and the effect on AuNPs signal duration was evaluated by comparing the results thus obtained with those obtained in no gas or vented mode. For the ICP-QMS instrument, on the other hand, the cell was pressurized only with He as in the configuration of this equipment at the time of the experiment did not allow to introduce H_2 or NH_3 as reaction gases (no getter was available). These different gases were selected aiming to assess the potential influence

of different strategies that are widely applied in ICP-QMS to overcome spectral overlap as commented on in Chapter 3: an inert gas, such as He, that can be used in the CRC to remove interferences *via* kinetic energy discrimination, and two reaction gases (H_2 and NH_3), for which a combination of collisions and reactions is relied on to overcome spectral overlap.

4.2.1. Effect of CRC mode

For this part of the work, different methods for the detection of AuNPs were developed using the Agilent 8900, an ICP-MS/MS instrument equipped with an octopole CRC, as this can be seen as the more suitable technique to study the in-cell chemistry in ICP-QMS.[108] In the case of no gas, He and H_2 modes, Au^+ was monitored at its original mass-to-charge ratio (m/z = 197 amu, on-mass mode), while for NH_3, both on-mass and the best suited product ion of the reaction between Au^+ and NH_3 (mass-shift approach) were monitored. For mass-shift method development, the reactivity between Au^+ and NH_3 was assessed in a similar way as described on Chapter 3: PIS at different NH_3 gas flow rates. $Au(NH_3)^+$ (m/z = 214 amu) was identified as best suited reaction product ion. It needs to be noted that the use of collision and/or reaction gases is (typically) not required for interference-free determination of Au,[132] and that the purpose of developing these methods was to demonstrate the influence of various CRC modes on the characterization of NPs *via* SP-ICP-MS. It can be reasonably hypothesized that the most important conclusions drawn by studying AuNPs as "model NPs" can also be extrapolated to other NP types. Table 4.1 and Figure 4.1 show the effect of the different CRC modes on the signal duration and peak shape of individual AuNP events.

Table 4.1. Average peak width (signal duration) of individual AuNP events (signal spikes) at 1, 10 and 50% of the maximum height for the different CRC modes evaluated in this work. 50 nm AuNPs were measured in all cases, except for NH3 mass-shift mode, for which 100 nm AuNPs were measured.

	1% peak width	10% peak width	50% peak width
CRC mode	**Average ± SD**	**Average ± SD**	**Average ± SD**
No gas	0.60 ± 0.10	0.40 ± 0.06	0.22 ± 0.03
No gas*	0.62 ± 0.13	0.41 ± 0.08	0.23 ± 0.04
H_2	0.63 ± 0.10	0.46 ± 0.09	0.24 ± 0.05
He	0.74 ± 0.13	0.46 ± 0.08	0.24 ± 0.04
NH_3 on-mass	2.59 ± 0.91	1.33 ± 0.79	0.49 ± 0.32
NH_3 mass-shift*	1.84 ± 0.86	1.22 ± 0.61	0.56 ± 0.13

*100 nm AuNPs were measured instead of 50 nm AuNPs.

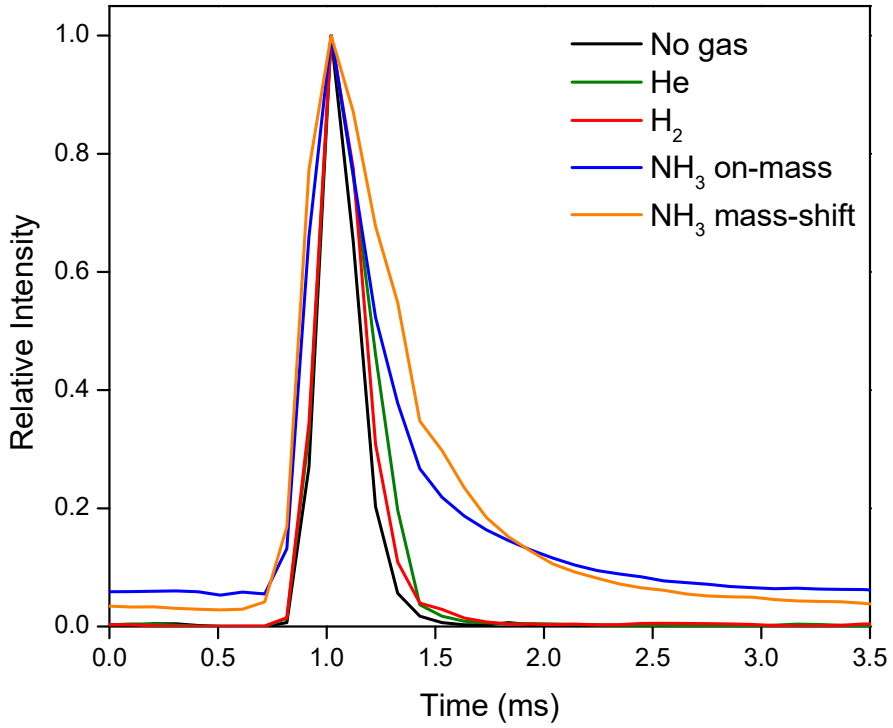

Figure 4.1. Effect of the different CRC modes on the signal duration and peak shape of individual NPs. In all cases, 50 nm AuNPs were measured, except for NH_3 mass-shift, for which 100 nm AuNPs were selected. The average normalized peak profile of approximately 1 000 NP events per CRC mode was calculated using the HDIP software.

For this experiment, highly monodisperse 50 nm AuNPs were measured using all modes, except for the NH_3 mass-shift approach, for which 100 nm AuNPs were selected due to the relatively low sensitivity of this method. To assess the potential influence of NP size on the signal duration, 100 nm AuNPs were also measured in no gas or "vented" mode, as a linear correlation between transit time of the ion cloud and particle diameter has been reported on in literature.[133] However, under the experimental conditions of this study, no significant difference was found between 50 and 100 nm AuNPs (average peak width at 1% of the maximum height of 0.60 ± 0.10 and 0.61 ± 0.13 ms, respectively), suggesting that within this NP size range and in the case of no gas mode, the influence of NP size can be considered negligible compared to the effect caused by using the CRC technology. As can be seen, also no significant difference was found between the no gas and H_2 modes (0.63 ± 0.10 ms), while a slight increase in signal duration (0.74 ± 0.13 ms) was already noticed when pressurizing the CRC with He. However, this effect turned to be drastically different when using NH_3, both for the on-mass and the mass-shift NH_3 methods, with a significant peak tailing leading to average peak widths at 1% of the maximum height of 2.59 ± 0.91 and 1.84 ± 0.86 ms for on-mass and mass-shift, respectively. In addition, Table 4.1 and Figure 4.1 also show an important peak broadening at 10 and 50% of the maximum height for both NH_3 methods, thus indicating that the effect of using NH_3 in the CRC is not limited to a longer peak tail.

These results demonstrated that the use of NH_3 gas into the CRC of an ICP-MS instrument can strongly modify the occurrence of NP events during SP-ICP-MS analysis. The significant differences between the use of NH_3 and the other CRC gases can most likely be attributed to the larger size of NH_3 molecules compared to that of H_2 molecules and/or He atoms *i.e.*, the larger collisional cross-section of the CRC gas increases the probability of collision/interaction with the ion plume created for each NP event, thus significantly disturbing the kinetic energy distribution of the ions generated from a single NP. Consequently, some of those ions might lose kinetic energy to a different extent, and thus, they will be detected at slightly different moments in time. The Figure 4.2 illustrates the effect of pressurizing a CRC system during the measurement of the fast-transient signal for an individual NP.

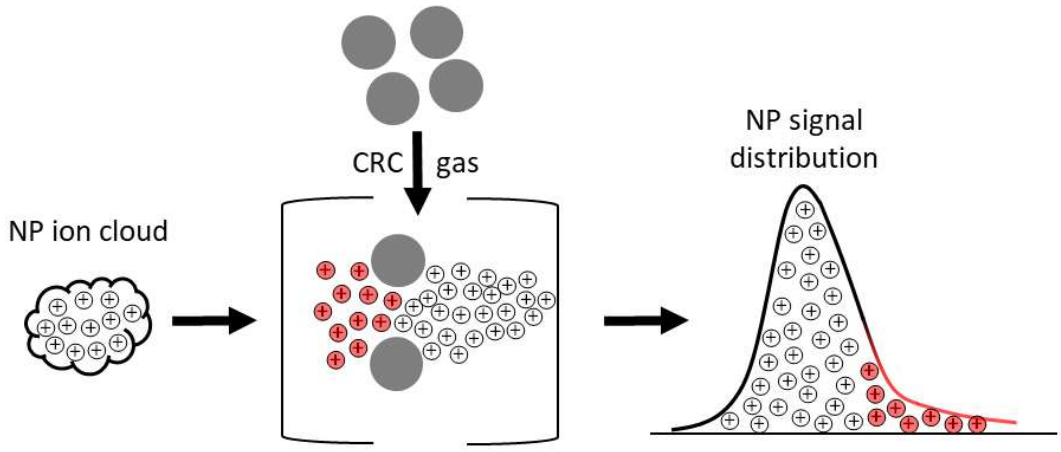

Fig. 4.2. Graphical illustration of the effect of introducing a gas in the CRC of an ICP-CRC-QMS instrument on the NP signal duration of individual NP events. The graphic shows the disturbances of the ion cloud generated by individual NPs as a result of interactions with a gas in the CRC system and the consequent effect on the NP signal distribution.

This effect explains the longer peak width and the relatively long tail observed for the AuNPs measured using both NH_3 modes. The larger standard deviations on signal duration calculated for the NH_3 methods also indicated a higher variability between NPs measured using NH_3, further supporting the different interactions between the ionic cloud and the reaction gas. The occurrence of this effect at an even larger magnitude might even split the population of a single NP event into various populations with, *e.g.*, a partially overlapped double peak, thus having a strong influence on the accurate characterization of NPs *via* SP-ICP-MS. However, the potential effect induced by the high reactivity of NH_3 gas cannot be ruled out as a potential explanation for the pronounced peak broadening observed when using this gas.

4.3. Effect of gas flow rate

4.3.1. Effect of NP size

In addition to the effect of different CRC modes, the gas pressure in the CRC or the gas flow rate may also have an influence on the signal duration of single NP events.

For evaluating this effect, Ag particles of different sizes (50, 75, 80, 100 and 200 nm) were measured using a single-quadrupole ICP-MS instrument equipped with a quadrupole CRC pressurized with He at different gas flow rates (0, 1, 2, 3, 4 and 5 mL min^{-1}). Figure 4.3A shows the signal duration as a function of the He gas flow rate for all Ag particle sizes studied. As can be seen, no significant differences in signal duration were observed in the absence of He (no gas mode – signal durations ranging from 0.76 to 0.81 ms, expressed as peak width at 1% of the maximum height), except in the case of 50 nm AgNPs for which a slightly shorter duration (0.62 ms) was found compared to all the other sizes. It needs to be noted, though, that the intensities of the NP spikes generated by 50 nm AgNPs were relatively low (7.2 counts at the maximum of the peak on average), so that the proximity to the LOD_{size} may compromise the accuracy of the signal duration measurements. Figure 4.3A indicates that the addition of He into the CRC increases the average signal duration of individual NP events proportionally to the gas flow rate for all the particle sizes, thus supporting the hypothesis of collisions between the ion cloud and the CRC gas as reason for the anomalously wide peak profiles (see Figure 4.2). In addition, Figure 4.3B shows the increase in particle event signal durations at 5 mL min^{-1} of He compared to 0 mL min^{-1} of He for the AgNPs of several sizes. The signal durations were established to be higher by a factor of 1.31, 1.44, 1.65, 2.25 and 2.95 at 5 mL min^{-1} He than in no gas mode for particles of 50, 75, 80, 100 and 200 nm, respectively. Interestingly, these results clearly demonstrated that also the particle size has an important influence on the extent of the effect exerted by using CRC technology on the signal duration of NP events. This different behavior for particles as a function of their size can most likely be explained by the denser ion cloud formed for the larger particles, thus increasing the probability of interactions with the cell gas. Thus, in addition to the CRC mode, type of gas and gas flow rate, attention also needs to be paid to the size of the particles prior to SP-ICP-MS analysis using CRC technology to overcome spectral overlap.

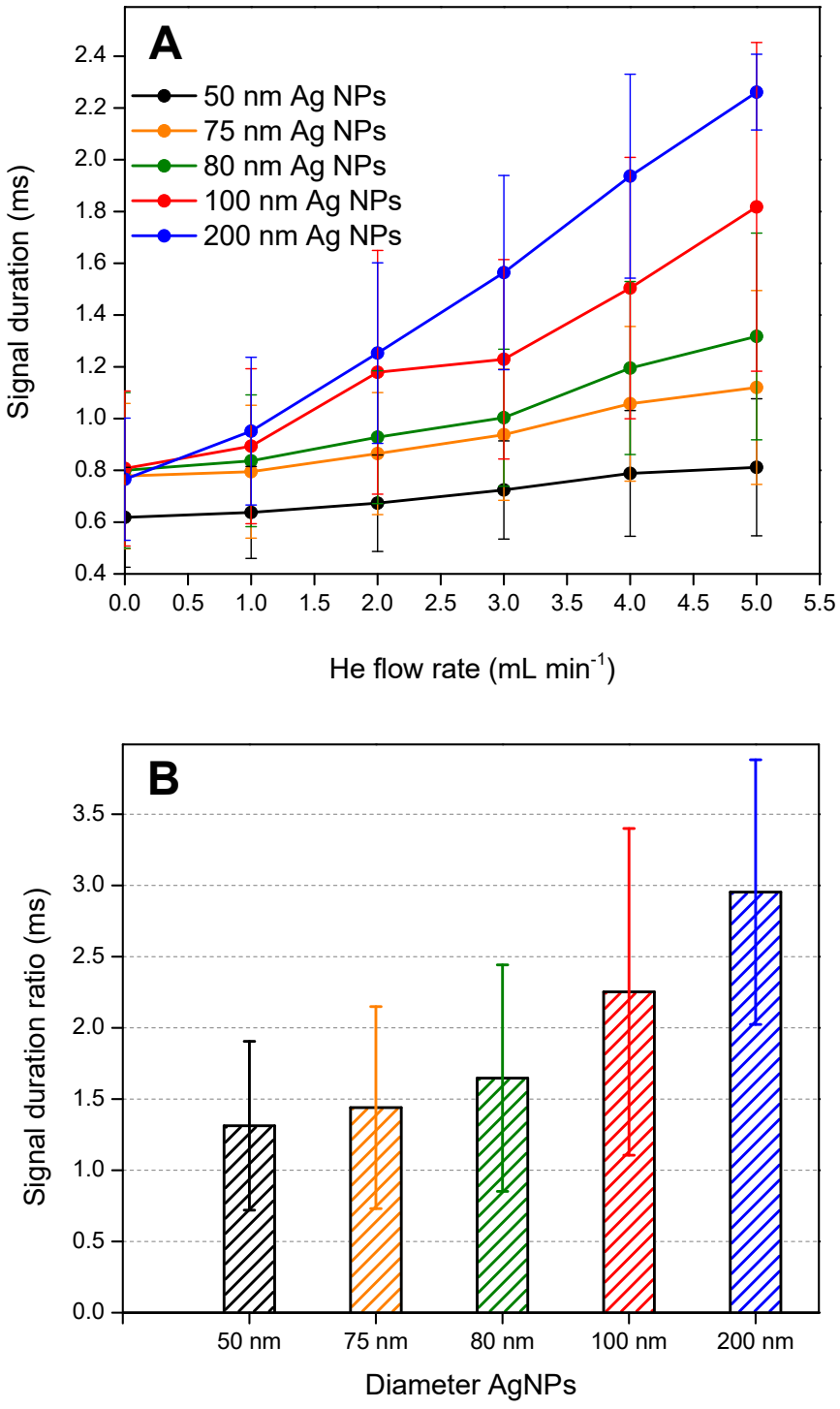

Figure 4.3. A: Increase of the signal duration as a function of the He flow rate for AgNPs of various sizes ranging from 50 to 200 nm. **B:** Increase of the signal duration ratio (NP signal duration at 5 mL min^{-1} relative to that at 0 mL min^{-1}) for AgNPs with different sizes.

4.3.2. Effect of NP type

To assess the potential effect of the chemical composition of the NPs, the signal durations for 50 and 100 nm AuNPs and for 50 and 70 nm PtNPs were measured under the same conditions as described in the previous section, *i.e.*, He gas flow rates ranging from 0 to 5 mL min^{-1}, and the results thus obtained were compared with those of AgNPs. The goal was assessing the potential differences in peak width for individual NPs with a different chemical composition, but with approximately the same diameter (Ag, Au and PtNPs of 50 nm, Ag and PtNPs of 70 and 75 nm, respectively, and Ag and AuNPs of 100 nm). Figures 4.4A (Ag and AuNPs) and 4.4B (Ag and PtNPs) show the effect of increasing the He flow rate on the signal duration for the different NP types. It is interesting to note that the results obtained in this experiment for 50 nm AuNPs were obtained using a single-quadrupole ICP-MS instrument equipped with a quadrupole CRC (0.62 ± 0.19 and 0.79 ± 0.25 for 0 and 5 mL min^{-1} He, respectively), which are not significantly different from those reported in section 3.1.1. for the same AuNPs using a tandem ICP-MS instrument equipped with an octopole CRC (0.60 ± 0.10 and 0.74 ± 0.13 for 0 and 5 mL min^{-1} He, respectively). Self-evidently, the influence of different types of mass spectrometers and/or of CRC technologies on the transit time of the ion cloud generated by individual NPs merits further study, but these results seem to indicate that the effect of introducing an additional quadrupole and/or of using different type of CRC (quadrupole *vs* octopole) might be negligible compared to the effect of adding a CRC gas.

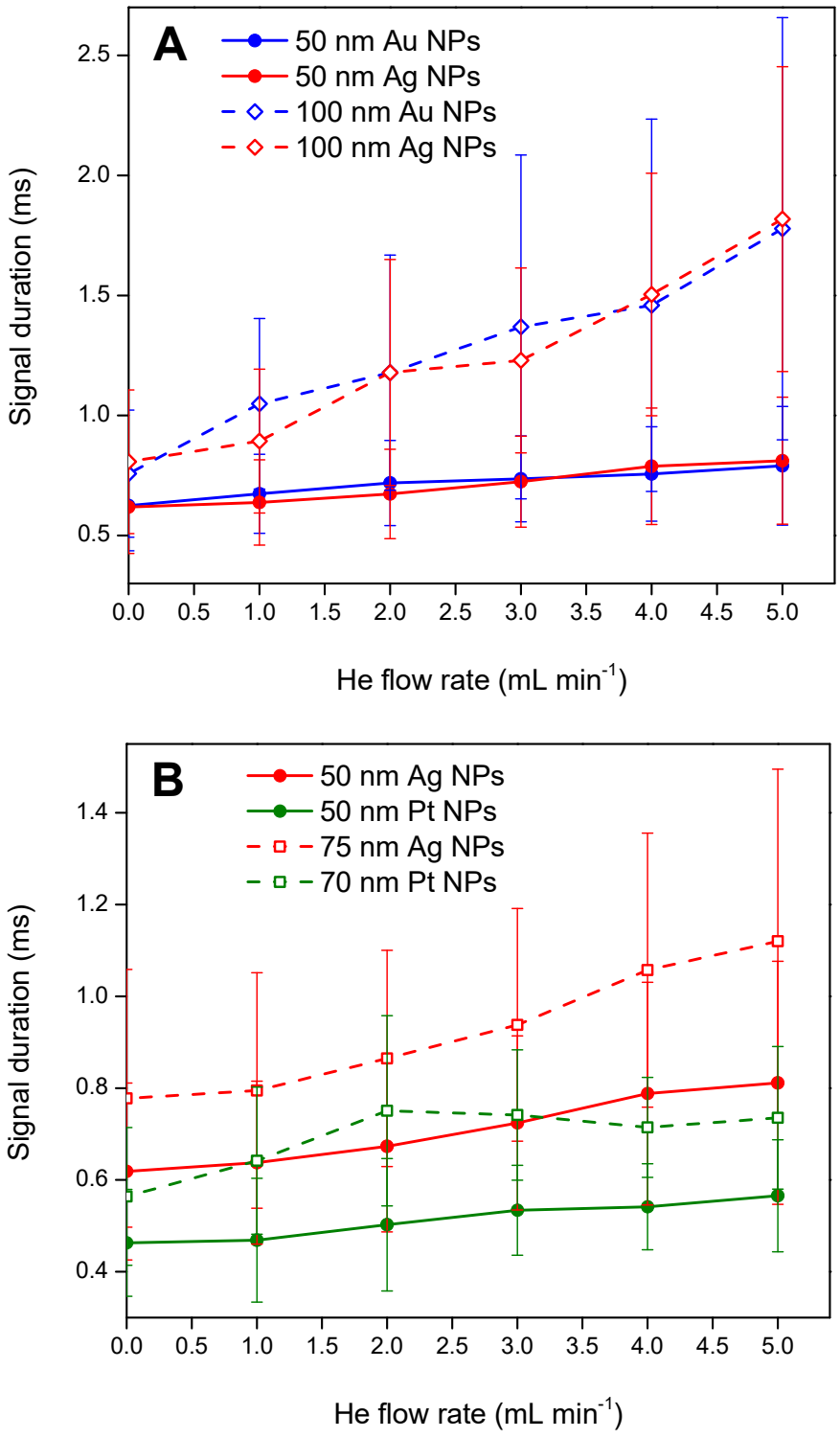

Fig. 4.4 Comparison of the signal duration of Ag and AuNPs (A) and Ag and PtNPs (B) as a function of increasing He flow rates.

In the comparison of different NP types, on the one hand, very similar results were obtained for Ag and AuNPs, both in terms of average signal duration and effect of the He flow rate. On the other hand, significantly shorter peak widths were found for PtNPs compared to AgNPs and AuNPs of the same size, while the effect of increasing the He flow also seemed less pronounced. In a previous work, Kéri *et al*.[133] reported significantly longer signal durations for AuNPs than for AgNPs and tried to attribute this difference to physical processes that can influence the transit time of the ion cloud (*e.g.*, temperature and enthalpy of melting and boiling, and/or ionization energy). However, all physical processes studied suggested that AgNPs should produce longer transient times than AuNPs, and it was concluded that, most likely, some effects occurring in the plasma (*e.g.*, charge-transfer reactions) can also contribute. In this work, the significant differences observed for PtNPs do not seem to be related with, *e.g.*, ionization energy (Au > Pt > Ag). In addition to the physicochemical properties of the constituting element, also the morphology of the NPs may influence the signal duration of single NP events. In order to shed light onto these differences, TEM images of Ag, Au and Pt NPs were obtained, and are shown in Figure 4.5.

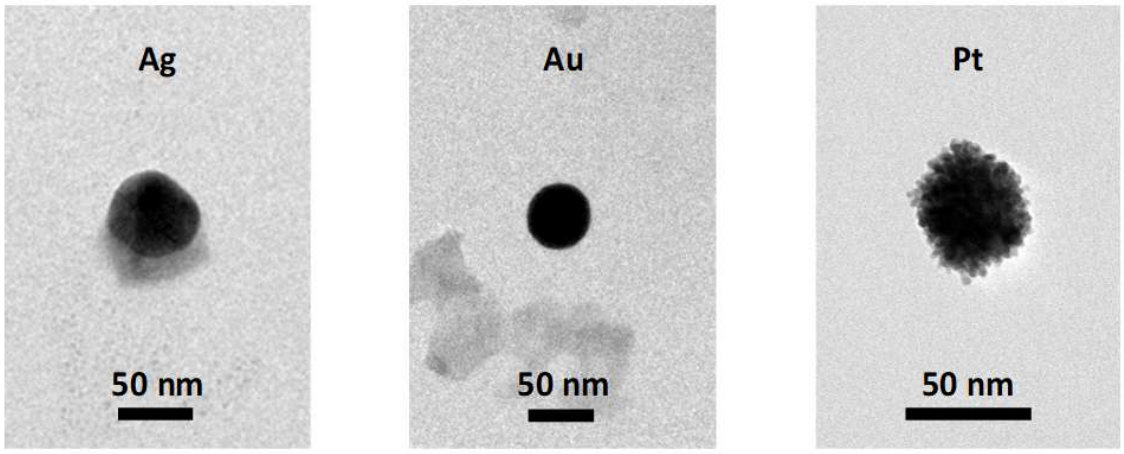

Figure 4.5. TEM images obtained for 50 nm Ag, Au and Pt NPs. It can be observed that the PtNPs are agglomerates of NPs of approximately 1 – 2 nm.

Interestingly, it was found that – in contrast to Ag and Au NPs – both 50 and 70 nm PtNPs are agglomerates of NPs of approximately 1 – 2 nm. This different morphology can be the cause of the significantly shorter signal duration established for PtNPs, although the influence of a different chemical composition and thus, different physicochemical properties cannot be ruled out. Ag and AuNPs showed a similar behavior, but both are spherical and metallic NPs from the same group within the periodic table. Thus, they are expected to have rather similar chemical and physical properties. In the case of PtNPs, the influence of the difference in chemical composition cannot be assessed, as the aberrant behavior can most likely be attributed to the different morphology. Based on these results, a full explanation for how NP type (composition) affects the signal duration of a single NP event cannot be provided, but these results suggest that the use of the temporally resolved information generated by SP-ICP-MS could also provide some nano-morphological information.

4.4. Characterization of Fe_3O_4NPs via SP-ICP-MS/MS operated in different CRC modes

4.4.1. Method development for interference-free determination of Fe using CRC technology and ICP-MS/MS

FeNPs are of the utmost interest for environmental, biological, industrial and technological applications[134–136]. Some types of FeNPs present magnetic properties and are also called magnetic nanoparticles (MNPs). MNPs interact with a magnetic field and do not present a residual field when the magnetic field is not applied. Furthermore, they are chemically stable in colloidal suspensions, biocompatible and biodegradable. In face of all these properties, new applications for MNPs have arisen, such as biomedical uses, water treatment and decontamination.[137] In the analytical chemistry field, MNPs are applied in preconcentration and separation, electrochemical detectors and magnetic separation.[138]

The characterization of FeNPs by SP-ICP-MS is hampered by the occurrence of spectral interferences, such as the ubiquitous ArO^+ polyatomic ions with the same

nominal m/z ratio as the most abundant Fe isotope (56, relative isotopic abundance of 91.75%), thus requiring the development of powerful ICP-MS methods able to address this problem of spectral overlap. Two strategies were developed for this purpose: (i) employing H_2 as a CRC gas, and (ii) employing NH_3 as a CRC gas.

(i) ICP-MS/MS method using H_2 as CRC gas

In this case, the ICP-MS/MS was set on the on-mass approach, as this gas reacts only with the interferent species and the measurement of Fe^+ ions is carried out at their original m/z ratio. The effective removal of the ArO^+ polyatomic interference can be achieved according to the following reactions:

$$Fe^+ + H_2 \rightarrow Fe^+ + H_2$$

(no reaction)

$$ArO^+ + H_2 \rightarrow ArOH^+ + H$$

(H addition – reaction mode)

$$ArO^+ + H_2 \rightarrow ArO^+ + H_2$$

(collision followed by kinetic energy discrimination – KED mode)

The optimum gas flow rate for H_2 was set at 6.5 mL min^{-1}, which was selected after optimization of the signal-to-background ratio (see Figure 4.6). After optimization, the sensitivity of this method was approximately 110 000 cps per 1 µg L^{-1} of an ionic standard solution of Fe.

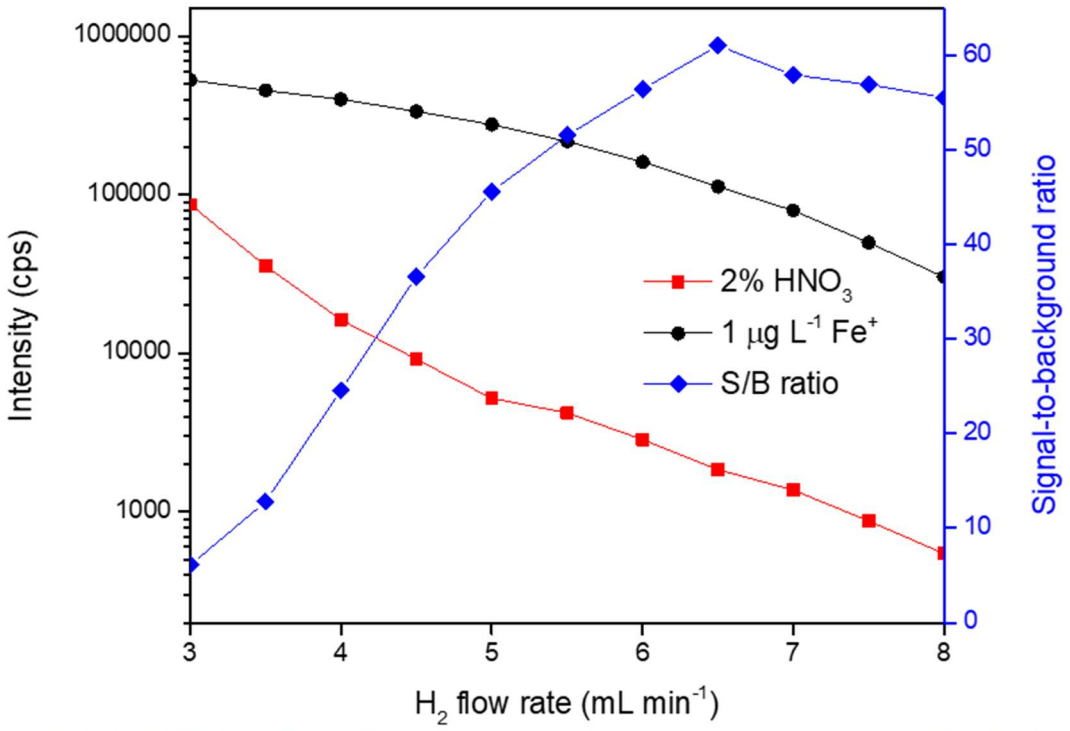

Figure 4.6. Optimization of the H_2 gas flow rate for the on-mass measurement of $^{56}Fe^+$ using the ramp cell gas option: signal intensity for 1 µg L^{-1} Fe and background signal (left y-axis, logarithmic scale) and signal-to-background ratio (right y-axis).

(ii) ICP-MS/MS method using NH_3 as CRC gas

In this method the ICP-MS/MS mass-shift approach was used, based on the formation of a NH_3-based reaction product ion ($Fe(NH_3)_x^+$).

$$Fe^+ + NH_3 \rightarrow Fe(NH_3)_x^+$$

(cluster formation – reaction mode)

It is important to note that a charge transfer reaction between the interferent species and NH_3 also occurs in this case:

$$ArO^+ + NH_3 \rightarrow ArO + NH_3^+$$

(charge transfer)

Product ion scans were performed (similarly as described in section 3.2.1) at different gas flow rates between 1 and 5 mL min^{-1} (Figure 4.7). The cluster $Fe(NH_3)_2^+$ at

m/z = 90 was identified as the best suited reaction product ion. Maximum sensitivity was obtained at 3 mL min^{-1} of NH_3.

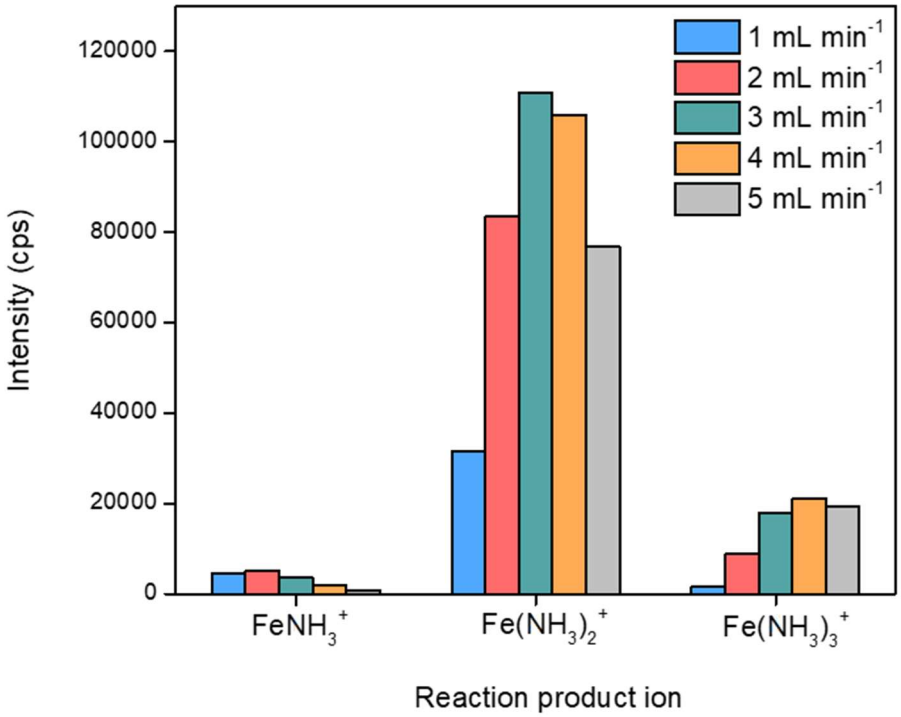

Figure 4.7: Search for the best suited $^{56}Fe(NH_3)_x^+$ reaction product ions (using a 1 µg L^{-1} Fe solution) at different gas flow rates using product ion scanning.

After optimization, the sensitivity of this method was also approximately 110 000 cps per 1 µg L^{-1} of an ionic standard solution of Fe. In addition, the effect of using the Axial Acceleration (AA) option available for the Agilent 8900 ICP-MS/MS instrument was evaluated in this approach. The AA function allows a voltage gradient to be applied to accelerate ions along the ion guide axis of the octopole, providing enhanced sensitivity when operating an ICP-MS/MS instrument in reaction cell mode. This counteracts the relatively low kinetic energy of newly created reaction product ions, reducing ion transmission efficiency due to collisional scattering or space charge repulsion. The axial acceleration voltage increases the kinetic energy of those reaction product ions, thus enhancing their transport out of the cell and into the second quadrupole.[139] The influence of AA on the signal intensities of the reaction product ion selected at different gas flow rates was studied by varying the AA voltage between -2 and +2 V (Figure 4.8).

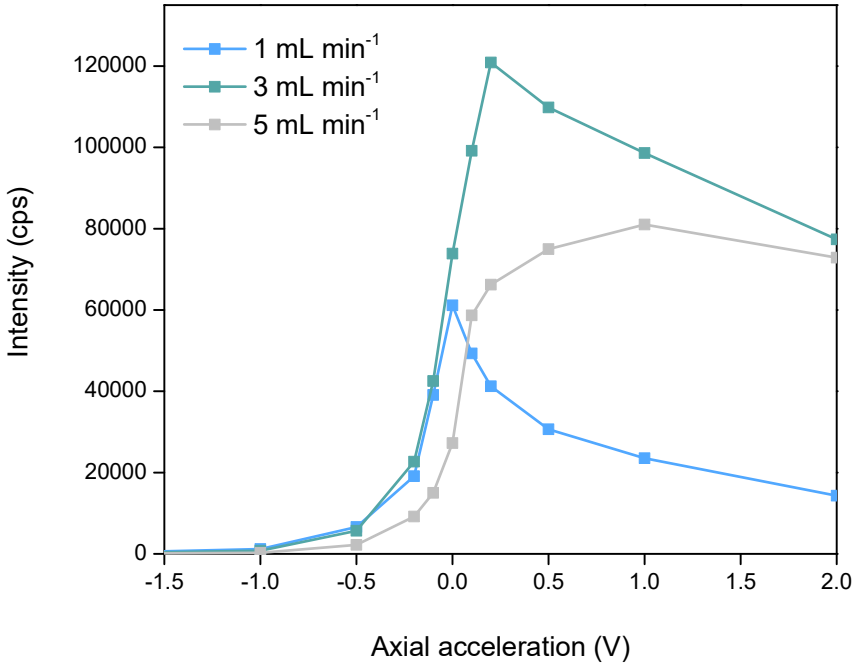

Figure 4.8: Effect of axial acceleration (AA) on the intensity of the reaction product ion selected ($^{56}Fe(NH_3)_2^+$) as a function of the gas flow rate.

It was observed that the optimum AA voltage increases with the increase of the gas flow rate (0.0, 0.1, 0.2, 0.5 and 1 V at 1, 2, 3, 4 and 5 mL min^{-1} NH_3, respectively). Based on these results, it was demonstrated that the use of higher gas flow rates in the CRC reduces the ion transmission efficiency of the reaction product ions, thus necessitating a higher AA voltage to compensate for this effect. After optimization of the AA, the highest signal intensity for $Fe(NH_3)_2^+$ was found at 3 mL min^{-1} of NH_3 and an AA setting of 0.2V (120 000 cps per 1 µg L^{-1} Fe). In this specific case, the operation of the ICP-MS/MS instrument with the AA off resulted in a reduction of the sensitivity (ion transmission efficiency) by a factor of ~2.

4.4.2. Effect of using CRC technology on the SP-ICP-MS analysis of 50 nm and 200 nm Fe_3O_4NPs

The two methods developed (based on H_2 on-mass monitoring and NH_3 mass-shift, respectively) were subsequently used to study the effect of using the CRC

technology on the characterization of 50 nm and 200 nm Fe_3O_4NPs by means of SP-ICP-MS/MS. Both methods provide approximately the same sensitivity for the interference-free determination of ^{56}Fe, and thus, they are a priori also expected to provide approximately the same NP detection capabilities when operating the ICP-MS/MS instrument in SP mode. However, while in the case of the H_2 on-mass approach, the signal spikes corresponding to individual NP events were found to be clearly separated from the background (ionic) signal for both 50 and 200 nm Fe_3O_4NPs, the use of NH_3 mass-shift did not allow to distinguish the 50 nm Fe_3O_4NP spikes from the background signal. As can be seen from Figure 4.9 (depicting the signal for individual events for Fe_3O_4NPs of 200 nm), this can be attributed to the effect of using NH_3 on the NP signal shape and height. Since the sensitivities of the H_2 on-mass and NH_3 mass-shift methods were approximately the same, the lower maximum peak height obtained for the same NPs using the NH_3-based method (160 counts) compared to that of H_2 (1500 counts) can only be explained by the more pronounced peak broadening. In contrast to the significant differences in peak height, the peak areas calculated using the HDIP software corresponded to 3900 and 3700 counts for H_2 and NH_3, respectively. In addition, it needs to be pointed out that the use of AA did not improve the situation, as similar peak widths were obtained when operating the ICP-MS/MS instrument with AA on/off.

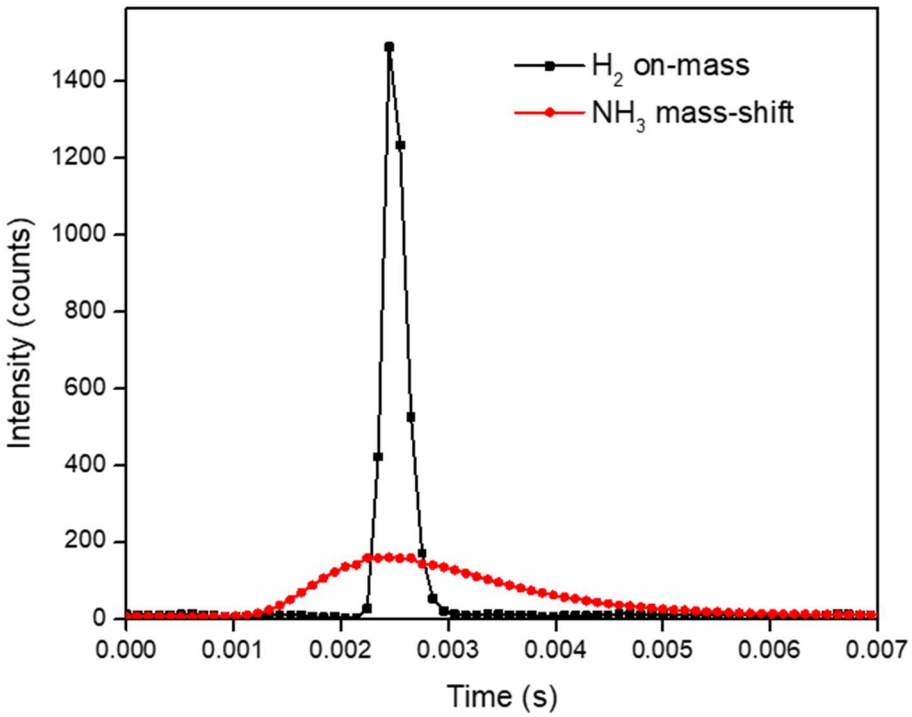

Figure 4.9: Effect of the use of H_2 on-mass and NH_3 mass-shift approaches on the NP signal duration and peak shape of 200 nm Fe_3O_4NPs. The average peak profile of approximately 1 000 NP events per CRC mode was calculated using the HDIP software.

As can be observed from Figure 4.9, a very pronounced peak broadening was observed as a result of the combination of (i) the use of NH_3 gas and (ii) the measurement of relatively large particles. As a result of these two effects, an average signal duration of 6.10 ± 1.60 ms was calculated for 200 nm Fe_3O_4NPs using the NH_3 mass-shift approach, while for the same NPs, the average signal duration was only 0.94 ± 0.49 ms when using the H_2 on-mass method.

The size distributions for 50 and 200 nm Fe_3O_4NPs obtained with the different approaches tested are shown in Figure 4.10. It is clear that the very pronounced increase in signal duration induced by the introduction of NH_3 gas into the CRC of an ICP-MS/MS instrument has a detrimental effect on the NP detection capabilities and it even precludes measuring 50 nm Fe_3O_4NPs using this approach, despite of the lower effect expected for 50 nm compared to 200 nm NPs. For 50 nm (H_2) and 200 nm (H_2 and NH_3), a very good agreement between the size distribution obtained using SP-ICP-MS/MS and the TEM results provided by the manufacturer was obtained. However, comparison of

the size distribution for the 200 nm Fe_3O_4NPs using both approaches showed a slightly wider distribution for the NH_3-based method compared to the use of H_2, while also NPs with sizes exceeding 300 nm appear when using the NH_3 mass-shift approach. This can also be attributed to the larger signal duration and the higher probability of overlap of peaks corresponding to individual NPs (double events).

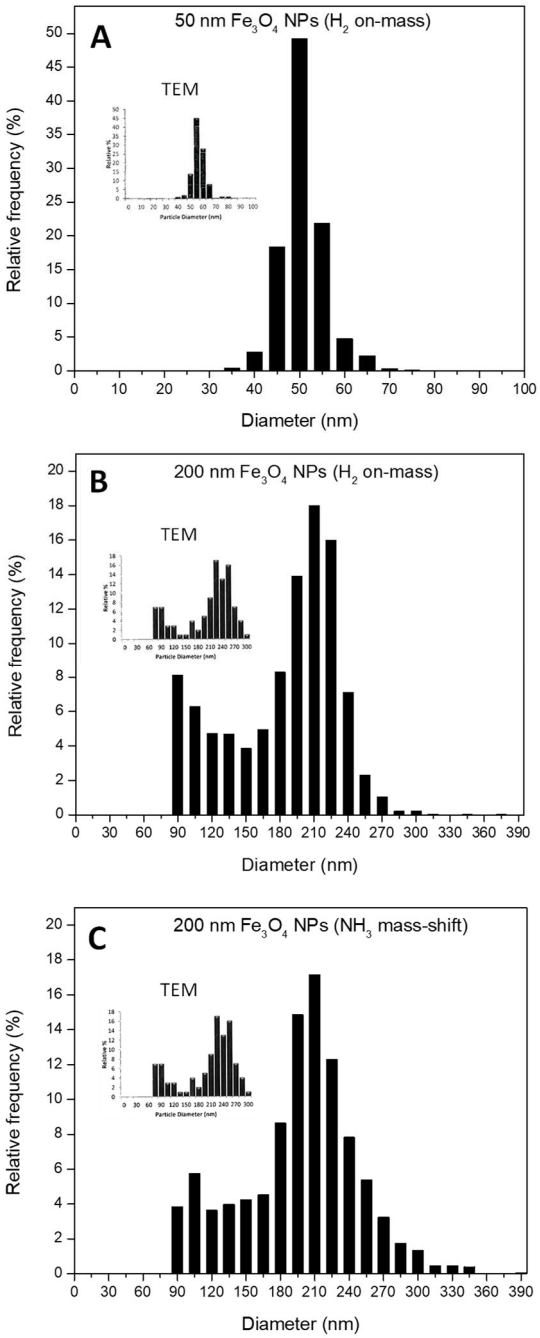

Figure 4.10: Size distribution of 50 (H_2 – A) and 200 (H_2 – B and NH_3 – C) nm Fe_3O_4NPs using SP-ICP-MS/MS. The TEM size distributions were provided by the manufacturer.

4.5. Influence of the signal duration on the accuracy of the SP-ICP-MS measurements

The increase of the transit time of the NP ion cloud as a result of the use of CRC technology in ICP-QMS instrumentation exerts a detrimental effect on the SP-ICP-MS analysis, thus necessitating the application of some additional measures to minimize the consequences in terms of accuracy of the NP size, particle number concentration and mass concentration results. The occurrence of double events might be seen as one of the consequences of an anomalously high NP signal duration. In SP-ICP-MS, the NPs are randomly distributed in the diluted aqueous dispersions, and these dispersions should be sufficiently diluted to avoid that two or more particles are detected at the same time. As previously discussed Poisson statistics can be used to estimate the probability of one or more than one particle reaching the plasma in a fixed time interval (Equation 1.2)[59,62,84,86]. In this equation, the parameter λ can be calculated using the following equation:

$$\lambda = Q_{NP} \times t = C_{NP} \times Q_{sam} \times \eta_{neb} \times t \quad \textbf{(4.1)}$$

Where C_{NP} is the particle number concentration, Q_{sam} is the sample flow rate, η_{neb} is the nebulization efficiency and t is the fixed period of time. This time has been considered as the dwell time (t_{dwell}) when working in the millisecond range, and as the peak width of the transient signal (w_{peak}) when working in the microsecond range (generally established at 0.5 ms). However, the assumption of a signal duration of ~0.5 ms is not valid when using CRC technology to avoid spectral overlap, as previously demonstrated. The peak widths obtained using this approach can range from 0.5 to 2.2 ms for larger Au and AgNPs and 6 ms for Fe_3O_4NPs. In order to further illustrate the effect of this longer signal durations on the probability of more than one event occurring within the same time interval (particle coincidence), the probabilities were calculated at different NP fluxes (5, 20 and 50 s^{-1}) and peak widths (0.5, 1, 2.5 and 5 ms) based on Poisson statistics and the corresponding results are shown in Table 4.2.

Table 4.2. Probability of particle coincidence of more than one nanoparticle (%) at different NP fluxes and peak widths calculated based on Poisson statistics.

	NP flux (Hz)		
Peak width (ms)	**5**	**20**	**50**
0.5	0.00031	0.0050	0.031
1.0	0.0012	0.020	0.12
2.5	0.0077	0.12	0.72
5.0	0.031	0.47	2.6

According to the previous table, it can be seen that for conventional NP fluxes, for instance 20 Hz, the probability of particle coincidence increases approximately 2 orders of magnitude for NP events with a peak width of 5 ms compared to 0.5 ms. This increase in the probability of particle coincidence will result in an underestimation of the particle number concentration and an overestimation of the NP size. Depending on the type of software used for NP data treatment, two individual NP events can be resolved, even if they partially overlap, as shown in Figure 4.11A. In this specific case, accurate results can still be achieved for the particle number concentration, but incomplete peak areas will lead to inaccurate NP sizes. A further refinement of this approach would lie in deconvolution of overlapping peaks, although the asymmetry of the NP peaks poses additional challenges. Therefore, an estimation of the signal duration of individual NP events prior to SP-ICP-MS using CRC technology is recommended in order to select an appropriate dilution factor. However, this approach requires an increase of the total measurement time to avoid inaccurate results because of poor counting statistics.

In addition to the occurrence of particle coincidence, the SP detection capabilities (LOD_{size}) can also be affected by pronounced peak broadening, as shown in the Figure 4.11B. The overlap of the signal from the NP with that of the background can potentially hamper the detection of the smallest NPs. As a result, the average NP size determined could be biased high, while an inaccurate particle number concentration will be obtained as a result of the counting of only the larger NPs.

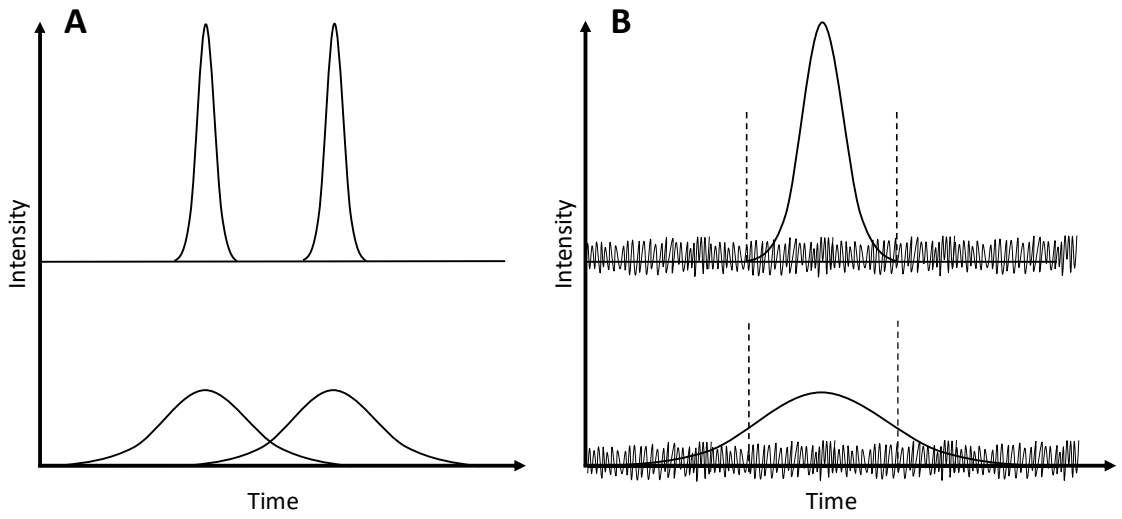

Fig. 4.11. (A) Probability of occurrence of double events (particle coincidence) as a function of the signal duration of individual NP events and (B) effect of signal broadening on the accuracy of NP characterization and their LOD_{size}.

In addition to the direct effect on the accuracy of the NP characterization, it needs to be noted that the use of some approaches reported on in the literature to calibrate the NP size based on the use of the NP signal durations can also be affected when using CRC technology.[133] If such approaches are intended, it has to be considered that the duration depends on the size and the collisions/interactions between the ion cloud and the CRC gas, and thus, higher variations are expected.

4.6. Conclusion

The use of CRC technology in SP-ICP-MS with quadrupole-based instrumentation is mandatory for those NPs strongly affected by the occurrence of spectral overlap (e.g., Fe_3O_4NPs). However, this work has demonstrated (using two different instrument types) that the introduction of a gas into the CRC has an important effect on the signal duration of a single NP event. The use of different CRC modes revealed that gases with a larger collisional cross-section (e.g., NH_3) induce a more pronounced peak broadening than do gases with a smaller one (e.g., He and H_2). In addition, the gas pressure in the CRC (determined by the gas flow rate) and even the type and morphology of the NPs might

influence the transit time of the NP ion cloud through the mass spectrometer. These conclusions have been further illustrated by the characterization of Fe_3O_4NPs, which are strongly affected by the occurrence of spectral interference. The detrimental effect of using a NH_3 mass-shift approach did not enable 50 nm Fe_3O_4NPs to be distinguished from the background signal, while this was not found to be the case when using a H_2 on-mass approach. The effect was found to be most pronounced for larger particles, and thus, the characterization of NPs of smaller dimensions are less affected by the use of CRC technology. To minimize the effect for larger particles, light gases and low gas flow rates are recommended. In addition, the effect of a longer NP signal width on the accuracy of the SP-ICP-MS measurements, such as higher probability of particle coincidence, higher LOD_{size}, inaccurate size distribution, particle number density and mass concentration results has been described into detail. This effect, however, could also be exploited for multi-isotope monitoring using sequential ICP-MS instrumentation operated in SP mode.

CHAPTER 5

Overcoming matrix effects on SP-ICP-MS: Matrix-matching of ionic calibration for AgNPs characterization in complex matrices

5.1. Introduction

As discussed in chapter one, the most common calibration approach used in SP-ICP-MS to quantify the NP mass (and consequently, NP diameter) and particle number concentration is based on the use of (aqueous) standard solutions of the analytes in the ionic form plus determination of the transport efficiency (TE). In this way, a mass-flux calibration curve is measured with ionic standards, taking into account the TE value for determining the values in the x-axis.[59,62,73] This approach, however, and similarly to any calibration carried out with ICP-MS, is also subjected to potential matrix effects, especially when complex matrices are targeted. It is important to point out that most SP-ICP-MS studies in the literature have been conducted with NPs on water or non-complex media, which is not prone to induce matrix effects. In fact, the direct analysis of NPs in complex media remains a big challenge on SP-ICP-MS that has not been fully addressed so far.

There are different approaches to surmount matrix effects in ICP-MS, which include different strategies of sample pre-treatment, use of different sample introduction systems, instrument optimization and use of different calibration strategies, such as internal standardization, standard addition, isotope dilution or matrix-matched calibration.[140] Application of these possibilities to SP-ICP-MS is not straightforward in some cases (e.g. internal standardization or isotope dilution would require the simultaneous measurement of two isotopes for a single NP). The use of matrix matching for SP-ICP-MS has been recommended in some papers,[141] but this possibility has not been systematically evaluated in the literature. Montaño *et.al.,*[73] for instance, reported in a review article different sensitivities for ionic gold and AuNPs in different matrices and deionized water media, and pointed out that the effects of using matrix-matching on the accuracy of NP sizing needed further assessment. Liu *et al.*[141] investigated matrix effects on the signals for AgNPs and Ag^+ with diluents that simulate biological and environmental media, such as water, 1 mM tris(hydroxymethyl)aminomethane, borate buffer, sodium carbonate buffers solutions, 1 mM sodium citrate, 1 mM sodium chloride, 1 mM glutathione and 0.1 mM sodium sulphide. The authors verified losses in the ionic signal due to the interaction of Ag^+ with matrix compounds, whereas the NP intensity remained the same among all the tested media, and hence matrix-matching was not

recommended. Finally, Vidmar *et.al.,*[142] on a study on different strategies for biological tissues pre-treatment for NP determination, investigated the potential use of matrix-matching for the ionic calibration for Ag and AuNPs characterization after alkaline and enzymatic digestion. NPs were suspended in ultrapure water, 1.0% Tetramethylammonium hydroxide (TMAH) and enzyme solution. In this case, differences in the transport efficiencies were reported for the different media, although the authors did not recommend the use of matrix-matching as better results (in terms of mass recovery and particle size) were obtained if calibration was conducted with ionic standards in ultrapure water. However, no systematic study of these effects was conducted.

The aim of this part of the work was investigating the effect of matrix-matching the ionic calibration standards for NP determination in complex matrices by SP-ICP-MS, using AgNPs extracted from biological tissues as a model for the study. In fact, AgNPs are one of the most used types of NPs worldwide, being well-known by their antibacterial and antimicrobial activity. This property has expanded their application to a wide variety of goods mostly related to medical, hygiene and food applications.[11] As a consequence of the intense use of AgNPs, the possibility of human and environmental exposition has increased, bringing about a higher circulation and accumulation of this nanomaterial in diverse environmental systems, human and animal tissues.[11,143]

Analysis of AgNPs in biological tissues is commonly carried out after alkaline or enzymatic extraction,[142,144,145] and TMAH, with or without the presence of Triton X-100 to avoid aggregation of AgNPs, is one of the most popular extraction media.[144,146] The aim of this work is to perform a systematic study about the capabilities of matrix-matched calibration approach to characterize AgNPs in TMAH + Triton X-100 media, resulting from the alkaline extraction of NPs from blood and other biological tissues.

5.2. AgNPs extraction from blood and biological tissues

This matrix-match ionic calibration study was conducted in the context of a larger study carried out at LGC (London) for extraction of Polyethylene Glycol (PEG)-coated

AgNPs from blood and biological tissues. These AgNPs are used in medical devices due to their antibacterial properties and may be released into the blood stream and/or accumulate in tissues, thus generating safety concerns. Before the study, PEG coated AgNPs samples were characterized in-house for their size and particle number concentration. Thereafter, the AgNPs samples were spiked in Seronorm^{TM} Trace Elements in whole blood, level 2 from Sero AS and pig brain from a local butcher.

A set of extraction conditions was investigated by LGC, such as extraction reagent's concentration, or storage conditions for NP stability. The critical parameter was found to be the reagent's concentration, with optimum values of 25% w w^{-1} TMAH for tissue digestion and 15% w w^{-1} TMAH for blood. For SP-ICP-MS determination, all samples had to be diluted 10 times and 0.1% w w^{-1} of Triton X-100 was added.

Therefore, for this reason, the chosen matrix-match for SP-ICP-MS analysis in this chapter was 2.5% w w^{-1} TMAH + 0.1% w w^{-1} Triton X-100.

5.3. Ionic Calibration in different media for AgNPs characterization

As a previous study to the AgNPs characterization, 3 different calibration curves were produced in the following media: 1 mM citrate (most commonly used NPs coating and stabilizer), 1% v v^{-1} HNO_3 (most commonly used media for SP-ICP-MS ionic calibration) and 2.5% w w^{-1} TMAH with 0.1% w w^{-1} Triton X-100 (matrix-matched media, commonly used for NPs extraction *via* alkaline digestion). The measurements of the 3 curves were performed in 3 different days, in which each curve is represented in the Figure 5.1.

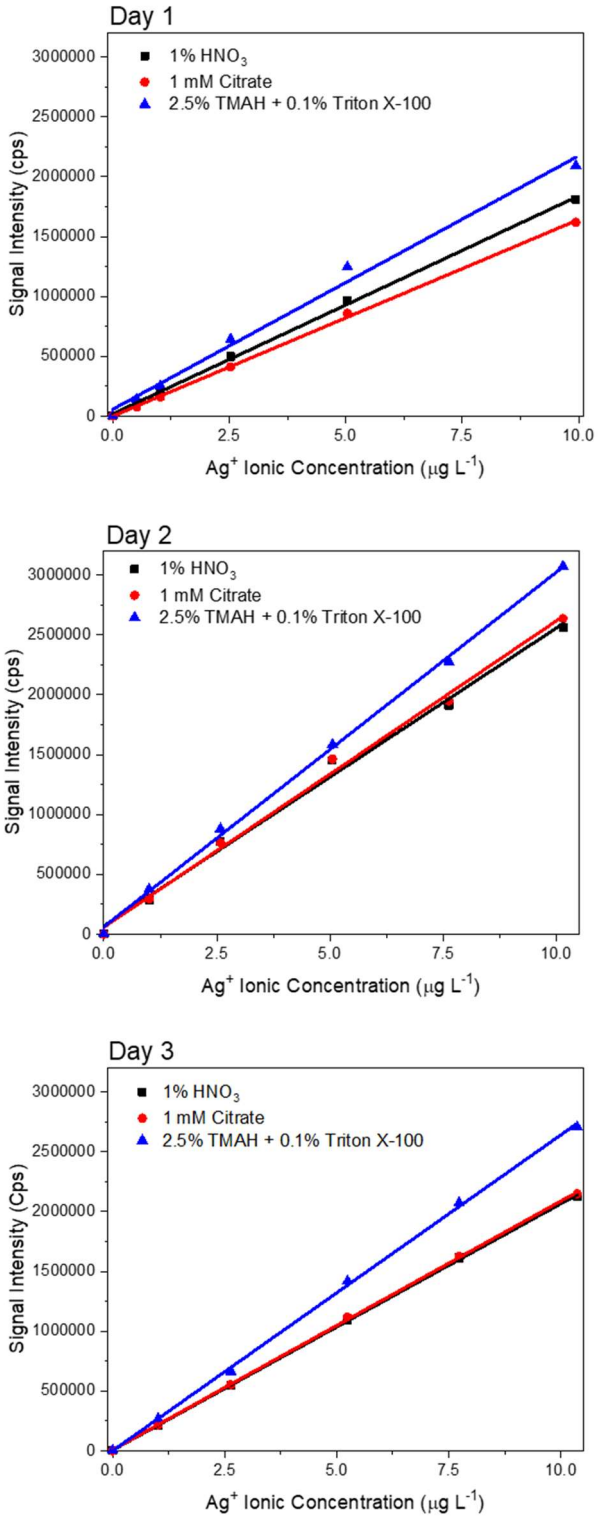

Figure 5.1: Calibration curves of ionic Ag in the three different tested media. The values of sensitivity (cps L μg^{-1}) and R^2 (in this order) were: **Day 1:** 1% HNO_3 181928 cps L μg^{-1} and 0.993; 1 mM Citrate: 164125 cps L μg^{-1} and 0.999; 2.5% TMAH + 0.1% Triton X-100: 211534 cps L μg^{-1} and 0.998. **Day 2:** 1% HNO_3 248694 cps L μg^{-1} and 0.992; 1 mM Citrate: 255723 cps L μg^{-1} and 0.995; 2.5% TMAH + 0.1% Triton X-100: 295967 cps L μg^{-1} and 0.990. **Day 3:** 1% HNO_3 207839 cps L μg^{-1} and 0.999; 1 mM Citrate: 205943 cps L μg^{-1} and 0.999; 2.5% TMAH + 0.1% Triton X-100: 263909 cps L μg^{-1} and 0.999.

According to the values of Figure 5.1, the obtained sensitivities for 1 mM citrate and 1% v v^{-1} HNO_3 disclose similar values, whereas the 2.5% w w^{-1} TMAH with 0.1% w w^{-1} Triton X-100 value is, approximately, 25% higher. To statistically corroborate the observed values in the Figure 5.1, the sensitivity values of each day were normalized (all the sensitivity values were divided by the higher sensitivity value, setting the higher value as 1) and a student t-test at a 95% confidence level was applied for these values. The calculated p-values were: (i) 0.8046 for HNO_3 and citrate curves; (ii) 0.0461 for citrate and TMAH + Triton X-100 curves and (iii) 0.0085 to HNO_3 and TMAH + Triton X-100 curves. Based on these values, it can be verified that the TMAH + Triton X-100 curve is statistically different from the citrate and HNO_3 curves (p-value < 0.05), whilst there are no statistically significant differences between the remaining two curves. These results indicate that considerable discrepancies on particle size determination may appear by applying the obtained sensitivities for non-complex media into the particle size estimation for AgNPs extracted in TMAH+Triton X-100.

5.3.1. Ionic calibration effects on AgNPs particle size determination

Taking into consideration the ionic calibrations on the 3 tested media, size determination for AgNPs with 40 and 75 nm nominal diameters in TMAH+ Triton X-100 was carried out. All the samples were daily freshly prepared in 2.5% w w^{-1} TMAH with 0.1% w w^{-1} Triton X-100 media. The TE determination was performed with the AgNPs CRM NIST 8017 in the same media of the samples, using the particle frequency method described by Pace[59] and achieving the following values: 12.47% in the Day 1, 11.20% in the Day 2 and 13.29% in the Day 3. Measurements for each sample were carried out in triplicate. The daily TE and sensitivities were used to characterize the NPs samples, with consequent determination of particle size, particle number concentration and mass concentration. Regarding the diameter determination, the mean of the average diameter values and the mode sizes (most frequent particle size) of each of the three replicates were used to calculate the final particle size value. Results are gathered in Table 5.1. As can be observed from this table, for the 40 nm AgNPs characterization, the

TMAH + Triton X-100 matrix-matching values are the closest to the values provided by the manufacturer.

Table 5.1: AgNPs Nanocomposix® 40 nm equivalent particle diameter values (average ± standard deviation, n = 9, 3 replicates per 3 days of analysis) obtained experimentally, determined with Particle Application Module of Agilent ICP-MS MassHunter Software (G5714A). TEM value provide by the manufacturer: 41 ± 4 nm.

Ionic Calibration Matrix	Most Frequent Size (nm)	Average (nm)
1 mM Citrate	47.0 ± 1.4	46.7 ± 1.6
1.0% HNO_3	47.1 ± 0.5	46.7 ± 0.5
2.5% TMAH + 0.1% Triton X-100	43.6 ± 0.6	43.3 ± 0.4

According to values in Table 5.1, the calculated diameter values with the ionic calibration in the acid and citrate media are overestimated, being around 46.7 nm for the average and, approximately, 47.0 nm for the most frequent size. The differences are better evidenced in Figure 5.2, where the diameter values with the respective standard deviations (Fig. 5.2A) and particle size distributions per matrix are represented: Fig. 5.2B: average of the 3 days and Fig. 5.2C: all the 9 replicates obtained over the 3 days.

According to Figure 5.2, the TMAH + Triton X-100 distributions are shifted to the left against the other distributions, with lower particle size and closer to the expected TEM value (41 ± 4 nm). To confirm this observation, a student t-test at a 95% confidence level was applied to the average diameter values obtained with each media, taking into account all the set of replicates (n = 9). The calculated p-values were: (i) 0.9373 for HNO_3 and citrate diameters; (ii) 0.0010 for citrate and TMAH + Triton X-100 diameters and (iii) 0.0000 for HNO_3 and TMAH + Triton X-100 diameters. The T-test values show that the estimated diameter with the TMAH + Triton X-100 media is statistically different from the other estimated diameters (p-value < 0.05), whereas the calculated diameters with citrate and HNO_3 did not present statistically significant differences. Therefore, the T-test indicates that, for 40 nm AgNPs sizing, the matrix-matched calibration approach impacts positively in the size determination, improving the accuracy of the diameter determination.

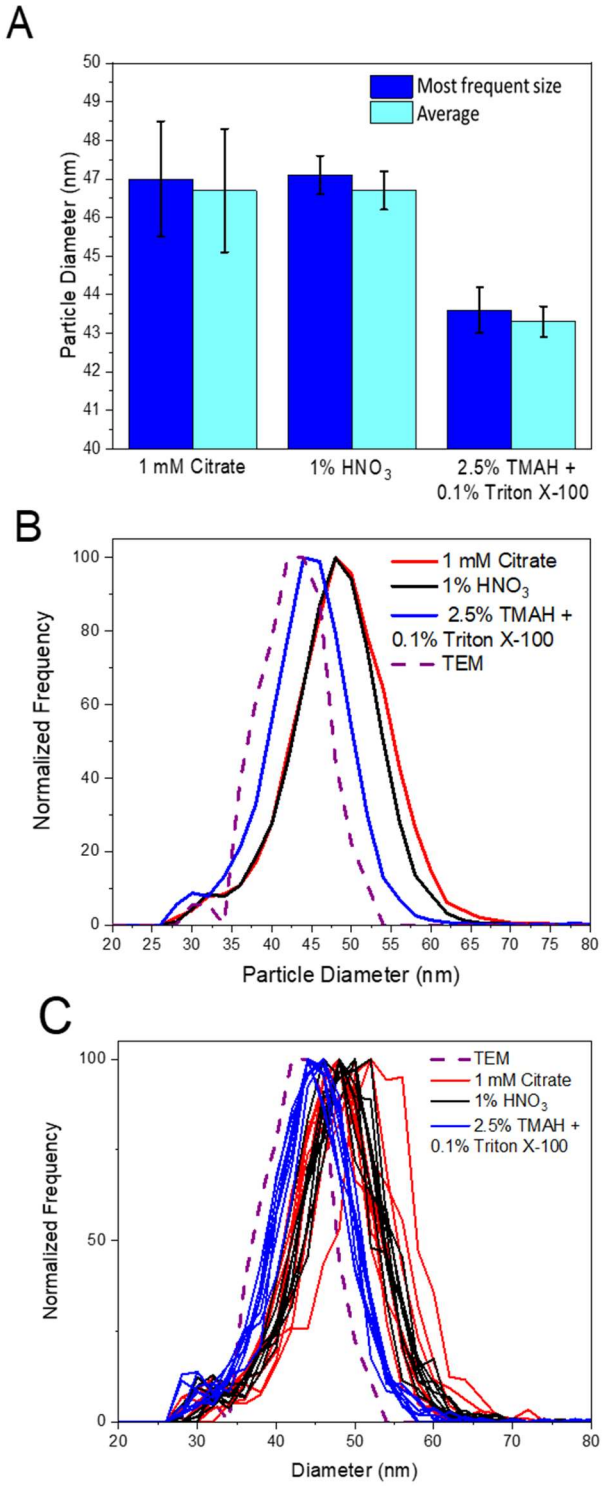

Figure 5.2: Results for size determination of AgNPs of 40 nm nominal diameter (obtained experimentally) using different matrices for ionic calibration; A. Most Frequent Size and Average Graphical Representation; B. Particle Size Distribution – representation of the average of 3 days results (n = 9, 3 replicates per 3 days of analysis), including TEM curve in dashed provided by the manufacturer. C. Particle Size Distribution – representation of the 9 replicates obtained over the 3 days of analysis, including TEM curve in dashed provided by the manufacturer.

For 75 nm AgNPs, on the other hand, size values obtained for calibration with all the tested media (both average and most frequent size) are above the TEM values provided by the manufacturer (74.6 ± 3.8 nm) (Table 5.2). Nevertheless, size values obtained with the TMAH + Triton X-100 calibration curve are the closest to the expected TEM diameters with 80.9 nm for the average value and 81.4 nm for the most frequent size value.

Table 5.2: AgNPs NIST 8017 75 nm equivalent particle diameter values (average ± standard deviation, n = 9, 3 replicates per 3 days of analysis), determined with Particle Application Module of Agilent ICP-MS MassHunter Software (G5714A). TEM value provide by the manufacturer: 74.6 ± 3.8 nm.

Ionic Calibration Matrix	Most Frequent Size (nm)	Average (nm)
1 mM Citrate	87.8 ± 3.7	87.8 ± 3.7
1.0% HNO_3	87.7 ± 1.3	87.7 ± 1.3
2.5% TMAH + 0.1% Triton X-100	81.4 ± 1.6	80.9 ± 2.0

Again, the diameter values calculated from the acid and citrate curves are very similar. The differences among the obtained diameters and particle size distributions are best evidenced by graphically observing such parameters (Figure 5.3). It can be seen that, with the ionic calibration in TMAH and Triton X-100 media, the particle size distribution appeared, one more time, shifted to the left against the other two distributions in both particle size distribution representations (average of three days in Figure 5.3B and set of all replicates in Figure 5.3C), with lower diameter values and closer to the reference TEM value.

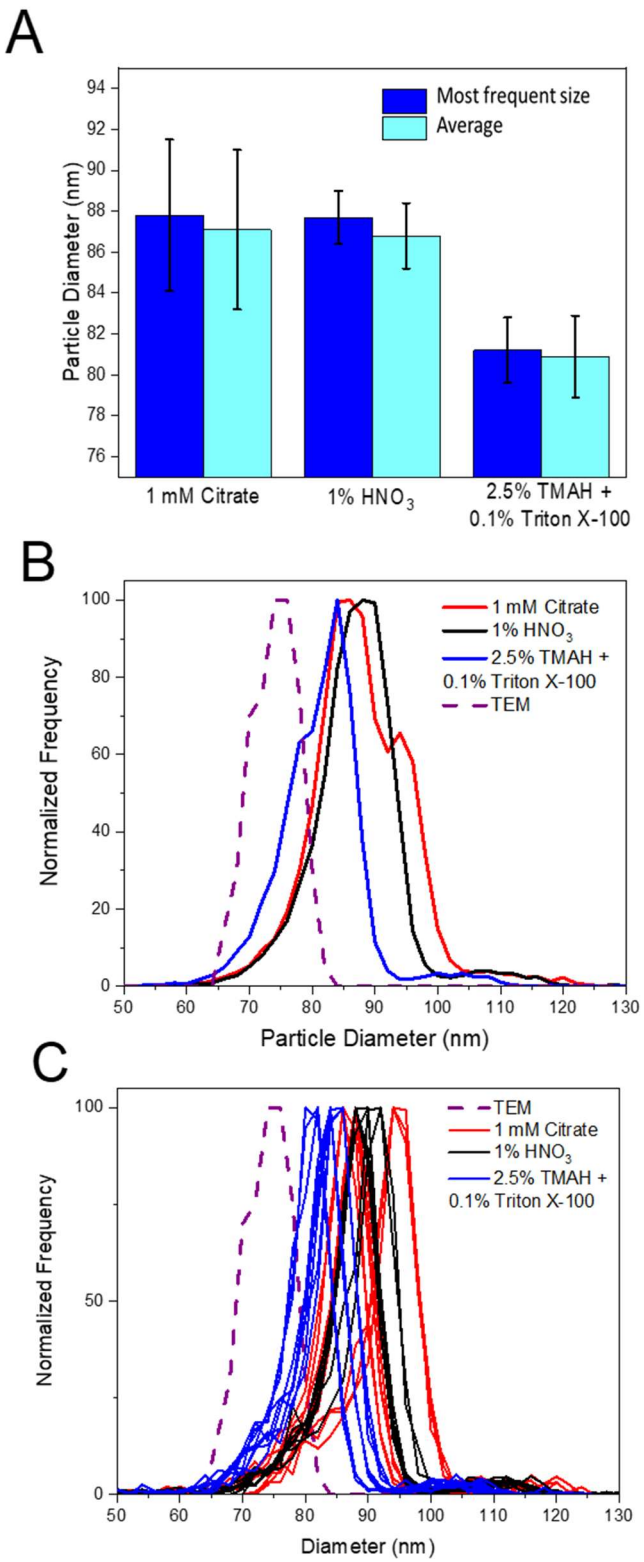

Figure 5.3: Results for size determination of AgNPs NIST 8017 of 75 nm nominal diameter (obtained experimentally) using different matrices for ionic calibration; A. Most Frequent Size and Average Graphical Representation; B. Particle Size Distribution – representation of the average of 3 days results (n = 9, 3 replicates per 3 days of analysis), including TEM curve in dashed provided by NIST. C. Particle Size Distribution – representation of the 9 replicates obtained over the 3 days of analysis, including TEM curve in dashed provided by NIST.

As for 40 nm AgNPs, a T-test was applied (n = 9) to compare these results, achieving the following p-values: (i) 0.8506 for HNO_3 and citrate diameters; (ii) 0.0012 for citrate and TMAH + Triton X-100 diameters and (iii) 0.0000 for HNO_3 and TMAH + Triton X-100 diameters. Again, statistically significant differences were found only between TMAH + Triton X-100 and the other curves (p-value < 0.05).

Different explanations for diameter oversizing can be hypothesized. First, and as indicated in the introduction, diameter calculations in SP-ICP-MS are based on the assumption that NPs are perfect spheres with a density similar to that of the bulk material. In this case, both assumptions might be wrong. As seen from Figure 5.4, where TEM pictures for the AgNPs investigated are shown, NPs are not perfect spheres in any of the cases considered. Besides, different density values have been recently reported for AgNPs in the range of 30 to 100 nm,[95] which could also contribute to the differences observed. A different explanation can be based on a possible underestimation of the determined TE. A TE underestimation would lead to overestimated diameters and underestimated particle number concentration. More details on this hypothesis will be provided in the next section. In any case, it seems clear that the use of matrix-matching for the calibration curves results in a better estimation of the particle size than the use of non matrix-matched media.

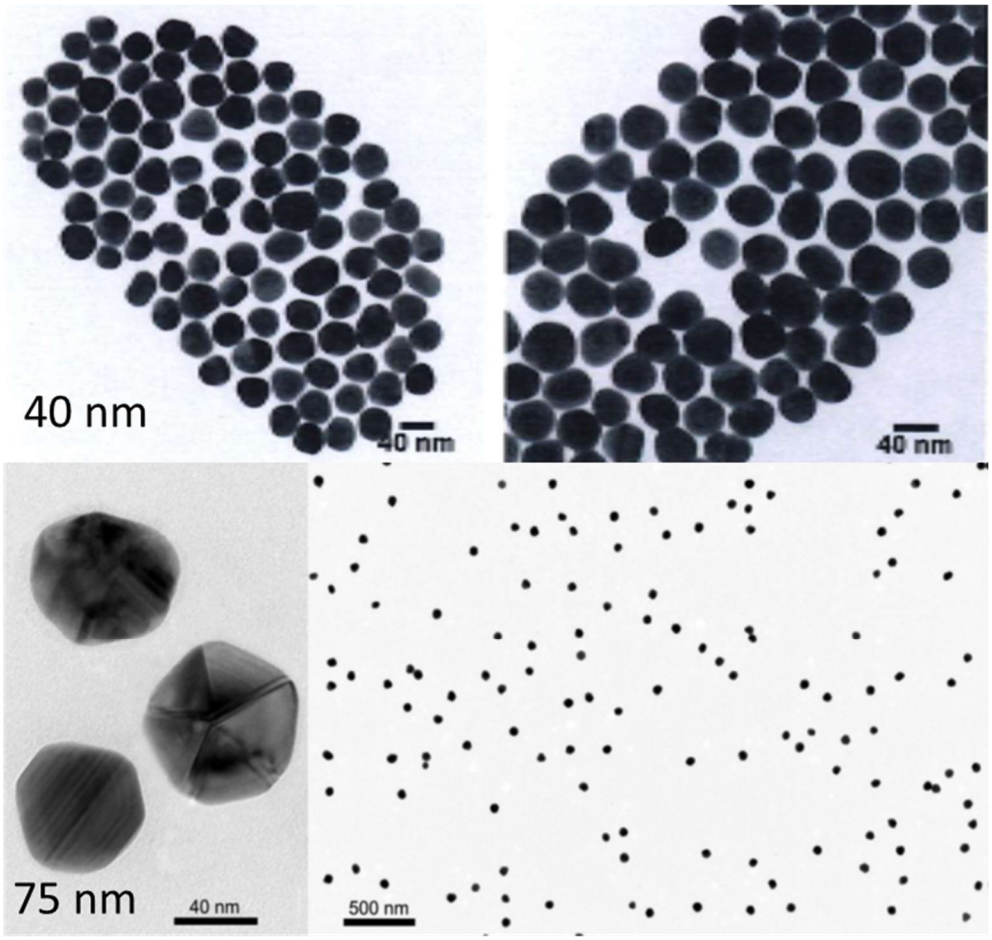

Figure 5.4: TEM pictures from (A) AgNPs 40 nm from Nanocomposix and (B) NIST 8017 AgNPs 75 nm (pictures provided by the manufacturers).

5.3.2. Particle mass and number concentration recoveries

For complete AgNPs characterization, and besides NP diameter value, it is common to report the values of total particle mass (relating to the NP fraction) and particle number concentration. Out of these parameters, only mass concentration depends on the ionic calibration (as it is calculated from the determined particle size), while the particle number concentration only depends on the transport efficiency. As commented on in the previous section, 3 replicates of each sample were measured in three different days, in which the respective TE calculated for each day was used for the particle number concentration and diameter calculation. The ionic calibration was used only for the diameter and, consequently, mass concentration calculations.

The Ag mass in the NP fraction and number concentration for the 40 and 75 nm AgNPs dispersions prepared in 2.5% w w^{-1} TMAH + 0.1% w w^{-1} Triton X-100 media are presented on Tables 5.3 and 5.4, respectively.

Table 5.3: Measured Ag Mass Concentration in the NP fraction and AgNPs Particle Number Concentration with respective recoveries for AgNPs Nanocomposix® 40 nm.
*****Recovery from the total mass given by Nanocomposix® certificate of analysis (~21 mg L^{-1})
****** Recovery from the obtained particle number concentration measured in house by revisited waste collection method (5.55 x 10^{13} part L^{-1}).[90]

Ionic Calibration Matrix	Mass Concentration of Ag in the NP Fraction (mg L^{-1})	NP mass concentration Recovery (%) *	Particle Number Concentration (x 10^{13} part L^{-1})	Particle Number Concentration Recovery (%) **
1 mM Citrate	23.40 ± 2.43	111 ± 10	3.96 ± 0.34	71 ± 8
1.0% HNO_3	23.50 ± 2.27	112 ± 10	3.96 ± 0.34	71 ± 8
2.5% TMAH + 0.1% Triton X-100	18.71 ± 1.21	89 ± 10	3.96 ± 0.34	71 ± 8

Table 5.4: Measured Ag Mass Concentration in the NP fraction and AgNPs Particle Number Concentration with respective recoveries for AgNPs NIST 8017 75 nm *Recovery from the total mass given by NIST certificate of analysis (~1072 mg L^{-1})
** Recovery from the obtained particle number concentration measured in house by revisited waste collection method (4.69 x 10^{14} part L^{-1}).[90]

Ionic Calibration Matrix	Mass Concentration of Ag in the NP Fraction (mg L^{-1})	NP mass concentration Recovery (%) *	Particle Number Concentration (x 10^{13} part L^{-1})	Particle Number Concentration Recovery (%) **
1 mM Citrate	1670 ± 117	156 ± 7	4.50 ± 0.25	96 ± 5
1.0% HNO_3	1643 ± 25	155 ± 2	4.50 ± 0.25	96 ± 5
2.5% TMAH + 0.1% Triton X-100	1319 ± 59	124 ± 5	4.50 ± 0.25	96 ± 5

As seen from these tables, for each measured AgNPs dispersion, the particle number concentration (and each respective recovery) is equal for the 3 studied calibration media, as this value depends only on the transport efficiency which was indirectly determined by the revisited waste collection method. For 40 nm AgNPs, the particle number concentration recovery observed was around 71%. This low particle number concentration recovery value could be due to (i) an underestimated TE, or (ii) to the dissolution of a part of the NPs in the stock solution. This latter effect has been

recently documented by Liu *et.al*[141] on a study regarding the long term of AgNPs stability. However, at the sight of results for 40 nm AgNPs, an underestimation of the TE cannot be ruled out. For these NPs, if TE was 29% higher, PNC recovery would have matched the expected value while calibration with the non matrix-matched media would have provided an accurate value for the particle size (as sensitivity with the TMAH+Triton X-100 media was 25% higher, *c.f.* section 5.2.2). Looking at results for 75 nm AgNPs, however, helps unravelling the situation. In fact, the particle number concentration recovery observed for 75 nm AgNPs was around 96%, which clearly points out at a correct determination of the TE, a poor stability for the smaller Ag NPs and a better size determination with the matrix matching approach.

As for mass concentration values, and as could be expected, recoveries are well above the expected values for 1 mM citrate and 1% HNO_3 media for both AgNP sizes, while in the case of the TMAH 2.5% + Triton X-100 media, recoveries slightly below or slightly above the expected values are obtained for the 40 nm AgNPs and the 75 nm AgNPs, respectively. These discrepancies are explained by the combination of the particle number concentration recoveries and the particle size results. In fact, and as a result of the cubic relation between the NP diameter and its mass, a small overestimation in the particle size entails a magnification of this error in the calculation of the particle mass and, consequently, the total mass concentration of the analyzed sample. This results in clearly overestimated values whenever particle size is overestimated, even for the 40 nm AgNPs for which a low particle number concentration recovery was obtained. Again, t-tests at the 95% confidence level were applied for comparing results with the different calibration media, taking into account all the replicates. For the 40 nm AgNPs the obtained p-values were (i) 0.9304 for HNO_3 and citrate; (ii) 0.0001 for citrate and TMAH + Triton X-100 and (iii) 0.0000 for HNO_3 and TMAH + Triton X-100. On the other hand, for the 75 nm Ag NPs the calculated p-values were: (i) 0.8627 for HNO_3 and citrate; (ii) 0.0000 for citrate and TMAH + Triton X-100 and for HNO_3 and TMAH + Triton X-100. These results indicate again that the values with the ionic calibration in TMAH + Triton X-100 media are statistically different from those obtained with 1% HNO_3 and 1mM citrate media; while the values of mass concentration obtained with the latter do not present significant statistical differences. In any case it can be concluded that, overall, the best results both in terms of particle size and mass

concentration recoveries are obtained when matching the ionic calibration with the sample media.

5.4. Conclusion

This part of the work has presented a systematic study that verifies the possibilities of matrix-matching of the ionic calibration curves for quantification of AgNPs in complex matrices by SP-ICP-MS. Significant differences were found on the sensitivity for Ag ionic calibration curves prepared in TMAH + Triton X- media (used for extracting AgNPs from biological samples), compared to HNO_3 or citrate media (frequently used for calibration in SP-ICP-MS). These differences result in different particle size values obtained for the determination of AgNPs in TMAH + Triton X-100 media, which agree better with the expected values if the matrix matched calibration curves are used. In this particular study, particle number concentration was not affected by the ionic calibration curve used, as an indirect waste collection method was used for TE determination. However, if the particle size method[59] was used for TE calculation, the media for the ionic calibration curves would have also have an impact in the results obtained, and better results would have been obtained with the matrix-matched calibration curves.

CHAPTER 6

Isotope ratio determination of individual nanoparticles for the sizing and counting of silver nanoparticles by means of SP-ICP-TOF-MS and isotope dilution analysis

6.1. Introduction

As discussed in previous chapters, SP-ICP-MS can suffer from matrix effects, which degrade the quality of measurements. As for conventional ICP-MS analysis, these effects can be categorized into spectral overlaps or non-spectral interferences, and each one shows consequences for this working methodology. On the one hand, the occurrence of matrix-induced spectral interferences in SP-ICP-MS results in elevated background signals with a direct impact in the NP size limits of detection (*c.f.* chapters 3 and 4). On the other hand, matrix can also induce intensity changes in the ICP-MS response which, as shown in chapter 6, can compromise calibration.[73]

Among all strategies available for dealing with matrix effects in ICP-MS,[140] isotope dilution analysis (IDA) is generally regarded as the most robust and effective, providing superior accuracy and uncertainty over other calibration methods. IDA relies on the intentional alteration of the isotope abundances of an endogenous element in a given sample by the addition of a known amount of an enriched isotope of the same element (spike).[147] Calculations are based on the measurement of the modified isotope ratios in the mixture "sample plus spike", which implies that, for proper application of IDA, it is necessary that two or more isotopes of the analyte element can be measured free of spectral interferences.

This prerequisite is not easy to fulfil for SP-ICP-MS as, with the most commonly used sequential ICP-MS instruments (equipped with either quadrupole or single collector-sector field spectrometers), only one isotope can be monitored on the time scale of the signal generated by one NP (300-500 µs).[148,149] As a consequence, only two papers in the literature have reported application of IDA to SP-ICP-MS after making some approximations for overcoming this limitation. In the work of Telgmann et al.,[150] the average 107/109 isotope ratio for a distribution of silver NPs was calculated for the most frequent NP size by ratioing the mean $^{107}Ag^+$ and $^{109}Ag^+$ signals of the NP frequency histogram obtained by Gaussian fitting. These ratios were introduced in the IDA equations to obtain the most frequent size of the NP distribution. This working strategy allows for rapid size determination of suspensions of NPs with a distinct size in complex matrices, but information on the particle size distribution is not available. This problem was circumvented by Sötebier et al.[151] by using a modification of the post-column

species-unspecific IDA equation.[152,153] In the case of SP-ICP-MS, the transient nature of the signal is given by the detection of the individual NPs over the constant signal of the spike. To measure the isotope ratios for every NP event needed for calculations, the authors used a ^{109}Ag-enriched spike (close to 100% ^{109}Ag) at a sufficiently high concentration as to be able to consider that the contribution of the NP intensity to the m/z=109 trace was negligible, so that the intensity for this trace was relatively constant from one measurement cycle to the next. On the other hand, NPs were detected in the m/z=107 trace where contribution of the spike was low. With this approximation it was possible to determine 109/107 ratios for every NP event thus obtaining information on the particle size distribution for the sample analysed. As a drawback, the long measurement cycles that had to be used for monitoring both silver isotopes (22 ms) resulted in only 45% of the NP events being effectively detected in the m/z=107 trace, so that long acquisition times (up to 10 minutes) were necessary to compensate for this fact.

All these problems could be solved if a simultaneous ICP-MS system with a time resolution in the micro or milli second range was used for analysis. An instrument of this sort, based on the use of a Time of Flight (TOF) spectrometer, was introduced as a prototype in 2013[154] and has been recently made commercially available. Different papers on the possibilities of such an instrument for multi-element analysis of nanoparticles have been published,[77,99,154] and the positive results obtained permit to foresee an increasing use of this instrument for SP-ICP-MS analysis in the future. However, no publication has reported its use for IDA so far. Moreover, deploying this calibration methodology implies accurate and precise determination of isotope ratios for individual nanoparticles, which again, has only been reported with multicollector-ICP-MS instruments.[155,156] It is the purpose of this chapter to evaluate the possibilities of an ICP-TOF-MS with millisecond time resolution for application of IDA to single particle analysis. Method development, including accurate and precise determination of isotope ratios for individual nanoparticles, will be explored for the case of silver NPs determination.

6.2. Isotope dilution equations for SP-ICP-MS

Considering that the analytical signal in SP-ICP-MS shows a transient nature, an isotope dilution equation adapted to online work was used for calculations. In particular, the basic equation for post-column species-unspecific isotope dilution (eq. 6.1) first proposed by Rottmann and Heumann[157,158] and described in detail by Rodríguez-González et al.[147] was used as a model.

$$c_S d_s f_s = c_{sp} d_{sp} f_{sp} \frac{M_s}{M_{sp}} \left(\frac{R_m A_{sp}^b - A_{sp}^a}{A_s^a - R_m A_s^b} \right) \textbf{(6.1)}$$

The original equation is designed to quantitatively determine the different species in a mixture, which are separated in a chromatographic column. After the separation, the effluent (sample) with a density $\boldsymbol{d_s}$ (ng mL^{-1}) and containing a concentration of the element of interest $\boldsymbol{c_s}$ (ng g^{-1}), is pumped at a flow rate $\boldsymbol{f_s}$ (mL min^{-1}) and mixed with the spike solution. The latter shows a density $\boldsymbol{d_{sp}}$ (ng mL^{-1}), contains a concentration of the element of interest $\boldsymbol{c_{sp}}$ (ng g^{-1}), and is pumped at a flow rate $\boldsymbol{f_{sp}}$ (mL min^{-1}). As for the rest of the parameters in eq. 6.1:

- M_s and M_{sp} are the atomic weights of the element in the sample and the spike.
- A_S^i and A_{sp}^i are the isotope abundances for the isotope *i* in the sample and the spike.
- Rm is the isotope ratio a/b in the mixture, which varies with time as a result of the chromatographic separation.

The units for the expression $c_S d_s f_s$ are ng min^{-1} as it represents the mass flow of the sample eluting from the column, MF_s, which also changes with time as a consequence of the varying element concentration after the chromatographic column. Quantification of the different species can be performed by simple integration of the different peaks in the mass flow chromatogram (MF_s vs. time).

In the particular case of SP-ICP-MS, each species of the analyte (both ionic and

the nanoparticulate forms) provides a different signal. Each NP event can be seen as a chromatographic peak in the mass flow chromatogram, so that equation (6.1) can be used with modifications. The determined MF_s obtained from equation (6.1) for each NP event can be converted into the mass of the detected NP (m_{NP}) according to equation (6.2), after introducing the transport efficiency η_n, and the dwell time (integration time in the case of TOF mass spectrometers, t_{int}) as additional parameters:

$$m_{NP} = \eta_n \cdot t_{int} \cdot c_s \cdot d_s \cdot f_s \quad \textbf{(6.2)}$$

As no chromatographic column is needed for the separate detection of the NPs and the dissolved material, on-line addition of the spike is not strictly necessary for SP-ICP-MS. Although online addition of the spike might have some advantages in terms of sample preparation, batch-spiking of sample aliquots might favor spike-sample equilibration thus reducing the uncertainty of the results.[140] For this reason, batch spiking of sample aliquots was used throughout this study. The final IDA equation used for calculations (eq. 6.3) combines equations (6.1) and (6.2) and considers batch-spiking of an aliquot of the NP dispersion giving a final concentration of the spike in the mixture c_{spike} (ng g^{-1}).

$$m_{NP} = \eta_n \cdot t_{int} \cdot c_{spike} \cdot d \cdot f \cdot \frac{M_s}{M_{sp}} \left(\frac{R_m A_{sp}^b - A_{sp}^a}{A_s^a - R_m A_s^b} \right) \quad \textbf{(6.3)}$$

In this equation, f refers to the nebulizer flow rate at which the spiked dispersion is introduced in the ICP-MS and d to the density of the spiked dispersion.

From all parameters included in eq. 6.3, most are either user defined (t_{int}, c_{spike}, f) or known (d, M_s, M_{sp}, A_s^i if a natural isotopic composition is assumed for the sample; A_{sp}^i if a certified spike with known isotopic composition is used). The only two parameters that have to be experimentally determined for IDA calculations are the transport efficiency η_n , and the isotope ratio R_m for each NP event. Measurement of these parameters with the best precision and accuracy is thus needed for the best results to be obtained. For transport efficiency calculation, the particle frequency method described by Pace *et al*.[59] was carried out, matrix-matching the media for the reference NP dispersion with the sample matrix. As for estimation of the isotope ratio

for each NP event (R_m), method development for optimizing accuracy and precision for the measurement of this parameter will be discussed in the following sections.

6.3. Method development for accurate and precise measurement of isotope ratios for individual nanoparticle events (Rm)

6.3.1. Data acquisition mode in ICP-TOF-MS for NP detection

The ICP-TOF-MS instrument deployed in this work can be operated in two data acquisition modes: either continuous- or trigger-mode.[100] In continuous acquisition mode, detection of the full mass spectra (7-275 amu) is possible at a rate of up to 1000 Hz (33 TOF extractions per mass spectrum). This detection speed is, however, limited by the data transfer from the analog-to-digital converter to computer hard drive. For the particular configuration used in this work, this limitation implies a maximum time resolution of 3 ms in continuous acquisition mode.

In trigger-mode acquisition, data is only recorded if the signal level from a specified m/z channel is above a user-defined threshold. Time resolution in trigger mode is only limited by the repetition rate of the TOF mass analyzer (30 µs), although at the cost of only being able to record 32 data points for each trigger event. It is important to note that selection of this acquisition mode for NP detection is only possible if a continuous signal for an isotope different to that used for NP detection can be used as a trigger, as otherwise signal for the BG needed for NP quantification is not recorded by the instrument. This can be easily achieved though. In the work by Hendriks et al.[100], for instance, the NP dispersion was doped with a ionic solution of Cs, an element of no interest for the analysis, and the signal of ^{133}Cs was used as trigger.

When aiming at NP detection, selecting one acquisition mode or the other is primarily affected by two opposing issues that must be evaluated by the analyst on each particular case. As extensively covered in the literature, signals generated by NPs in ICP-MS typically show a duration of 300-500 µs[62] and hence, selection of integration times in the order of 50-100 µs (at present only offered by the trigger-mode) would be

preferred for improving size detection limits (LOD_{size}), as contribution of the BG to the signal is then minimized. On the other hand, the possibility of simultaneously detecting the full mass range is exclusive to ICP-TOF-MS instruments in continuous-mode and might well justify the marginal loss of detection power derived from selection of a longer integration time when unknown samples are targeted.

In addition to these two factors, a third consideration turns to be relevant for the particular case of IDA. In fact, application of IDA equations shown in section 6.1 requires the calculation of the isotope ratio of the mixture NP+spike for each individual NP event (R_m) and, as will be shown in section 6.2.2.1, precision and accuracy of these ratios is affected by the integration time selected. In practice, shorter integration times lead to larger uncertainties for R_m values. This uncertainty adds to the noise of the ICP-TOF-MS measurement which result in distorted (wider) NP-size distributions if compared with "true" (as characterized by other techniques) values.[100]

In this work, the continuous mode with 3 ms time resolution (spectral averaging time) was selected for evaluation of the IDA calibration methodology under compromise conditions (sizing and counting of 75 nm nominal diameter Ag NPs). However, selection of the trigger-mode acquisition and fine tuning of the integration time might be needed for particular situations requiring the best detection capabilities.

6.3.2. Effect of integration time (t_{int}) and composition/concentration of the spike ($\boldsymbol{A_{sp}^{i}, c_{spike}}$)

The basic working principle of an ICP-TOF-mass spectrometer is to inject an isokinetic packet of ions sampled from the plasma into a field-free flight tube, at the end of which there is an ion detector. Isotopes of different mass-to-charge ratios travel at different speeds through the flight tube, such that they reach the detector at different moments and are hence separated. Even though detection occurs at different moments in time, each one of these packets of ions is sampled simultaneously, such that the level of correspondence achieved for different nuclides is very high, permitting most sources of noise related to the ICP ion source to be filtered out when isotope ratios are calculated. Under these conditions, isotope ratio precision achievable with this type of

instruments is mostly limited by counting statistics, which depends in turn on signal intensity (in cps) and integration time (t_{int}) selected.[100]

When IDA analysis is carried out in digested samples, these parameters can be tuned to a certain extent to get better precision values. Generally speaking, the longer the integration time and the higher the analyte concentration, the better the counting statistics and the isotope ratio precision. This is shown in Figure 6.1A, where precision values attained for $^{107}Ag/^{109}Ag$ isotope ratios, for ionic silver solutions of different concentrations, are displayed as a function of the integration time selected. These data were acquired at a spectral averaging time of 3 ms, while isotope signals were summed in data post-processing for achieving the extended integration times shown in the figure. As seen in the figure, isotope ratio precision improves for longer integration times and higher analyte concentration values, and in all cases experimental data fit reasonably well the expected precision according to counting statistics.[159] A similar experiment was conducted in the work by Hendriks et al.[100] but for longer integration times, and the conclusion was that accordance to counting statistics can be expected for t_{int} up to 100 s. From this value on, problems with mass calibration drifts worsens the RSD.

The situation for isotope ratio determination of individual NP events is different, and analyte concentration and integration time cannot be tuned in a similar manner for optimizing precision. In fact, each NP event has a fixed duration in the 300-500 µs range and provides a given intensity that depends on the NP size and the instrument absolute sensitivity (in counts per atom). Precision obtained is barely affected by the integration time selected at the millisecond time and increasing the NP concentration in the suspension monitored does not result in events of increased intensity (and hence better counting statistics) but in more frequent events of the same intensity. This is shown in Figure 6.1B, where precision values attained for $^{107}Ag/^{109}Ag$ isotope ratios for a suspension of Ag NPs of 75 nm nominal diameter are shown as a function of integration time. Data obtained for a 2.5 µg L^{-1} Ag ionic solution of natural abundance, providing similar intensity values (in counts) for 3 ms, are also displayed for comparison purposes. Every NP event provides an intensity value of approximately 40-50 counts (for the most frequent size) for each silver isotope, regardless of the integration time selected. Self-evidently, increasing the integration time does not have any effect on the isotope ratio precision for individual NPs, which remains at a constant value corresponding well with

the counting statistics prediction for the recorded signal. For the 2.5 μg L^{-1} Ag ionic solution, signal intensity (in counts) for each silver isotope increases with the integration time and isotope ratio precision improves accordingly. Also, in this case, the RSD obtained corresponds well with data predicted from counting statistics.

As concluded from results shown in Figure 6.1 and as expected, precision attainable for isotope ratio determination of individual nanoparticles in ICP-TOF-MS instrument is ultimately determined by the instrument absolute sensitivity (in counts per atom) and little can be done in method development to improve this value. In the case of IDA, however, R_m is monitored, which includes the signal coming from the individual NP and that of the spike. Signal for the individual NP is fixed, but signal obtained for the spike depends on the composition and concentration of the ionic spike and the integration time. These parameters are interrelated and influence the total amount of counts recorded per event, and hence precision attained for R_m. As explained in the upcoming sections, we followed a straightforward approach for proper selection of these parameters where we first decided on the integration time (according to general considerations for SP-ICP-MS analysis) and later adjusted spike composition and concentration.

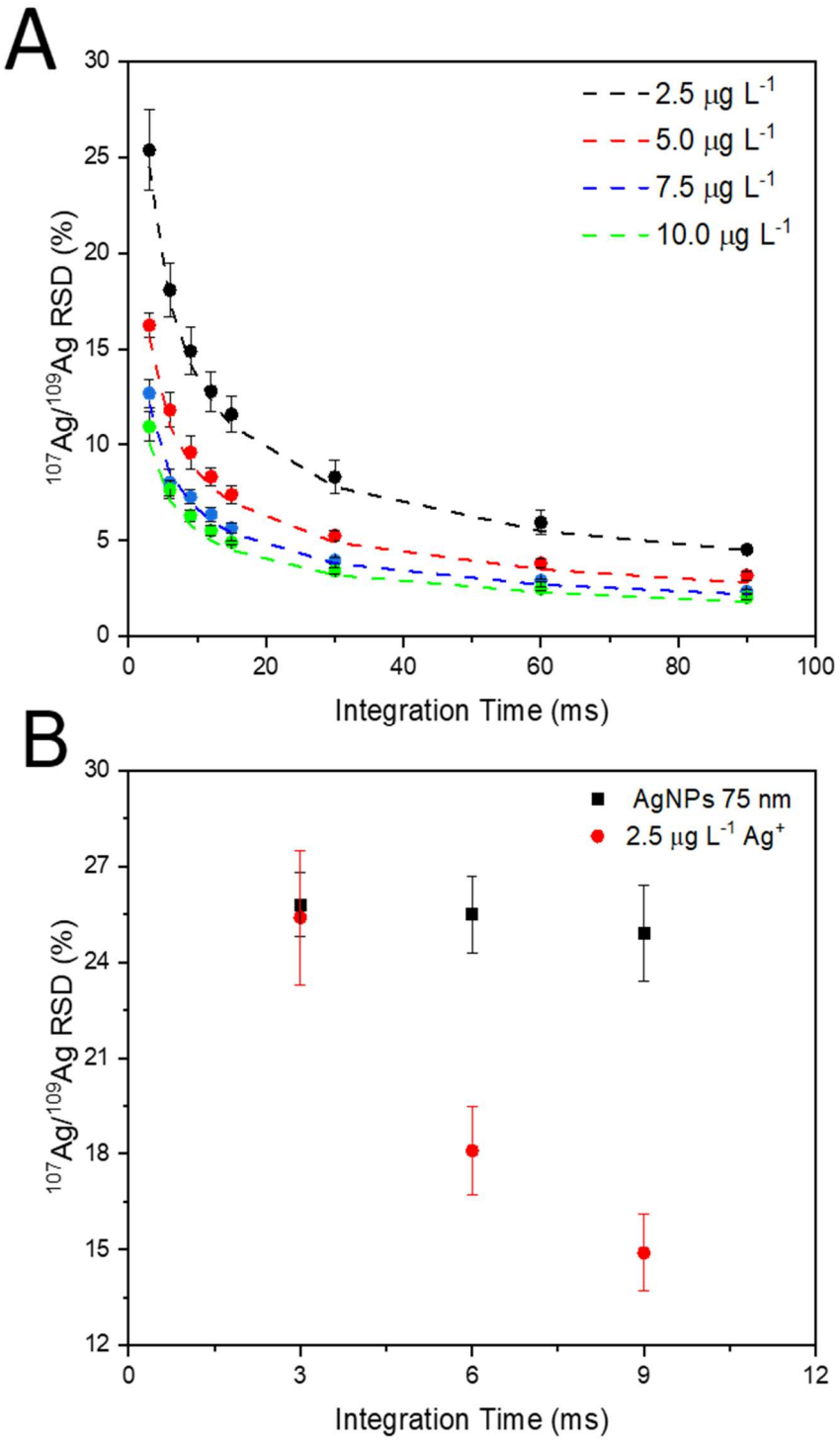

Figure 6.1: (A) Isotope ratio precision (% RSD) for Ag ionic solutions of different concentration as a function of integration time. The dotted lines represent the theoretical RSD value according to counting statistics, while dots represent experimental values. (B) Isotope ratio precision (% RSD) for a 75 nm AgNPs suspension and a 2.5 µg L^{-1} Ag ionic solution. In both figures, error bars represent one standard deviation (n=3, measured in different days).

6.3.3. Selection of integration time and correction for split events

For conventional SP-ICP-MS (calibration with external ionic solutions), and when integration (or dwell) times in the millisecond range are used, the best option seems to be selecting an integration time sufficiently low to minimize the background contribution to the signal, but long enough to minimize the probability of splitting the signal of a single NP in various events.[62] Additionally, the particle number concentration of the NP dispersions measured is also critical in this methodology as the probability of measuring two or more NPs in a single integration time needs to be minimized. In this regard, there tends to be an agreement in the SP-ICP-MS community to use dwell (integration) times of 3–5 ms as the most suitable.[60,72]

According to these principles, 3 ms (the minimum possible for continuous acquisition mode) was selected as integration time in this particular case. As will be discussed in more detail in section 6.2.2.2, this measure together with selection of an ^{109}Ag enriched spike close to 100% purity ($A_{sp}^{109}\sim 1$) allows to improve the LOD_{size} for analysis. Particle number concentration for the NP dispersions measured was adjusted by dilution of the original suspensions in order to minimize the occurrence of double particle events (probability below 5%) with this integration. On the other hand, and as analyzed in detail in the paper by Liu et al.,[141] for integration times in the millisecond range a significant amount of NP signals is still split into different events (what we called *split events*) when such short times (below 5ms) are selected, and implementation of a proper method for correction would be advisable.

The theoretical probability of split events was calculated prior to data treatment. Equation 6.4 shows the probability of split events according to the Poisson Statistics:

$$P_{split} = \frac{t_{pulse}\,\lambda e^{-\lambda}}{t_{dwell}(1 - e^{-\lambda})} \quad (\mathbf{6.4})$$

Where t_{pulse} is the NP pulse duration in the plasma (s), t_{dwell} is the dwell or, in this case, integration time (S) and λ is the nanoparticle detection frequency (NPs s^{-1}) multiplied by the dwell time (s). Considering the daily values for particle number

concentration, sample flux and TE, the following particle frequency values were obtained: 17.1 Hz for day 1, 17.8 Hz for day 2 and 17.3 Hz for day 3. With these values, the theoretical probability of split events (for t_{dwell} of 3 ms and average t_{pulse} of 400 µs) is, approximately, 13.0% for each day of analysis.

After carrying out all the analyses, it was experimentally confirmed that, with this integration time, a significant amount of NP signals was split into different events. For the proper correction of these events, these signals have to be integrated as one coming from a single NP, in a similar manner as instruments with integration (dwell) times in the µs range work. For this purpose, a script was written in GNU Octave that performs the following actions:

(i) **Split events identification**: split events are identified when two adjacent intense signals over a user-defined threshold are detected for the m/z=107 trace (where contribution of the spike to the signal is negligible as composition of the spike was selected to be $A_{sp}^{109}\sim1$). This threshold was set as 3 times the standard deviation of the average background for m/z=107 trace, as for the acquisition conditions used in this work the probability for two adjacent signals coming from two different NPs instead of a split one is negligible.[160]

(ii) **NP mass integration:** the masses obtained for these adjacent signals after application of the IDA equation (eq. 7.3) are integrated by the script.

(iii) **NP diameter calculation:** the diameter of the NP is calculated with the integrated value.

With the described script, an average percentage of split events of 10.0 ± 0.6 % was detected in the different experiments conducted in this work (n=5), which corresponds well with the expected value based on Poisson probability calculations.[160] Implementing this correction script is important for the correct determination of the NP size distribution as shown in Figure 6.2. As seen from this figure, the occurrence of abundant split events artificially increases the number of small NPs (if compared with reference distribution from NIST), which (i) decreases the average size of the NPs and (ii) hampers setting of the threshold for defining a NP. After correction for split events

this region is much better defined, which results in better LOD_{size}.

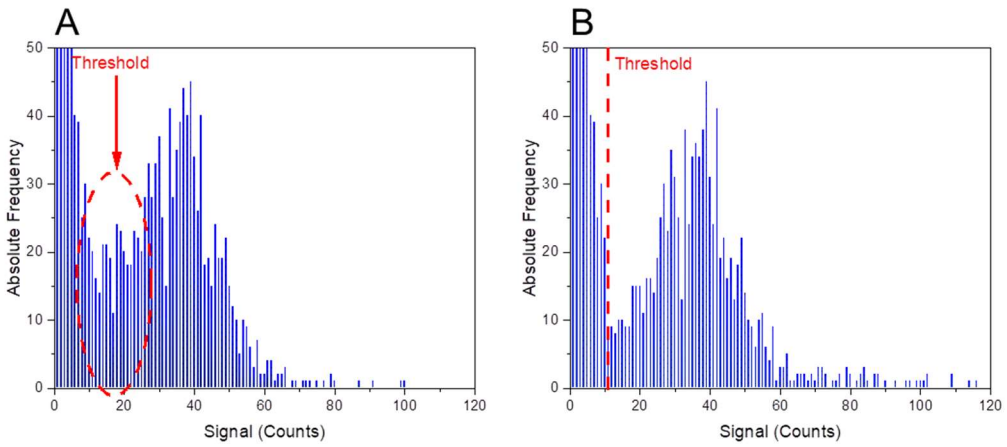

Figure 6.2: Signal distributions for ^{107}Ag isotope obtained for a 75 nm nominal diameter AgNPs dispersion (the threshold for separation of BG and NP distribution indicated in red in the figure was defined according to the 5σ criteria). (A) without split event correction and (B) with split event correction using the GNU octave script.

Particle number recovery without correction was, on average, 106 ± 7 %, while after correction with the GNU octave script it was 96 ± 6 %. It is important to note that this correction is only effective for events providing a signal above the 5σ threshold applied for particle identification. This could be a problem for NP distributions close to the detection limit, as some small NPs might pass undetected if split in two. In such situations, selection of an integration time in the microsecond range would be preferred for reaching the best detection capabilities. On the other hand, selection of longer integration times would reduce the occurrence of split events, but higher dilution factors would be needed to minimize the probability of occurrence of double particle events, the measuring time would have to be enlarged for compensating for dilution, and the LOD_{size} would increase due to a larger contribution of the background to the m/z=107 signal.

6.3.4. Selection of spike composition and concentration

Spike composition was selected to be $A_{sp}^{109} \sim 1$ as to minimize its contribution to the 107 trace, which is used for NP identification. This permits to improve the LOD_{size}. For the same reason, concentration of the spike would need to be kept sufficiently low. However, and considering the inherent imprecision bond to isotope ratios determined for individual NPs as discussed in Figure 6.1, it was confirmed that too low a spike concentration has detrimental effects for results. In fact, too low spike concentrations result, first, in experimental R_m values above the expected natural ratio (107/109=1.075), which in turn result in negative mass values for the detected NPs once equation 6.3 is applied. This occurrence of negative mass values was also observed by Sötebier et al. in their work,[151] which they solved by just removing the negative values from the NP distributions claiming that this measure does not affect final results. To test the validity of this statement, IDA analysis of an AgNPs dispersion doped with different amounts of the selected isotopic spike with composition $A_{sp}^{109} \sim 1$ was carried out. Results are presented in Figure 6.3 and Table 6.1.

Table 6.1: Percentage of negative values and average Rm value ($^{107}Ag/^{109}Ag$) obtained (standard deviation of 3 days of analysis) for analysis of a 75 nm Ag NP suspension by IDA as a function of the spike concentration deployed.

Spike (μg L^{-1})	Negative Values (%)	Average Rm ± SD
0.25	14.2%	0.8633 ± 0.0511
0.50	3.4%	0.7167 ± 0.0198
0.75	0.4%	0.5969 ± 0.0116
1.00	0.1%	0.5217 ± 0.0069
1.50	0.0%	0.4063 ± 0.0065
2.00	0.0%	0.3217 ± 0.0019

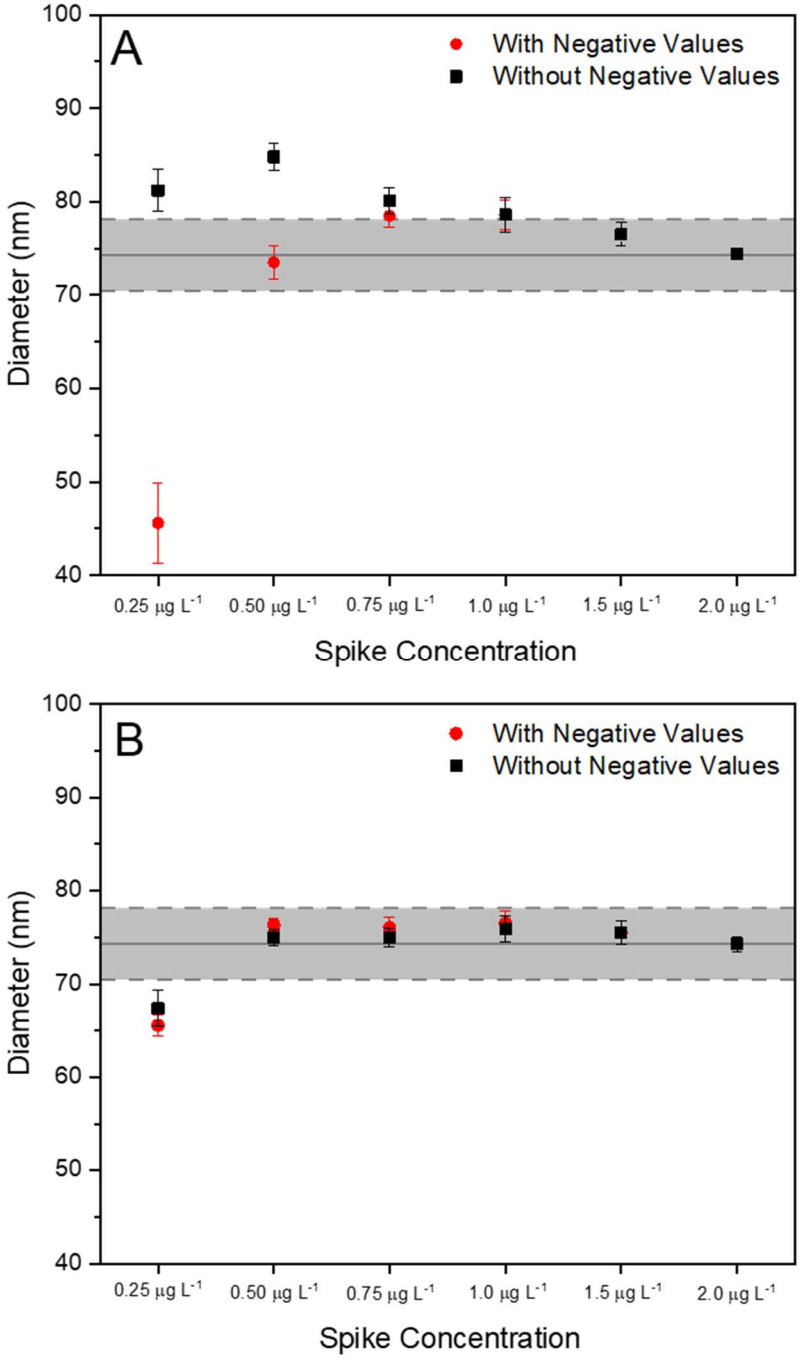

Figure 6.3: Average (A) and median (B) diameter values obtained for analysis of a 75 nm nominal diameter AgNP suspension as a function of the ^{109}Ag spike solution concentration deployed for 2 different types of data treatment: with and without the consideration of negative values. Error bars represent 95 % confidence intervals (n = 15 – 5 replicates per day, 3 days of measurement). The hatched area represents the reference average diameter and standard deviation obtained by TEM analysis (74.3 ± 3.8 nm), according to the certificate of analysis provided by NIST.

As seen from Table 6.1, the higher the spike concentration the lower the percentage of negative values obtained. For concentration values above 0.75 µg L^{-1}, which provide R_m values of about 0.6 for the most frequent size NP, the percentage of negative values is already negligible, which is consistent with results shown in Figure 6.1. In fact, if precision values attainable for isotope ratio determination of individual NPs is about 25-30%, probability for the experimental isotope ratios to exceed the natural value of 1.075 for an expected ratio of 0.6 would be rather small.

For too low spike concentrations providing a significant percentage of negative values (e.g. 0.25 µg L^{-1}), on the other hand, the effect of these negative values on the sizing of the NPs is evident from Figure 6.3. As could be expected, if negative values are included in the distribution, an average diameter biased low is obtained. On the other hand, if negative values are just removed from the distribution as recommended by Sötebier et al.,[151] results improve but a positive bias on the average diameter determined is observed instead. For spike concentrations above 0.75 µg L^{-1} (providing a negligible number of negative values) the effect is much less pronounced and no significant differences from certificate values are observed. It is possible to note that the median values are much less affected by the presence of negative results as seen from Figure 6.3B. This is not surprising considering that the median is known to be much more robust towards the influence of outliers.

To understand the change from negative to positive bias in the results observed, a closer look to the NP distributions obtained is needed. In fact, an additional effect is observed if spike concentration is not appropriately selected. Similarly to what was indicated in section 6.2.1 for the integration time, selection of a lower spike concentration results in poorer counting statistics and larger uncertainties for R_m values. This uncertainty adds to the noise of the ICP-TOF-MS measurement which result in distorted (wider) NP-size distributions if compared with “true” (as characterized by other techniques) values.[100] This can be observed in Figure 6.4, where the size distributions obtained for IDA analysis of a 75 nm Ag NP dispersion with different spike concentrations is presented. Negative values, if present, were removed from the graphics.

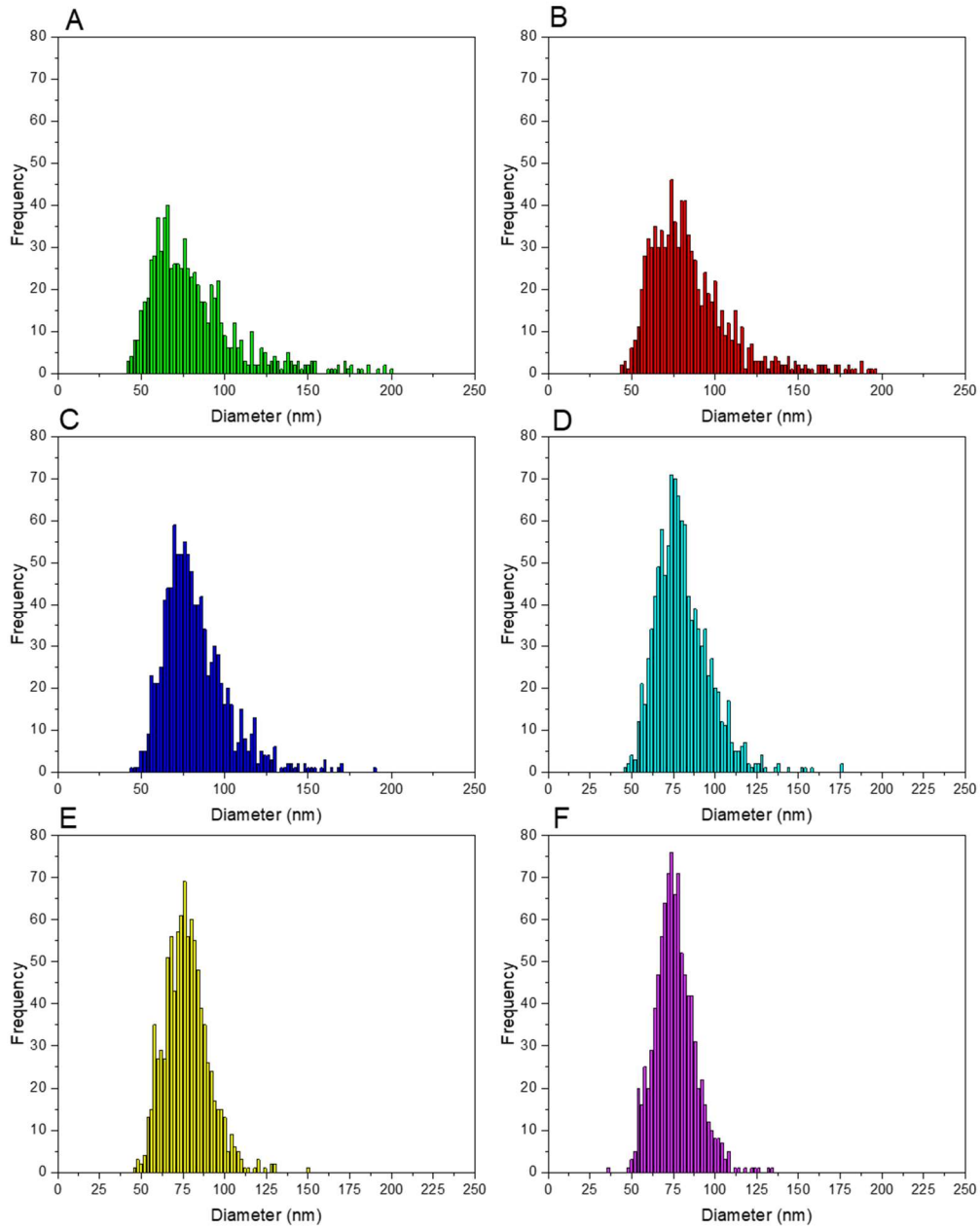

Figure 6.4: Particle size distributions obtained for the analysis of a 75 nm nominal diameter AgNPs dispersion spiked with different concentrations of the ^{109}Ag isotopically enriched solution: (A) 0.25 $\mu g \cdot L^{-1}$ spike concentration; (B) 0.50 $\mu g \cdot L^{-1}$ spike concentration; (C) 0.75 $\mu g \cdot L^{-1}$ spike concentration; (D) 1.00 $\mu g \cdot L^{-1}$ spike concentration; (E) 1.5 $\mu g \cdot L^{-1}$ spike concentration and (F) 2.0 $\mu g \cdot L^{-1}$ spike concentration. For distributions A, B and C, negative values have been removed for the sake of simplicity.

As seen from Figure 6.4, the lower the spike concentration the wider the NP distribution obtained, the effect being more pronounced to the right wing of the distribution. This is more evident from Figure 6.5, which includes boxplots for all the NP distributions obtained with IDA analysis and different spike concentration plus the one obtained with external calibration and that provided by the NIST certificate of analysis, both included for comparison purposes. As seen from this figure, narrower distributions are obtained as the spike concentration increases. Taking the distribution obtained for external calibration as a reference (which is biased but is not affected by the effect of the spike concentration), it can be concluded that acceptable agreement is obtained for spike concentrations above 1.5 μg L^{-1}. This fact is also supported by the varying mass concentration recoveries obtained for each distribution, which are gathered in Table 6.2. In that table, the results are given as the median value of the 3 days measurements. In the third day of measurements, the results of particle mass concentration obtained were considerably higher than those obtained the other two days of measurements. Thus, in this case, the median displays a better observation of the particle mass recovery than the average value. The average value of the two first days is also provided for comparison.

Table 6.2: Particle mass recovery by each spike condition (median values for the three days of analysis and average ± standard deviation of the two first days of analysis).

Spike (μg L^{-1})	Particle Mass Recovery (Median) (%)	Particle Mass Recovery (Average) ± SD (%)
0.25	338	270 ± 96
0.50	293	373 ± 159
0.75	168	167 ± 36
1.00	142	138 ± 6.0
1.50	119	112 ± 10
2.00	98	98 ± 0.1

As seen from this table, low spike concentrations result in significant positive bias for the mass concentration recovery, which is consistent with the enlargement of the distribution towards larger diameter values seen in Figures 6.4 and 6.5. For values above 1.5 μg L^{-1} mass concentration recoveries are closer to 100%, which serves as an indicator that spike concentration is adequate.

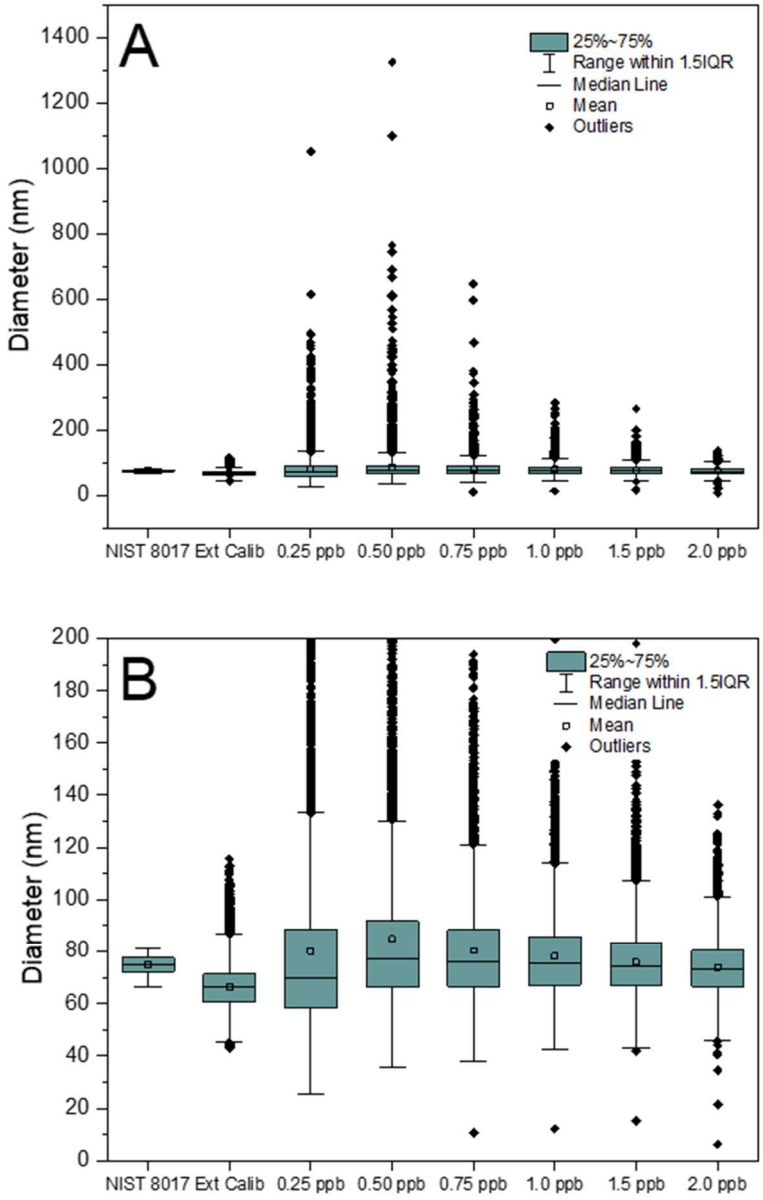

Figure 6.5. Boxplots for the analysis of a 75 nm nominal diameter AgNPs dispersion (without negative values) spiked with different concentrations of the ^{109}Ag isotopically enriched solution (2 days of analysis). The thick horizontal line across each box marks the median of the corresponding particle size distribution, the square dot inside the box represents the mean, and the bottom and top of the box indicate the 25th and 75th percentiles, respectively. The bottom and top whiskers indicate the range of data within 1.5 times the interquartile range. Individual diamonds represent values outside 1.5 times the interquartile range (outliers). The boxplot labelled NIST 8017 represents data gathered in NIST report of analysis, for which individual data outside 1.5 times the interquartile range are not available. (A) Complete representations of outliers (B) Zoom-in of A in order to compare all the median, mean, 25th and 75th percentiles individual values

As for the SP-ICP-MS NP distribution data provided by NIST and gathered in Figure 6.5, comparison cannot be complete as no individual values are provided in the Certificate of Analysis, although it seems that the NP distributions obtained by SP-ICP-TOF-MS (with either external calibration of IDA) are wider than those reported by NIST, especially towards larger diameters. This could be due to NP aggregation. However, it has to be mentioned in this regard that, according to literature,[161] relatively large differences in NP distribution data are common for different analytical techniques or even different operators, such that data provided on mass concentration recovery can be considered as a good indicator of the quality of the results.

Finally, influence of the spike concentration on the LOD_{size} must be evaluated. As indicated above, too high a spike concentration could result in higher background for the 107 trace, which is used for NP identification, which would degrade LOD_{size}. LOD_{size} for the different spike concentrations used in the study were calculated following the equation proposed by Laborda et. al[60] (eq. 1.12 on Chapter 1). A summary of LOD_{size} is included in Table 6.3. As seen from this table, there are no significant differences in LOD_{size} for the spike concentrations deployed in this work, such that selection of the spike is better done in terms of the shape for the NP distribution obtained as explained above. Accordingly, 1.5 µg L^{-1} was used for further analysis in this study.

Table 6.3: LOD_{size} by each spike condition (standard deviation of 2 days of analysis).

Spike (µg L^{-1})	**LOD_{size} ± SD (nm)**
0.25	33.83 ± 1.70
0.50	33.06 ± 0.80
0.75	32.57 ± 0.57
1.00	32.70 ± 0.50
1.50	32.36 ± 0.32
2.00	32.25 ± 0.74

6.3.5. Mass discrimination correction

It is well known that heavier isotopes are better transmitted in ICP-MS instruments. This mass discrimination effect is known to be produced in the interface (nozzle effect) or in the ion optics (space-charge effect).[147] ICP-TOF-MS instruments have similar introduction systems to regular quadrupole instruments, so that these sources of mass discrimination are also present and must be corrected for.

Among the different methods existing for mass bias correction, the sample standard bracketing method was considered as the most appropriate in this particular case. It has been documented[100] that there is a mass peak drift in ICP-TOF-MS when integration times are long, so it is important to mass calibrate the instrument often. In the sample-standard bracketing method, a mass-bias correction factor, K, is calculated as $K = R_{true}/R_{measured}$ for a standard with well-known or certified isotopic composition, and this factor is later applied to the sample measured ratios to obtain the true values. For elements that do not show natural variations in their isotopic abundances, such as Ag, any standard (with natural isotopic composition) can be used for correction. For this particular case, moreover, a dispersion of Ag NP of natural isotopic composition can be also used for correction. Calculation of the K factor was carried out in this work with these two options: a 75 nm Ag NP dispersion on the one side, and a set of ionic solutions with concentrations of 2.5; 5.0; 7.5 and 10.0 µg L^{-1} on the other. Results are compared in Table 6.4. As seen from this table, there are no significant differences in the median K values obtained with one option or the other, but uncertainty with the ionic standards is much lower than with the AgNPs dispersion. As a result, calculation of the K factor with the ionic standards was carried out in all IDA experiments.

Table 6.4: Median K factor obtained after measurement of a 75nm nominal diameter AgNP dispersion and for a set of Ag ionic solutions of 2.5, 5, 7.5 and 10 µg L^{-1}. Confidence intervals represent one standard deviation of 3 different days.

Sample	K factor ± SD
NPs	1.0562 ± 0.0126
Ionic Solutions	1.0554 ± 0.0033

6.4. Application of the IDA developed method on AgNPs characterization by means ICP-TOF-MS

Table 6.5 gathers all the important parameters obtained for the AgNPs characterization by IDA approach, using the experimental parameters commented on in the previous sections. As previously indicated, the results of the third day of measurements are biased high in comparison the two other days of analysis. For this reason, the results given in the Table 6.5 are expressed as the average of the first 2 days of analysis.

Table 6.5: Comparison of the AgNPs characterization parameters values obtained with optimized IDMS conditions. All the values are expressed by the average and standard deviation of the result obtained by 2 days of analysis (n = 2). Certified diameter provided by NIST certificate of analysis: 74.6 ± 3.8 nm.

Parameter	1.5 ppb spike
Median diameter (nm)	74.8 ± 0.9
Average diameter (nm)	76.0 ± 1.0
Mass concentration recovery (%)	112 ± 10
Particle number concentration recovery (%)	96 ± 1.9

As seen from this table, good median and average diameter values were achieved with the optimized IDA method. Also, this approach also presents good mass and particle number concentration recoveries.

Despite the wide study of the IDA method presented in this chapter, some aspects can be improved, such as the impact of spikes higher than 2.0 µg L^{-1} in the particle size distribution, the application of this method to different types of matrices for an eventual replacement of the conventional approach of the characterization of NPs by means SP-ICP-MS and the possibility of working with ultra-short integration times in order to avoid the split and double events generated when integration times on the millisecond scale are used. However, it is clear that the method developed in this work presents itself as a possible solution for the characterization of NPs in complex matrices by means SP-ICP-TOF-MS.

6.5. Conclusions

According to the study described throughout this chapter, the method developed for NPs characterization by IDA approach may be an alternative to the classic method of NPs characterization by means SP-ICP-MS in complex matrices (TE determination and mass-flux ionic calibration). Appropriate adaptations were made to apply the general IDA equation for standard ICP-MS operation to SP analysis, such as the inclusion of TE and the time of integration in the equation. Furthermore, a systematic study on the effect of different parameters in the precision attained for analysis was carried out in an ICP-TOF-MS. This instrument is the only ICP-MS in the market that records a quasi-simultaneous full MS spectrum, enabling the calculation of the isotope ratio of the Ag isotopes from the same AgNP. The isotope ratio is calculated particle by particle and thus, it is possible to calculate the mass and, consequently, the diameter of each single particle by applying the IDA equation. The development of this method is not straightforward, however, and attention must be paid to instrumental parameters (data acquisition mode and integration time), optimization of the spike concentration and data treatment (split events correction and mass calculation). After the optimization of all discussed parameters and choosing the 1.5 µg L^{-1} spike, the IDA method was applied for the AgNPs characterization and satisfactory diameter values, particle number values and mass concentration recoveries were obtained. The optimized method presented promising results and further studies would be fair to be carried out in order to apply this method on several types of samples with complex matrices.

CHAPTER 7

Final Conclusions

7.1. Final Conclusions

As described in Chapter 1, the SP-ICP-MS technique still faces challenges regarding to the development of reliable methods that can be applied in samples with complex matrices. As well as in the ICP-MS technique, SP-ICP-MS also suffers the effects of spectral interferences from species ubiquitous in the plasma, jeopardizing the analyses of NPs composed by elements such as Si and Fe, for example. Furthermore, this technique also faces potential matrix effects when analysis of samples with complex matrices is aimed at. Thus, proper strategies to overcome those effects are still needed. In particular, this doctoral thesis explored two main approaches for the development of reliable methods for NPs characterization by SP-ICP-MS: (i) use of collision and reaction gases to eliminate spectral interferences; and, (ii) new calibration strategies to eliminate matrix effects for the characterization of NP in complex samples.

In the first part of this doctoral thesis (Chapters 3 and 4), ICP-MS/MS instrumentation was used due to minimize spectral interferences through the use of reactions in a CRC, which is placed between two quadrupole mass analyzers.[108] The use of this instrumentation for NPs analysis made possible the characterization of SiO_2 and Fe_3O_4NPs free from spectral interferences, greatly improving LOD_{size}. The method developed for SiO_2NPs, for example, was one of the first studies in the literature that used the ICP-MS/MS instrumentation for NPs characterization. In this work, a minimum dwell time of 3 ms could be used, which made possible the characterization of SiO_2NPs for sizes > 100 nm using H_2 as the reaction gas and working with the "on-mass" mode. With this same method, it was also possible to characterize SiO_2NPs down to 80 nm with a deconvolution approach, using the OriginLab software to separate both background and NPs distribution and estimate the SiO_2NPs diameter.

During this doctoral thesis, manufacturers for ICP-MS instruments have been continuously improving the performance of their products, enabling the use of dwell times in the microsecond range (10 – 500 µs). The use of ultra-short dwell times brought a great advance to the SP-ICP-MS technique and to this doctoral thesis, since it was possible to obtain less intense background intensities and lower LOD_{size}. Applying this dwell time on the previous SiO_2NPs method, it was possible to obtain lower LOD_{size} for

SiO_2NPs and characterize 80 nm SiO_2NPs without the need for the use of the deconvolution approach previously mentioned. With this instrumentation, it was also possible to develop a method for Fe_3O_4NPs characterization free from spectral interferences.

One of the main objectives of this doctoral thesis was to study the effects of the use of CRCs on the duration of NP signals. Until the date in which this work started, the vast majority of SP-ICP-MS works targeted Au and AgNPs, which should not suffer from severe spectral overlap and, therefore, do not require the use of CRC for any method development. Therefore, there was no information in the literature regarding the effect that CRC gases could have on the time of detection of NPs. In this study, it was observed that the type, flow and reactivity of the reaction gas may affect the duration of NPs. Gases with a larger molecular size such as NH_3 tend to produce a larger peak broadening than smaller gases like H_2 and He. Furthermore, a very interesting behavior was observed when using NH_3 as a reaction gas for the characterization of Fe_3O_4NPs: peaks of up to 6 ms were observed for 200 nm NPs, which indicates that the time of detection of NPs must be studied prior to any analysis with methods that made use of a collision/reaction gas in the CRC.

The second part of this doctoral thesis (Chapters 5 and 6) explored the development of strategies that could mitigate the matrix effects in complex samples when SP-ICP-MS is deployed. Matrix-matching and isotope Dilution were chosen as strategies to overcome such matrix effects. It is important to highlight that in both methods, the TE was determined in the same matrix of the sample and was determined by the Particle Frequency Method described by Pace et al,[59] as this is, up to this date, the most accepted method described in the SP-ICP-MS literature for the TE determination. In Chapter 5, it was observed that it is essential to perform matrix matching of the ionic calibration standards for the characterization of AgNPs in samples of 2.5% TMAH + 0.1% Triton X-100, resulting from the alkaline digestion of tissues and blood. In chapter 6, on the other hand, adaptation of the IDA approach for AgNPs characterization by SP-ICP-MS was explored. Application of the IDA approach requires an ICP-TOF-MS instrument, due to its possibility of quasi-simultaneous monitorization of all isotopes in the mass range 14-275 u, enabling the calculation of the isotope ratios of a single NP, which is not possible with quadrupole ICP-MS instruments. The post-

column equation used for chromatography isotope dilution methods was adapted to SP-ICP-MS for the calculation of the nanoparticle mass. The post-column equation for NP characterization considers the TE and the selected integration time in addition of the sample flow, isotope abundance and isotope ratios (in the spike and sample). A systematic study was carried out to optimize the different parameters that affect the quality of the results.

The application of this method is not straightforward, and attention must be paid to instrumental parameters (data acquisition mode and integration time), optimization of the spike concentration and data treatment (split events correction and mass calculation). The optimized method presented promising results and further studies would be fair to be carried out in order to apply this method on several types of samples with complex matrices.

7.2. Conclusiones Finales

Como se describe en el Capítulo 1, la técnica SP-ICP-MS aún enfrenta desafíos con respecto al desarrollo de métodos confiables que se puedan aplicar en muestras con matrices complejas. Así como en la técnica ICP-MS, SP-ICP-MS también sufre los efectos de interferencias espectrales de especies presentes en el plasma, comprometiendo los análisis de NPs compuestas por elementos como Si y Fe, por ejemplo. Además, esta técnica también se enfrenta a posibles efectos de matriz cuando se pretende analizar muestras con matrices complejas. Por lo tanto, aún se necesitan estrategias adecuadas para superar esos efectos. En particular, esta tesis doctoral exploró dos enfoques principales para el desarrollo de métodos confiables para la caracterización de NPs mediante SP-ICP-MS: (i) uso de gases de colisión y reacción para eliminar interferencias espectrales; y, (ii) nuevas estrategias de calibración para eliminar efectos de matriz para la caracterización de NP en muestras complejas.

En la primera parte de esta tesis doctoral (Capítulos 3 y 4), se utilizó instrumentación de ICP-MS / MS para minimizar las interferencias espectrales mediante el uso de reacciones en una CRC, la cual se ubica entre dos analizadores de masas cuadrupolo. El uso de esta instrumentación para el análisis de NPs hizo posible la caracterización de SiO_2 y Fe_3O_4NPs libres de interferencias espectrales, mejorando enormemente el límite de detección en tamaño (LOD_{size}). El método desarrollado para SiO_2NPs, por ejemplo, fue uno de los primeros estudios en la literatura que utilizó la instrumentación ICP-MS/MS para la caracterización de NPs. En este trabajo se pudo utilizar un tiempo de integración mínimo de 3 ms, lo que posibilitó la caracterización de SiO_2NPs para tamaños > 100 nm utilizando H_2 como gas de reacción y midiendo enla masa del analito (modo "*on-mass*"). Con este mismo método, también fue posible caracterizar SiO_2NPs hasta 80 nm mediante deconvolución de las señales obtenidas para el ruido de fondo y las nanopartículas utilizando el software OriginLab.

Durante el tiempo de elaboración de esta tesis doctoral, los fabricantes de instrumentos ICP-MS han mejorado el rendimiento de sus productos, permitiendo el uso de tiempos de permanencia (*dwell time*) en el rango de microsegundos (10 - 500 µs). El uso de tiempos de permanencia ultracortos supuso un gran avance en la técnica SP-ICP-MS y en esta tesis doctoral, ya que fue posible obtener intensidades de contribución de

fondo menos intensas y, en consecuencia, menores LOD_{size}. Aplicando este tiempo de integración en el método anterior de SiO_2NPs, fue posible obtener un LOD_{size} más bajo para SiO_2NPs y caracterizar SiO_2NPs de 80 nm sin la necesidad del uso de la deconvolución mencionada anteriormente. Con esta instrumentación, también fue posible desarrollar un método para la caracterización de Fe_3O_4NPs libre de interferencias espectrales.

Uno de los principales objetivos de esta tesis doctoral fue estudiar los efectos del uso de las celdas de colisión/reacción (CRC) sobre la duración de las señales de las NPs. Hasta la fecha en que se inició este trabajo, la gran mayoría de los trabajos de SP-ICP-MS tenían como objetivo nanopartículas de Au y Ag, que no están afectadas por interferencias importantes en el ICP-MS y, por lo tanto, no requieren el uso de CRC para el desarrollo de ningún método. Por lo tanto, no había información en la literatura sobre el efecto que el uso de las CRC podrían tener en las señales de las NPs. En este estudio, se observó que el tipo, flujo y reactividad del gas de reacción pueden afectar a la duración de las NP, aumentándola considerablemente. Los gases con un mayor tamaño, como el NH_3, tienden a producir un ensanchamiento de pico mayor que los gases más pequeños como el H_2 y el He. Además, se observó un comportamiento muy interesante al utilizar NH_3 como gas de reacción para la caracterización de Fe_3O_4NPs: se observaron picos de hasta 6 ms de duración para NPs de 200 nm de diámetro nominal, lo que indica que el tiempo de detección de las NPs debe ser estudiado antes de cualquier análisis cuando se vaya a utilizar la CRC.

La segunda parte de esta tesis doctoral (Capítulos 5 y 6) exploró el desarrollo de estrategias que podrían mitigar los efectos de la matriz en muestras complejas cuando se implementa SP-ICP-MS. Se eligieron la compatibilización de matrices y la dilución isotópica como estrategias para superar dichos efectos de matriz. Es importante destacar que, en ambos métodos, la eficiencia de transporte se determinó en la misma matriz de la muestra por el Método de Frecuencia de Partículas descrito por Pace et al,[59] ya que este es, hasta la fecha, el método descrito más aceptado en la literatura de SP-ICP-MS para la determinación de la eficiencia de transporte. En el Capítulo 5 se observó que es fundamental realizar la compatibilización de matrices de los estándares de la calibración iónica para la caracterización de AgNPs en muestras de TMAH al 2.5% + Triton % X-100, resultantes de la digestión alcalina de tejidos biológicos y sangre. En el

capítulo 6, por otro lado, se exploró la adaptación del enfoque IDA para la caracterización de AgNPs mediante SP-ICP-MS. La aplicación del enfoque IDA requiere un instrumento ICP-TOF-MS, debido a su posibilidad de monitorización cuasi-simultánea de todos los isótopos en el rango de masa 14-275 u, lo que permite el cálculo de las relaciones isotópicas de una sola NP, lo que no es posible con los instrumentos ICP-MS equipados con cuadrupolo como separador de masas. La ecuación de post-column utilizada para los métodos de dilución isotópica por cromatografía se adaptó a SP-ICP-MS para el cálculo de la masa de las nanopartículas. La ecuación post-column adaptada para la caracterización de NPs considera la TE y el tiempo de integración seleccionado, además del flujo de muestra, la abundancia de los isótopos consideradas y las relaciones isotópicas medidas para la mezcla muestra+ estándar isotópico. Se realizó un estudio sistemático para optimizar los diferentes parámetros que inciden en la calidad de los resultados. La aplicación de este método no es sencilla y se debe prestar atención a los parámetros instrumentales (modo de adquisición de datos y tiempo de integración), optimización de la concentración de picos y tratamiento de datos (corrección de eventos divididos y cálculo de masas). El método optimizado presentó resultados prometedores para la determinación del tamaño, concentración de NPs y concentración en masa para AgNPs de 75 nm de diámetro nominal. Sin embargo, habrá que realizar más estudios para aplicar este método en varios tipos de muestras con matrices más complejas.

Bibliography

(1) Gubala, V. Johnston, L. J., Liu, Z., Krug, H., Moore, C. J., Ober, C. K., Schwenk M. & Vert, M. (2018). "Engineered Nanomaterials and Human Health: Part 1. Preparation, Functionalization and Characterization (IUPAC Technical Report)". ***Pure Appl. Chem,*** 90 (8), pp. 1283–1324. DOI: 10.1515/pac-2017-0101

(2) Ashby, M. F., Ferreira, P. J. & Schodek, D. L. (2009). "Chapter 1 - Nanomaterials and Nanotechnologies: An Overview". Ashby, M. F. Ferreira, P. J. Schodek, D. L. ***Nanomaterials, Nanotechnologies and Design,*** Boston: Butterworth-Heinemann, pp. 1–16. DOI:10.1016/B978-0-7506-8149-0.00003-9

(3) Ramsden, J. J. (2014). "Chapter 1 - What Is Nanotechnology?". Ramsden, J. J. ***Applied Nanotechnology (Second Edition)***, Oxford: Micro and Nano Technologies, pp. 3–12. DOI: 0.1016/B978-1-4557-3189-3.00001-4

(4) Roco, M. C. (2011). "The Long View of Nanotechnology Development: The National Nanotechnology Initiative at 10 Years". ***J. Nanopart. Res.***, 13 (2), pp. 427–445. DOI: 10.1007/s11051-010-0192-z

(5) ISO (2005). ISO/TC 229 - Nanotechnologies. Available in: https://www.iso.org/cms/render/live/en/sites/isoorg/contents/data/committee/38/19/381983.html (accessed: September 26th, 2020).

(6) Foresight (2020). About Nanotechnology. Available in: https://foresight.org/nano/ (accessed: September 26th, 2020).

(7) IUPAC (2005 - 2021). Nano. Available in, https://goldbook.iupac.org/terms/view/N04082 (accessed: September 26th, 2020).

(8) ISO (2017). ISO/TR 18401:2017(en), Nanotechnologies — Plain language explanation of selected terms from the ISO/IEC 80004 series. Available in: https://www.iso.org/obp/ui/#iso:std:iso:tr:18401:ed-1:v1:en (accessed: September 28th, 2020).

(9) ISO (2015).ISO/TS 80004-2:2015(en), Nanotechnologies — Vocabulary — Part 2: Nano-objects. Available in: https://www.iso.org/obp/ui/#iso:std:iso:ts:80004:-2:ed-1:v1:en (accessed: July 21th, 2020).

(10) Krystek, P., Ulrich, A., Garcia, C. C., Manohar, S. & Ritsema, R. (2011)."Application of Plasma Spectrometry for the Analysis of Engineered Nanoparticles in Suspensions and Products". ***J. Anal. At. Spectrom****.* 26 (9), pp. 1701-1721. DOI: 10.1039/c1ja10071h

(11) Calderón-Jiménez, B., Johnson, M. E., Montoro Bustos, A. R., Murphy, K. E., Winchester, M. R. & Vega Baudrit, J. R. (2017). "Silver Nanoparticles: Technological Advances, Societal Impacts, and Metrological Challenges". ***Front. Chem.***, 5, pp. 1-26. DOI:10.3389/fchem.2017.00006

(12) Krug, H. F. & Wick, P. (2011). "Nanotoxicology: An Interdisciplinary Challenge". ***Angew. Chem. Int. Ed.,*** 50 (6), pp. 1260–1278. DOI: 10.1515/pac-2017-0101

(13) Vert, M., Doi, Y., Hellwich, K.-H., Hess, M., Hodge, P., Kubisa, P., Rinaudo, M. & Schué, F. (2012). "Terminology for Biorelated Polymers and Applications (IUPAC Recommendations 2012)". ***Pure Appl. Chem,*** 84 (2), pp. 377–410. DOI:10.1351/PAC-REC-10-12-04

(14) Sharma, V. K., Filip, J., Zboril, R. & Varma, R. S. (2015). "Natural Inorganic Nanoparticles – Formation, Fate, and Toxicity in the Environment". ***Chem. Soc. Rev***., 44 (23), pp. 8410–8423. DOI:10.1039/C5CS00236B

(15) Dolez, P. I. (2015). "Nanomaterials Definitions, Classifications, and Applications". ***Nanoengineering - Global Approaches to Health and Safety Issues,*** Dolez, P. I. Canadá: Elsevier, pp. 3–40. DOI: 10.1016/B978-0-444-62747-6.00001-4

(16) Mourdikoudis, S., Pallares, R. M. & Thanh, N. T. K. (2018). "Characterization Techniques for Nanoparticles: Comparison and Complementarity upon Studying Nanoparticle Properties." ***Nanoscale,*** 10 (27), pp. 12871–12934. DOI: 10.1039/C8NR02278J

(17) López-Serrano, A., Olivas, R. M., Landaluze, J. S. & Cámara, C. (2014). "Nanoparticles: A Global Vision. Characterization, Separation, and Quantification Methods. Potential Environmental and Health Impact." ***Anal. Methods,*** 6 (1), pp. 38–56. https://doi.org/10.1039/C3AY40517F

(18) Pitkänen, L. & Striegel, A. M. (2016). “Size-Exclusion Chromatography of Metal Nanoparticles and Quantum Dots”. ***Trends Anal. Chem.,*** 80, pp. 311–320. DOI: 10.1016/j.trac.2015.06.013

(19) Bleeker, E. A. J., de Jong, W. H., Geertsma, R. E., Groenewold, M., Heugens, E. H. W., Koers-Jacquemijns, M., van de Meent, D., Popma, J. R., Rietveld, A. G., Wijnhoven, S. W. P., Cassee, F. R. & Oomen, A. G. (2013). "Considerations on the EU Definition of a Nanomaterial: Science to Support Policy Making". ***Regul. Toxicol. Pharmacol.,*** 65, pp. 119–125. DOI: 10.1016/j.yrtph.2012.11.007

(20) Hassellöv, M., Readman, J. W., Ranville, J. F. & Tiede, K. (2008). "Nanoparticle Analysis and Characterization Methodologies in Environmental Risk Assessment of Engineered Nanoparticles". ***Ecotoxicology***, 17 (5), pp. 344–361. DOI: 10.1007/s10646-008-0225-x

(21) Aschberger, K., Micheletti, C., Sokull-Klüttgen, B. & Christensen, F. M. (2011). "Analysis of Currently Available Data for Characterising the Risk of Engineered Nanomaterials to the Environment and Human Health — Lessons Learned from Four Case Studies" ***Environ. Int***, 37, pp. 1143–1156. DOI: 10.1016/j.envint.2011.02.005

(22) Gottschalk, F. & Nowack, B. (2011). "The Release of Engineered Nanomaterials to the Environment". ***J. Environ. Monit.***, 13 (5), pp. 1145-1155. DOI: 10.1039/c0em00547a

(23) Noguera-Oviedo, K. & Aga, D. S. (2016). "Lessons Learned from More than Two Decades of Research on Emerging Contaminants in the Environment." ***J. Hazard. Mater.,*** 316, pp. 242–251. DOI: 10.1016/j.jhazmat.2016.04.058

(24) Boverhof, D. R., Bramante, C. M., Butala, J. H., Clancy, S. F., Lafranconi, M., West, J. & Gordon, S. C. (2015). "Comparative Assessment of Nanomaterial Definitions and Safety Evaluation Considerations". ***Regul. Toxicol. Pharmacol.,*** 73 (1), pp.137–150. DOI: 10.1016/j.yrtph.2015.06.001

(25) Lövestam, G., Rauscher, H., Roebben, G., Klüttgen, B. S., Gibson, N., Putaud, J.-P. & Stamm, H. (2010). **"*Considerations on a Definition of Nanomaterial for Regulatory Purposes"***, European Union: European Commission.

(26) European Commission (2011). Commission Recommendation of 18 October 2011 on the Definition of NanomaterialText with EEA Relevance. Available in: https://ec.europa.eu/research/industrial_technologies/pdf/policy/commission-recommendation-on-the-definition-of-nanomater-18102011_en.pdf (accessed: October 12th, 2020).

(27) Australian Government, Department of Health (2020). Categorization of chemicals at the nanoscale. Available in: https://www.industrialchemicals.gov.au/help-and-guides/extra-resources-help-you-categorise-your-introduction/categorisation-chemicals-nanoscale (accessed: September 28th, 2020).

(28) Government of Canada (2010). Interim Policy Statement on Health Canada's Working Definition for Nanomaterials. Available in: https://www.canada.ca/en/health-canada/services/science-research/consultations/interim-policy-statement-health-canada-working-definition-nanomaterials/document.html (accessed: September 28th, 2020).

(29) Environmental Protection Agency (2017). Chemical substances when manufactured or processed as nanoscale materials: TSCA reporting and recordkeeping requirements. Available in: https://www.regulations.gov/document?D=EPA-HQ-OPPT-2010-0572-0137 (accessed: September 28th, 2020).

(30) Food and Drug Administration (2011). "Guidance for Industry Considering Whether an FDA-Regulated Product Involves the Application of Nanotechnology". ***Biotechnology Law Report***, 30 (5), pp. 613–616. DOI: 10.1089/blr.2011.9814

(31) Linsinger, T. P. J., Roebben, G., Gilliland, D., Calzolai, L., Rossi, F., Gibson, N. & Klein, C., (2012) "Requirements on Measurements for the Implementation of the European Commission Definition of the Term "Nanomaterial*"",* Luxembourg: ***Institute for Reference Materials and Measurements***, pp. 1-48

(32) Laux, P., Tentschert, J., Riebeling, C., Braeuning, A., Creutzenberg, O., Epp, A., Fessard, V., Haas, K.-H., Haase, A., Hund-Rinke, K., Jakubowski, N., Kearns, P., Lampen, A., Rauscher, H., Schoonjans, R., Störmer, A., Thielmann, A. & Mühle, U., Luch, A. (2018). "Nanomaterials: Certain Aspects of Application, Risk Assessment and Risk Communication. ***Arch. Toxicol.,*** 92 (1), pp. 121–141. DOI: 10.1007/s00204-017-2144-1

(33) López-Sanz, S., Guzmán Bernardo, F. J., Rodríguez Martín-Doimeadios, R. C. & Ríos, Á. (2019). " Analytical Metrology for Nanomaterials: Present Achievements and Future Challenges". ***Anal. Chim. Acta,*** 1059, pp. 1–15. DOI: 10.1016/j.aca.2019.02.009

(34) European Chemicals Agency (2019). Guidance on Information Requirements and Chemical Safety Assessment https://echa.europa.eu/guidance-documents/guidance-on-information-requirements-and-chemical-safety-assessment (accessed: October 20th, 2020) .

(35) López-Lorente, Á. I. & Valcárcel, M. (2016). "The Third Way in Analytical Nanoscience and Nanotechnology: Involvement of Nanotools and Nanoanalytes in the Same Analytical Process". ***Trends Anal. Chem.,*** *75*, pp. 1–9. DOI: 10.1016/j.trac.2015.06.011

(36) Sharma, D., Kanchi, S., Bisetty, K. & Nuthalapati, V. N. (2016). "Chapter 1 Perspective on Analytical Sciences and Nanotechnology". Hussain, C.M. & Kharisov, B. ***Advanced Environmental Analysis Applications of Nanomaterials, Volume 1***. Cambridge: Royal Society of Chemistry, pp. 1–34. DOI: 10.1039/9781782623625-00001

(37) López-Lorente, Á. I. & Valcárcel, M. (2014). "Chapter 1 - Analytical Nanoscience and Nanotechnology". ***Compr. Anal. Chem*****,** 66, pp. 3–35. DOI: 10.1016/B978-0-444-63285-2.00001-8

(38) Valcárcel, M. & Simonet, B. M. (2011). "Nanomaterials for Improved Analytical Processes". ***Anal. Bioanal. Chem.,*** 399 (1), 1–2. DOI: 10.1007/s00216-010-4315-2

(39) Powers, K. W., Brown, S. C., Krishna, V. B., Wasdo, S. C., Moudgil, B. M. & Roberts, S. M. (2006). "Research Strategies for Safety Evaluation of Nanomaterials. Part VI. Characterization of Nanoscale Particles for Toxicological Evaluation". ***Toxicol. Sci.,*** 90 (2), pp. 296–303. DOI: 10.1093/toxsci/kfj099

(40) Soriano, M. L., Zougagh, M., Valcárcel, M. & Ríos, Á. (2018). "Analytical Nanoscience and Nanotechnology: Where We Are and Where We Are Heading". ***Talanta***, 177, pp. 104–121. DOI: 10.1016/j.talanta.2017.09.012

(41) Contado, C. (2015). "Nanomaterials in Consumer Products: A Challenging Analytical Problem". ***Front. Chem.***, *3*. pp. 1 - 20 DOI: 10.3389/fchem.2015.00048

(42) Laborda, F., Bolea, E., Cepriá, G., Gómez, M. T., Jiménez, M. S., Pérez-Arantegui, J. & Castillo, J. R. (2016). "Detection, Characterization and Quantification of Inorganic Engineered Nanomaterials: A Review of Techniques and Methodological Approaches for the Analysis of Complex Samples". ***Anal. Chim. Acta*****,** *904*, pp. 10–32. http://dx.doi.org/10.1016/j.aca.2015.11.008

(43) Gräfe, M., Donner, E., Collins, R. N. & Lombi, E. (2014). "Speciation of Metal(Loid)s in Environmental Samples by X-Ray Absorption Spectroscopy: A Critical Review". ***Anal. Chim. Acta*****,** 822, pp. 1–22. DOI: 10.1016/j.aca.2014.02.044

(44) Resano, M., Aramendía, M. & Belarra, M. A. (2014). "High-Resolution Continuum Source Graphite Furnace Atomic Absorption Spectrometry for Direct Analysis of Solid Samples and Complex Materials: A Tutorial Review". ***J. Anal. At. Spectrom.***, 29 (12), 2229–2250. DOI: 10.1039/C4JA00176A

(45) Leopold, K., Brandt, A. & Tarren, H. (2017). "Sizing Gold Nanoparticles Using Graphite Furnace Atomic Absorption Spectrometry". ***J. Anal. At. Spectrom.***, *32* (4), pp. 723–730. DOI: 10.1039/C7JA00019G

(46) Resano, M., Garcia-Ruiz, E. & Garde, R. (2016). "High-Resolution Continuum Source Graphite Furnace Atomic Absorption Spectrometry for the Monitoring of Au Nanoparticles". ***J. Anal. At. Spectrom.***, 31 (11), pp. 2233–2241. DOI: 10.1039/C6JA00280C

(47) Ray, S.S. (2013). "Techniques for Characterizing the Structure and Properties of Polymer Nanocomposites". Ray, S.S. ***Environmentally Friendly Polymer Nanocomposites***. Woodhead Publishing, pp 74–88. DOI: 10.1533/9780857097828.1.74

(48) Klein, T., Buhr, E. & Georg Frase, C. (2012). "Chapter 6 - TSEM: A Review of Scanning Electron Microscopy in Transmission Mode and Its Applications. In *Advances in Imaging and Electron Physics"* Hawkes, P. W., ***Advances in Imaging and Electron Physics.*** Elsevier, 171, pp. 297–356. DOI: 10.1016/B978-0-12-394297-5.00006-4

(49) Mahmood, I. A., Moheimani, S. O. R. & Bhikkaji, B. A (2011). "New Scanning Method for Fast Atomic Force Microscopy". ***IEEE T. Nanotechnol.,*** *10* (2), pp. 203–216. DOI: 10.1109/TNANO.2009.2036844.

(50) Dhawan, A. & Sharma, V. (2010). "Toxicity Assessment of Nanomaterials: Methods and Challenges". ***Anal, Bioanal. Chem.,*** *398* (2), pp. 589–605. DOI: 10.1007/s00216-010-3996-x.

(51) Kranz, C. & Mizaikoff, B. (2014). "Chapter 6 - Microscopic Techniques for the Characterization of Gold Nanoparticles". Valcárcel, M. & López-Lorente, Á. I., ***Comprehensive Analytical Chemistry***, Elsevier, 66, pp. 257–299. DOI: 10.1016/B978-0-444-63285-2.00006-7.

(52) Bartczak, D., Vincent, P. & Goenaga-Infante, H. (2015). "Determination of Size- and Number-Based Concentration of Silica Nanoparticles in a Complex Biological Matrix by Online Techniques". ***Anal. Chem.*** 87 (11), pp. 5482–5485. DOI: 10.1021/acs.analchem.5b01052.

(53) Hoo, C. M., Starostin, N., West, P. & Mecartney, M. L. (2008). "A Comparison of Atomic Force Microscopy (AFM) and Dynamic Light Scattering (DLS) Methods to Characterize Nanoparticle Size Distributions". ***J Nanopart Res,*** 10, pp. 89–96. DOI: 10.1007/s11051-008-9435-7.

(54) Dhawan, P. A., Sharma, V. & Parmar, D. (2009). "Nanomaterials: A Challenge for Toxicologists". ***Nanotoxicology,*** 3 (1), pp. 1–9. DOI: 10.1080/17435390802578595.

(55) Cagno, S., Brede, D. A., Nuyts, G., Vanmeert, F., Pacureanu, A., Tucoulou, R., Cloetens, P., Falkenberg, G., Janssens, K., Salbu, B. & Lind, O. C. (2017). "Combined Computed Nanotomography and Nanoscopic X-Ray Fluorescence Imaging of Cobalt Nanoparticles in *Caenorhabditis Elegans"*. ***Anal. Chem.***, 89 (21), pp. 11435–11442. DOI: 10.1021/acs.analchem.7b02554.

(56) Hernandez-Viezcas, J. A., Castillo-Michel, H., Andrews, J. C., Cotte, M., Rico, C., Peralta-Videa, J. R., Ge, Y., Priester, J. H., Holden, P. A. & Gardea-Torresdey, J. L. (2013). "In Situ Synchrotron X-Ray Fluorescence Mapping and Speciation of CeO2 and ZnO Nanoparticles in Soil Cultivated Soybean (Glycine Max)". ***ACS Nano,*** 7 (2), pp. 1415–1423. DOI: 10.1021/nn305196q.

(57) Fiedler, H. D., Drinkel, E. E., Orzechovicz, B., Leopoldino, E. C., Souza, F. D., Almerindo, G. I., Perdona, C. & Nome, F. (2013). "Simultaneous Nondestructive Analysis of Palladium, Rhodium, Platinum, and Gold Nanoparticles Using Energy Dispersive X-Ray Fluorescence". ***Anal. Chem.*** 85 (21), pp. 10142–10148. DOI: 10.1021/ac402419r

(58) Ban, E., Yoo, Y. S. & Song, E. J. (2015). "Analysis and Applications of Nanoparticles in Capillary Electrophoresis". ***Talanta***, 141, pp. 15–20. DOI: 10.1016/j.talanta. 2015.03.020

(59) Pace, H. E., Rogers, N. J., Jarolimek, C., Coleman, V. A., Higgins, C. P. & Ranville, J. F. (2011). "Determining Transport Efficiency for the Purpose of Counting and Sizing Nanoparticles via Single Particle Inductively Coupled Plasma Mass Spectrometry". ***Anal. Chem.***, 83 (24), pp. 9361–9369. DOI: 10.1021/ac201952t

(60) Laborda, F., Bolea, E. & Jiménez-Lamana, J. (2014). "Single Particle Inductively Coupled Plasma Mass Spectrometry: A Powerful Tool for Nanoanalysis". ***Anal. Chem.,*** 86 (5), pp. 2270–2278. DOI: 10.1021/ac402980q.

(61) Montaño, M. D., Badiei, H. R., Bazargan, S. & Ranville, J. F. (2014). "Improvements in the Detection and Characterization of Engineered Nanoparticles Using SpICP-MS with Microsecond Dwell Times". ***Environ. Sci.: Nano*****,** 1 (4), pp. 338–346. DOI: 10.1039/C4EN00058G.

(62) Olesik, J. W. & Gray, P. J. (2012). "Considerations for Measurement of Individual Nanoparticles or Microparticles by ICP-MS: Determination of the Number of Particles and the Analyte Mass in Each Particle". ***J. Anal. At. Spectrom.*****,** 27 (7), pp. 1143-1155. DOI: 10.1039/c2ja30073g

(63) Crider, W. L. (1968). "Spectrothermal Emission Aerosol Particle Analyzer (SEAPA)". ***Review of Scientific Instruments***, 39 (2), pp, 212–215. DOI: 10.1063/1.1683316

(64) Hieftje, G. M. & Malmstadt, H. V. (1968). "Unique System for Studying Flame Spectrometric Processes". ***Anal. Chem.*****,** 40 (12), pp. 1860–1867. DOI: 10.1021/ac60268a024

(65) Kawaguchi, H., Fukasawa, N. & Mizuike, A. (1986). "Investigation of Airborne Particles by Inductively Coupled Plasma Emission Spectrometry Calibrated with Monodisperse Aerosols". ***Spectrochim. Acta, Part B*** **,** 41 (12), pp. 1277–1286. DOI: 10.1016/0584-8547(86)80006-4

(66) Nomizu, T., Kaneco, S., Tanaka, T., Yamamoto, T. & Kawaguchi, H. (1993). "Determination of Femto-Gram Amounts of Zinc and Lead in Individual Airborne Particles by Inductively Coupled Plasma Mass Spectrometry with Direct Air-Sample Introduction". ***Anal. Sci.***, 9 (6), pp. 843–846. DOI: 10.2116/analsci.9.843

(67) Degueldre, C., Favarger, P.Y. & Bitea, C. (2004). "Zirconia Colloid Analysis by Single Particle Inductively Coupled Plasma–Mass Spectrometry". ***Anal. Chim. Acta***, 518 (1), pp. 137–142. DOI: 10.1016/j.aca.2004.04.015

(68) Degueldre, C., Favarger, P.Y., Rossé, R. & Wold, S. (2006). "Uranium Colloid Analysis by Single Particle Inductively Coupled Plasma-Mass Spectrometry". ***Talanta*****,** 68 (3), pp. 623–628. DOI: 10.1016/j.talanta.2005.05.006

(69) Degueldre, C. & Favarger, P.Y. (2003). "Colloid Analysis by Single Particle Inductively Coupled Plasma-Mass Spectroscopy: A Feasibility Study". ***Colloids Surf., A,*** 217 (1), pp. 137–142. DOI: 10.1016/S0927-7757(02)00568-X

(70) Degueldre, C. & Favarger, P.Y. (2004). "Thorium Colloid Analysis by Single Particle Inductively Coupled Plasma-Mass Spectrometry". ***Talanta,*** 62 (5), pp. 1051–1054. DOI: 10.1016/j.talanta.2003.10.016

(71) Laborda, F., Jiménez-Lamana, J., Bolea, E. & Castillo, J. R. (2011). "Selective Identification, Characterization and Determination of Dissolved Silver(i) and Silver Nanoparticles Based on Single Particle Detection by Inductively Coupled Plasma Mass Spectrometry". ***J. Anal. At. Spectrom.*** **,** 26 (7), pp. 1362-1271. DOI: 10.1039/c0ja00098a

(72) Peters, R., Herrera-Rivera, Z., Undas, A., van der Lee, M., Marvin, H., Bouwmeester, H. & Weigel, S. (2015). "Single Particle ICP-MS Combined with a Data Evaluation Tool as a Routine Technique for the Analysis of Nanoparticles in Complex Matrices". ***J. Anal. At. Spectrom.*****,** 30 (6), pp. 1274–1285. DOI: 10.1039/C4JA00357H

(73) Montaño, M. D., Olesik, J. W., Barber, A. G. & Challis, K., Ranville, J. F. (2016). "Single Particle ICP-MS: Advances toward Routine Analysis of Nanomaterials". ***Anal Bioanal Chem*****,** 408 (19), pp. 5053–5074. DOI: 10.1007/s00216-016-9676-8

(74) Montoro Bustos, A. R., Purushotham, K. P., Possolo, A., Farkas, N., Vladár, A. E., Murphy, K. E. & Winchester, M. R. (2018). "Validation of Single Particle ICP-MS for Routine Measurements of Nanoparticle Size and Number Size Distribution". ***Anal. Chem.*****,** 90 (24), pp. 14376–14386. DOI: 10.1021/acs.analchem.8b03871

(75) Hendriks, L., Ramkorun-Schmidt, B., Gundlach-Graham, A., Koch, J., Grass, R. N., Jakubowski, N. & Günther, D. (2019). "Single-Particle ICP-MS with Online Microdroplet Calibration: Toward Matrix Independent Nanoparticle Sizing". ***J. Anal. At. Spectrom.***, 34 (4), pp. 716–728. DOI: 10.1039/C8JA00397A

(76) Hendriks, L., Gundlach-Graham, A., Hattendorf, B. & Günther, D. (2017). "Characterization of a New ICP-TOFMS Instrument with Continuous and Discrete

Introduction of Solutions". ***J. Anal. At. Spectrom.*****,** 32 (3), pp. 548–561. DOI: 10.1039/C6JA00400H

(77) Naasz, S., Weigel, S., Borovinskaya, O., Serva, A., Cascio, C., Undas, A. K., Simeone, F. C., Marvin, H. J. P. & Peters, R. J. B. (2018). "Multi-Element Analysis of Single Nanoparticles by ICP-MS Using Quadrupole and Time-of-Flight Technologies". ***J. Anal. At. Spectrom.*****,** 33 (5), pp. 835–845. DOI: 10.1039/C7JA00399D

(78) Hegetschweiler, A., Borovinskaya, O., Staudt, T. & Kraus, T. (2019). " Single-Particle Mass Spectrometry of Titanium and Niobium Carbonitride Precipitates in Steels". ***Anal. Chem.*****,** 91 (1), pp. 943–950. DOI: 10.1021/acs.analchem.8b04012

(79) Huang, Y., Tsz-Shan Lum, J. & Sze-Yin Leung, K. (2020). "Single Particle ICP-MS Combined with Internal Standardization for Accurate Characterization of Polydisperse Nanoparticles in Complex Matrices". ***J. Anal. At. Spectrom.*****,** 35, pp. 2148–2155. DOI:10.1039.D0JA00180E

(80) Rua-Ibarz, A., Bolea-Fernandez, E., Pozo, G., Dominguez-Benetton, X., Vanhaecke, F. & Tirez, K. (2020). "Characterization of Iron Oxide Nanoparticles by Means of Single-Particle ICP-Mass Spectrometry (SP-ICP-MS) – Chemical versus Physical Resolution to Overcome Spectral Overlap". ***Anal. At. Spectrom.*****,** 35 (9), pp. 2023–2032. DOI: 10.1039/D0JA00183J

(81) Azimzada, A., Farner, J. M. , Hadioui, M., Liu-Kang, C., Jreije, I., Tufenkji, N. &Wilkinson, K. J. (2020). "Release of TiO_2 Nanoparticles from Painted Surfaces in Cold Climates: Characterization Using a High Sensitivity Single-Particle ICP-MS". ***Environ. Sci. Nano.,*** 7 (1), pp. 139–148. DOI: 10.1039/C9EN00951E

(82) Mozhayeva, D. & Engelhard, C. (2020). "A Critical Review of Single Particle Inductively Coupled Plasma Mass Spectrometry – A Step towards an Ideal Method for Nanomaterial Characterization". ***J. Anal. At. Spectrom.***, 35, pp. 1740–1783 DOI: 10.1039/C9JA00206E

(83) Montaño, M. D., Majestic, B. J., Jämting, Å. K., Westerhoff, P. & Ranville, J. F. (2016). "Methods for the Detection and Characterization of Silica Colloids by

Microsecond SpICP-MS". ***Anal. Chem.*****,** 88 (9), 4733–4741. DOI: 10.1021/acs.analchem.5b04924

(84) Abad-Álvaro, I., Peña-Vázquez, E., Bolea, E., Bermejo-Barrera, P., Castillo, J. R. & Laborda, F. (2016). "Evaluation of Number Concentration Quantification by Single-Particle Inductively Coupled Plasma Mass Spectrometry: Microsecond vs. Millisecond Dwell Times". ***Anal. Bioanal. Chem.*****,** 408 (19), pp. 5089–5097. DOI: 10.1007/s00216-016-9515-y

(85) Kaňa, A., Loula, M., Koplík, R., Vosmanská, M. & Mestek, O. (2019). "Peak Bordering for Ultrafast Single Particle Analysis Using ICP-MS". ***Talanta*****,** *197*, pp. 189–198. DOI: 10.1016/j.talanta.2019.01.030

(86) Laborda, F., Jiménez-Lamana, J., Bolea, E. & Castillo, J. R (2013). "Critical Considerations for the Determination of Nanoparticle Number Concentrations, Size and Number Size Distributions by Single Particle ICP-MS". ***J. Anal. At. Spectrom.***, 28 (8), 1220. DOI: 10.1039/c3ja50100k

(87) Laborda, F., Bolea, E. & Jiménez-Lamana, J. (2016). "Single Particle Inductively Coupled Plasma Mass Spectrometry for the Analysis of Inorganic Engineered Nanoparticles in Environmental Samples" ***Trends Environ. Anal. Chem.,*** 9, pp. 15–23. DOI: 10.1016/j.teac.2016.02.001

(88) Liu, J., Murphy, K. E., Winchester, M. R. & Hackley, V. A (2017). "Overcoming Challenges in Single Particle Inductively Coupled Plasma Mass Spectrometry Measurement of Silver Nanoparticles". ***Anal. Bioanal. Chem.***, 409 (25), pp. 6027–6039. DOI: 10.1007/s00216-017-0530-4

(89) Montoro Bustos, A. R., Petersen, E. J., Possolo, A. & Winchester, M. R. (2015). "Post Hoc Interlaboratory Comparison of Single Particle ICP-MS Size Measurements of NIST Gold Nanoparticle Reference Materials". ***Anal. Chem.*****,** 87 (17), pp. 8809–8817. DOI: 10.1021/acs.analchem.5b01741

(90) Cuello-Nuñez, S., Abad-Álvaro, I., Bartczak, D., del Castillo Busto, M. E., Ramsay, D. A., Pellegrino, F. & Goenaga-Infante, H. (2020). "The Accurate Determination of Number Concentration of Inorganic Nanoparticles Using SpICP-MS with the

Dynamic Mass Flow Approach". ***J. Anal. At. Spectrom.*****,** 35, pp. 1832-1839 10.1039.C9JA00415G. DOI: 10.1039/C9JA00415G

(91) Tuoriniemi, J., Cornelis, G. & Hassellöv, M. (2012). "Size Discrimination and Detection Capabilities of Single-Particle ICP-MS for Environmental Analysis of Silver Nanoparticles". ***Anal. Chem.*****,** 84 (9), pp. 3965–3972. DOI: 10.1021/ac203005r

(92) Cornelis, G. & Hassellöv, M. A. (2014). "Signal Deconvolution Method to Discriminate Smaller Nanoparticles in Single Particle ICP-MS". ***J. Anal. At. Spectrom.,*** 29 (1), pp. 134–144. DOI: 10.1039/C3JA50160D

(93) Jiménez-Lamana, J., Abad-Álvaro, I., Bierla, K., Laborda, F., Szpunar, J. & Lobinski, R. (2018). "Detection and Characterization of Biogenic Selenium Nanoparticles in Selenium-Rich Yeast by Single Particle ICPMS". ***J. Anal. At. Spectrom.***, 33 (3), pp. 452–460. DOI: 10.1039/C7JA00378A

(94) Lee, S., Bi, X., Reed, R. B., Ranville, J. F., Herckes, P. & Westerhoff, P. (2014). "Nanoparticle Size Detection Limits by Single Particle ICP-MS for 40 Elements". ***Environ. Sci. Technol.***, 48 (17), pp. 10291–10300. DOI: 10.1021/es502422v

(95) Tadjiki, S., Montaño, M. D., Assemi, S., Barber, A., Ranville, J. & Beckett, R. (2017). "Measurement of the Density of Engineered Silver Nanoparticles Using Centrifugal FFF-TEM and Single Particle ICP-MS". ***Anal. Chem.*****,** 89 (11), pp. 6056–6064. DOI: 10.1021/acs.analchem.7b00652

(96) NIST (2020). SRM Order Request System RM 8012 - Gold Nanoparticles, Nominal 30 nm Diameter. Available in: https://www-s.nist.gov/srmors/view_detail.cfm?srm=8012 (accessed: October 19th, 2020)

(97) NIST (2020). SRM Order Request System RM 8013 - Gold Nanoparticles, Nominal 60 nm Diameter. Available in: https://www-s.nist.gov/srmors/view_detail.cfm?srm=8013 (accessed: October 19th, 2020)

(98) LGC Standards (2020). Colloidal gold nanoparticles. Available in: https://www.lgcstandards.com/ES/es/Colloidal-gold-nanoparticles/p/LGCQC5050 (accessed: October 19th, 2020)

(99) Borovinskaya, O., Gschwind, S., Hattendorf, B., Tanner, M. & Günther, D. (2014) "Simultaneous Mass Quantification of Nanoparticles of Different Composition in a Mixture by Microdroplet Generator-ICP-TOF-MS". ***Anal. Chem.,*** 86 (16), pp. 8142–8148. DOI: 10.1021/ac501150c

(100) Hendriks, L., Gundlach-Graham, A., Hattendorf, B. & Günther, D. (2017). "Characterization of a New ICP-TOFMS Instrument with Continuous and Discrete Introduction of Solutions". ***J. Anal. At. Spectrom.,*** 32 (3), pp. 548–561. DOI: 10.1039/C6JA00400H

(101) Heroult, J., Nischwitz, V., Bartczak, D. & Goenaga-Infante, H. (2014). "The Potential of Asymmetric Flow Field-Flow Fractionation Hyphenated to Multiple Detectors for the Quantification and Size Estimation of Silica Nanoparticles in a Food Matrix". ***Anal. Bioanal. Chem.,*** 406 (16), pp. 3919–3927. DOI: 10.1007/s00216-014-7831-7

(102) Speed, D., Westerhoff, P., Sierra-Alvarez, R., Draper, R., Pantano, P., Aravamudhan, S., Chen, K. L., Hristovski, K., Herckes, P., Bi, X., Yang, Y., Zeng, C., Otero-Gonzalez, L., Mikoryak, C., Wilson, B. A., Kosaraju, K., Tarannum, M., Crawford, S., Yi, P., Liu, X., Babu, S. V., Moinpour, M., Ranville, J., Montaño, M., Corredor, C., Posner, J. & Shadman, F. (2015). "Physical, Chemical, and in Vitro Toxicological Characterization of Nanoparticles in Chemical Mechanical Planarization Suspensions Used in the Semiconductor Industry: Towards Environmental Health and Safety Assessments". ***Environ. Sci.: Nano,*** 2 (3), pp. 227–244. DOI: 10.1039/C5EN00046G

(103) May, T. W. & Wiedmeyer, R. H. (1998), "A Table of Polyatomic Interferences in ICP-MS. ***Atomic Spectroscopy,*** 19 *(5)*, pp. 150–155

(104) Tanner, S. D., Baranov, V. I. & Vollkopf, U. (2000). "A Dynamic Reaction Cell for Inductively Coupled Plasma Mass Spectrometry (ICP-DRC-MS)". ***J. Anal. At. Spectrom.,*** 15 (9), pp. 1261–1269. DOI: 10.1039/b002604m

(105) Fernández, S. D., Sugishama, N., Encinar, J. R. & Sanz-Medel, A. (2012). "Triple Quad ICPMS (ICPQQQ) as a New Tool for Absolute Quantitative Proteomics and Phosphoproteomics". ***Anal. Chem.,*** 84 (14), pp. 5851–5857. DOI: 10.1021/ac3009516

(106) Balcaen, L., Woods, G., Resano, M. & Vanhaecke, F. (2013). "Accurate Determination of S in Organic Matrices Using Isotope Dilution ICP-MS/MS". ***J. Anal. At. Spectrom.,*** 28 (1), pp. 33–39. DOI: 10.1039/C2JA30265A

(107) Balcaen, L., Bolea-Fernandez, E., Resano, M. & Vanhaecke, F. (2015). "Inductively Coupled Plasma - Tandem Mass Spectrometry (ICP-MS/MS): A Powerful and Universal Tool for the Interference-Free Determination of (Ultra)Trace Elements - A Tutorial Review", ***Anal. Chim. Acta,*** 894, pp. 7–19. DOI: 10.1016/j.aca.2015.08.053

(108) Bolea-Fernandez, E., Balcaen, L., Resano, M. & Vanhaecke, F. (2017). "Overcoming Spectral Overlap via Inductively Coupled Plasma-Tandem Mass Spectrometry (ICP-MS/MS). A Tutorial Review". ***J. Anal. At. Spectrom.,*** 32 (9), pp. 1660–1679. DOI: 10.1039/C7JA00010C

(109) Bolea-Fernandez, E., Balcaen, L., Resano, M. & Vanhaecke, F. (2014). "Potential of Methyl Fluoride as a Universal Reaction Gas to Overcome Spectral Interference in the Determination of Ultratrace Concentrations of Metals in Biofluids Using Inductively Coupled Plasma-Tandem Mass Spectrometry". ***Anal. Chem.,*** 86 (15), 7969–7977. DOI: 10.1021/ac502023h

(110) Bolea-Fernandez, E., Van Malderen, S. J. M., Balcaen, L., Resano, M. & Vanhaecke, F. (2016). "Laser Ablation-Tandem ICP-Mass Spectrometry (LA-ICP-MS/MS) for Direct Sr Isotopic Analysis of Solid Samples with High Rb/Sr Ratios". ***J. Anal. At. Spectrom.,*** 31 (2), pp. 464–472. DOI: 10.1039/C5JA00404G

(111) Virgílio, A., Amais, R. S., Amaral, C. D. B., Fialho, L. L., Schiavo, D. & Nóbrega, J. A. (2016). "Reactivity and Analytical Performance of Oxygen as Cell Gas in Inductively Coupled Plasma Tandem Mass Spectrometry". ***Spectrochim. Acta, Part B,*** 126, pp. 31–36. DOI: 10.1016/j.sab.2016.10.013

(112) Amais, R. S., Amaral, C. D. B., Fialho, L. L., Schiavo, D. & Nóbrega, J. A. (2014). "Determination of P, S and Si in Biodiesel, Diesel and Lubricating Oil Using ICP-MS/MS". ***Anal. Methods*****,** 6 (13), pp. 4516–4520. DOI: 10.1039/C4AY00279B

(113) Gourgiotis, A., Ducasse, T., Barker, E., Jollivet, P., Gin, S., Bassot, S. & Cazala, C. (2017). "Silicon Isotope Ratio Measurements by Inductively Coupled Plasma Tandem Mass Spectrometry for Alteration Studies of Nuclear Waste Glasses" ***Anal. Chim. Acta*****,** 954, pp. 68–76. DOI: 10.1016/j.aca.2016.11.063

(114) Aureli, F., D'Amato, M., Raggi, A. & Cubadda, F. (2015). "Quantitative Characterization of Silica Nanoparticles by Asymmetric Flow Field Flow Fractionation Coupled with Online Multiangle Light Scattering and ICP-MS/MS Detection". ***J. Anal. At. Spectrom.*****,** 30 (6), pp. 1266–1273. DOI: 10.1039/C4JA00478G

(115) Feldmann, I., Jakubowski, N. & Stuewer, D. (1999). "Application of a Hexapole Collision and Reaction Cell in ICP-MS Part I: Instrumental Aspects and Operational Optimization". ***Fresenius J Anal Chem,*** 365 (5), pp. 415–421. DOI: 10.1007/s002160051633

(116) Resano, M., Aramendía, M., Volynsky, A. B. &Belarra, M. A. (2004). "Solid Sampling-Graphite Furnace Atomic Absorption Spectrometry for the Direct Determination of Trace Amounts of Silicon in Polyamide. Comparison of the Performance of Platinum and Palladium as Chemical Modifiers". ***Spectrochim. Acta, Part B*****,** *59* (4), pp. 523–531. DOI: 10.1016/j.sab.2003.12.022

(117) De Schrijver, I., Aramendía, M., Resano, M., Dumoulin, A. & Vanhaecke, F. (2008). "Novel Strategies for Rapid Trace Element Analysis of Polyamide by Graphite Furnace Atomic Absorption Spectrometry and Inductively Coupled Plasma Mass Spectrometry. Dissolution in an Organic Solvent versus Direct Solid Sampling Approaches". ***J. Anal. At. Spectrom.*****,** 23 (4), pp. 500-507. DOI: 10.1039/b717257e

(118) Tanner, S. D., Baranov, V. I. & Bandura, D. R. (2002). “Reaction Cells and Collision Cells for ICP-MS: A Tutorial Review”. ***Spectrochim. Acta, Part B*****,** 57 (9), pp. 1361–1452. DOI: 10.1016/S0584-8547(02)00069-1

(119) Lee, W.-W. & Chan, W.-T. (2015). “Calibration of Single-Particle Inductively Coupled Plasma-Mass Spectrometry (SP-ICP-MS)”. ***J. Anal. At. Spectrom.*****,** 30 (6), pp. 1245–1254. DOI: 10.1039/C4JA00408F

(120) Garcia, C. C., Murtazin, A., Groh, S., Horvatic, V. & Niemax, K. (2010). “Characterization of Single Au and SiO_2 Nano and Microparticles by ICP OES Using Monodisperse Droplets of Standard Solutions for Calibration”. ***J. Anal. At. Spectrom.*****,** 25 (5), pp. 645–653. DOI: 10.1039/B921041E

(121) Kálomista, I., Kéri, A., Ungor, D., Csapó, E., Dékány, I., Prohaska, T. & Galbács, G. (2017). “Dimensional Characterization of Gold Nanorods by Combining Millisecond and Microsecond Temporal Resolution Single Particle ICP-MS Measurements”. ***J. Anal. At. Spectrom.*****,** 32 (12), pp. 2455–2462. DOI: 10.1039/C7JA00306D

(122) Fréchette-Viens, L., Hadioui, M. & Wilkinson, K. J. (2017). “Practical Limitations of Single Particle ICP-MS in the Determination of Nanoparticle Size Distributions and Dissolution: Case of Rare Earth Oxides”. ***Talanta*****,** 163, pp. 121–126. DOI: 10.1016/j.talanta.2016.10.093

(123) Jakubowski, N., Moens, L. & Vanhaecke, F. (1998). “Sector Field Mass Spectrometers in ICP-MS”. ***Spectrochim. Acta, Part B*****,** 53 (13), pp. 1739–1763. DOI: 10.1016/S0584-8547(98)00222-5

(124) Jakubowski, N., Prohaska, T., Rottmann, L. & Vanhaecke, F. (2011). “Inductively Coupled Plasma- and Glow Discharge Plasma-Sector Field Mass Spectrometry”. ***J. Anal. At. Spectrom.*****,** 26 (4), pp. 693–726. DOI: 10.1039/C0JA00161A

(125) Tuoriniemi, J., Cornelis, G. & Hassellöv, M. (2015). “A New Peak Recognition Algorithm for Detection of Ultra-Small NanoParticles by Single Particle ICP-MS Using Rapid Time Resolved Data Acquisition on a Sector-Field Mass

Spectrometer". ***J. Anal. At. Spectrom.***, 30 (8), pp. 1723–1729. DOI: 10.1039/C5JA00113G

(126) Bandura, D. R., Baranov, V. I. & Tanner, S. D. (2001) "Reaction Chemistry and Collisional Processes in Multipole Devices for Resolving Isobaric Interferences in ICP–MS". ***Fresenius J. Anal. Chem***., 370 (5), pp. 454–470. DOI: 10.1007/s002160100869

(127) Hattendorf, B. & Günther, D. (2004). "Suppression of In-Cell Generated Interferences in a Reaction Cell ICP-MS by Bandpass Tuning and Kinetic Energy Discrimination". ***J. Anal. At. Spectrom.***, 19 (5), pp. 600–606. DOI: 10.1039/B312155K

(128) Yamada, N. (2015). "Kinetic Energy Discrimination in Collision/Reaction Cell ICP-MS: Theoretical Review of Principles and Limitations". ***Spectrochim. Acta, Part B***, 110, pp. 31–44. DOI: 10.1016/j.sab.2015.05.008

(129) Kálomista, I., Kéri, A. & Galbács, G. (2016). "On the Applicability and Performance of the Single Particle ICP-MS Nano-Dispersion Characterization Method in Cases Complicated by Spectral Interferences". ***J. Anal. At. Spectrom.***, 31 (5), pp. 1112–1122. DOI: 10.1039/C5JA00501A

(130) Klencsár, B., Sánchez, C., Balcaen, L., Todolí, J., Lynen, F. & Vanhaecke, F. (2018). "Comparative Evaluation of ICP Sample Introduction Systems to Be Used in the Metabolite Profiling of Chlorine-Containing Pharmaceuticals via HPLC-ICP-MS". ***J. Pharmaceut. Biomed.,*** 153, pp. 135–144. DOI: 10.1016/j.jpba.2018.02.031

(131) Malderen, S. J. M. V., Managh, A. J., Sharp, B. L. & Vanhaecke, F. (2016). "Recent Developments in the Design of Rapid Response Cells for Laser Ablation-Inductively Coupled Plasma-Mass Spectrometry and Their Impact on Bioimaging Applications". ***J. Anal. At. Spectrom.***, 31 (2), pp. 423–439. DOI: 10.1039/C5JA00430F

(132) Simpson, L. A., Thomsen, M., Alloway, B. J. & Parker, A. (2001) "A Dynamic Reaction Cell (DRC) Solution to Oxide-Based Interferences in Inductively Coupled

Plasma Mass Spectrometry (ICP-MS) Analysis of the Noble Metals". ***J. Anal. At. Spectrom.,*** 16 (12), pp. 1375–1380. DOI: 10.1039/B107818F

(133) Kéri, A., Kálomista, I., Ungor, D., Bélteki, Á., Csapó, E., Dékány, I., Prohaska, T. & Galbács, G. (2018). "Determination of the Structure and Composition of Au-Ag Bimetallic Spherical Nanoparticles Using Single Particle ICP-MS Measurements Performed with Normal and High Temporal Resolution". ***Talanta,*** 179, pp. 193–199. DOI: 10.1016/j.talanta.2017.10.056

(134) Gupta, A. K. & Gupta, M. (2005). "Synthesis and Surface Engineering of Iron Oxide Nanoparticles for Biomedical Applications". ***Biomaterials,*** 26 (18), pp. 3995–4021. DOI: 10.1016/j.biomaterials.2004.10.012

(135) Xu, P., Zeng, G. M., Huang, D. L., Feng, C. L., Hu, S., Zhao, M. H., Lai, C., Wei, Z., Huang, C., Xie, G. X. & Liu, Z. F. (2012). "Use of Iron Oxide Nanomaterials in Wastewater Treatment: A Review". ***Sci. Total Environ.,*** 424, pp. 1–10. DOI: 10.1016/j.scitotenv.2012.02.023

(136) Fernández, J. G., Sánchez-González, C., Bettmer, J., Llopis, J., Jakubowski, N., Panne, U. & Montes-Bayón, M. (2018). "Quantitative Assessment of the Metabolic Products of Iron Oxide Nanoparticles to Be Used as Iron Supplements in Cell Cultures". ***Anal. Chim. Acta,*** 1039, pp. 24–30. DOI: 10.1016/j.aca.2018.08.003

(137) Alonso, E.V., Guerrero, M. M.L., Cordero, M. T.S., Pavón, J. M.C. & de Torres, A.G. (2016). "Characterization of Solid Magnetic Nanoparticles by Means of Solid Sampling High Resolution Continuum Source Electrothermal Atomic Absorption Spectrometry". ***J. Anal. At. Spectrom.,*** 31 (12), pp. 2391–2398. DOI: 10.1039/C6JA00225K

(138) Aguilar-Arteaga, K., Rodriguez, J. A. & Barrado, E. (2010). "Magnetic Solids in Analytical Chemistry: A Review". ***Anal, Chim. Acta,*** 674 (2), pp. 157–165. DOI: 10.1016/j.aca.2010.06.043

(139) Agilent Technologies (2020). Agilent 8900 triple quadrupole ICP-MS. Technical overview.

(140) Agatemor, C. & Beauchemin, D. (2011) “Matrix Effects in Inductively Coupled Plasma Mass Spectrometry: A Review”. ***Anal. Chim. Acta*****,** 706 (1), pp. 66–83. DOI: 10.1016/j.aca.2011.08.027

(141) Liu, J., Murphy, K. E., Winchester, M. R. & Hackley, V. A. (2017). “Overcoming Challenges in Single Particle Inductively Coupled Plasma Mass Spectrometry Measurement of Silver Nanoparticles”. ***Anal. Bioanal. Chem.,*** 409 (25), pp. 6027–6039. DOI: 10.1007/s00216-017-0530-4

(142) Vidmar, J., Buerki-Thurnherr, T. & Loeschner, K. (2018). “Comparison of the Suitability of Alkaline or Enzymatic Sample Pre-Treatment for Characterization of Silver Nanoparticles in Human Tissue by Single Particle ICP-MS”. ***J. Anal. At. Spectrom.,*** 33 (5), pp. 752–761. DOI: 10.1039/C7JA00402H.

(143) Vidmar, J., Loeschner, K., Correia, M., Larsen, E. H., Manser, P., Wichser, A., Boodhia, K., Al-Ahmady, Z. S., Ruiz, J., Astruc, D. & Buerki-Thurnherr, T. (2018) “Translocation of Silver Nanoparticles in the *Ex Vivo* Human Placenta Perfusion Model Characterized by Single Particle ICP-MS”. ***Nanoscale,*** 10 (25), pp. 11980–11991. DOI: 10.1039/C8NR02096E

(144) De la Calle, I., Menta, M. & Séby, F. (2016). “Current Trends and Challenges in Sample Preparation for Metallic Nanoparticles Analysis in Daily Products and Environmental Samples: A Review”. ***Spectrochim. Acta, Part B*****,** 125, pp. 66–96. DOI: 10.1016/j.sab.2016.09.007

(145) Gray, E. P., Coleman, J. G., Bednar, A. J., Kennedy, A. J., Ranville, J. F. & Higgins, C. P. (2013). “Extraction and Analysis of Silver and Gold Nanoparticles from Biological Tissues Using Single Particle Inductively Coupled Plasma Mass Spectrometry”. ***Environ. Sci. Technol.*****,** 47 (24), pp. 14315–14323. DOI: 10.1021/es403558c

(146) Bolea, E., Jiménez-Lamana, J., Laborda, F., Abad-Álvaro, I., Bladé, C., Arola, L. & Castillo, J. R. (2014) “Detection and Characterization of Silver Nanoparticles and Dissolved Species of Silver in Culture Medium and Cells by AsFlFFF-UV-Vis-ICPMS: Application to Nanotoxicity Tests”. ***Analyst*****,** 139 (5), pp. 914–922. DOI: 10.1039/C3AN01443F

(147) Rodríguez-González, P., Marchante-Gayón, J. M., García Alonso, J. I. & Sanz-Medel, A. (2005) “Isotope Dilution Analysis for Elemental Speciation: A Tutorial Review”. ***Spectrochim. Acta, Part B*****,** 60 (2), pp. 151–207. DOI: 10.1016/j.sab.2005.01.005

(148) Olesik, J. W. (1997). “Investigating the Fate of Individual Sample Droplets in Inductively Coupled Plasmas”. ***Appl. Spectrosc.***

(149) Garcia, C. C., Murtazin, A., Groh, S., Horvatic, V., Niemax, K. (2010) “Characterization of Single Au and SiO_2 Nano and Microparticles by ICP OES Using Monodisperse Droplets of Standard Solutions for Calibration”. ***J. Anal. At. Spectrom.*****,** 25 (5), pp. 645–649. DOI: 10.1039/b921041e

(150) Telgmann, L., Metcalfe, C. D. & Hintelmann, H. (2014). “Rapid Size Characterization of Silver Nanoparticles by Single Particle ICP-MS and Isotope Dilution”. ***J. Anal. At. Spectrom.*****,** 29 (7), pp. 1265–1272. DOI: 10.1039/C4JA00115J

(151) Sötebier, C. A., Kutscher, D. J., Rottmann, L., Jakubowski, N., Panne, U. & Bettmer, J. (2016). “Combination of Single Particle ICP-QMS and Isotope Dilution Analysis for the Determination of Size, Particle Number and Number Size Distribution of Silver Nanoparticles”. ***J. Anal. At. Spectrom.*****,** 31 (10), pp. 2045–2052. DOI: 10.1039/C6JA00137H

(152) Rottmann, L. & Heumann, K. G. (1994). “Development of an On-Line Isotope Dilution Technique with HPLC/ICP-MS for the Accurate Determination of Elemental Species”. ***Fresenius J. Anal. Chem.*****,** 350 (4), pp. 221–227. DOI: 10.1007/BF00322473

(153) Rottmann, Lothar. & Heumann, K. G. (1994). “Determination of Heavy Metal Interactions with Dissolved Organic Materials in Natural Aquatic Systems by Coupling a High-Performance Liquid Chromatography System with an Inductively Coupled Plasma Mass Spectrometer”. ***Anal. Chem.*****,** 66 (21), pp. 3709–3715. DOI: 10.1021/ac00093a027

(154) Borovinskaya, O., Hattendorf, B., Tanner, M., Gschwind, S. & Günther, D. (2013). "A Prototype of a New Inductively Coupled Plasma Time-of-Flight Mass Spectrometer Providing Temporally Resolved, Multi-Element Detection of Short Signals Generated by Single Particles and Droplets". ***J. Anal. At. Spectrom.*****,** 28 (2), pp, 226–233. DOI: 10.1039/C2JA30227F

(155) Yongyang, S., Wei, W., Zhiming, L., Hu, D., Guoqing, Z., Jiang, X. & Xiangjun, R. (2015). "Direct Detection and Isotope Analysis of Individual Particles in Suspension by Single Particle Mode MC-ICP-MS for Nuclear Safety". ***J. Anal. At. Spectrom.*****,** 30 (5), pp. 1184–1190. DOI: 10.1039/C4JA00339J

(156) Kappel, S., Boulyga, S. F., Dorta, L., Günther, D., Hattendorf, B., Koffler, D., Laaha, G., Leisch, F. & Prohaska, T. (2013). "Evaluation Strategies for Isotope Ratio Measurements of Single Particles by LA-MC-ICP-MS". ***Anal Bioanal Chem*****,** 405 (9), pp. 2943–2955. DOI: 10.1007/s00216-012-6674-3

(157) Rottmann, L. & Heumann, K. G. (1994). "Development of an On-Line Isotope Dilution Technique with HPLC/ICP-MS for the Accurate Determination of Elemental Species". ***Fresenius J Anal Chem*****,** 350 (4), pp. 221–227. DOI: 10.1007/BF00322473

(158) Rottmann, Lothar. & Heumann, K. G. (1994). "Determination of Heavy Metal Interactions with Dissolved Organic Materials in Natural Aquatic Systems by Coupling a High-Performance Liquid Chromatography System with an Inductively Coupled Plasma Mass Spectrometer". ***Anal. Chem.*****,** 66 (21), pp. 3709–3715. DOI: 10.1021/ac00093a027

(159) Ulianov, A., Müntener, O., Schaltegger, U. (2015). "The ICP-MS Signal as a Poisson Process: A Review of Basic Concepts. ***J. Anal. At. Spectrom.*****,** 30 (6), pp. 1297–1321. DOI: 10.1039/C4JA00319E

(160) Liu, J., Murphy, K. E., MacCuspie, R. I., Winchester, M. R. (2014). "Capabilities of Single Particle Inductively Coupled Plasma Mass Spectrometry for the Size Measurement of Nanoparticles: A Case Study on Gold Nanoparticles". ***Anal. Chem.*****,** 86 (7), pp. 3405–3414. DOI: 10.1021/ac403775a

(161) Petersen, E. J., Montoro-Bustos, A. R., Toman, B., Johnson, M. E., Ellefson, M., Caceres, G. C., Neuer, A. L., Chan, Q., Kemling, J. W., Mader, B., Murphy, K., Roesslein, M. (2019). “Determining What Really Counts: Modeling and Measuring Nanoparticle Number Concentrations”. ***Environ. Sci.: Nano*****,** 6 (9), pp. 2876–2896. DOI: 10.1039/C9EN00462A